INFLUENCE OF CHARGE ASYMMETRY IN HEAVY ION COLLISIONS AT INTERMEDIATE ENERGIES

A THESIS

submitted to the

THAPAR UNIVERSITY, PATIALA

for the degree of

DOCTOR OF PHILOSOPHY

IN THE FACULTY OF SCIENCE

By

Anupriya Jain

Regn. No. 901012003

SCHOOL OF PHYSICS AND MATERIALS SCIENCE

THAPAR UNIVERSITY

PATIALA-147004, PUNJAB (INDIA)

.

I dedicate this work to my parents,
who guided and loved me through my life,
taught me again and again to never give up and to follow my dreams.
And to my Guru ji from whom I learned a lot of principles
and the best ones are the principles of life.

THAPAR UNIVERSITY, PATIALA

CANDIDATE'S DECLARATION

I hereby certify that the work which is being presented in this thesis entitled "**INFLUENCE OF CHARGE ASYMMETRY IN HEAVY ION COLLISIONS AT INTERMEDIATE ENERGIES**" in partial fulfillment of the requirements for the award of Degree of Doctor of Philosophy and submitted in the School of Physics and Materials Science, Thapar University, Patiala, is an authentic record of my own work carried out during the period from September 2010 to May 2013 under the supervision of **Dr. Suneel Kumar**, Associate Professor, Thapar University, Patiala and **Professor Rajeev K. Puri**, Department of Physics, Panjab University, Chandigarh. The matter presented in this thesis has not been submitted by me in part or full for the award of any other degree in any other university or institute.

Anupriya Jain

(Anupriya Jain)

This is to certify that the above statement made by the candidate is correct to the best of our knowledge.

S Kumar

Dr. Suneel Kumar
(Supervisor)

Prof. Rajeev K. Puri
(Co-Supervisor)

Head of the Department

Dean R & SP

A. K. Srivastava 31/10/2013

External Examiner

Date: 31-10-2013

Acknowledgments

A dream realized the joy that occurs when standing on the destination and sees that path which we cover to reach the destination. The journey was not easy if, I ever meet, my friends and my well wishers, who have helped and supported me along this long but fulfilling road. At the end of this journey of Ph.D, I would like to thank all the people who helped me to complete my thesis and leave an unforgettable picture of some beautiful moments on my mind.

First of all, I would like to pay homage to my supervisor, **Dr. Suneel Kumar**, Associate Professor, Thapar University, Patiala. For me, he is a pillar of support, an epitome of strength, as loving as a mother, as strict as a father, as caring as a friend, a disciplinarian yet always so approachable and warm at heart. I am glad to be his student, a million thanks to him, as he gave me the strength, to make my dreams come true. For the world he is one person, but for one person, he is the world, and that person is me. I admire him, for the challenges, he has made me to face, for they gave me the courage to lead every race. It is not a fair task to thank him with a few words. I can never forget what he has done for me.

I am also extremely indebted to my co-supervisor, **Professor Rajeev K. Puri**, Panjab University, Chandigarh. He has especially contributed a lot to this thesis. Everything he says feels right. Everything about him looks nice. I am lucky to have a teacher like him. Words are not enough to express his ability to get an intuitive feel of the most difficult ideas. It is a fortunate for me being associated with him in research field. Despite of his busy schedule he used to review my thesis progress, give his valuable suggestions and made corrections. His steady courage and conviction will always inspire me.

I would not have contemplated my Ph.D if **Dr. Prem Singh Pundir**, Assistant Professor, S.D. College, Ambala Cant, has not been motivated me. I will forever be thankful to him as, he is the only person because of whom I met Dr. Suneel Kumar.

I offer special thanks to **Dr. Kulvir Singh**, Head of School of Physics and Materials Science, Thapar University, Patiala, for providing all the necessary facilities in the department. He patiently provided the vision, encouragement and advice necessary for me to proceed through the doctorial program and complete my dissertation.

I can never forget to acknowledge the funding agencies for providing me financial assistance, the University Grant Commission (UGC) in the form of Project Fellow and Council of Scientific & Industrial Research (CSIR) in the form of Senior Research Fellow which buttressed me to perform my work comfortably.

I acknowledge the useful suggestions of the members of my doctoral committee Drs. Manoj Kumar Sharma, Alka Upadhyay and Rajesh Kumar. Their guidance has served me well and I owe them my heartfelt appreciation. Thanks to Dr. Parmod K. Bajpai, Dean, research and sponsored projects for providing the possible research facilities here at Thapar University campus.

With great appreciation I shall acknowledge all my lab mates Chandani Khurana, Parveer Kaur, Mintu Tyagi, Deepika Jain, Rajni Mittal and many others research scholars here at Thapar University, Patiala. I also acknowledge with thanks the support and encouragement extended by theory group at Chandigarh, particularly Rajni Bansal, Sukhjit Kaur and Dr. Sakshi Gautam. My special appreciation goes to my very close friends Mr. Karan Singh Vinayak and Ms. Rubina Bansal for all their help and support throughout this study. You guys were always real pals. I would like to acknowledge my three friends Dr. Shinjinee Das Gupta, VECC Kolkata, Mr. Vijay Raj Sharma, A. M. University, Aligarh and Virendra Kumar Passi, IIT Mumbai, who always helped me to find the research papers which were not accessible at Thapar University Campus.

During my Ph.D at Thapar University, I never felt home sickness. It's all because of my wonderful and dearest sister Rishu. She was always there to help me whenever I feel depressed. Thank you so much for all your love, support and care. I love you so much.

I owe a special thanks to my family, my Mom and Papa and my brother Bhavesh, who supported me and helped me throughout my life and during my Ph.D. Mom and Papa, I really do not know how to thank you enough for providing me with the opportunity to be where I am today. I dedicate this work to you all.

Last but not the least, I would like to pay high regards to Saraswati the Goddess of knowledge who gave me some intellect and wisdom to reach where I am today.

Date : (Anupriya Jain)

Patiala

List of Publications :

A. Journals :

1. Influence of charge asymmetry and isospin dependent cross-section on nuclear stopping.
   Anupriya Jain, Suneel Kumar and Rajeev K. Puri
   Phys. Rev. C **84**, 057602 (2011) (*4 pages*).

2. Anisotropic distribution of nucleons participating in elliptical flow.
   Anupriya Jain and Suneel Kumar
   Nucl. Phys. A **876**, 109 (2012) (*10 pages*).

3. Effect of isospin dependent cross-section on fragment production in the collision of charge asymmetric nuclei.
   Anupriya Jain and Suneel Kumar
   Pramana Journal of physics **78**, 749 (2012) (*10 pages*).

4. Influence of charge asymmetry and isospin-dependent cross section on elliptical flow.
   Anupriya Jain, Suneel Kumar and Rajeev K. Puri
   Phys. Rev. C **85**, 064608 (2012) (*6 pages*).

5. The study of participant-spectator matter and thermalization for charge asymmetric nuclear collision.
   Anupriya Jain and Suneel Kumar
   Phys. Scr. **85**, 065306 (2012) (*6 pages*).

6. Phase space analysis of anisotropic flow.
   Anupriya Jain and Suneel Kumar
   International Journal of Modern Physics E **21**, 1250071 (2012) (*9 pages*).

7. Consequence of isospin effects on the rapidity distribution of anisotropic flows.
   Suneel Kumar and Anupriya Jain
   AIP Conf. Proc. **1524**, 247 (2013) (*5 pages*).

8. Effect of momentum dependent interactions and nucleonic cross-section on directed flow (v_1).
   Anupriya Jain, Karan Singh Vinayak and Suneel Kumar
   Annals of Physics **334**, 334 (2013) (*7 pages*).

9. On the fragment mass independence of balance energy.
   Anupriya Jain and Suneel Kumar
   Phys. Scr. **88**, 025201 (2013) (*5 pages*).

10. Isospin effects on the system mass dependence of nuclear stopping around balance energy.
    Anupriya Jain and Suneel Kumar
    Nucl. Phys. A (Under review).

11. Analyzing the role of isospin content and colliding geometry on the transition energy for symmetric colliding nuclei.
    Anupriya Jain and Suneel Kumar
    Phys. Scr. (Under review).

12. Isospin effects on p_t differential flow in heavy-ion collisions at intermediate energies.
    Rubina Bansal, Anupriya Jain and Suneel Kumar
    Annals of Physics (Under review).

13. Correlation between directed transverse flow and nuclear stopping for the mass asymmetric nuclear matter.
    Rubina Bansal, Anupriya Jain and Suneel Kumar
    Cent. Eur. J. Phys. (Under review).

B. Symposia/Workshops/Conferences:

14. Intermediate Mass Fragment Production in Symmetric Collisions.
    Anupriya Jain, Bahadur Singh and Suneel Kumar
    5^{th} Chandigarh Science Congress, PS-59, Panjab University, Chandigarh, India (2011).

15. Effect of isospin dependent cross-section on nuclear stopping.
    Anupriya Jain and Suneel Kumar
    DAE Symposium on Nuclear Physics, Vol. **56**, 798 (2011).

16. Consequence of colliding geometry and rapidity range on anisotropic flow.
    Anupriya Jain, Suneel Kumar and R. K. Puri
    DAE Symposium on Nuclear Physics, Vol. **57**, 676 (2012).

17. Correlation between nuclear stopping and directed flow at intermediate energies.
    Suneel Kumar and Anupriya Jain
    DAE Symposium on Nuclear Physics, Vol. **57**, 702 (2012).

18. Consequence of isospin dependent cross section and charge asymmetry on anisotropic flow.
    Anupriya Jain and Suneel Kumar
    11^{th} International Conference on Nucleus-Nucleus Collisions, San Antonio, Texas (USA), (Poster presentation)
    May 27-June 1 (2011).

19. Sensitivity of the transition energy towards mass asymmetry of the colliding nuclei.
    Anupriya Jain, Sangeeta and Suneel Kumar
    International Nuclear Physics Conference (INPC), Firenze, Italy, 2-7 June 2013 (Under review).

20. Analyzing the role of fragment charge on nuclear stopping for symmetric colliding nuclei.
    Anupriya Jain, T. Sahil and Suneel Kumar
    XXXIII Mazurian Lakes Conference on Physics, Piaski, Poland, 1-7 September 2013 (in press).

21. Influence of density dependent of symmetry energy on neutron-proton directed transverse flow (v_1).
    Rubina Bansal, Anupriya Jain and Suneel Kumar
    DAE Symposium on Nuclear Physics, 02-06 December 2013
    Bhabha Atomic Research Centre, Mumbai (INDIA) (accepted)

22. Correlation between temperature, density and nuclear stopping in heavy-ion collisiins

    Suneel Kumar, Anupriya Jain and Rubina Bansal

    DAE Symposium on Nuclear Physics, 02-06 December 2013

    Bhabha Atomic Research Centre, Mumbai (INDIA) (accepted)

Contents

ABSTRACT

In heavy-ion collisions, lots of effort have been made to understand the properties of stable nuclei. With the development of radioactive beam facilities, the study of isospin degree of freedom has gained a major boost. At intermediate energies, both attractive mean field and nucleon-nucleon collisions play an important role. Both these regimes together, lead the matter from a fused state to total disassembly. Therefore, one is also interested to understand the mechanism behind this. This mechanism has motivated the nuclear physics community to study the hot and dense nuclear matter under extreme conditions of density and temperature in heavy-ion collisions at intermediate energies. This energy regime offers an excellent opportunity to study various phenomena like multifragmentation, collective flow and nuclear stopping. However, the phenomena at higher incident energy are characterized by the production of sub-threshold particles and their isospin dependence. Our aim in this thesis to study the effect of isospin asymmetry (charge asymmetry) and isospin dependent nucleon nucleon cross section on fragment production, collective flow as well as on nuclear stopping. The term charge asymmetry means the collision of nuclei in which neutron number is not equal to the proton number. Here we fix the mass of the colliding nuclei but varied their proton number (isobaric nuclei).

Firstly, we have focused on multifragmentation, which constitutes fragments of different charge/mass. In the present work, we study the isospin effects on the multiplicity of free nucleons (FN's) [$A_f = 1$], light mass fragments (LMF's) [$2 \leq A_f \leq 4$] and intermediate mass fragments (IMF's) [$5 \leq A_f \leq A_{tot}/6$] for isospin asymmetric nuclei. We find that the multiplicity of FN's, LMF's and IMF's depends more on the mass of the colliding nuclei compared to N/Z of the system. We also find that, the isospin dependence of nucleon-nucleon cross-section shows a small influence on the multiplicity of FN's, LMF's and IMF's with incident energy. Moreover, we observe a uniform effect of σ_{iso} ($\sigma_{np} = 3\sigma_{nn} = 3\sigma_{pp}$) and σ_{noiso} ($\sigma_{np} = \sigma_{nn} = \sigma_{pp}$) on the N/Z dependence of the multiplicity of FN's and LMF's. Our theoretical calculations follow the similar trend as given by the experimental findings of ALADiN collaboration. Moreover, the multiplicity of IMF's is not influenced by the two forms of cross-section discussed here.

The another phenomena linked with the interplay between the attractive mean field and

repulsive nucleon-nucleon scattering is the global stopping of nuclear matter. Therefore, as a next step, we study the isospin effects on nuclear stopping for isobaric nuclei. We have discussed the isospin dependence of nucleon-nucleon cross-section on nuclear stopping. We find that, like multifragmentation even in nuclear stopping, small influence is observed due to σ_{iso} and σ_{noiso}. Participant (spectator) matter decreases (increases) with increase in the neutron content of the system whatever be the definition of the participant matter. The variation of the slope of $\langle participant \rangle_{norm}$ (normalized participant matter) with incident energy gives an indication about the global equilibrium of the system and the variation of the slope of $\langle spectator \rangle_{norm}$ (normalized spectator matter) with incident energy gives an indication about the local equilibrium of the system. The isospin content of the colliding nuclei has again a small influence on $\langle R \rangle$ and $\langle 1/Q_{zz} \rangle$. Moreover, our theoretical calculations follow the similar trend as the experimental findings of the INDRA collaboration. We also investigate the reasons of failure by earlier theoretical attempts made in this direction, and we find that in addition to the choice of centrality, strength of nucleon-nucleon cross-section has a major role to play in reaction dynamics.

Additional promising observable for the understanding of isospin asymmetry in the momentum distribution includes the directed, elliptical, triangular and quadrupole flow. The absolute value of flow results from the above interplay. This interplay is responsible for the transition from a fused state to total disassembly. In the present study, we conclude that the directed flow of both neutrons and protons is affected by the isospin dependence of nucleon-nucleon cross-section. Isospin dependent cross-section (σ_{iso}) is found to be more compatible with the experimental data. Although, it has been proven experimentally that, fragment charge/mass does not influence the balance energy. We have proved this theoretically for the first time using Isospin dependent Quantum Molecular Dynamics (IQMD) model. In case of elliptical flow, we have studied that, the distribution of nucleons and fragments is not symmetric around the beam axis. Moreover, the elliptical flow depends on the isospin dependence of nucleon-nucleon cross-section. Transition energy is however not affected by the change in isotopic content of the system. Our theoretical calculations of the excitation function of elliptical flow are able to reproduce the experimental findings of GSI collaboration. Higher order anisotropic flows are more sensitive to the isotopic content and the isospin dependence of the nucleon-nucleon cross-section,

indicating the strong dependence of these observables on the initial configuration of the system.

Isospin effects have been found to be due to the interplay between Coulomb potential, symmetry energy, nucleon-nucleon cross-section. To shed light on the relative importance of above mentioned observables, we studied the effect of isospin degree of freedom on nuclear stopping throughout the mass range between 50 and 350 for two sets of isotopic systems as well as isobaric systems. Analysis is carried out at incident energy below, at and above the energy of vanishing flow (EVF). Our findings reveal that nuclear stopping does not show any particular behavior at EVF. Moreover, system size effects dominate the isospin effects throughout the range of colliding geometry. The Coulomb effect becomes important at higher colliding geometry. The comparative study of counterbalancing of Coulomb and mean field by removing nucleon-nucleon collisions clearly indicates the dominance of nucleon-nucleon cross-section over the repulsive Coulomb potential.

Finally, we conclude that, collective flow can act as a better tool compared to multifragmentation and nuclear stopping to study the reaction dynamics involving the nuclei having isospin asymmetry.

Chapter 1

Introduction

"The intuitive mind is a sacred gift and the rational mind is a faithful servant. We have created a society that honors the servant and has forgotten the gift".....Albert Einstein

1.1 Introduction to the nuclear physics

Nuclear physics is about the study of nuclei which lie at the core of every atom in the Universe. The nuclei occupy almost 99.9% of the mass of all ordinary matter in the Universe. One of the major motivations for studying the atomic nucleus is simply to gain deeper understanding of our nature, including its origin and future, as well as its present state. Study of nuclear physics can be divided into different branches. One of its branch is related to the study of *quark gluon plasma*. Its second branch led to the development of the *low energy γ-ray spectroscopy*. The third branch deals with the study of nuclear collectivity through *giant resonances*. Last branch known as intermediate energy heavy-ion collisions, grew out of compound nucleus and fission studies and matured through the low energy deep inelastic scattering [1, 2, 3].

In early fifties of last century, the field was dominated by shooting light particles on heavy targets. Due to which, only limited phenomena like fusion of two nuclei or fission etc. could be studied. But now a days, with the help of high energy accelerators, one is able to study a variety of phenomena in heavy-ion reactions.

The main interest to study the low energy nuclear physics is to look for the nuclear interactions, fusion, fission, cluster-radioactivity, formation of super heavy nuclei, the halo-nuclei [4] etc. The structure of nuclei is the main concern in this energy regime. The reaction cross-section at low incident energy composes of three categories i.e, the fusion-

evaporation, fusion-fission and deep inelastic scattering. Naturally, all these processes depend on the projectile-target combination, on the bombarding energy of the projectile as well as on the angular momentum. But now a days, one is able to accelerate the heavy ions with bombarding energies comparable to their rest mass. This opened up new dimensions which is termed as intermediate energy heavy-ion physics.

The reactions at intermediate energy gives the possibility to study the properties of nuclear matter under the extreme conditions of density and temperature. This high density and temperature region is often called "fireball". The residues of the target and the projectile outside the overlapping region, are excited by collisions. They constitute "spectator" matter that de-excites by evaporation or multifragmentation. The study of the behavior of hadrons in hot and dense nuclear matter is one of the central topics in present day research. Naturally, like all other materials, the properties of nuclear matter are also influenced by the pressure, density and temperature. This can be further understood in terms of phase diagram.

1.1.1 The phase transition of nuclear matter

Normal nuclear matter exists at the density $\rho_0 = 0.15$ to $0.17\ fm^{-3}$. In Fig.1.1, the black dot represents the ground state. The shell model [5] was invented when mass measurements revealed the existence of magic numbers. Because of short range of the interaction, nuclei have properties reminiscent of liquid drops. This led to the development of the liquid-drop model for explaining macroscopic nuclear properties.

On increasing the temperature, and/or pressure the nuclear material shows a phase transition from liquid-like state to the gaseous phase in which the nucleons move freely in the nuclear volume like Van der Waals gas. In this state, the matter consists of hadrons. The second phase transition of nuclear matter occur, on further increasing the temperature and/or density. This phase is known as quark gluon plasma [7].

In Fig.1.1, the dashed lines indicate the path followed by the early Universe in the first minute of its existence. As already stated, the exact position and nature of the phase transition is still under investigation. The nuclear equation of state (NEOS) of nuclear matter is useful to describe the relationship between the macroscopic quantities like temperature and density. The determination of the NEOS can be regarded as the

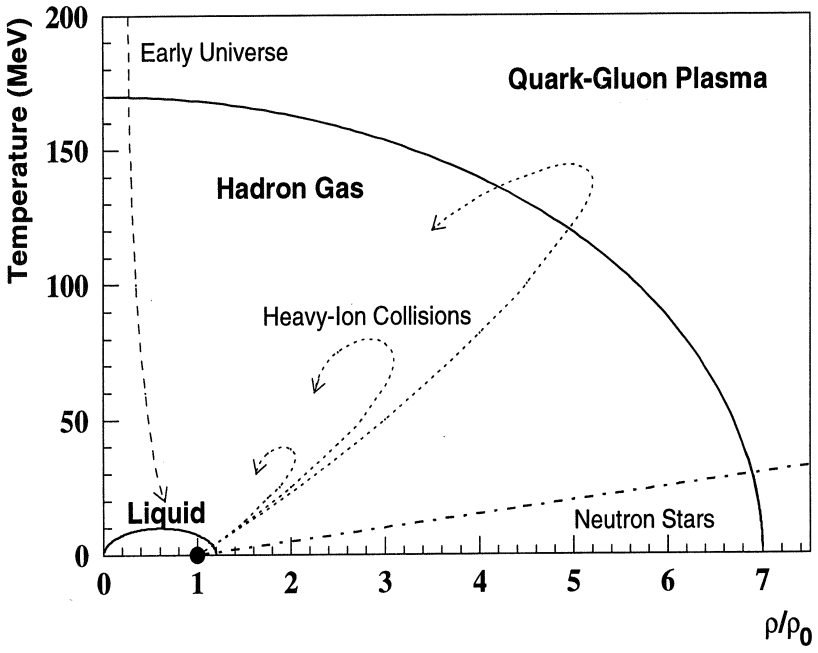

Figure 1.1: *Phase diagram of nuclear matter. The y-axis indicates the temperature (in MeV) and the x-axis indicates the baryons density normalized to the density of the ground state of nuclear matter. The figure is taken from the reference [6].*

Holy Grail of this field of physics [8].

During a heavy-ion collision, due to larger compression of nuclear matter, density as well as temperature reaches to very high values that helps to probe the pressure-density phase of the nuclear matter. With the invention of many accelerator facilities such as: BEVALAC at Berkeley (which was shut down in early 1993), the GSI accelerator complex with the UNILAC and the heavy-ion Synchrotron SIS at Darmstadt, the SATURNE Synchrotron at Saclay, the GANIL Cyclotron at France as well as the heavy-ion collider NICA at JINR (Dubna) and RHIC at Brookhaven, which provide heavy-ion beams with relativistic energies, it became possible to study the hot and dense nuclear matter through the heavy-ion collisions in a laboratory environment, and indeed, this new field of physics with all its fascinating features is opened for investigations [9, 10, 11, 12].

NEOS plays a central role in hot and dense nuclear matter physics, because it is useful for the understanding of the physics of early Universe as well as the static and dynamical behavior of stars (e.g. supernova explosion) and contains the intriguing possibilities of various phase transitions (liquid-gas, meson condensate, quark-gluon plasma etc.) [13].

Since bulk nuclear properties are mainly determined by the nuclear matter equation of state, is therefore one of the main goals of heavy-ion physics to extract the NEOS, i.e. the density dependence of the thermostatic properties of nuclear matter (energy and pressure) from observations. In the next section, we will discuss the basic concept of nuclear equation of state.

1.2 The concept of nuclear equation of state (NEOS)

An equation of state (EOS) is a relation between thermodynamic variables pressure, temperature and density of the matter under consideration. Nuclear equation of state describe the possibility of compressing nuclear matter. If we try to change the density (e.g. by compression) we have to overcome the repelling forces i.e we have to pump compressional energy into the system. Nuclear equation of state describe compressional energy which corresponds to density. Jha *et al.,* [14] studied the EOS for dense matter in the core of a compact stars using a mean-field approach.

To understand the concept of nuclear equation of state more clearly, consider an infinite nuclear matter, consisting of nucleons only. The energy content in the piece of volume "V" of the nuclear matter is given by [15]:

$$E_V = \int_V \rho(r) \cdot W[\rho(r), T(r)]dV \tag{1.1}$$

In the simple scenario, the energy density functional *W(ρ,T)* is known as the equation of state (EOS). It contains all the important thermodynamical features of nuclear matter. For example the pressure is given by [16].

$$\begin{aligned} P(V,T) &= -(\frac{\partial E}{\partial V})_{T,N=constant} = \frac{N}{V^2}(\frac{\partial E}{\partial \rho})_{T,N=constant} \\ &= \frac{N^2}{V^2}(\frac{\partial}{\partial \rho}\ \frac{E}{N})_{T,N=constant} = \rho^2(\frac{\partial W}{\partial \rho})_{T,N=constant} \end{aligned} \tag{1.2}$$

The minimum of the energy density functional *W(ρ,T)* occur at T = 0 and at saturation or equilibrium density ρ_0. Fits to nuclear binding energies and density distributions lead to [17, 18, 19]

$$\rho_0 = 0.166 \pm 0.027 fm^{-3} \qquad W(\rho_0, T=0) = -16 \pm 0.5 \text{ MeV/nucleon.}$$

The compressibility of nuclear matter is characterized by the curvature of *W(ρ, T=0)* near ρ_0. Larger the curvature, more is the energy required for the compression. The nuclear (in)compressibility constant K is defined by the change in energy of a nucleus w.r.t the change in the radius.

$$K = R^2 \frac{d^2W}{dR^2} = 9(\frac{P}{\rho} + \rho^2 \frac{\partial^2 W}{\partial \rho^2})_{T,N=constant} \tag{1.3}$$

At $\rho = \rho_0$, the pressure P vanishes as per definition and the compressibility constant (K) is given by:

$$K = 9\rho_0^2 (\frac{\partial^2 W}{\partial \rho^2})_{T,N=constant} \tag{1.4}$$

To get an idea of what might be expected for the incompressibility, one might run a parabola through two known points on the curve of $\frac{E}{A}(\rho)$. Then the resulting incompressibility has a value of $K \approx 290$ MeV. If the actual incompressibility turns out to be below this benchmark value, we may consider EOS to be soft, and stiff in opposite case.
Though, large efforts have been made in pinning down the nuclear matter of symmetric nature as well as various associated phenomena. These phenomena depend on the asymmetry of the matter and are useful to understand the new degree of freedom, i.e. the isospin degree of freedom. We shall now discuss this degree of freedom.

1.3 Symmetry energy

The isospin dependent part of the nuclear equation of state can be expressed in terms of the nuclear symmetry energy. Fig.1.2 shows an illustration of the concept of symmetry energy. The lower line represents the symmetric nuclear matter, whereas the upper line represents the pure neutron matter. The difference between the two lines is the symmetry energy, which express the effect of isospin on nuclear matter energy density.

A binding energy formula expresses the energy E of a nucleus in terms of charge Z and mass A i.e. $E = E(A, Z)$. The Bethe-Weizsacker (BW) mass [20, 21], formula is sum of five terms namely,

$$E = -a_V A + a_S A^{2/3} + \frac{a_C Z(Z-1)}{A^{1/3}} + \frac{a_A (N-Z)^2}{A} + \delta. \tag{1.5}$$

For the details of these terms, reader is referred to the Ref. [21]. The fourth term in the formula, $a_A(N-Z)^2/A$, with $a_A \approx 21$ MeV, is commonly known as symmetry energy

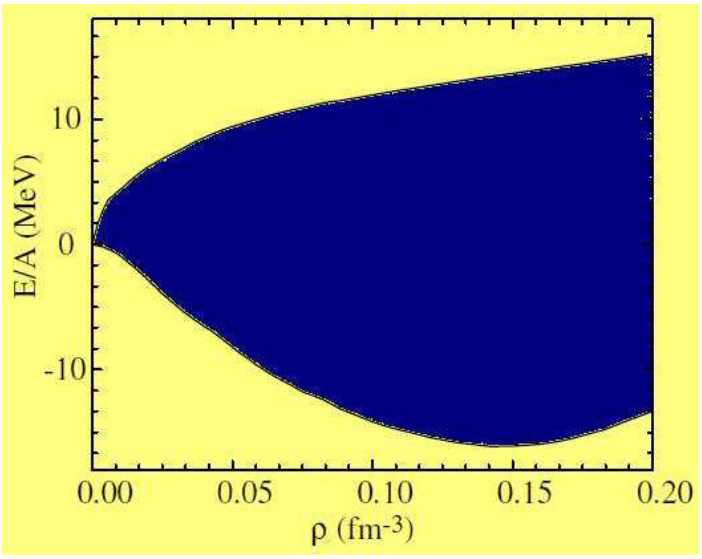

Figure 1.2: *An illustration of the nuclear symmetry energy. The envelopes of the blue area depict the energy per nucleon as a function of density for cold symmetric matter (lower boundary) and cold neutron matter (upper boundary). The figure is taken from the Ref. [22] Copyright @ 1998 World Scientific.*

term.

This symmetry energy as a function of density has been parametrized in different terms as [23]

$$V_1^{Sym} = cF_1(u)\delta\tau_z, \tag{1.6}$$

$$V_2^{Sym} = cF_2(u)\delta\tau_z + \frac{1}{2}cF_2(u)\delta^2, \tag{1.7}$$

$$V_3^{Sym} = cF_3(u)\left[\delta\tau_z - \frac{1}{4}\delta^2\right], \tag{1.8}$$

with $\tau_z = 1$ for neutrons, and -1 for protons.

where $F_1(u) = u$, $F_2(u) = u^2$ and $F_3(u) = u^{1/2}$ and, $u = \frac{\rho}{\rho_0}$; δ is the relative neutron excess $\delta = \frac{\rho_n-\rho_p}{\rho_n+\rho_p} = \frac{\rho_n-\rho_p}{\rho}$; ρ, ρ_0, ρ_n and ρ_p are the total, normal, neutron and proton densities respectively. The strength of c is of the order of 32 MeV to reproduce the 4^{th} term of the Bethe Weizsacker mass formula.

The Isospin-dependent Quantum Molecular Dynamic (IQMD) model [24] developed by C. Hartnack and collaborators reduces the above symmetry potentials into a form:

$$V_{ij}^{Sym} = t_6\frac{1}{\varrho_0}T_3^iT_3^j\delta(r_i{}' - r_j), \tag{1.9}$$

where, T_3^i, T_3^j are their respective T_3 components (i.e. 1/2 for protons and -1/2 for neutrons), t_6 = 100 MeV and $\delta(r_i' - r_j)$ represents the distance between two nucleons. Here again the strength of the symmetry energy is found to be of the order of 32 MeV.

1.4 Isospin dependence of nucleon-nucleon cross-section

In several areas including shielding against ions originating from either space radiations or terrestrial accelerators, cosmic ray propagation studies in galactic medium or radiobiological effects resulting from the work place or clinical exposures, the transportation of energetic ions in bulk matter is of direct interest. The knowledge of beam composition and interaction is necessary for carcinogenesis, terrestrial radiation therapy and radiobiological research to properly evaluate the effects on human & animal tissues. For the proper assessment of radiation exposures, both reliable transport codes and accurate input parameters are needed. One such important input is nucleon-nucleon cross-section [25]. In nuclear and particle physics, the concept of cross-section is used to express the likelihood of interaction between the particles.

The widely used energy dependent nucleon-nucleon cross-section was developed by Cugnon [26]. This cross-section is a fit to the experimental cross-section. Schmidt *et al.* [27] and Cugnon *et al.* [28] reported for the first time the in-medium modifications in connection with the mean free path of a nucleon in hot dense matter. Faessler *et al.* [29] calculated the in-medium nucleon-nucleon cross-section at zero temperature in the framework of Bruekner theory based on Reid potential. They reported the strong modifications of free nucleon-nucleon cross-section with increasing density. Li *et al.* [30] studied the density dependence of in-medium nucleon-nucleon cross-section for symmetric nuclear matter. Alm *et al.* [31] calculated the in-medium nucleon-nucleon cross-section from the thermodynamic T matrix at finite temperatures. They reported that the energy dependent in-medium nucleon-nucleon cross-section at a given density shows a strong temperature dependence. A significant influence of nuclear density on resulting in-medium cross-section was observed in their density, angular and energy dependencies. Cassing *et al.* [32] used G-matrix theory to estimate the in-medium nucleon-nucleon cross-section. The cross-sections used in the IQMD model are deduced from the G-matrix [33, 34, 35, 36]. The actual cross-sections used are basically the parameterized forms taken from the imag-

inary part of G-matrix. The isospin degree of freedom enters via the real part in terms of iso-vector (symmetry) potential and Coulomb potential and into imaginary part as isospin dependent in-medium nucleon-nucleon cross-section and Pauli blocking.

The isospin dependence of nucleon-nucleon cross-section in asymmetric matter is of great interest because it is useful to explore the isospin dependence of nucleon effective interactions. In asymmetric matter, the cross-section becomes isospin dependent beyond the usual and well-known differences between the neutron-proton and the proton-proton/neutron-neutron cases. It depends on the total density and the relative proton and neutron concentrations, which of course also implies that the proton-proton and the neutron-neutron cases will in general be different from each other. This is because of the differences in the transition matrices of the isospin $T = 1$ and $T = 0$ channels, and the fact that both the iso-singlet and iso-triplet channels contribute to neutron-proton (np) scattering, their cross-sections (σ_{np}^{free}) in free space are higher than those for proton-proton (pp) (σ_{pp}^{free}) or neutron-neutron (nn) scattering (σ_{nn}^{free}) where only iso-triplet channels are involved. In general, neutron-proton cross-section is about a factor of 2 to 3 larger that the proton-proton or neutron-neutron cross-section [37].

Usually, the isospin averaged free nucleon-nucleon cross-section is used as an input to the Glauber model. This model is used for extracting information about the structure of radioactive nuclei, such as the radii and the distribution of the constituent neutrons and protons, the total interaction cross-section in the optical limit is determined by a transmission function, which is a convolution of the nucleon-nucleon cross-section and the density distribution of nucleons from both target and projectile in the overlapping region. Knowing the proton density distribution (which can be determined from other means such as electron scattering) and nucleon-nucleon cross-section, the neutron density distribution can then be determined. The role of different nucleon-nucleon cross-section on observables such as transverse momentum and the disappearance of flow has been investigated extensively [38, 39, 40]. Both experimentally [41] and theoretically [42] isospin effects in heavy-ion collisions have been explored to obtain the information about the nucleon-nucleon cross-section. The aim of the present study is to explore which of these observables can act as probe for extracting information about the isospin dependence of nucleon-nucleon cross-section in intermediate energy regime by taking isospin asymmetric

systems. To identify the isospin effects on the various observables of heavy-ion collisions, we compare the cases when the isospin dependence of nucleon-nucleon cross-section is either turned on (σ_{iso}) or off (σ_{noiso}) in chapters 3, 4 and 5.

1.5 Various phenomena at intermediate energies

1.5.1 Multifragmentation

Due to the collision of projectile and target, an excited system is formed. If the excitation energy is comparable with the binding energy of a nucleus, it breaks into many fragments of different masses. This phenomena is known as "multifragmentation". The name "Multi-fragmentation" was introduced by Bondorf in 1976. The word "Multi" means more than two. The produced particles include the free nucleons (FN's) [$A_f = 1$], light mass fragments (LMF's) [$2 \leq A_f \leq 4$], intermediate mass fragments (IMF's) [$5 \leq A_f \leq A_{tot}/6$] as well as the heavy fragments. The energy of the projectile can be between few MeV/nucleon and few GeV/nucleon. During collision, one can experience:

1. Formation of Excited System.
2. Expansion of the system and formation of the fragments.
3. Secondary decay of the fragments.

Several studies revealed that multifragmentation depends on the entrance channel parameters like the mass of the colliding nuclei [43], beam energy [44, 45], colliding geometry [46], mass asymmetry of colliding nuclei [47, 48].

1.5.2 Collective flow

In a non-central collision, the overlap region of two nuclei is almond (or lens) shaped. In this overlap region of two nuclei, the transverse plane has a short axis, which is parallel to the vector connecting the center of two nuclei, and the long axis is perpendicular to it. The particles along the minor axis suffer more pressure gradient compared to the particles along the long axis. This pressure dependent correlation between particles position and momentum is known as *collective flow*. This initial state is characterized by a "spatial anisotropy" in the azimuthal plane. On account of multiple inter-particle collisions, this

initial spatial anisotropy gives rise to the final momentum anisotropy. Moreover, there will be no flow, if either of the two namely initial spatial anisotropy and rescattering is missing. Therefore, the collective flow provides a measure of re-scattering in the non-central collisions. In other words, collective flow provides information on the equation of state of the matter produced in collisions. It also helps to understand the processes such as thermalization, creation of quark gluon plasma (QGP), phase transition etc.
Collective flow is of various types, namely *radial*, *directed*, *elliptical*, *triangular*, *quadrupole flow* and higher order anisotropic flows. In the following subsections the some of the flows will be introduced.

1. **Radial flow**

   Radial flow (or radial expansion) arises in the central collisions. The overlap region of two colliding nuclei is symmetric in central collisions. Therefore, it results in an isotropic distribution of the emitted particles in the transverse plane. Due to this, the pressure gradients may intervene and results in an azimuthally asymmetric collective flow of the final state particles, which is called *radial flow*. This effect is superimposed onto the random thermal motion, thus can be observed by studying the transverse momentum distribution of the various particle species. For details of the radial flow reader is refer to Ref. [49].

2. **Directed flow**

   The emission of different fragments or particles sideward from the hot and dense region formed by the overlap of projectile and target is called directed flow. As, the directed flow depends on the pressure created in the system, therefore it is sensitive to the compressibility of the highly thermalized nuclear matter. It depends on the colliding geometry and is maximum for semi-central collisions and vanishes for central collisions, due to symmetry, and for peripheral collisions due to the lack of a sizable pressure gradient [50]. Because of its sensitivity towards the EOS, the magnitude and shape of the directed flow is of special interest. It was experimentally observed that the mean transverse momentum changes sign from negative to positive as the bombarding energy is increased above 100 MeV/nucleon [51]. In fact, at low incident energies, nuclear interactions are dominated by the attractive part of nuclear mean field deflecting the particles to the negative angles [52].

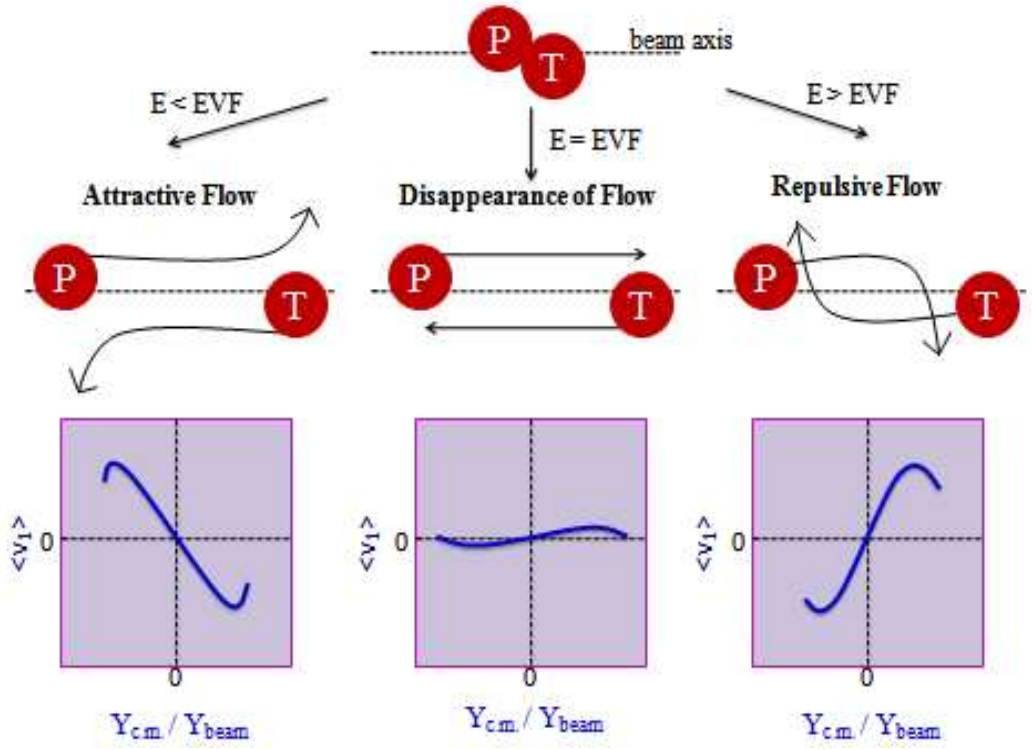

Figure 1.3: Pictorial view of the energy dependence of directed flow.

The nucleon-nucleon collisions and the repulsive part of the mean field dominate the dynamics at energies of few hundred MeV to 1 GeV/nucleon, therefore the particles gets emitted in the positive angles [53]. In fact, at higher incident energies particles are forced to move in the forward hemisphere making in-plane flow positive. Therefore, the attractive interactions could be balanced by the repulsive interactions while going from low to higher incident energies. The energy at which the flow becomes zero is known as the energy of vanishing flow (EVF) or balance energy (E_{bal}) [54]. A schematic illustration is given in Fig.1.3. Due to the decrease in the transition time between two colliding nuclei [55], the directed flow reduces at higher incident energies. At higher energies, it is easier to study the elliptical flow [56].

3. **Elliptical flow**

The elliptical flow refers to the anisotropy of the ϕ distribution at mid-rapidity and its value indicates whether the particle emission is in-plane or out-of-plane.

In-plane emission occurs if azimuthal distribution peaks at 0^0 and 180^0. On the other hand the out-of-plane emission (or squeeze-out) occurs if distribution peak at $\pm 90^0$. The squeeze-out occur in non-central collisions. In fact, the squeeze-out emission depends on the pressure build up during the compression stage compared to the energy density and the passage time for the removal of (projectile-) and (target-)like spectator of the fireball model.

4. **Triangular and Quadrupole flow**

   Recent developments in understanding the initial geometry in heavy-ion collisions points to a "lumpy" initial state. The fluctuations in the initial geometry lead to dipole asymmetry and triangular anisotropy in azimuthal particle production through the collective expansion of the medium [57]. The recent studies in the high energy heavy-ion collisions at Relativistic Heavy Ion Collider (RHIC) have also demonstrated the presence of higher order flows ($\langle v_3 \rangle$ and $\langle v_4 \rangle$) [58]. These anisotropic flows have been shown to achieve large values at intermediate and large transverse momenta in non-central heavy-ion collisions and contain important physics of heavy-ion collisions [59]. Recently, the scaling of these anisotropic flows have also been studied [60] and is found to be originated from nucleonic coalescence.

1.5.3 Nuclear stopping

Nuclear stopping is a measure of the efficiency of converting the incoming longitudinal energy of the projectile and target into transverse degree of freedom, thus slowing down the incoming nucleons. In case of full stopping, there is a complete memory loss of the incoming momentum due to the breakup of the initial correlations among the nucleons of projectile and target. The nuclear stopping has gained a lot of interest because it provides the possibility to study the degree of thermalization or equilibration reached in the matter. The degree of nuclear stopping however may vary drastically with incident energy, mass of colliding nuclei and colliding geometry [61]. The detailed analysis of nuclear stopping is performed in chapter 4.

1.6 Review of experimental attempts

The early natural accelerator available to the mankind was cosmic rays. They are ionized nuclei - about 90% protons, 9 % alpha particles and rest are heavier nuclei - and they are distinguished by their high energies. It is generally accepted that primary cosmic ray nuclei such as H, He, C, N, and O, are accelerated in supernova remnants. After being accelerated, cosmic rays are released in the circumstellar environment, where they diffuse through the turbulent magnetic fields and interact with interstellar matter (ISM). The collisions of these nuclei with interstellar gas are believed to be the mechanism producing the secondary cosmic ray nuclei, such as Li, Be, and B, which are under-abundant in the thermal ISM. The secondary-to-primary boron-to-carbon (B/C) ratio is widely used to study the cosmic-ray propagation processes in the Galaxy. It is usually assumed that secondary nuclei such as Li-Be-B are generated entirely by collisions of heavier cosmic ray nuclei with the interstellar medium (ISM) [62]. It was realized later on that the energetic particles obtained in the cosmic rays consist of elements of different masses with different energies leading to inclusive experiments. The exclusive experiments, however, need fixed incident energy as well as mass. This was possible in accelerators only.

1.6.1 Review of experimental attempts on multifragmentation

One of the phenomena in heavy-ion collisions is nuclear fragmentation, which was discovered almost 77 years ago [63] in the cosmic-rays studies as a puzzling phenomenon by the collisions of relativistic protons with target and resulting in the emission of slow nuclear fragments. The resulting fragments were heavier than those of α-particles, but lighter than those of fission fragments. These particles were named as intermediate mass fragments (IMF's) ($3 \leq Z_f \leq 20$).

Later on in 1950's, Perfilov & Lozhkin [64] observed this phenomena in experiments at the accelerators. However, a dramatic change occur after 1982, when Jakobsson *et al.* observed a multiple emission of IMF's in emulsion irradiated by the carbon beam of 250 MeV/nucleon at Berkeley Bevalac [65]. This result created the interest of the nuclear community toward multifragmentation. Warwick *et al.* [66] found that multifragmentation is a dominant reaction channel at beam energies higher than 35 MeV/nucleon. Another interesting phenomena of multifragmentation (spinodal decomposition) was discussed first

in 1983 by Siemens [67]. Many papers by Purdue University group [68] and Dubna group [69] reported the study of multifragmentation phenomena to get new insights into the problem of nuclear equation of state. Since then, lots of complicated 4π-devices were created to study the each and every aspect in detail.

Recently, Ogul *et al.* [70] studied the N/Z dependence of projectile fragmentation at relativistic energies with ALADiN spectrometer. They reported that global fragmentation observables depend weakly on the N/Z ratio of the projectile while substantial differences are observed for the isotope distribution of light mass fragments ($Z \leq 10$). The FASA multidetector setup has been designed for systematic studies of nuclear multifragmentation caused by relativistic light nuclei (from protons to oxygen nuclei). The old versions of the setup were described in [71]. The new setup is located on the beam of the Nucletron superconducting accelerator at the Joint Institute for Nuclear Research (JINR). The use of a new upgraded FASA module will make it possible to measure correlations of the relative velocities and angles of genetically related fragments and raise the trigger efficiency several fold. The new module is also expected to offer a chance to determine the total time scale of the process [72].

1.7.1.1 ALADiN spectrometer

To study the mass and isospin effects on the breakup of projectile spectators, an experiment has been performed by ALADiN (A Large Acceptance Dipole magNet) collaboration at GSI laboratory. To cover the various combination of masses and N/Z ratios in the entrance channel, four different projectiles $^{197}_{79}Au_{118}$, $^{124}_{57}La_{67}$, $^{124}_{50}Sn_{74}$ *and* $^{107}_{50}Sn_{57}$, with an incident energy of 600 MeV/nucleon have been investigated. The two latter beams have been delivered by the FRagment Spectator (FRS) of the GSI as products of the fragmentation of a primary ^{142}Nd beam at 1.1 GeV/nucleon on ^{9}Be production target. Secondary beams have also been used to extend the range of isotopic compositions.

Fig.1.4, display a cross-sectional view of the setup used. The isotopic composition of the secondary beams was determined and monitored from the magnetic rigidity measured at the FRS, from a velocity measurement along the 80-m flight path between the FRS and the ALADiN setup, and from the charge measurement with the TP-MUSIC IV detector. The dash-dotted lines represent the beam directions before and after the deflection by 7^0 in the field of the ALADiN magnet.

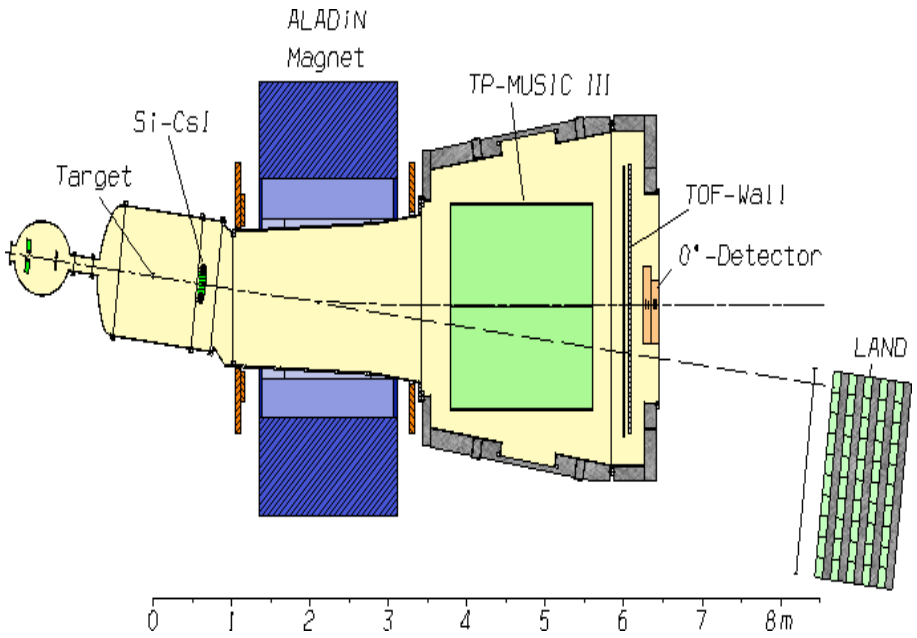

Figure 1.4: *Cross-sectional view of the ALADiN setup. The figure is taken from the Ref. [73].*

The measurement of the charge and the momentum vector of all projectile fragments with $Z \geq 2$ has been performed with high efficiency and high resolution with the TP-MUSIC IV detector [46, 70, 74]. We have compared our theoretical results of mean multiplicity of intermediate mass fragments $< M_{IMF} >$ obtained from this experiment in chapter 3. The details of the experiment has been taken from the Ref. [75].

1.6.2 Review of experimental attempts on collective flow

To describe the collision of nucleons and nuclei, the fluid-dynamics was first used by Belenkij & Landau [76] in 1955. Later on, in 1959 the shock waves that could be formed when a high energy proton or pion exceeding the speed of sound passes through the nucleus were considered by Glassgold, Heckrotte & Watson [77]. They proposed a way to determine the nuclear compressibility coefficient.

In an ideal fluid hydrodynamics, the importance of transverse expansion was first shown by Scheid, Müller & Greiner [17]. It was predicted that in the first 15 fm/c after penetration, with an incident energy of 12.5 MeV/nucleon the longitudinal border of the stopped

and shocked matter was expanding slower than the transverse border. They proposed that the matter is pushed outward perpendicular to the relative motion of two nuclei [17]. Experimentally, the first evidence for the occurrence of sideward flow [78] was obtained by so-called 4π-detectors, the Streamer Chamber [79] & the Plastic-Ball/Wall [80] at Bevalac in Berkeley. Experimentally, out-of-plane emission termed as *squeeze-out* was first observed in 1989 at nearly same time by two competing collaborators. The Diogene collaboration at Saturne Synchrotron in Saclay (France) observed few peaks in the azimuthal distribution of the particles at mid-rapidity in Ne-induced reactions at 800 MeV/nucleon [81]. At BEVELAC in Berkeley, the Plastic Ball/Wall group observed out-of-plane emission in ${}^{197}_{79}Au_{118} + {}^{197}_{79}Au_{118}$ collisions at 400 MeV/nucleon [82]. For the reactions at semi-peripheral collisions, the out-of-plane emission is strongest. The effect is more pronounced at mid-rapidity, but extends quite far towards projectile or target spectators [83]. The transition from in-plane to out-of-plane emission was first observed for the reaction of ${}^{64}_{30}Zn_{34} + {}^{58}_{28}Ni_{30}$ at GANIL facility by the NAUTILUS collaboration in 1994 [84]. The transition energy increases with impact parameter.

Other collaborations: FOPI, ALADiN at GSI, and INDRA at GANIL emphasis on the transition of elliptical flow for different kind of fragments from in-plane to out-of-plane in intermediate energy heavy-ion collisions [85, 86]. On the other hand INDRA & ALADiN collaborations presented new results of flow analysis for the set of reactions ${}^{124,129}_{54}Xe_{70,75}$ & ${}^{112,124}_{50}Sn_{62,74}$ [87]. We have compared our theoretical predictions of elliptical flow with the experimental findings of GSI in chapter 5. The data has been obtained by the INDRA and ALADiN collaborations using the 4π INDRA detector, stable Xe beams from the SIS synchrotron at GSI & isotopically enriched Sn targets.

1.6.3 Review of experimental attempts on nuclear stopping

Nuclear stopping is a measure of the efficiency of converting the incoming longitudinal energy of projectile and target into transverse degree of freedom, thus, slowing down the incoming nucleons. Experimentally, Lehaut *et al.* [88] studied the global nuclear stopping at intermediate energies by analyzing the kinematically complete events recorded with the help of 4π multi-detector for symmetric and asymmetric reactions such as ${}^{197}_{79}Au_{118} + {}^{197}_{79}Au_{118}$, ${}^{129}_{54}Xe_{75} + {}^{118}_{50}Sn_{68}$ and ${}^{58}_{28}Ni_{30} + {}^{58}_{28}Ni_{30}$ etc. Nuclear stopping was reported to be

highly sensitive towards the isospin dependence of the in-medium nucleon-nucleon cross-section. FOPI collaboration [89] also studied the nuclear stopping for the reactions of ${}^{40}_{20}Ca_{20} + {}^{40}_{20}Ca_{20}$, ${}^{58}_{28}Ni_{30} + {}^{58}_{28}Ni_{30}$, ${}^{96}_{44}Ru_{52} + {}^{96}_{44}Ru_{52}$, ${}^{129}_{54}Xe_{75} + CsI$ and ${}^{197}_{79}Au_{118} + {}^{197}_{79}Au_{118}$ at an incident energy between 90 and 1930 MeV/nucleon. They reported that, degree of stopping is found to be highly correlated to the amount of sideward‘flow.

1.7 Various radioactive ion beam facilities

The isospin degree of freedom plays a significant role in the various phenomena in the nuclear physics and therefore, attracted the attention of nuclear physics community. This has become possible only because of the several advances in the experiments with radioactive beams. Several phenomena such as understanding of the nuclear force at the nucleon-nucleon level and its link to collective behavior of the nucleus, the effect of large N/Z ratio on the magic numbers etc. have been discovered. In order to have better understanding of these phenomena and to build a theoretical model with high degree of predictive power, a substantial data of nuclear structure, decay and reaction cross-sections is required from a systematic study of as many nuclei as possible. Within the limits of stability, thousands of nuclei have been identified experimentally. But, only few hundred are stable. Therefore, we have very limited data on which our theoretical models are based. Although, the heavy-ion beams have viaduct the gap, yet one needs radioactive ion beams to produce large number of nuclei to have enough systematics. Therefore, the invention of new RIBs have opened new doors in the nuclear physics to explore the features of nuclear matter at extreme isospin asymmetry. Review of few experimental radioactive ion beam facilities is discussed below in brief.

There are some other facilities like the Radioactive Isotopes Beam Facilities (RIBF) at some major laboratories like RIKEN (2007-12) in Japan [90], Heavy Ion Research Facility of Lanzhou (HIRFL) at Lanzhou in China [91], Legnaro National Lab (LNL) at Padua in Italy [92], TRI-University Meson Facility (TRIUMF) in Canada, National Superconducting Cyclotron Laboratory (NSCL) at Michigan State University in USA, Holifield Radioactive Ion Beam Facility (HRIBF) at Oak Ridge National Laboratory (ORNL) [93] and last but not the least Facility for Antiproton and Ion research (FAIR) at GSI [94] etc., which represent the major efforts, the world over, and produce exotic beams. This

leads to the discovery of new isotopes, and to a deeper understanding of the nuclear force at the nucleon-nucleon level and its link to collective behavior of the nucleus, and the effect of large neutron/proton (N/Z) ratio on the magic numbers [95].

At RIKEN, using the in-flight fast Radioactive Isotope Beam (RIB), 45 new isotopes were produced (using 345 MeV/nucleon U beam) including $^{128}_{46}Pd_{82}$, $^{78}_{28}Ni_{50}$, and $^{138}_{50}Sn_{88}$. Deformed halo nucleus $^{31}_{10}Ne_{21}$ was discovered. This is an excellent achievement in just five years. Moreover, collective enhancement towards the drip line was noted in 2009 and deformed magic number at N = 64 in Zr was identified in 2011. At PRISMA (2009-11) spectrometer with AGATA Gamma-ray Detector Array at Legnaro, neutron-rich nuclei Si-Os were studied. At Argonne, Rare Isotope Beam (RIB) by fission, Californium Rare Ion Breeder Upgrade (CARIBU) provides neutron rich, re-accelerated beams at energies above the Coulomb barrier. It is better compared to standard Isotope Separator On-Line (ISOL) type facility. The gas cather, transforms the fission recoils into a beam with good optical properties. At Isotope Separator On Line-Detector (ISOLDE), CERN, using 1.4 GeV protons, 700 different nuclei of 76 elements were produced. The β-delayed fission and island of inversion at N = 32 were studied.

Stability of the shell structure and the effect of neutron/proton excess on magic shells at Z, N = 20, 28, 40, 50 and 82 are being studied for exotic nuclei at both ends of the nuclear chart. At ORNL, isotopes of $^{242-244}_{94}Pu_{148-150}$, $^{241-243}_{95}Am_{146-148}$, $^{244}_{96}Cm_{148}$, $^{248}_{97}Bk_{151}$ and $^{249-251}_{98}Cf_{151-153}$ were produced using actinide targets with $^{48}_{20}Ca_{28}$ beam [95].

Asia's second advanced facility for conducting experiment of Unstable and Rare-Isotopes Beams will come up at the Rajarhat campus of Kolkata. Japan is the only other Asian country to have this facility. The USA, France and Canada are the other three countries to have similar research facilities. The new facility called Advanced National facility for Unstable & Rare-Isotope Beams (ANURIB), will give us the complete information on nuclear forces and nuclear equation of state which controls the supernova explosions where all elements heavier than Iron are produced. In addition to this, it is quite possible that it may also help in the discovery of many isotopes, which could have great applications in the field of medicine and material science [96].

1.8 Review of various theoretical models

In order to have the first hand information of different theoretical models and algorithms suitable at intermediate (and relativistic) energies, we have to keep in the mind the dynamics involved at these incident energies. The key point to remember is that the heavy-ion collisions involve very complicated non-equilibrium physics, therefore, its numerical modeling is not straight forward. In the last few decades, major efforts were made to develop microscopic models which can describe the dynamics of heavy-ion collisions from the start where the nuclei are well separated to the end where matter is cold and fragmented. The nuclear reactions at intermediate energies led to several rare phenomena like collective flow, multifragmentation, nuclear stopping as well as sub-threshold particle production. The reaction dynamics depends on the incident energy as well as on the impact parameter of a reaction. At low incident energy, reaction dynamics is governed by the attractive mean field or by the mutual two and three body interactions. Therefore, due to the lack of available free space for scattering at low incident energy, about 98% of the binary collisions are blocked. On the other hand, the repulsive interactions decide the fate of a reaction at higher incident energies. The availability of the large phase space at relativistic energies practically reduce Pauli-blocking to a significant level and hence dynamics is governed by the repulsive nucleon-nucleon scattering alone. On the contrary, both the cascade and mean field picture emerges at intermediate energies. Beside this, the isospin picture also comes into existence in this energy range. Therefore, one needs proper transport theories to simulate a heavy-ion reaction. No single transport model is capable of describing the reaction dynamics throughout the incident energy range. Various theoretical models can be divided into two categories namely statistical and dynamical models.

Statistical models include, *Statistical Multifragmentation model (SMM)* [97] and the *Berlin Multifragmentation model (BMM)* [98], which is based on the assumption that nuclear fragments are produced simultaneously in the explosive breakup of a thermalized nuclear system formed at intermediate stage of a highly dissipative nuclear reaction. It also incorporates the specific nuclear effects such as finite size, nuclear and Coulomb interactions, de-excitation of primary fragments etc. Another statistical model includes *Participant-Spectator model* [99] for high energy fragmentation reactions with two neutron halo nuclei. The model originated in the sudden approximation where one of the halo constituents, the

participant were, instantly removed in the fragmentation reaction while the other two, the spectators, were left undisturbed. This model incorporates both nuclear and Coulomb interactions between the projectile and target. Therefore, is applicable for all targets from light to heavy ones. Additional static models include *Lattice Gas Approach* [100] and *Expanding Emitting Source (EES)* model [101]. These approaches have the virtue of providing relatively simple schematic algorithms suitable for the exploration of critical phenomena in finite systems. The limitation of the statistical models are:

1. The situation at the start of reaction is based on some assumption for the degree of thermalization [102] and

2. The statistical models give a better description only of the later/final stage of the reaction.

The dynamical approach such as *Time dependent Hartree Fock (TDHF)* approximation was pioneered by Bonche, Koonin, and Negele [103] for the microscopic description of the dynamics of nuclear system. Since then, many theoretical investigations were initiated [104]. In the *TDHF* approximation, the fermions are assumed to interact only through the mean field & collisions between particles as the residual interactions are neglected. Numerical solution [105] of the *TDHF* equation provides interesting insight into the dynamics of interacting fermion systems. Since, the collision between the particles are neglected, therefore it is not suitable to study the reaction dynamics at intermediate energy, where one treats the nucleon-nucleon scattering and mean field on equal footing. Some attempts were made in the literature to extend the *TDHF* theory to take care of the residual nucleon-nucleon interactions, which are responsible for the two-body collisions. This was dubbed as *Extended Time dependent Hartree-Fock (ETDHF)* theory [106]. However, its numerical implementation prohibited its use for large scale investigations of heavy-ion collisions.

In addition to this, several advances have been made recently in the theoretical approaches. F. J. Hambsch, member of International Atomic Energy Agency (IAEA) reported the Monte Carlo Code *FREYA* for prompt n-emission, event by event fission model, developed for complete kinematic information on fragments, neutrons etc. G. F. Bertsch, described the fission dynamics, potential energy surface, on how the nucleus travels, descends from

the barrier, and of the conflict between statistical and inertial dynamics and tunneling under the barriers. In addition to this, he also disscussed the channel statistics at the barriers, and pairing, using time dependent mean field theory (MFT) based on Hartree Fock Bogoliubov wave functions for connecting hamiltonian to dynamics. A. S. Umar gave microscopic theory for channel coupling to compute fusion barriers from *Density Constrained Time Dependent Hartree Fock Theory (DC-TDHF)*. It yields a dynamical path in relation to the multidimension [107].

In the first attempt, semi-classical version of *ETDHF* theory i.e. *Vlasov equation* [108] was coupled with nucleon-nucleon collisions and thus, a new realization, named as *Boltzmann-Uehling-Uhlenback equation (BUU)* was reported. In classical statistical dynamics, one can describe the transport processes which are special cases of non-equilibrium processes by the Boltzmann equation. In the 1930's, this equation was modified by Nordheim, Uehling and Uhlenbeck to incorporate also quantum mechanical effects of fermionic systems. The resulting equation is the so-called *Boltzmann-Uehling- Uhlenbeck equation (BUU equation)* [109]. In the beginning 1980's *BUU* models started to replace the simpler Cascade models in heavy-ion collision simulations [108]. In the late 80's, the theory group at the Justus Liebig University (JLU) Giessen started to use the *BUU* model to describe heavy-ion collisions and later on also photon induced processes. The *BUU* model use test particle method in which the evolution of one-body phase space distribution is studied. The main drawback of such models is that the correlations and fluctuations are not preserved and thus, they are suitable in the study of one-body observables only, like collective flow, stopping and particle production. However, Bonasera *et. al.* [110], solved the collision integral using the concept of mean free path. In this method, N parallel events are performed and the average physical values of various quantities are calculated over large number of events. Since N parallel runs do not communicate with each other, event by event correlations are preserved.

Then a very interesting picture is given by *Classical Molecular Dynamics (CMD)* [111]. This approach is capable of predicting the fragments production. It also incorporates complete classical N-body dynamics which is necessary to describe the formation of the fragments. In this approach, the classical nucleons interact via classical potentials and no binary collision takes place. However, both potentials as well as a Pauli corrected

stöchastic scattering are necessary to describe heavy-ion collisions properly. This approach was later extended by Aichelin and Stöcker to incorporate the quantum features like the Pauli principle, stöchastic scattering and particle production and was dubbed as *Quantum Molecular Dynamics (QMD)* model [112].

One needs reliable theoretical tools, in order to extract information of the EOS of neutron rich matter from heavy-ion reactions induced by neutron rich beams. Transport models that include explicitly the isospin degree of freedom and thus the isospin-dependent physical quantities such as the iso-vector (symmetry) potential and isospin-dependent in-medium nucleon-nucleon cross-sections and Pauli-blocking can be used to extract such information. As discussed above, the semi-classical models include mainly the two types: the *BUU* and the *QMD* model. Several rather comprehensive isospin-dependent, but mostly semi-classical transport model such as *IBUU* [23], *SMF* [113] and *IQMD* [24] have been successfully developed in recent years to describe nuclear reactions induced by neutron-rich nuclei at intermediate energies due to the development of radioactive ion beam physics.

Several isospin dependent phenomena in heavy-ion collisions at intermediate energies [23] has been successfully explained by the *Isospin-dependent Boltzmann-Uehling-Uhlenbeck (IBUU)* transport model. In this model, the isospin dependence was included in the dynamics through nucleon-nucleon collisions by using isospin-dependent cross-sections and Pauli blocking factors, the symmetry potential $V_{sym}(\rho, \delta)$, and the Coulomb potential. The initial neutron and proton density distributions of projectile and target are obtained by using the Skyrme-Hartree-Fock Theory. The isospin dependence resides in the fact that the cross-section of neutron-proton collision is about three times that of neutron-neutron or proton-proton collisions. This model was used to calculate the ratio of yield of neutron and protons in pre-equilibrium emission [114]. The *BUU* equation provides an accurate description of the time dependence of the one body distribution function. The nucleons are represented as an ensemble of particles which are initially uniformly distributed in a sphere representing the nucleus. The *BUU* equation can be solved numerically using the test particle method. The density fluctuations that lead to the fragment production are suppressed in the *BUU* equation, so the calculation of fragment yield directly via *BUU* model is not feasible. Therefore, alternate model such as, *Stochastic Mean Field (SMF)*

model [113] and *Isospin Quantum Molecular Dynamics (IQMD)* model [24] has been developed to address the density fluctuations.

The *SMF*, like *IBUU*, describes the time evolution of the collision using self-consistent mean field. It generates an ensemble of single particle density matrices by incorporating density fluctuations (quantal or thermal) in the initial state. Each matrix element is a Gaussian random number. In this approach, single particle wave function are determined by the self-consistent mean-field of each event. In fact, it is a one body dissipation and fluctuations mechanism consistent with quantal fluctuation-dissipation theorem. The application of the *SMF* model to the unstable situations relies on the knowledge of the most important unstable modes, which may be difficult to identify in case where the modes are not known a prior.

The dynamics in HIC's at intermediate energies is mainly governed by three component, namely the mean field, two-body collisions and Pauli blocking. Therefore, for an isospin-dependent reaction dynamics model, it is essential that all three components should reasonably include isospin degree of freedom. Since there exists a large difference between neutron and proton β stability line, therefore it is essential that in initialization of projectile and target nuclei, the samples of neutrons and protons in phase space should be treated separately. In fact, one should sample a stable initialized nucleus (particularly for neutron rich nucleus) with neutron-skin structure and therefore one can directly explore the nuclear structure effects through a microscopic transport model. Based on the above mentioned ideas, the *QMD* model [112] has been improved. The isospin degree of freedom enters into the calculations via symmetry potential and cross-sections [115, 116]. The model incorporate the N-body correlations, explains the nuclear equation of state and includes the many quantum features like Pauli blocking, Stöchastic scattering, particle production, isospin dependent potential and cross-section.

Once phase space of a reaction is generated, one can analyze various phenomena based on single particle dynamics or on cluster dynamics. To study the phenomena based on clusters, one need to identify fragments. The phase space generated can be subjected to various cluster recognization methods to identify fragments.

1.9 Organization of thesis

The thesis is organized as follows:

- In **chapter 2**, we will give the brief survey of various theoretical models used in literature to study heavy-ion collisions. We shall present the detailed discussion of *Isospin-dependent Quantum Molecular Dynamics (IQMD) model*.

- In **chapter 3**, we shall study the influence of isospin dependence of nucleon-nucleon cross-section on the multiplicity of FN's and fragments for isobaric nuclei. We shall compare the theoretical calculations for the mean multiplicity of IMF's with the experimental findings of ALADiN collaboration [117].

- In **chapter 4**, we shall study the N/Z dependence of participant-spectator matter, anisotropic ratio $\langle R_a \rangle$, relative momentum $\langle K_R \rangle$. In addition to this, the isospin dependence of nucleon-nucleon cross-section on nuclear stopping as well as on the multiplicity of FN's and LMF's for isobaric nuclei at an incident energy between E = 100 and 300 MeV/nucleon spanning the whole colliding geometry will also be discussed. Moreover, the theoretical results on the anisotropy ratio $\langle R \rangle$ shall compared with the experimental findings of INDRA collaboration [75].

- In **chapter 5**, we shall discuss different aspects of directed flow (such as excitation function, effect of colliding geometry) throughout the mass range. We shall also present the descriptive analysis to study the effect of nucleonic cross-section (isospin dependent and isospin-independent) on the neutron-proton directed flow ($\langle v_1 \rangle$). Investigation to study the influence of fragment mass on the balance energy at different colliding geometries as well as the incident energy and the impact parameter dependence of reduced flow ($\frac{\partial v_1}{\partial y}|_{midr}$) throughout the mass range shall also be made. Not only the directed flow, we shall also discuss the phase space distribution of the nucleons coming from participant matter that are contributing in elliptical flow ($\langle v_2 \rangle$). Study will also include the effect of isospin content of colliding nuclei and isospin dependence of nucleon-nucleon cross-section on $\frac{dN}{d(\langle Cos\phi \rangle)}$ and on different aspects of elliptical ($\langle v_2 \rangle$), triangular ($\langle v_3 \rangle$) and quadrupole flow ($\langle v_4 \rangle$). We shall explore the effect of isospin content (N/Z) and colliding geometry on the transition

energy throughout the mass range between 72 and 394 for isotopes, isobars as well as isotones. We shall compare theoretical results with the experimental findings of INDRA(GSI+GANIL) [88], MSU [85] and FOPI [40, 118] collaborations.

- In **chapter 6**, we shall discuss the effect of isospin degree of freedom on nuclear stopping throughout the mass range between 50 and 350 for two sets of isotopic systems with N/Z = 1.16 and 1.33 as well as isobaric systems with N/Z = 1.0 and 1.4. Analysis will be carried out at an incident energies below, at, and above the energy of vanishing flow (EVF).

- Our results are summarized in **chapter 7**, which also contains an outlook of the work.

Chapter 2

Methodology

2.1 Introduction

As stated in chapter 1, among variety of theoretical models, models based on molecular dynamic picture can give better description of a reaction. Since these are dynamical in nature and are capable to identify the fragments. Therefore, we shall discuss *Quantum Molecular Dynamics (QMD) Model*. Since our main focus is to analyze the isospin physics, we shall use *Isospin dependent Quantum Molecular Dynamics (IQMD) model*. In the following we shall discuss the various realizations of QMD model and its isospin version $IQMD$ model.

2.2 Quantum Molecular Dynamics (QMD) Model

The basic idea of QMD [112] approach can be best described by comparing it with the *Classical molecular dynamics (CMD)* approach [111]. The CMD is based on the assumption that nucleons behave like classical particles interacting by forces and is a N-body theory. The information about the system is obtained by solving the N-body Liouville equation. The solution is time reversible if the potentials are conservative. The time reversible means if one replace $t = \tau$ and all momenta $\mathbf{p}$ by $-\mathbf{p}$, then the system goes back to its initial configuration at $t = 2\tau$. The fluctuations and correlations are preserved because no information is lost in the time evolution. This property differentiate it from the one-body theories like the Boltzmann equation [109], which produces entropy in the course of the time evolution by discarding all correlations. In fact, in this approach, the Pauli principle for nucleons is not taken into account and the scattering angle is uniquely determined by the impact parameters.

However, in *Quantum Molecular Dynamics approach (QMD)*, both the stochastic scattering as well as the time evolution of the particles along classical orbits are incorporated. The stochastic scattering [119] is described by the higher order terms in $\hbar$. After scattering, if nucleons tends to occupy the regions of phase space already occupied or partially occupied by the other nucleons those collisions are suppressed due to Pauli principle. In these partially occupied phase space regions, the scattering angles as well as the blocking of collisions are treated statistically. The time reversibility of the classical equations is destroyed by this procedure.
However in QMD approach it is possible to describe the time evolution of all correlations because one can solve N-body equation without reducing to one-body level. The simulation models like BUU [108], QMD [112] etc. has three distinct steps.

1. *Initialization*, in which one has to generate the nuclei. It is important to check that our initialization does not destabilize the cold nuclei.

2. *Propagation*, in which the nuclei propagate under the influence of surrounding mean field.

3. *Nucleon-nucleon binary collisions* in which the nucleons are bound to collide if they come too close to each other. The role of Pauli blocking is also checked.

We shall discuss the principle structure of QMD model and then will discuss in detail the $IQMD$ model.

2.2.1 Principal structure of QMD model

As already mentioned, the QMD model [112] has three steps:

1. *Initialization* of the target and projectile.

2. *Propagation* of the nucleons, resonances and newly produced particles due to their mutual potential interactions. and

3. The *nucleon-nucleon binary collisions* which further depends on the energy dependent nucleon-nucleon cross-section for the various channels along with the Pauli blocking.

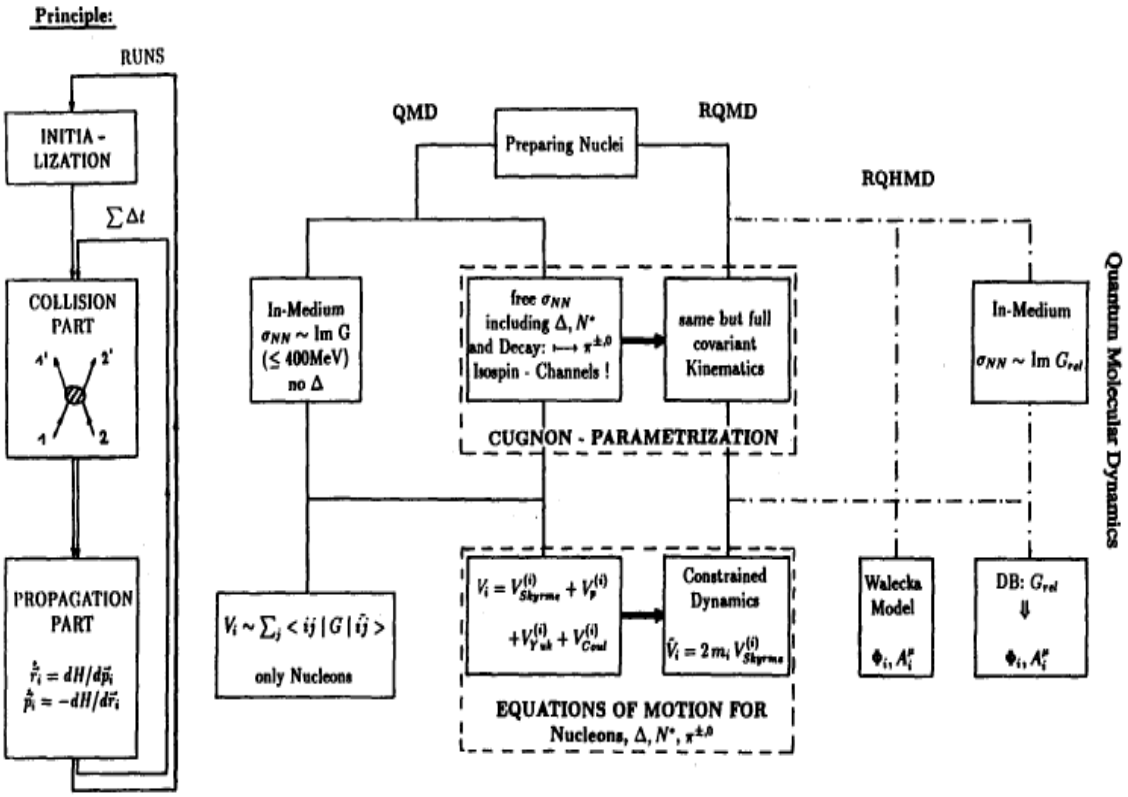

Figure 2.1: *Schematic view of simulation package of QMD/RQMD. Lines connecting the blocks asign the different possibilities to use the package. Figure is taken from Ref.[120].*

Fig.2.1, describes the basic picture of QMD model.

The above principal structure is common for all QMD realizations. However, difference lies in the details and initialization of the projectile and target nuclei. Here, we will discuss some realization of the QMD model.

1. **PQMD**

   In order to give a reasonable overall reproduction of gross the properties of uniform nuclear matter and finite nuclei, Peilert *et al.* [121] employed a quassi-classical molecular dynamics model which incorporates a Pauli-potential. They employed Gaussian Pauli potential introduced by Dorso *et al.* [122]. The thermostatic properties of the system are obtained by averaging over several hundred statistically distributed manifestations of the system, sampled by means of Metropolis procedure [123] on the basis of appropriate canonical weight. Screened Coulomb interactions are used to describe both the finite and infinite nuclear matter. Two parameters of Yukawa potentials have been adjusted to obtain reasonable simulation of finite nuclei. In fact, Pauli potential is a strong repulsive potential that prevents two identical fermions being too close in space. Due to the strong momentum dependent nature of the Pauli potential, it has a different physical input compared to other discussed flavors. This model has also been utilized for the analysis of the FOPI data at low incident energies [124].

2. **G-matrix QMD**

   One has to assume a certain form of nucleon-nucleon cross-section in a medium in order to describe hard nucleon-nucleon collisions. Then vary these parameters to see their influence on the observables in heavy-ion collisions. One hopes to determine the equation of state (EOS) with experimental values. This strategy has the limited success due to the following reasons:

   (a) The results depend not only on the equation of state but also on the mean field potential in the whole density, momentum plane as well as on the nucleon-nucleon cross-section in the medium. Moreover, the potential is proportional to the gradient of the real part of T (or Brueckner G) matrix, whereas the cross-section is proportional to $|T|^2$ ($|G|^2$) [112].

(b) The simple phenomenological form of the mean-field potential such as Skyrme type should not be adequate.

In fact, the nuclear equation of state and the optical potential alone are not sufficient to obtain the nuclear potential in the whole density and momentum plane unambiguously. These problems can be avoided if one starts from the basic nucleon-nucleon interaction and calculates the equation of state and the nucleon-nucleon cross-section in a medium microscopically in a consistent way.

3. **TQMD**

Another realization of QMD model is done by Puri and Faessler and co-workers by incorporating temperature-dependent mean field potentials of nucleons and is dubbed as *Temperature dependent Quantum Molecular Dynamics (TQMD) model* [36]. In actual QMD simulations, one first calculate the so called local temperature at the position of particle i in each time step, then use this temperature to get the temperature dependent potential which finally used in the equation of motion. Clearly, the temperature has to be defined at thermal equilibrium but in an intermediate energy heavy-ion reactions no thermal equilibrium is reached. Puri *et al.* [36] reported a method to extract a reasonable defined temperature T, which is an extension of the usual definition in thermal equilibrium using a local density approximation obtained from the simulation of the heavy-ion collisions. These temperature dependent potentials are obtained by solving the Bethe-Goldstone equation for a realistic force in nuclear matter at finite temperature. The Skyrme type parametrization is employed for density and temperature dependent potentials. The effects of these temperature dependent potentials are found to be stronger in heavier nuclei [36].

4. **MQMD**

Another realization of the primary QMD code written by Frankfurt theoretical physics group of Germany was reconstructed by Jianye and Guang [125] and is dubbed as *Modified Quantum Molecular Dynamics (MQMD).* In this realization, they coupled QMD to the *Reconstructed Aggregation Model (RAM)* [126] which gives the reasonable description of cluster formation. The reason for using RAM is that, at the point of instability, the nucleons aggregate into compact clusters and

don't stay as unphysical filamented objects which is the case if one restrict to quantum molecular dynamics only. This modified version can describe the dynamical process of the colliding systems well, especially multifragmentation because of the explicit treatment of many-body correlations.

5. **DQMD**

   In order to study different observables in heavy-ion collisions at higher incident energies Waged *et al.* [127] developed a new realization in the framework of Glauber plus QMD model dubbed as $DQMD$ model. This model suggests that, the reaction process could be divided into two parts namely the *direct reaction* and the *dynamical formation of highly-excited fragments*. First, one is treated using the Classical Glauber approach [128] and the second one (dynamical aspect of collisions) is followed by utilizing the QMD model. For energies well above several GeV/nucleon, these two processes are assumed to be well separated in their time scale.

   The study of $DQMD$ showed that this is a promising direction to generalize the QMD simulations to high energy. But care should be taken at higher energies because in primary nucleon-nucleon interactions a large number of pions should be produced and their evolution inside the system may influence the distribution of excitation energy in its interior.

6. **BQMD**

   In order to study the low energy fragmentation data, the original QMD was rewritten by Bohnet *et al.* [129]. It was dubbed as $BQMD$, because it was designed for describing the proper binding of a nucleus in order to describe fragmentation process [130]. In addition to this, an improvement on the stability against artificial particle evaporation was also achieved in $BQMD$. In contrast to the original QMD model, in which, a sphere is used for the distribution of the centroid of Gaussian, in $BQMD$, the nucleons are distributed within a sphere with a Wood-Saxon-type density Profile. Like in the QMD model, in order to keep all the nucleons bound, maximum Fermi-momentum is limited by the local binding energy of the nucleon. The normal nuclear matter density and the Gaussian width of nucleons are chosen to be $\rho_0 = 0.15fm^{-3}$ and $L = 4.33fm^2$, respectively. The coupling constant t, of the Skyrme-type two body interaction is also modified in order to keep the nuclear

equation of state and binding energy independent of the Yukawa interactions and also to keep the proper binding energy. Both the range of the Yukawa interactions as well as the binary nucleon-nucleon cross-sections are same as used in original QMD model. In addition to this, like original QMD model, it also uses nucleons and deltas only and all the nucleons interact with the same average cross-section without distinction in isospin.

7. **HQMD**

   To study the influence of different modules, Huber and Aichelin [131] incorporated higher resonances (such as $N^*(1440)$), free pions and the proper isospin coupling in addition to the nucleons and deltas. It is an upgraded version of the QMD model that also uses certain optional features of $BQMD$ model. This upgraded version of QMD model was dedicated to the question concerning the meson production. It is quoted as $HQMD$ because it contains higher resonances. It has been used extensively to study kaons production.

8. **CoMD**

   By incorporating Pauli potential, another realization of QMD has been given by Papa *et al.* [132] dubbed as *Constrained Molecular Dynamics (CoMD)*. In this approach , a stochastic process is added to the usual QMD in order to prevent the violation of Pauli principle. Thus, it constrained the phase space to full fill the Pauli principle at each time step. In particular, this model is used:

   (a) To describe the fermionic nature of N-body system with the more general condition that the occupation probability should be less than one.

   (b) To realize a model for which the computational time is short enough to allow the study of the heaviest systems.

   This model was proved to be quite successful in explaining the fragmentation data at 35 MeV/nucleon [132]. A drawback of the Pauli-potential is, however, that the kinetic momenta of the nucleons are not anymore equivalent to their canonic momenta, i.e. the nucleons carry the correct Fermi-momentum, but their velocity is zero. Furthermore, the Pauli-potential leads to a wrong specific heat and changes the dynamics of fragment formation. A big advantage of the Pauli-potential is that

the initialized nuclei remain absolutely stable whereas in the conventional initialization and propagation without the Pauli-Potential the nuclei start evaporating single nucleons after approximately 20-30 fm/c.

9. **RQMD**

   To extend the QMD model upto relativistic energies (AGS and CERN/SPS domain) a new approach named as the *Relativistic Quantum Molecular Dynamics (RQMD)* has been developed by Sorge and Greiner and later on new realization was put forward by Faessler and co-workers [133]. Compared to the standard QMD model, various improvements done in this model are:

   (a) Covariant dynamics.

   (b) An improved and extended collision term containing heavy baryon-resonances, strange particles and string-excitation for high energy hadron-hadron interactions.

   The time evolution of many-body system has been described within this model using classical co-variant equations of motion. The system propagates in a 8N-dimensional phase space with 6N degrees of freedom representing the classical configuration and momentum space. The eigentime and energy of each particle is contained in remaining 2N degrees of freedom. The necessity of employing an 8N-dimensional phase space is based on the *no-interaction theorem* (NIT) given by Curri *et al.* [134]. Also the $RQMD$ model calculations are found to agree with the QMD calculations in non-relativistic limits, even for highly sensitive observables like directed in-plane flow.

10. **UrQMD**

    For the general understanding of the dynamics of heavy-ion collisions over vast energy range, i.e. ultra relativistic version of QMD model was developed. As bombarding energy increases, the velocity of particles become comparable to the velocity of light, therefore relativistic effects become very important. The Frankfurt group reported a new version named *Ultra-relativistic Quantum Molecular Dynamics (UrQMD) model* [135]. This microscopic transport approach based on the co-variant propagation of all hadrons on classical trajectories in combination with stochastic

binary scattering, color string formation and resonance decay. It can be applied to study hadron-hadron, hadron-nucleus and heavy-ion reactions from E_{lab} = 100 MeV/nucleon to $\sqrt{S_{NN}}$ = 200 GeV. It simulates multiple interactions of in-going and newly produced particles, the excitation and fragmentation of color strings and the formation as well as the decay of hadronic resonances. The treatment of sub-hadronic degrees of freedom is of major importance towards higher energies [135]. The $UrQMD$ approach includes:

(a) The cross-section of various meson-meson, meson-baryon, and baryon-baryon interactions. It takes into account $\sim$ 50 baryons and $\sim$ 45 mesons.

(b) The string fragmentation and formation time of particles.

(c) The potential interactions between the particles, especially, Yukawa, Coulomb and Pauli potentials [135].

In order to provide an improved description of later, purely hadronic stage of the reaction, so-called microscopic plus macroscopic (micro+macro) hybrid approaches have also been reported during past decades. The detailed investigation of these can be found in Ref. [136]. For describing the soft physics at RHIC, such hybrid micro/macro transport calculations are to date the most successful approaches. The termination of the calculations at a fixed freeze-out temperature can be overcome by combining *Relativistic Fluid Dynamics (RFD)* calculation with a microscopic hadronic model. This kind of hybrid approach dubbed as hydro+micro was pioneered in Ref.[137] and then taken by some other groups also [138]. The advantage of adding RFD part of the calculation is that, it directly incorporates an equation of state as input.

The main drawback of its addition is that, it requires thermalized initial conditions, and one is not able to do an *ab initio* calculations.

11. **FMD**

In the initialization of QMD type models, the initialized nuclei are not really in their ground state with respect to the Hamiltonian used for their propagation. The parameters of the Hamiltonian are adjusted in accordance with the equation of state of infinite nuclear matter and to the properties of finite nuclei such as binding en-

ergy and their root mean square radius. However, nucleus then generated, would collapse to a single point in momentum space, if the energy of the nucleons within the nucleus is minimized according to the Hamiltonian in a self consistent fashion. The appropriate solution to this problem is the inclusion of fermionic properties of nucleons via the antisymmetrization of the wave function of the nucleus. This approach was developed by Feldmeier [139] and is dubbed as *Fermionic Molecular Dynamics (FMD)*. This model combines from the very beginning Fermi-Dirac statistics with a semi-quantal trajectory picture. It turns into classical molecular dynamics in the limit where the system becomes dilute in phase space i.e. low density and for high temperature. This model does not describe all wave mechanical interference effects thus is not called as fully quantum mechanical. However, the Fermi-Dirac statistics is included on the many-body level. The basic idea of this model is to find a parametrization which contain essential degrees-of-freedom of the system. It is a true quantum mechanical treatment that represents the many-body state as an antisymmetrized Slater determinant, built from single particle wave packets of Gaussian form. The spin-isospin degree of freedom of the nucleons are included and they are assumed to move in a mean field. The Pauli principle is also incorporated correctly because of the Slater determinant.

12. **AMD**

    The above FMD approach has been restricted by neglecting the time variation of the width parameters and that of spin wave functions [140]. By doing so it becomes possible to treat many-nucleon systems. In addition to this, they have also demonstrated that the antisymmetrized version of the molecular dynamics combined with the frictional cooling method [141] is very powerful for the study of nuclear structure since this method is free from model assumptions such as axial symmetry and that of clustering structure. However, it is indispensable to incorporate the two nucleon collision process to treat heavy-ion collisions. Ono *et al.* [142] have been succeeded in incorporating two nucleon collisions into the antisymmetrized version of molecular dynamics dubbed as *Antisymmetrized Molecular Dynamics (AMD)*. Another difference of this approach from the FMD approach is the width parameter which is constant in AMD, compared to FMD, where it is a dynamical variable.

The main drawback of this approach is that, the total angular momentum conservation is violated by two-nucleon collisions and therefore the calculated values of spins of the AMD fragments may not be so reliable. Moreover, the use of both AMD and FMD models are restricted due to serious numerical problems, to lighter systems only.

In the following we present, details of the isospin version of QMD model. This model is used in our present analysis.

2.3 Isospin-dependent Quantum Molecular Dynamics (IQMD) model

Isospin-dependent Quantum Molecular Dynamics (IQMD) model is an extension of the QMD model that incorporates the isospin degree of freedom [24]. A symmetry potential (to achieve corrected distribution of protons and neutrons in a nucleus), and explicit Coulomb forces between Z_P & Z_T protons are included. This model treats different charge states of nucleons, deltas and pions explicitly. This model has been reported to be successful in reproducing large number of observable [24]. The isospin degree of freedom enters into the calculations via both cross-section and mean field [115]. Since it is an extension of the QMD model, it also consists of three steps namely the *initialization*, *propagation* and *nucleon-nucleon binary collisions*. However it differs some what from the original QMD model in all three aspects. In the following chapter, we shall discuss all these parts in detail.

2.3.1 Initialization

An almost identical time evolution of the nuclear density is found for beam energies greater than 25 MeV/nucleon, if one compare the quantal ($TDHF$) and the classical (Vlasov) mean field. This is quite surprising because the initial density distribution is given by Slater determinant in the quantal calculations whereas point-like nucleons randomly distributed in a sphere of radius $R = 1.12A^{1/3}$ fm, (where A is the mass number of nucleus under consideration)corresponding to a normal nuclear matter density used in Vlasov equation. Therefore, detailed form of the wave function has only a minor influence on the time evolution of the bulk of the system, provided it fulfills, the minimal requirements

like approximate constant density over the proper region in co-ordinate space. Therefore, one can start with any form of wave function which is easy to handle. Both in QMD as well as in $IQMD$ models, the nucleons are represented by the Gaussian wave packets that interact by mutual (two-) and (three-) body forces. The model simulates the heavy-ion collisions on an event-by-event basis and as a consequence, preserves the correlations and fluctuations among nucleons. In $IQMD$ model, the centroids of Gaussian in a nucleus are randomly distributed in a co-ordinate space sphere of radius $R = 1.12A^{1/3}\ fm$ and in a momentum space sphere of the radius of the corresponding Fermi momentum (p_F). The wave function for i^{th} nucleon which has a mean position $\mathbf{r_i(t)}$ and mean momentum $\mathbf{p_i(t)}$ is given by

$$\psi_i(\mathbf{r},\ \mathbf{p}_i(t),\ \mathbf{r}_i(t)) \ = \ \frac{1}{(2\pi L)^{3/4}} exp\left[\frac{i}{\hbar}\ \mathbf{p}_i(t)\cdot\mathbf{r} \ - \ \frac{(\mathbf{r} \ - \ \mathbf{r}_i(t))^2}{4L}\right]. \tag{2.1}$$

The parameter L, is related to the extension of the wave packet in phase-space and is a measure of interaction range of nucleons. In the QMD model, L is 1.08 fm^2 and is independent of system size, whereas in the $IQMD$ model, L varies with size of the system. This system mass dependence of L is introduced so as to obtain maximum stability of density profile. Its value is 2.16 fm^2 for Au+Au, 1.08 fm^2 for Ca+Ca, and in between these two values for middle mass nuclei. The total N-body function is assumed to be the direct product of coherent states of Eqn.2.1:

$$\Phi \ = \ \prod_i \psi_i(\mathbf{r},\ \mathbf{r_i}, \mathbf{p_i}, t). \tag{2.2}$$

As discussed earlier, we donot use a Slater determinant and thus, neglect the anti-symmetrization. First successful attempts to simulate the heavy-ion reactions with anti-symmetrized states have been performed for smaller systems [139, 142]. As the model is semi-classical, therefore to keep the formulation as closed as possible to classical transport theory, instead of wave functions, Wigner densities were used. The Wigner representation of A_{tot} (total mass of projectile and target) nucleon system is given by

$$f_i(\mathbf{r},\mathbf{p},t) = \frac{1}{\pi^3\hbar^3}\ e^{-(\mathbf{r}-\mathbf{r_i}(t))^2\frac{2}{L}}\ e^{-(\mathbf{p}-\mathbf{p_i}(t))^2\frac{L}{2\hbar^2}}. \tag{2.3}$$

where $\mathbf{r_i}(t)$, $\mathbf{p_i}(t)$ define the classical orbit or the center of the Gaussian wave packets in phase-space. The parameter L is assumed to be independent of time. The Wigner

distribution of Gaussian wave packets obey the uncertainty relation

$$\Delta x \Delta p_x \geq \frac{1}{2}\hbar$$

In order to initialize a nucleus, one has assign the co-ordinates and momenta to all nucleons. In three dimensional space, the centers of Gaussian wave packet $\mathbf{r_i}$ are uniformly distributed in polar co-ordinates by

$$\begin{aligned} r &= R\ c_1^{1/3}, \\ cos\theta &= 1\ -\ 2c_2, \\ \phi &= 2\pi\ c_3, \end{aligned} \tag{2.4}$$

where c_1, c_2 and c_3 are the random numbers. The co-ordinates of nucleons are rejected if the distance between them is less than 1.5 fm. The nucleons are initialized in accordance with the liquid drop model. Each nucleon occupies a volume of h^3, so that phase-space is uniformly filled. The initial momenta are randomly chosen between 0 and Fermi momentum, without any further local constraint. This Fermi momentum depends on the ground state density. This possibility, however gives a reduced binding energy per nucleon as compared to Weizsäcker mass formula. Hence, the initialized nuclei are less stable. But, this situation makes available the full Fermi-energy calculated from the Skyrme ansatz. The full Fermi pressure yields a stronger stability of the density profile against vibration modes. On contrary, in QMD model, the Fermi momentum is determined by the local potential. The nucleons close to the surface may be unbound initially, because the momenta are uniformly distributed within a momentum sphere. This in turn, leads to the lesser binding energy of the initialized nuclei. The center of each Gaussian wave packet p_i are uniformly distributed in polar co-ordinates

$$\begin{aligned} \mathbf{p_i} &= p_F(\mathbf{r_i})c_4^{1/3}, \\ cos\theta &= 1\ -\ 2c_5, \\ \phi &= 2\pi c_6. \end{aligned}$$

where, c_4, c_5 and c_6 are again the random numbers. A limited sequence of random numbers does not create the ground state of a nucleus but create a metastable excited

state which decays by the emission of nucleons due to fluctuations. In order to obtain a smoother distribution of nucleons in phase-space we introduced a minimum distance d_{min} and require nucleons in phase-space to satisfy

$$|\mathbf{r_i} - \mathbf{r_j}|^2 |\mathbf{p_i} - \mathbf{p_j}|^2 \geq d_{min} \tag{2.5}$$

Typically only 1 out of 50,000 initializations is accepted under the present criteria. The accepted configurations are quite stable. In a time span of 200 fm/c [143] only few light nuclei emit at most 1 nucleon spontaneously. Moreover, the $IQMD$ model performs a Lorentz contraction of the nucleus co-ordinate distribution, which becomes important at higher energies.

2.3.1.1 Numerical tests to check the stability of nuclei

The nuclei may start emitting nucleons after the lapse of hundred fm/c which are prepared within transport model. Therefore, it is very important to make sure that our initialization does not destabilize the cold nuclei. If the interactions among the nucleons ceases to exist, then the formation of the stable fragments takes place. Extensive tests were conducted by *Heidelberg-Nantes-Franfurt-Tubingen-Chandigarh* groups to study the properties of different single nuclei. We have also carried out various checks by calculating the time evolution of r.m.s radius and the momentum of four nuclei ranging in mass from Li to Au. Fig.2.2 shows the time evolution of the radii (left panels) and momentum (right panels) of 10 differently initialized nuclei. One can see that, for the heavy nuclei there occur the oscillations around the mean value, but no nucleons are emitted. On the other hand light nuclei (like Li) are a little less stable. One or two of the nuclei emit one nucleon in the time span of 200 fm/c because the local density approximation is not very good for these light nuclei. Nevertheless, one can see that majority of nuclei remains stable for couple of hundred fm/c, which is long enough for the present calculations.

Another check of the stability is done by plotting the phase-space distribution of the four nuclei ranging from Li to Au at different time steps, shown in Fig.2.3. For more clarity we have also shown a circle of radius $R = 1.12A^{\frac{1}{3}}$. Again one can see that for the heavy nuclei, most of the nucleons remain inside the radius and very few gets emitted in the time span of 200 fm/c. Thus we can say that, the nucleons remain confined in a sphere. Which indicates the stability of heavier nuclei. But for the lighter nuclei the approximation is again not good.

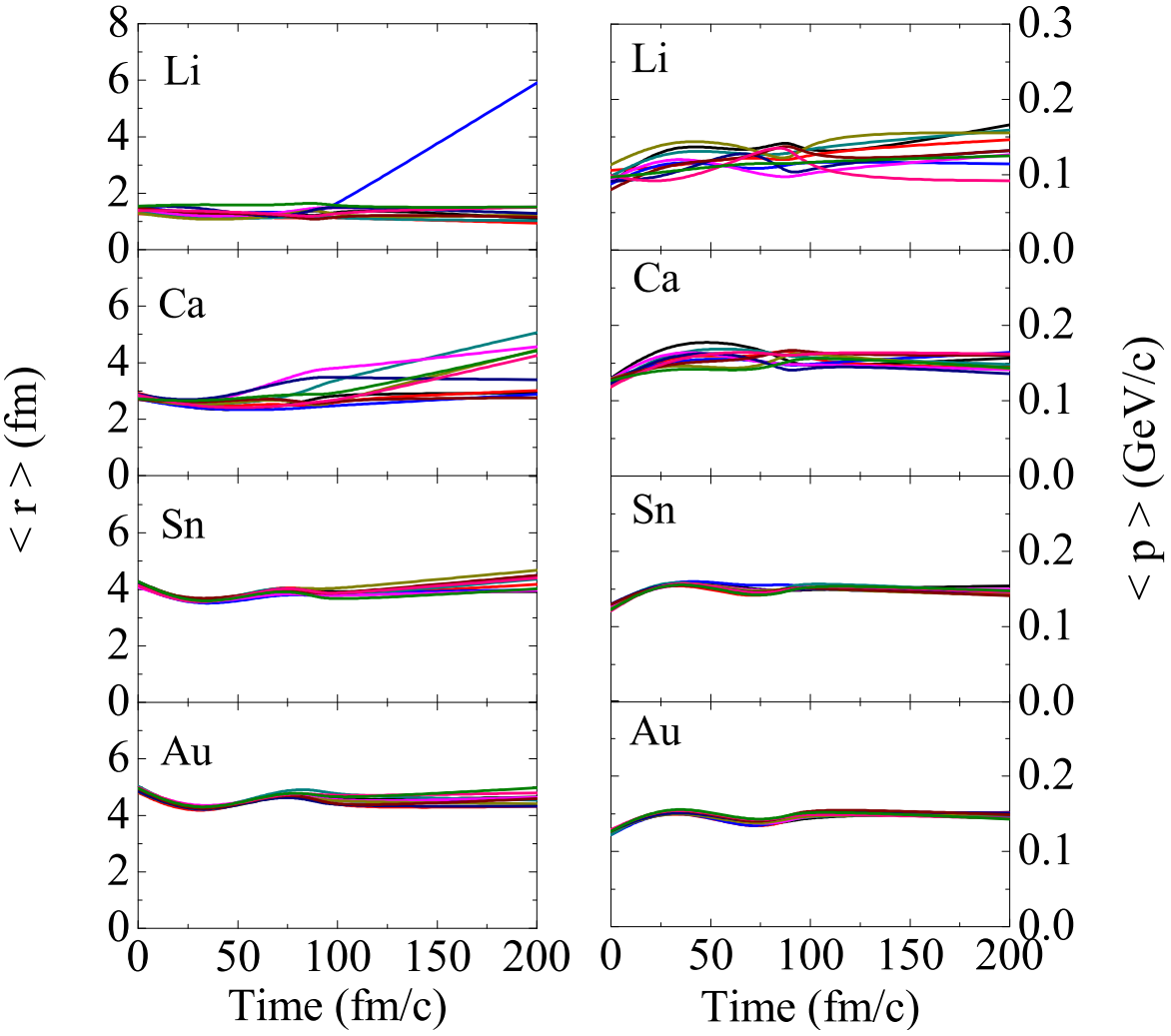

Figure 2.2: *Time evolution of the root mean square radius and momentum. For each nucleus we display the radius and momentum for ten different initializations.*

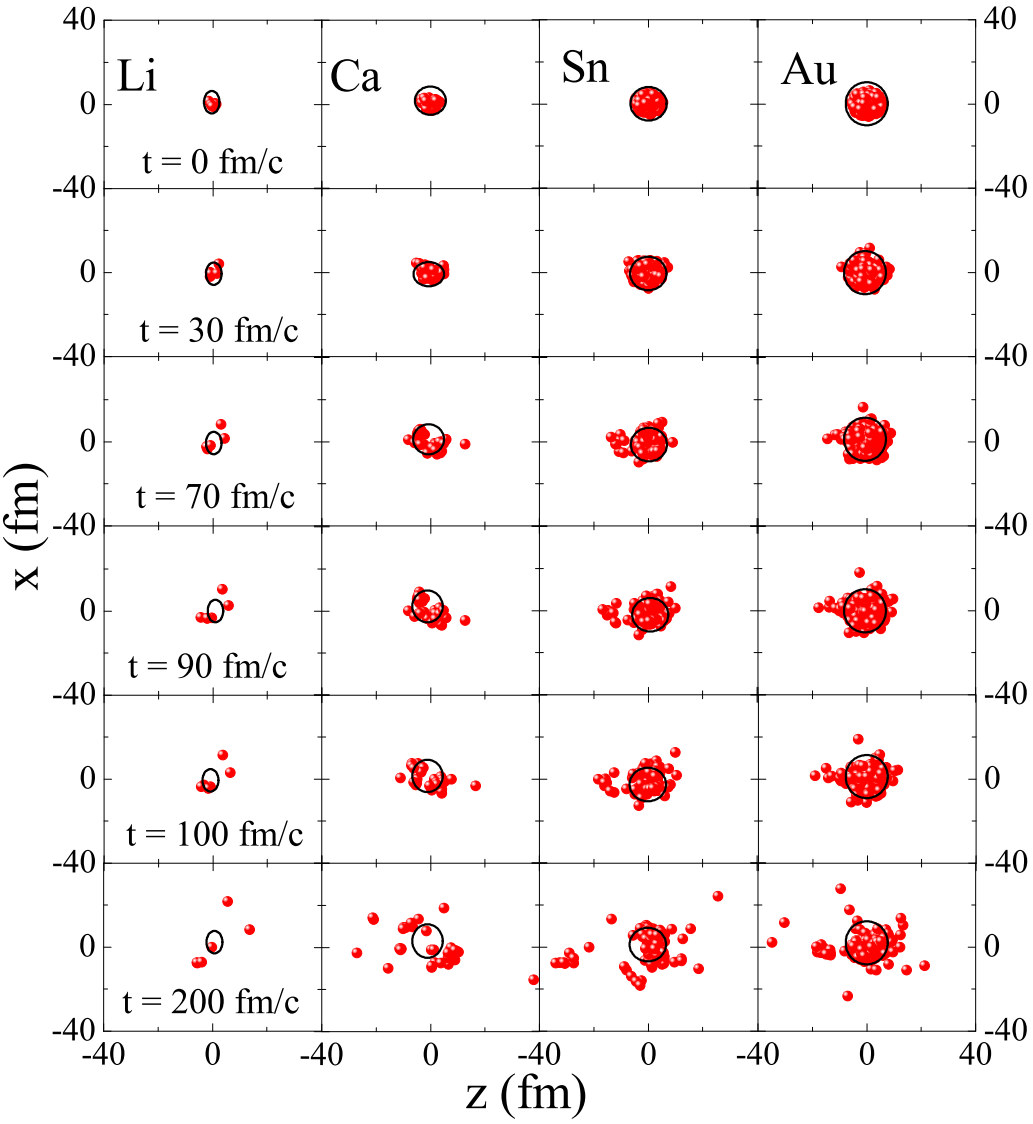

Figure 2.3: *Phase-space distribution of four different nuclei in the co-ordinate space.*

To keep the nuclei stable for several thousand fm/c Franfurt group [121] reported the inclusion of Pauli-potential in the mean field. On the other hand, Nantes group [112] checked the stability in terms of root mean square radius as well as binding energy.
Once the target and projectile are generated with proper initialization, we boost them with proper center-of-mass velocity. We shall now first discuss the propagation and then the nucleon-nucleon collisions.

2.3.2 Propagation

Nuclei which have been successfully initialized are then boosted towards each other with proper center-of-mass velocity using relativistic kinematics. The centers of projectile and target move along Coulomb trajectories upto a distance of 2 fm between the surface projectile and target. The equation of motion of many body system is then calculated by means of Ritz variational principle [144] to determine the further time evolution of the system. We start from the action

$$S = \int_{t_1}^{t_2} \mathcal{L}[\Phi, \Phi^*] d\tau, \tag{2.6}$$

with the Lagrange functional

$$\mathcal{L} = \langle \Phi | i\hbar \frac{d}{dt} - H | \Phi \rangle, \tag{2.7}$$

where the total time derivative includes the derivation with respect to the parameters. The time evolution is obtained by the requirement that the action is stationary under the allowed variation of the wave function

$$\delta S = \delta \int_{t_1}^{t_2} \mathcal{L}[\Phi, \Phi^*] dt = 0. \tag{2.8}$$

Which yields an Euler Lagrange equation for each parameter. We obtain for each parameter λ an Euler-Lagrange equation

$$\frac{d}{dt}\frac{\partial \mathcal{L}}{\partial \dot{\lambda}} - \frac{\partial \mathcal{L}}{\partial \lambda} = 0. \tag{2.9}$$

If the true solution of the Schrödinger equation is contained in the restricted set of wave function $\psi(\mathbf{r}, \mathbf{p_i}(t), \mathbf{r_i}(t))$, this variation of the action gives the exact solution of the Schrödinger equation. For the coherent states and a Hamiltonian of the form,

$$H_N = \sum_i T_i + \frac{1}{2} \sum_{i,j;i\neq j} V(\mathbf{r_i}(t) - \mathbf{r_j}(t)) \quad (i = 1, N). \tag{2.10}$$

The potential energy $V(\mathbf{r_i}(t) - \mathbf{r_j}(t))(\equiv V_{ij})$ between two particles is obtained by folding the two-body interaction with the densities of both particles. i.e.,

$$V(\mathbf{r_i}(t) - \mathbf{r_j}(t)) = \int f_i(\mathbf{r_i}, \mathbf{p_i}; t) f_j(\mathbf{r_j}, \mathbf{p_j}; t) V(\mathbf{r_i}, \mathbf{r_j}) d^3\mathbf{r_i} d^3\mathbf{r_j} d^3\mathbf{p_i} d^3\mathbf{p_j}. \tag{2.11}$$

Using classical Liouville equation, we find that the equations of motion of $\mathbf{r_i}$ and $\mathbf{p_i}$ show similar structure like classical Hamilton equations (provided the Hamiltonian can be written as in Eqn.2.10). The nucleons of the target and projectile interact via two and three body Skyrme forces, a Yukawa potential and momentum dependent interactions. The isospin degree of freedom is treated explicitly by employing a symmetry potential and explicit Coulomb forces between protons of colliding target and projectile. The hadrons propagate using Hamilton equations of motion

$$\dot{\mathbf{r_i}} = \frac{\partial H_N}{\partial \mathbf{p_i}}; \qquad \dot{\mathbf{p_i}} = \frac{-\partial H_N}{\partial \mathbf{r_i}}. \tag{2.12}$$

Suppose the Hamiltonian for the system is given by local Skyrme nucleon-nucleon interaction consisting of two-body and three-body interactions only:

$$V_{loc} = t_1 \delta(\mathbf{r_1} - \mathbf{r_2}) + t_2 \delta(\mathbf{r_1} - \mathbf{r_2}) \delta(\mathbf{r_1} - \mathbf{r_3}), \tag{2.13}$$

where t_1 and t_2 are (two-) and (three-) body coefficients, respectively. It is well known that the three-body part of above equation is equivalent to a density-dependent two-body force, however, since $IQMD$ model is an N-body theory, we prefer to use the three-body form rather than the density-dependent form. For three-body interactions (that includes three Gaussian overlap), the Hamiltonian becomes

$$H_N = \sum_i \frac{\mathbf{p_i}^2(t)}{2m} + \frac{1}{2} \sum_{i,j;i\neq j} V_{ij} + \frac{1}{3!} \sum_{i,j,k;i\neq j\neq k} V_{ijk} \equiv \sum_i H_i, \tag{2.14}$$

where

$$H_i = T_i + \frac{1}{2} \sum_{j;j\neq i} V_{ij} + \frac{1}{3!} \sum_{j,k;j\neq k\neq i} V_{ijk}, \tag{2.15}$$

where V_{ij} between two particles is obtained by folding two-body interaction with densities of the both particles and mentioned in Eqn.2.11. V_{ijk} among three particles is obtained by folding the three-body interaction with the densities of the three particles

$$V_{ijk} = \int f_i(\mathbf{r_i}, \mathbf{p_i}; t) f_j(\mathbf{r_j}, \mathbf{p_j}; t) f_k(\mathbf{r_k}, \mathbf{p_k}; t) V(\mathbf{r_i}, \mathbf{r_j}, \mathbf{r_k}) d^3\mathbf{r_i} d^3\mathbf{r_j} d^3\mathbf{r_k} d^3\mathbf{p_i} d^3\mathbf{p_j} d^3\mathbf{p_k}. \tag{2.16}$$

For the two-body interaction part of Eqn.2.15, according to Eqn.2.11, we have,

$$\begin{aligned}
\frac{1}{2}\sum_{j;i\neq j} V_{ij} &= \frac{1}{2}\sum_{j;i\neq j}\int f_i(\mathbf{r_i},\mathbf{p_i};t)\ f_j(\mathbf{r_j},\mathbf{p_j};t)\ V(\mathbf{r_i},\mathbf{r_j}) \\
&\quad \times\ d^3\mathbf{r_i}\ d^3\mathbf{r_j}\ d^3\mathbf{p_i}\ d^3\mathbf{p_j}, \\
&= \frac{1}{2}\sum_{j;i\neq j}\int f_i(\mathbf{r_i},\mathbf{p_i};t)\ f_j(\mathbf{r_j},\mathbf{p_j};t)\ t_1 \\
&\quad \times\delta(\mathbf{r_i}-\mathbf{r_j})d^3\mathbf{r_i}\ d^3\mathbf{r_j}\ d^3\mathbf{p_i}\ d^3\mathbf{p_j}, \\
&= \frac{1}{2}\sum_{j;i\neq j} t_1\int f_i(\mathbf{r_i},\mathbf{p_i};t)\ f_j(\mathbf{r_j},\mathbf{p_j};t) \\
&\quad \times\ d^3\mathbf{r_i}\ d^3\mathbf{p_i}\ d^3\mathbf{p_j}, \\
&= \frac{1}{2}\sum_{j;i\neq j} t_1\int \frac{1}{(\pi\hbar)^3}e^{-(\mathbf{r}-\mathbf{r_i}(t))^2 2/L}e^{-(\mathbf{p}-\mathbf{p_i}(t))^2 L/2\hbar^2} \\
&\quad \times\frac{1}{(\pi\hbar)^3}e^{-(\mathbf{r}-\mathbf{r_j}(t))^2 2/L}\ e^{-(\mathbf{p}-\mathbf{p_j}(t))^2 L/2\hbar^2}\ d^3\mathbf{r_i}\ d^3\mathbf{p_i}\ d^3\mathbf{p_j}, \\
&= \frac{1}{2}\sum_{j}\ t_1\frac{1}{(4\pi L)^{3/2}}e^{-(\mathbf{r_i}-\mathbf{r_j})^2/4L}, \\
&= \frac{t_1}{2}\sum_{j;i\neq j}\rho_{ij}. \qquad (2.18)
\end{aligned}$$

where, the interaction density ρ_{ij} is given by:

$$\rho_{ij} = \int d^3\mathbf{r}\ \rho_i(\mathbf{r})\ \rho_j(\mathbf{r}) = \frac{1}{(4\pi L)^{3/2}}e^{-(\mathbf{r}_i-\mathbf{r}_j)^2/4L}. \qquad (2.19)$$

The three-body interactions can be calculated as follows:

$$\begin{aligned}
\frac{1}{3!}\sum_{j,k;i\neq j\neq k} V_{ijk} &= \frac{1}{3!}\sum_{j,k;i\neq j\neq k}\int f_i(\mathbf{r_i},\mathbf{p_i},t)\ f_j(\mathbf{r_j},\mathbf{p_j},t)\ f_k(\mathbf{r_k},\mathbf{p_k},t)\ V(\mathbf{r_i},\mathbf{r_j},\mathbf{r_k}) \\
&\quad \times\ d^3\mathbf{r_i}\ d^3\mathbf{r_j}\ d^3\mathbf{r_k}\ d^3\mathbf{p_i}\ d^3\mathbf{p_j}\ d^3\mathbf{p_k}, \\
&= \frac{1}{3!}\sum_{j,k;i\neq j\neq k}\int f_i(\mathbf{r_i},\mathbf{p_i},t)\ f_j(\mathbf{r_j},\mathbf{p_j},t)\ f_k(\mathbf{r_k},\mathbf{p_k},t)\ t_2 \\
&\quad \times\delta(\mathbf{r_i}-\mathbf{r_j})\ \delta(\mathbf{r_i}-\mathbf{r_k})d^3\mathbf{r_i}\ d^3\mathbf{r_j}\ d^3\mathbf{r_k}\ d^3\mathbf{p_i}\ d^3\mathbf{p_j}\ d^3\mathbf{p_k}, \\
&= \frac{1}{3!}\frac{t_2}{(2\pi L)^3\cdot 3^{3/2}}\sum_{j,k;i\neq j\neq k} e^{-\left[(\mathbf{r_i}-\mathbf{r_j})^2+(\mathbf{r_i}-\mathbf{r_k})^2+(\mathbf{r_k}-\mathbf{r_j})^2\right]/6L}, \\
&= \frac{1}{3!}\frac{t_2}{(2\pi L)^3 3^{3/2}}\sum_{j,k;i\neq j\neq k} e^{-\left[(\mathbf{r_i}-\mathbf{r_j})^2+(\mathbf{r_i}-\mathbf{r_k})^2\right]/6L\times\frac{3}{2}}, \\
&= \frac{1}{3!}\frac{t_2\ (4\pi L)^{3/2\times 2}}{(2\pi L)^3\cdot 3^{3/2}}\left[\sum_{j\neq i}\frac{1}{(4\pi L)^{3/2}}e^{-(\mathbf{r_i}-\mathbf{r_j})^2/4L}\right]^2, \\
&= \frac{1}{3!}\frac{t_2\ 2^3}{3^{3/2}}\left[\sum_{j\neq i}\rho_{ij}\right]^2. \qquad (2.20)
\end{aligned}$$

From the above equation, we notice that for three-body interaction, the mean field can be written as $[\sum_{j\neq i}\rho_{ij}]^2$. We can show that for $\acute{\gamma}$+1-body ($\acute{\gamma}$ is an integer) interaction, the mean field can be written as $[\sum_{j\neq i}\rho_{ij}]^{\acute{\gamma}}$. Therefore, if we have two-body and ($\acute{\gamma}$+1)-body interactions we have for the Hamiltonian:

$$\begin{aligned} H_N &= \sum_i \frac{\mathbf{p_i}^2(t)}{2m} + \frac{1}{2}\sum_{i,j;i\neq j} V_{ij} + \frac{1}{(\acute{\gamma}+1)!}\sum_{i_1,i_2.....i_{\acute{\gamma}+1};i_1\neq i_2.....\neq i_{\acute{\gamma}+1}} V_{i_2,i_3....i_{\acute{\gamma}+1}} \\ &= \sum_i \frac{\mathbf{p_i}^2(t)}{2m} + \frac{1}{2}\sum_i \left[\sum_{j\neq i} t_1 \frac{1}{(4\pi L)^{3/2}} e^{-(\mathbf{r_i}-\mathbf{r_j})^2/4L}\right] \\ &+ \frac{1}{(\acute{\gamma}+1)!}\frac{t_2 2^3}{(\acute{\gamma}+1)^{3/2}}\sum_{i_1}\left[\sum_{i_2\neq i_1}\frac{1}{(4\pi L)^{3/2}} e^{-(\mathbf{r_i}1-\mathbf{r_i}2)^2/4L}\right]^{\acute{\gamma}} \end{aligned} \tag{2.21}$$

As we know that the purpose of heavy-ion collisions is to probe the equation of state of nuclear matter, therefore, the parameters t_1 and t_2 in the above equation are determined by the requirement that the Hamiltonian of above equation should reproduce the equation of state in infinite nuclear matter limits. Thus, we require that Eqn.2.21 should reproduce the Skyrme parametrization of nuclear matter EOS which is

$$\frac{E}{N}(or\frac{E}{A}) = \frac{1}{\rho}\frac{E}{V} = \frac{3}{5}\frac{\hbar^2 k_F^2}{2m} + \frac{\alpha}{2}\frac{\rho}{\rho_0} + \frac{\beta}{\acute{\gamma}+1}\frac{\rho^{\acute{\gamma}}}{\rho_0^{\acute{\gamma}}}, \tag{2.22}$$

where $k_F(=\frac{3}{2}\pi^2\rho)^{1/3}$ is the Fermi vector in nuclear matter. Therefore, in infinite nuclear matter limits the potential energy part of Eqn.2.21 can be written as

$$V_N \Rightarrow^{nuclearmatter} \frac{1}{2}Nt_1\rho + \frac{1}{(\acute{\gamma}+1)!}\frac{t_2 2^{\frac{3\acute{\gamma}}{2}}}{(\acute{\gamma}+1)^{3/2}}N\rho^{\acute{\gamma}} \tag{2.23}$$

Comparing the above equation with Eqn.2.22, we can determine t_1 and t_2 by:

$$\frac{t_1}{2} \Rightarrow \frac{\alpha}{2\rho_0} \tag{2.24}$$

and

$$\frac{1}{(\acute{\gamma}+1)!}\frac{t_2 2^{\frac{3\acute{\gamma}}{2}}}{(\acute{\gamma}+1)^{3/2}} \Rightarrow \frac{\beta}{\acute{\gamma}+1}\frac{1}{\rho_0^{\acute{\gamma}}} \tag{2.25}$$

Till now, we have only discussed about the local Skyrme interaction. But, besides Skyrme interaction we have a finite range Yukawa term V^{Yuk}, and Coulomb interaction V^{Coul} which read as:

$$V^{Yuk} = t_3\frac{exp\{-|\mathbf{r_i}-\mathbf{r_j}|\}/\mu}{|\mathbf{r_i}-\mathbf{r_j}|/\mu}. \tag{2.26}$$

$$V^{Coul} = \frac{Z_i Z_j \ e^2}{|\mathbf{r_i} - \mathbf{r_j}|}. \tag{2.27}$$

The Yukawa potential is also short ranged in $IQMD$ model, with t_3= -6.66 MeV and μ = 0.4 fm (in QMD, μ = 1.5 fm). It has been added to improve the surface properties of the interaction which are very important for multi-fragmentation. In nuclear matter where the density is constant, the interaction density coincides with the single particle density, and $V_{loc}^{(2)}$, as well as $V_{Yuk}^{(2)}$, are directly proportional to $(\frac{\rho}{\rho_o})$. The three-body part $V_{loc}^{(3)}$ of the interaction is proportional to $(\frac{\rho}{\rho_o})^2$. In nuclear matter, the local potential energy has the form

$$V_{loc} = \frac{\alpha}{2}\left(\frac{\rho}{\rho_o}\right) + \frac{\beta}{\zeta+1}\left(\frac{\rho}{\rho_o}\right)^2. \tag{2.28}$$

The above potential has two free (α and β) parameters, which can be fixed by the requirement that at normal nuclear matter density the average binding energy should be -16 MeV and total energy should have a minimum at ρ_o. In order to investigate the influence of different compressibilities, one can generalize the above potential energy (Eqn.2.28) to

$$V_{loc} = \frac{\alpha}{2}\left(\frac{\rho}{\rho_o}\right) + \frac{\beta}{\zeta+1}\left(\frac{\rho}{\rho_o}\right)^\zeta. \tag{2.29}$$

This equation leads to the nuclear matter equation of state which connects the pressure and energy [112]. In the study of heavy-ion collisions, one usually has the so-called Skyrme parameterization of nuclear equation of state (EOS), which contains two sets of parameter giving the same correct binding energy and saturation density, but, two different incompressibility K (one corresponds to soft EOS with K = 200 MeV (at smaller value of ζ), another corresponds to hard EOS with K = 380 MeV (at larger value of ζ)). The total Skyrme potential then can be written as

$$V^{Skyrme} = \sum_{j;i\neq j} t_1\delta(\mathbf{r_i} - \mathbf{r_j}) + t_2\delta(\mathbf{r_i} - \mathbf{r_j})\rho^{\acute{\gamma}-1}((\mathbf{r_i} + \mathbf{r_j})/2). \tag{2.30}$$

When momentum-dependent potential (which is optional) is introduced [145], we have to readjust the parameters of the Skyrme force to have correct saturation properties for normal nuclear matter and the same incompressibilities as those of the soft and hard EOS. The parametrized form of the momentum-dependent interactions (which is fitted to the experimental data [146]) is give as

$$V^{MDI} = \sum_{j;i\neq j} t_4 ln^2(t_5(\mathbf{p_i} - \mathbf{p_j})^2 + 1)\delta(\mathbf{r_i} - \mathbf{r_j}), \tag{2.31}$$

where t_4 = 1.57 MeV and $t_5 = 5 \times 10^{-4}\ MeV^{-2}$. The new parameter sets with the momentum dependence are called SM and HM, respectively. These set of parameters are listed in Table 2.1 together with incompressibilities. As we have already stated that, the

Table 2.1: *Parameter sets used in the IQMD model [115].*

EOS	α(MeV)	β(MeV)	ζ	δ(MeV)	K(MeV)
S	-356	303	1.17		200
SM	-390	320	1.14	1.57	200
H	-124	71	2.00		380
HM	-130	59	2.09	1.57	380

isospin effects in the $IQMD$ model enters via Coulomb and Symmetry potential. In this model, we use charge i.e. $Z_{proton} = 1$ and $Z_{neutron} = 0$ to include the isospin dependence of Coulomb potential. On the other hand, in QMD model, one has effective charge (Z_{eff}) for all nucleons without distinguishing between protons and neutrons. The symmetry potential between protons and neutrons is also added and is given by

$$V^{sym} = \sum_{j;i\neq j} t_6(1/\rho_0)T_{3i}T_{3j}\delta(\mathbf{r_i} - \mathbf{r_j}), \tag{2.32}$$

where t_6 = 100 MeV and T_{3i} and T_{3j} denote the isospin projection of particles i and j (being +1/2 and -1/2 for protons and neutrons, respectively). The total baryon-baryon potential in $IQMD$ model can be written as:

$$\begin{aligned} V_{ij} &= V_{ij}^{Skyrme} + V_{ij}^{Yukawa} + V_{ij}^{Coul} + V_{ij}^{MDI} + V_{ij}^{Sym} \\ &= \left(t_1\delta(\mathbf{r_i} - \mathbf{r_j}) + t_2\delta(\mathbf{r_i} - \mathbf{r_j})\rho^{\zeta-1}\left(\frac{\mathbf{r_i} + \mathbf{r_j}}{2}\right)\right) \\ &\quad + t_3\frac{exp(|\mathbf{r_i} - \mathbf{r_j}|/\mu)}{(|\mathbf{r_i} - \mathbf{r_j}|/\mu)} + \frac{Z_iZ_je^2}{|\mathbf{r_i} - \mathbf{r_j}|} \\ &\quad + t_4\ln^2[t_5(\mathbf{p_i} - \mathbf{p_j})^2 + 1]\delta(\mathbf{r_i} - \mathbf{r_j}) \\ &\quad + t_6\frac{1}{\varrho_0}T_{3i}T_{3j}\delta(\mathbf{r_i} - \mathbf{r_j}). \end{aligned} \tag{2.33}$$

2.3.3 Nucleon-Nucleon collisions

The nucleon-nucleon collisions are included in $IQMD$ model by employing the collision terms of the well-known VUU-BUU equations [103, 115]. Like in all cascade models [147] the collisions are done stochastically. However, there is a difference in parameterizations considered for the nucleon-nucleon scattering cross-sections in QMD and $IQMD$ models.

In QMD model, Cugnon parametrization has been taken into account (without distinguishing between isospin). Whereas in the case of $IQMD$, parameterizations of VerWest and Arndt have been taken [115]. Although, the collision treatment is done in the same way as in the QMD model, yet the Pauli blocking becomes isospin dependent i.e. the occupancy of phase-space of scattering partners is checked for the particles having same isospin as that of the scattered one. In fact, during the propagation, two nucleons are supposed to suffer a binary collision if the distance between their centroids is fulfilled by condition

$$|\mathbf{r_i} - \mathbf{r_j}| \leq \sqrt{\frac{\sigma_{tot}}{\pi}}, \quad \sigma_{tot} = \sigma(\sqrt{s}, type), \tag{2.34}$$

where "type" denotes the ingoing collision partners (N-N, N-Δ, N-π,....). In addition, Pauli blocking (of the final state) the baryons is taken into account by checking the phase space densities in the final states. The final phase space fractions P_1 and P_2 which are already occupied by the other nucleons are determined for each of the scattering baryons. The collision is then blocked with probability

$$P_{block} = 1 - (1 - P_1)(1 - P_2). \tag{2.35}$$

Delta decays are checked in an analogous fashion with respect to the phase space of the resulting nucleon. Moreover, parameterized free np and pp cross-sections are used instead of an averaged nucleon-nucleon cross-section like in the QMD model.

Total cross-section is the sum of the elastic and all inelastic cross-sections are:

$$\sigma_{tot} = \sigma_{el} + \sigma_{inel} = \sigma_{el} + \sum_{channels} \sigma_i. \tag{2.36}$$

In addition to nucleons and deltas (as in the QMD model), pions are also formed in the $IQMD$ model via the decay of delta resonances. The following inelastic channels are explicitly taken into account and constitute the imaginary part of the pion optical potential

$$\begin{aligned} N\ N &\rightarrow\ \Delta\ N \qquad (a),\\ \Delta &\rightarrow\ N\ \pi \qquad (b),\\ \Delta\ N &\rightarrow\ N\ N \qquad (c),\\ N\ \pi &\rightarrow\ \Delta \qquad (d). \end{aligned} \tag{2.37}$$

Elastic $\pi - \pi$, $\pi - N$, $\pi - \Delta$, $\Delta - \Delta$, $\Delta - N$ scatterings are not taken into account. Experimental cross-sections are used for the processes (a) and (d) [115], as well as for the elastic nucleon-nucleon cross-sections. Experimentally inaccessible channels like

Table 2.2: *a(s) and b(s) as a function of the c.m. energy.*

$\acute{x} = \sqrt{s}\ (GeV)$	$a\ (fm)$	b
2.104 - 2.12	$294.6(\acute{x} - 2.014)^{2.578}$	$19.71(\acute{x} - 2.014)^{1.551}$
2.12 - 2.43	$\frac{0.01224}{(\acute{x}-2.225)^2 + 0.004112}$	$19.71(\acute{x} - 2.014)^{1.551}$
2.43 - 4.50	$\left(\frac{2.343}{\acute{x}}\right)^{43.17}$	$33.14\ arctan(0.5404(\acute{x} - 2.146)^{0.9784})$

ΔN $\rightarrow$ NN are calculated from their reverse reactions (here $NN \rightarrow \Delta N$) using modified detailed balance formula [148]. The angular distribution for the elastically scattered nucleons is given by:

$$\frac{d\sigma_{el}}{d\Omega} \sim e^{A(s)\cdot t} \tag{2.38}$$

where,

$$t = -2p^2(1 - cos\theta) \quad and \quad A(s) = 6\frac{[3.65(\sqrt{s} - 1.8766)]^6}{1 + [3.65(\sqrt{s} - 1.8766)]^6}, \tag{2.39}$$

with $\sqrt{s}$ the c.m. energy in GeV and A(s) is given in $(GeV/c)^{-2}$. The inelastic channels are treated in an analogous fashion. The parametrization suggested by Huber and Aichelin [131] is used: fitted differential cross-sections are extracted from one-boson-exchange (OBE) calculations:

$$\frac{d\sigma_{in}}{d\Omega} \approx a(s)exp\left[b(s)cos\theta\right]. \tag{2.40}$$

The $a(s)$ and $b(s)$ are functions of $\sqrt{s}$ and vary in their definition for different intervals of $\sqrt{s}$ (see Table 2.2). θ is the polar angle.

2.3.3.1 Numerical test

In order to look for the changes in phase-space with reference to the nucleon-nucleon collisions. We display in Fig.2.4, the trajectory of participant nucleon in the co-ordinate space, for the reactions of Li+Li, Ca+Ca, Sn+Sn and Au+Au, for a single participant nucleon (denoted by circle) which has suffered large number of collisions. The numeric values in the boxes represents the number of collisions suffered by a nucleon and the subscripts to those values denote the time interval (in fm/c) during which these collisions happened. One can see that, the participant nucleons after suffering frequent collisions,

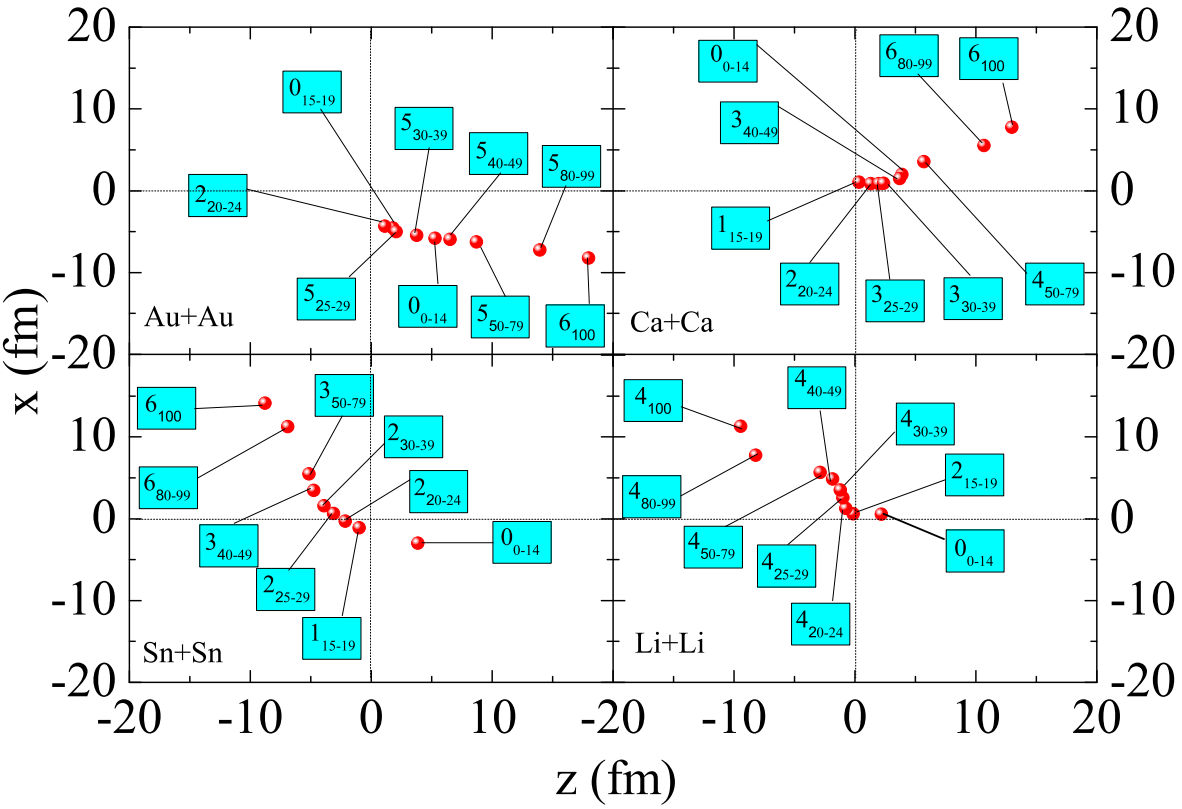

Figure 2.4: *The trajectory of participant nucleon in the co-ordinate space, for the reactions of Li+Li, Ca+Ca, Sn+Sn and Au+Au.*

move in the transverse direction.

The above mentioned models are "primary models" that are used to generate the phase space of nucleons. We need "secondary models" to clusterize the nucleons into fragments. We will discuss these clusterization methods in detail in the next chapter.

Summarizing, we discussed the details of various theoretical approaches in this chapter. These approaches contain one- as well as many-body features. We discuss the creation of nuclei, their propagation as well as binary collisions. In the following chapters, we shall present the detailed analysis of the isospin effects in the flow, its disappearance and other related phenomena like participant-spectator matter, density, temperature and thermalization achieved in heavy-ion reactions.

Chapter 3

Isospin effects on fragment production

3.1 Introduction

The heavy-ion collisions at intermediate energies typically yield various fragments consists of free nucleons (FN's) ($A_f = 1$), light mass fragments (LMF's) ($2 \leq A_f \leq 4$), medium mass fragments (MMF's) ($5 \leq A_f \leq 9$) and intermediate mass fragments (IMF's) ($5 \leq A_f \leq A_{tot}/6$). The emission of IMF's from highly excited nuclei, or multifragmentation, provides an important probe of collective behavior on a fast time scale. In this chapter, we plan to study fragmentation with reference to isospin effects. The gateway of a reaction is the density achieved in a reaction. We define density as:

$$\rho_i(r,t) = \sum_i^{A_{tot}} \frac{1}{(2\pi L)^{3/2}} e^{-[\mathbf{r}-\mathbf{r_i}(t)]^2/2L}. \tag{3.1}$$

Fig.3.1 shows the evolution of the scaled density $< \rho/\rho_0 >$ as a function of time. Different lines in the figure indicate the analysis at different bombarding energies. One can see that, density during compression is closely related to the violence of binary collision. The variation of final stage density is quite different from the saturation density at different incident energies.

One also notices from Fig.3.2 that the maximum density achieved in the reaction shows a rise and fall behavior with increase in the incident energy. The first increase in the density is due to the increase in the collision probability with incident energy, the decay after maximum is due to the fact that system becomes more transparent at higher incident energies. On contrary, the saturation density shows a sharp decay with incident energy. This happens because the number of binary collision decreases due to transparency at higher

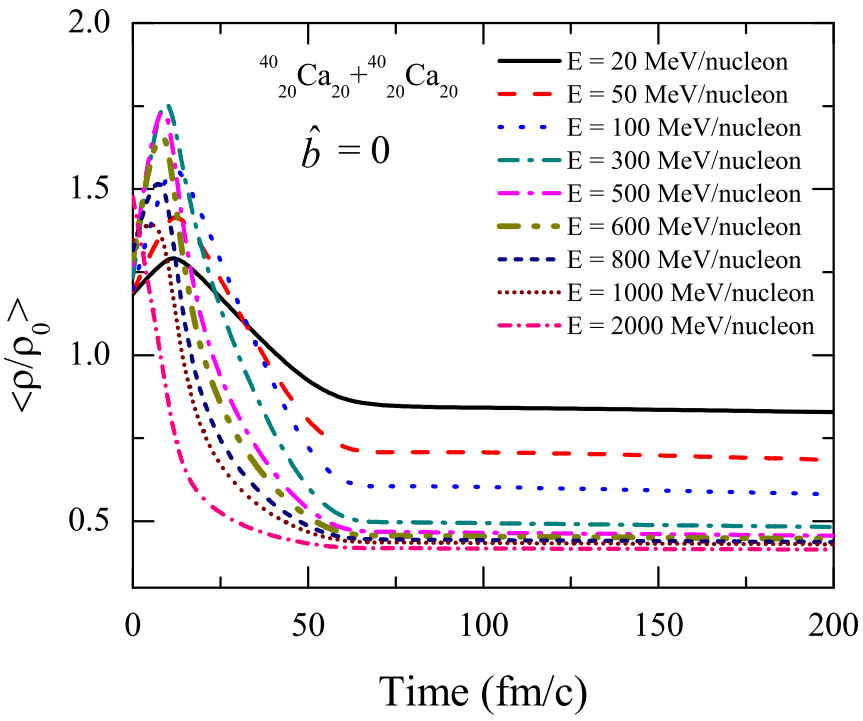

Figure 3.1: *The evolution of mean density as a function of time at different incident energies.*

incident energy. That leads to the evaporation of the material and thus the density decreases at higher incident energy due to the decrease in nucleon-nucleon cross-section. This saturation time of the density depends strongly on the mass of the colliding nuclei. For heavier systems, it will take far more time before the density saturates.

One of the major model ingredient in heavy-ion collisions is the symmetry energy, whose form and strength are two of the hot topics these days. In heavy-ion collisions, highly compressed matter can be formed for short time-span. Thus, the study of such a dynamical process can provide useful information on the high-density dependence of symmetry energy. Even at low incident energy, which belong to even smaller baryonic densities, the isospin dependence of the mean-field potential was shown to yield the same result obtained with potentials that have no isospin dependence. Recently, theoretical studies on the high-density symmetry energy have been started by investigating heavy-ion collisions of asymmetric systems [149, 150]. Comparisons of collisions of neutron rich to that of neutron-deficient systems provide a means of probing the asymmetry term experimen-

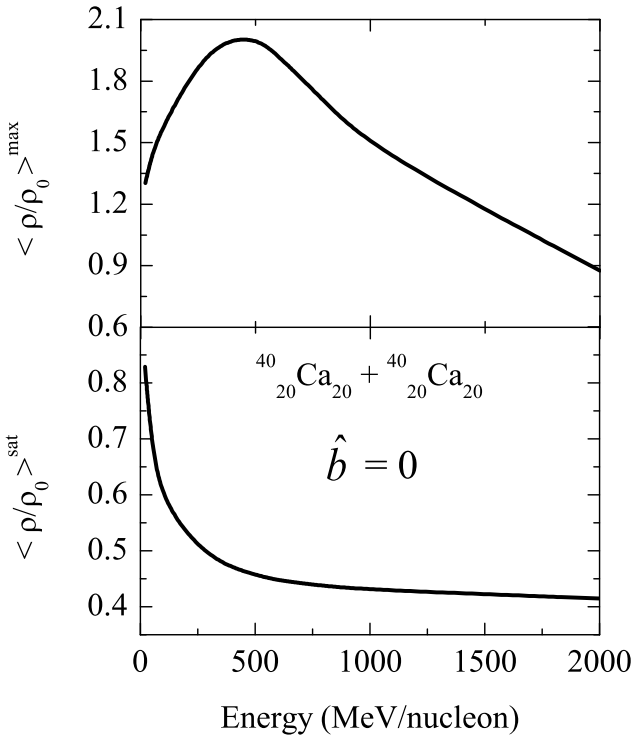

Figure 3.2: *Incident energy dependence of maximum and saturation density.*

tally [151, 152, 153]. So, it would be of interest to extract information of symmetry energy and its density dependence in heavy ion collisions. Many microscopic and/or phenomenological many-body theories using various interactions [154] predict that the symmetry energy increases continuously at all densities. However, other models [155] predict that the symmetry energy first increases to a maximum and then may start decreasing at certain supra-saturation densities. Many groups have estimated the different values of E_{sym} [156, 157] in order to study the influence of compressibility through symmetry energy. L. W. Chen *et al.* [156] expressed the density dependence of the symmetry energy as

$$E_{sym} = E^0_{sym}(\frac{\rho}{\rho_0})^\gamma \tag{3.2}$$

where $E^0_{sym} = 32$ MeV for normal nuclear density ρ_0, ρ is instantaneous density, γ is the stiffness parameter. Fig.3.3, shows the various forms of density dependent symmetry energy. One can see that, curve having $\gamma = 2$ is stiffer compared to other forms. The stiffness increases with increase in γ. Two different types of the density dependent forms

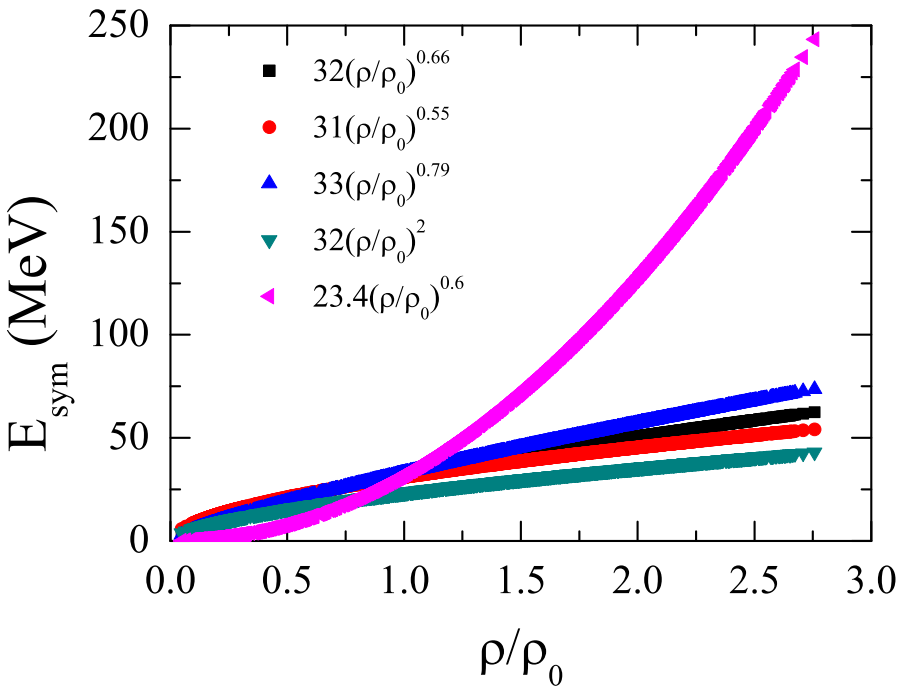

Figure 3.3: *Schematic view of the density dependence of symmetry energy suggested by various groups.*

of symmetry energy have been observed. One, where the symmetry energy increases monotonically with increasing density ("stiff" dependence) and the other, where the symmetry energy increases initially up to normal nuclear density and then decreases at higher densities ("soft" dependence). The symmetry energy with E^0_{sym} = 31-32 MeV and $\gamma \approx$ 0.55-0.69 are in agreement with the observation of various groups [158].

In addition to symmetry energy, multifragmentation is also influenced by the isospin dependence of nucleon-nucleon cross-section. C. Zeitlin *et al.* [159] experimentally studied the effect of cross-section on fragment production. R. Wada and co-workers [160] reported that the nucleon-nucleon cross-section decreases with increase in incident energy. The experimental analysis of the isospin effects on fragment production has yielded several interesting observations. Lozhkin *et al.* [161] studied the isotopic effects in the production of IMF's from light-ion-induced reactions on heavy nuclei. Their study reveals the high degree of equilibration in the isotopic degree of freedom. Dempsey *et al.* [162], in their investigation of ${}^{124,136}_{51}Xe_{73,85} + {}^{112,124}_{50}Sn_{62,74}$ at 55 MeV/nucleon, found that multiplicity of intermediate mass fragments (IMF's) increases with the neutron excess of the

system. A more comprehensive study by Buyukcizmeci *et al.* [163] showed that symmetry energy of the hot fragments produced in the statistical freeze-out is very important for isotope distributions, but its influence is not very large on the mean fragment mass distributions. Effect of symmetry energy on isotope distributions can survive after secondary de-excitation. Moreover, Schmidt *et al.* [164] in their investigation on the analysis of light charged particles production and isospin dependence of ${}^{124}_{50}Sn_{74}+{}^{64}_{28}Ni_{36}$, ${}^{124}_{50}Sn_{74}+{}^{58}_{28}Ni_{30}$, ${}^{124}_{50}Sn_{74}+{}^{27}_{13}Al_{14}$ at 35 MeV/nucleon and 25 MeV/nucleon collisions found that isospin effects were demonstrated in the observables, such as the angular distribution of light particles emitted in central collisions at 35 MeV/nucleon and LCP's (light charged particles) emission.

In view of the above facts, it is challenging to investigate the role of isospin degree of freedom on multifragmentation and to study the influence of change in isotopic content of colliding nuclei on fragment production. Our present aim is to look for the influence of isospin dependence of nucleon-nucleon cross-section on fragmentation due to the collision of isobaric nuclei.

3.2 Method of clusterization

Beside nucleon-nucleon interactions and cross-section, the clusterization approach one uses has an important role to play in final outcome of the reaction. The phase space configuration of nucleons generated by $IQMD$ model does not give fragment configuration as such. In order to identify the bound clusters one requires secondary algorithm. These algorithms are also important to know the clusterization mechanism at intermediate energies which is still not fully understood. One of the simplest algorithm to recognize the fragment distribution using spatial correlations only is the "*minimum spanning tree (MST)*" algorithm [112, 165, 166]. We shall throw light on MST in following subsection.

3.2.1 Minimum Spanning Tree (MST) method

In configuration space, a particle i belongs to a cluster if there is another particle j that belongs to same cluster with the condition

$$|\mathbf{r_i} - \mathbf{r_j}| \leq R_{clus}, \tag{3.3}$$

where $\mathbf{r_i}$ and $\mathbf{r_j}$ are the spatial positions of both nucleons. The minimum distance R_{clus} has been used as a free-parameter which varies between 2-4 fm. The algorithm that recognizes these clusters is known as the "*minimum spanning tree (MST)*" algorithm.

3.3 Results and discussion

To study the influence of isospin dependence of nucleon-nucleon cross-section on fragmentation, we have simulated the reactions of ${}^{124}_{50}Sn_{74} + {}^{124}_{50}Sn_{74}$ and ${}^{107}_{50}Sn_{57} + {}^{107}_{50}Sn_{57}$ at an incident energy of 600 MeV/nucleon spanning over the entire colliding geometry. The phase space generated using $IQMD$ model has been analyzed using the *minimum spanning tree (MST)* algorithm [121]. The results obtained are discussed in the following subsections [167].

3.3.1 Incident energy dependence of fragment multiplicity

Fig.3.4 shows the incident energy dependence of fragment multiplicity for the reactions of ${}^{124}_{50}Sn_{74} + {}^{124}_{50}Sn_{74}$ and ${}^{107}_{50}Sn_{57} + {}^{107}_{50}Sn_{57}$. It has been observed that multiplicity of FN's and LMF's increases with increase in incident energy. On the other hand, one can see a "rise and fall" in the multiplicity of IMF's. This behavior is similar to the behavior shown by Aladin group [75]. Moreover, the multiplicity of FN's and LMF's is more compared to IMF's because for central collisions, interactions among the nucleons increases, and therefore a large number of FN's and LMF's are produced. It is clear from the figure that the slope of the curve is steeper for the reaction of ${}^{124}_{50}Sn_{74} + {}^{124}_{50}Sn_{74}$ compared to ${}^{107}_{50}Sn_{57} + {}^{107}_{50}Sn_{57}$ and this theoretical observation is in agreement with the experimental observation of Sfienti *et al.* [75]. This is because maximum of fragment production depends more on the mass than on the N/Z of the colliding nuclei.

3.3.2 N/Z dependence of fragment multiplicity

To study the influence of nucleon-nucleon cross-section on fragmentation for isobaric nuclei, we have chosen two sets of reactions, one where the mass of the colliding nuclei is fixed to be 40 units, but charge varies from 14 to 23. For the first set, the chosen reactions are ${}^{40}_{Z_1}X_m + {}^{40}_{Z_1}X_m$, where Z_1 = (14, 15, 16, 17, 18, 20, 21 and 23). For the second set we have chosen the reactions for which the mass of the colliding nuclei is fixed to be 124

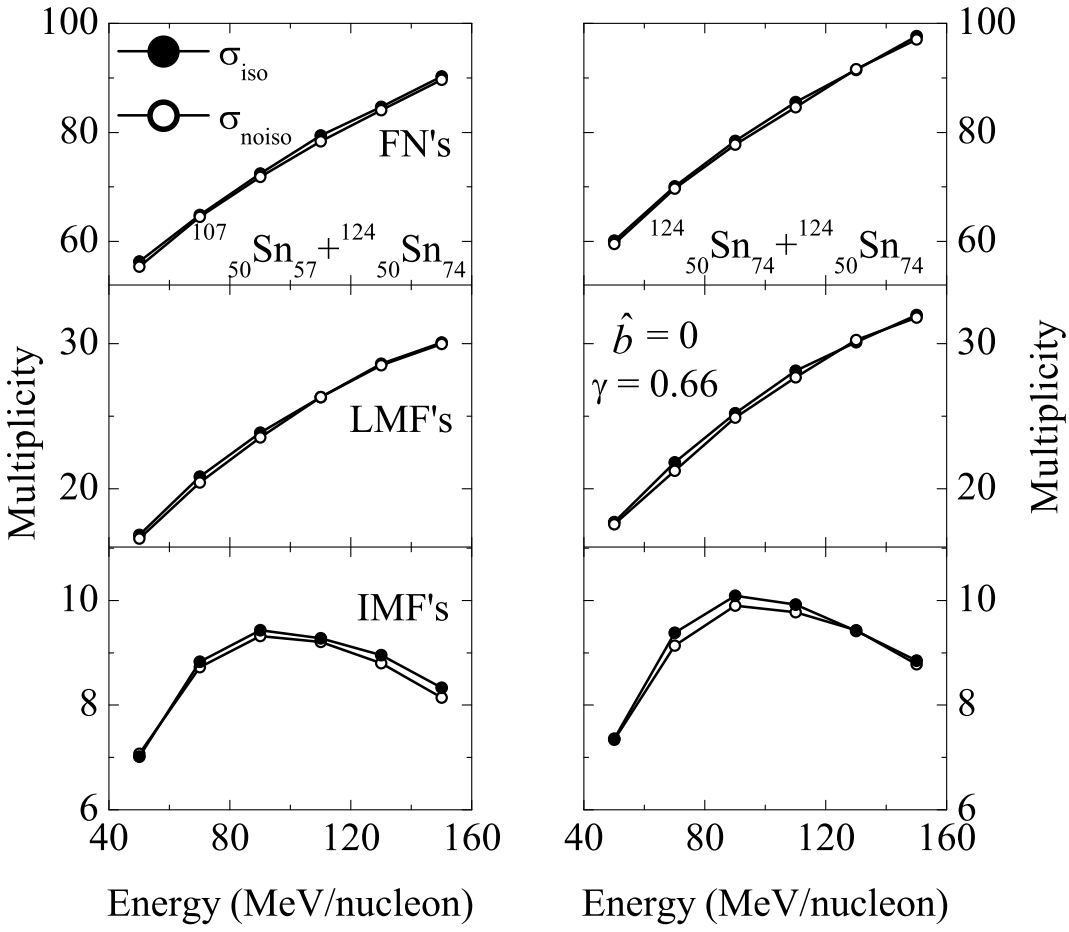

Figure 3.4: *Multiplicity of FN's, LMF's and IMF's with energy at fixed scaled impact parameter for* ${}^{124}_{50}Sn_{74} + {}^{124}_{50}Sn_{74}$ *and* ${}^{107}_{50}Sn_{57} + {}^{107}_{50}Sn_{57}$.

units, but charge varies from 47 to 59. The chosen reactions are ${}^{124}_{Z_2}Y_n + {}^{124}_{Z_2}Y_n$, where Z_2 = (47, 48, 49, 50, 53, 55, 56, and 59). The simulations are carried out at scaled impact parameter of $\hat{b} = 0.3$ and at an incident energy of 100 MeV/nucleon for symmetry energy corresponding to $\gamma = 0.66$. Here we take three different nucleon-nucleon cross-sections namely σ_{iso}, σ_{noiso} and constant cross-section for which $\sigma = 55$ mb. At low incident energy, cross-sections have very large influence on fragment production. Moreover, these have a small effect on fragment production for central collisions, whereas fragment production is strongly influenced at semi-central ($\hat{b} = 0.3$ in this case) collisions [168]. In Fig.3.5, we

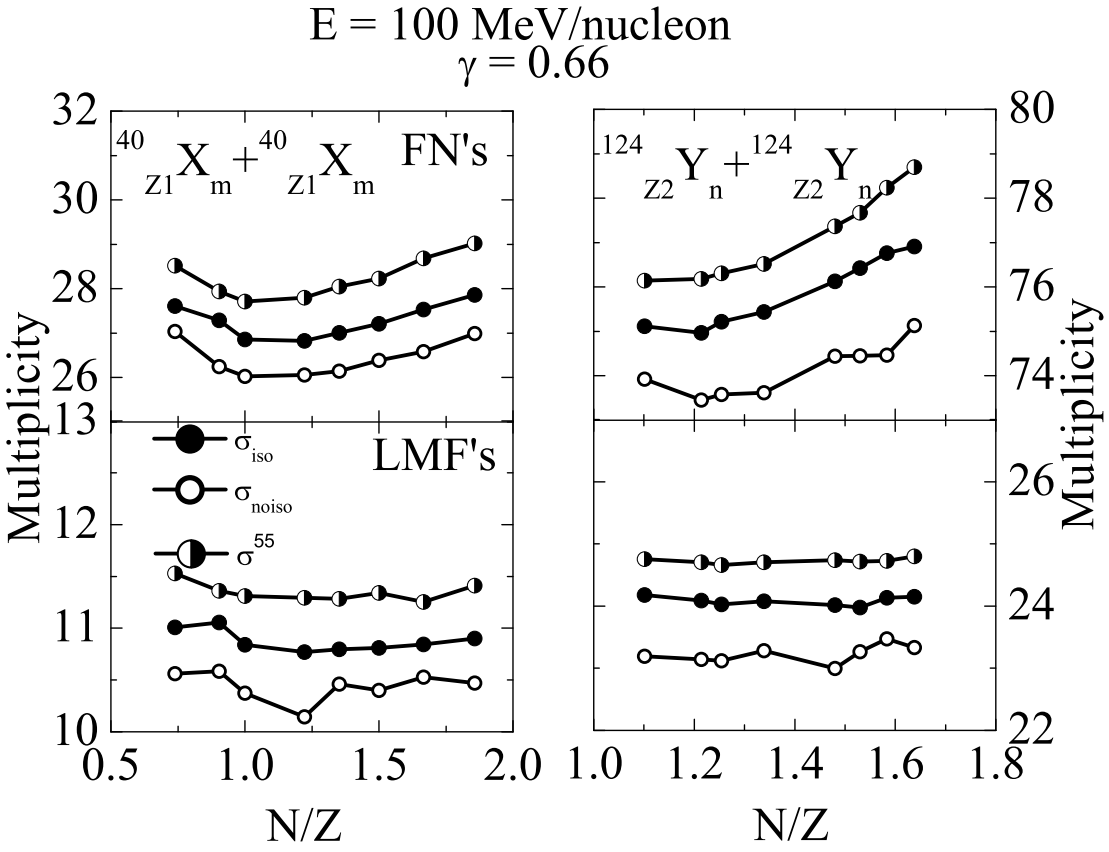

Figure 3.5: *Multiplicity of free nucleons and LMF's with N/Z. The left panels represents the set of reactions of* ${}^{40}_{Z_2}X_m + {}^{40}_{Z_2}X_m$*, where* Z_1 *= (14, 15, 16, 17, 18, 20, 21 and 23) and right panels for the reactions of* ${}^{124}_{Z_1}Y_n + {}^{124}_{Z_1}Y_n$*, where* Z_2 *= (47, 48, 49, 50, 53, 55, 56, and 59).*

display the multiplicity of FN's and LMF's as a function of N/Z of the system. Figure reveals that:

1. Multiplicity of the fragments is influenced by the isospin dependence of nucleon-nucleon cross-section. Multiplicity of FN's and LMF's increases for σ_{iso} ($\sigma_{np} = 3\sigma_{nn} = 3\sigma_{pp}$) compared to σ_{noiso} ($\sigma_{np} = \sigma_{nn} = \sigma_{pp}$). This is due to the increase in nucleon-nucleon binary collisions as discussed in chapter 1. If we fix cross-section to 55 mb, then multiplicity of FN's and LMF's is more compared to the other cross-sections due to further increase in nucleon-nucleon binary collisions.

2. Multiplicity is least when N/Z = 1, i.e. for symmetric collisions. The nuclei offer very interesting isospin situation where, the symmetry potential, Coulomb interaction and isospin-dependent nucleon-nucleon cross-section are simultaneously present. The Coulomb interaction is an important asymmetry term which can bring an important isospin effect into the observable quantities in the intermediate energy heavy-ion collisions.

3. The symmetry energy affects the multiplicity of LMF's more compared to FN's. The $(N - Z)^2$ plays a crucial role [157, 158, 169]. It has been observed that the isospin effects play more important role in LMF's compared to FN's.

From Fig.3.5, it is clear that minima in the fragment multiplicity is observed at N = Z in the case of FN's because they are produced from the participant zone. But for LMF's the fragment multiplicity is nearly constant. Moreover, it is clear from figure, that multiplicity of FN's and LMF's shows the similar trend for the two sets of reactions (one with mass = 40 units and other with mass = 124 units). However, for FN's the slope of the curve is steeper for the set of reactions with mass = 40 units compared to the set of reactions with mass = 124 units. This is due to the N/Z effect because the set of reactions with mass = 40 units are neutron-deficient reactions but the set of reactions with mass = 124 units are neutron-rich reactions.

3.3.3 Multiplicity of IMF's as a function of Z_{bound}

Fig.3.6, shows the mean multiplicity of IMF's as a function of Z_{bound}. The quantity Z_{bound} is defined as the sum of all atomic charges Z_i of all fragments with $Z_i > 2$. One can see that at semi-peripheral collisions, the multiplicity of IMF's shows a peak because most of the spectator part does not take part in the collision and hence large number of IMF's

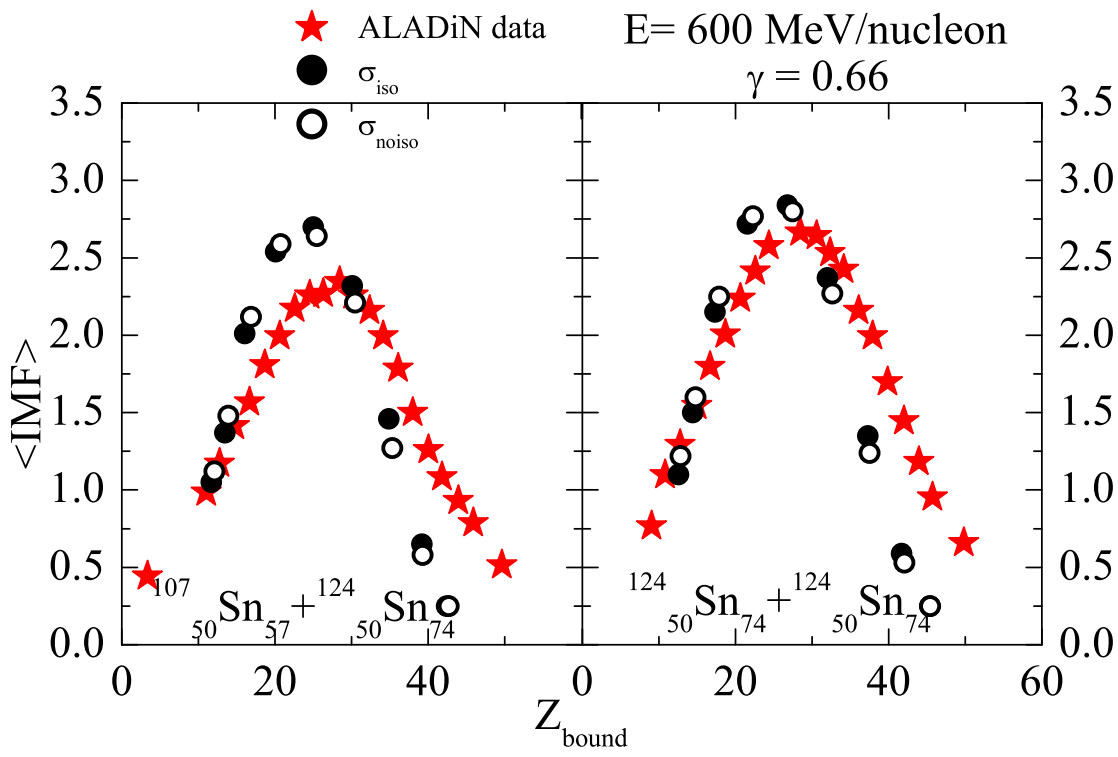

Figure 3.6: *Multiplicity of IMF's as a function of Z_{bound}. Experimental data has been taken from [75].*

are observed. At zero impact parameter, violent phase of collision occur and most of the nuclear matter emitted as FN's and LMF's. Therefore, only small number of IMF's are produced. At peripheral collisions, small portion of the target and the projectile overlap and again only small number of IMF's are observed because most of the fragments goes out as HMF's. In this way we get a clear "rise and fall" in multifragmentation emission. But the influence of isospin dependence of nucleon-nucleon cross-section is negligible because IMF's are produced from the spectator zone. Our theoretical calculations follow the similar trend as the experimental findings. One can see that for two choices of cross-section, we don't expect a significant difference on fragment production. Therefore, in multifragmentation we cannot pin down which choice of nucleon-nucleon cross-section is more realistic.

3.4 Summary

We have studied the influence of isospin dependence of nucleon-nucleon cross-section on the multiplicity of fragments. We find that, the isospin dependence of nucleon-nucleon cross-section shows a small influence on the multiplicity of FN's, LMF's and IMF's with incident energy. Moreover, we observe a uniform influence of σ_{iso} and σ_{noiso} on the N/Z dependence of FN's and LMF's. The multiplicity of FN's, LMF's and IMF's depends more on the mass of the colliding nuclei compared to the N/Z of the system. Comparison of theoretical calculations for both σ_{iso} and σ_{noiso} on the mean multiplicity of IMF's follow the similar trend with the experimental findings of ALADiN collaboration. From this we conclude that multifragmentation cannot be used to pin down which choice of nucleon-nucleon cross-section is more realistic.

Chapter 4

Thermalization in isospin asymmetric nuclear collisions

4.1 Introduction

The amount of nuclear stopping is defined as the percentage change of kinetic energy loss of the projectile nucleons in the nucleus-nucleus collision. It is of crucial importance for the increase of energy as well as for particle density. In order to get the first hand information for estimating the energy and particle density of the compressed nuclear matter at an early stage of the participant fireball, one of essential observable in heavy ion collision is the degree of nuclear stopping. It is closely related to the question, whether the thermalization (equilibrium) can be reached or not for a colliding system in order to obtain the information about the reaction dynamics. However, the story does not end here. Ions of heavy elements, such as gold, consists of many nucleons (protons and neutrons). The collision between two heavy ions is the superposition of many independent nucleon-nucleon collisions. Moreover, these collisions experienced by the nucleons are not independent, which makes the collision a little more complex. A nucleon of one nucleus can collide with many nucleons of the other nucleus and in this way it loses a large part of its energy in the collision region. Because of this energy loss a nucleon slows down as it passes through the nucleus, called *nuclear stopping*. The amount of stopping determines how much energy is lost by the nucleon. This problem has been studied extensively both theoretically as well as experimentally [170, 171]. Recently, Puri & co-workers [61] reported the correlation between multifragmentation and global nuclear stopping. Their findings revealed that light charged particles (LCP's) production behave in a similar fashion like anisotropy ratio. They, however did not take the isospin of the system into account.

Due to the advancement in the radioactive ion beam facilities, it become possible for the scientific community to investigate the isospin effects in heavy ion collisions [22, 23, 172] with respect to the above mentioned phenomena [36, 173, 174, 175, 176].

In low energy regime, systematic studies on isospin degree of freedom are available [177]. It has been reported in the literature that, in the energy region below Fermi energy, the nuclear stopping is sensitive to both the in-medium nucleon-nucleon cross-section and the symmetry potential. However, such studies at intermediate energy are rarely available [172]. One of the cause could be the much more complex dynamics involved at intermediate energies. Heavy ion collisions (HIC's) provide a unique opportunity to produce small amount of nuclear matter with high density and high temperature in a controlled fashion. The idea of studying nuclear stopping phenomena was introduced by Bass *et al.* [178] via the "isospin-mixing" method. In 1988, Bauer [179], pointed out that the nuclear stopping at intermediate energies is determined by both mean field as well as by in-medium nucleon-nucleon cross-section. It is worth mentioning that symmetry potential was not included in their analysis. G. Peilert *et al.* [180] suggested that the degree of approaching isospin equilibration provides a mean to probe the mechanism and power of the nuclear stopping in heavy ion collisions. Fu *et al.* [181] calculated both the radial flow and degree of nuclear stopping using the reactions of ${}^{207}_{82}Pb_{125} + {}^{207}_{82}Pb_{125}$ and ${}^{58}_{28}Ni_{30} + {}^{58}_{28}Ni_{30}$ at 0.4, 0.8 and 1.2 GeV/nucleon. They found that the expansion velocity as well as the degree of nuclear stopping are higher in heavier systems irrespective of the incident energy. Li *et al.* [182] studied the dependence of nuclear stopping $\langle\, Q_{ZZ}/A \,\rangle$ and $\langle\, \mathrm{R} \,\rangle$ in intermediate energy heavy-ion collisions on system size, initial N/Z, isospin symmetry potential and medium corrections of two-body cross-sections. They showed that the effect of initial N/Z ratio as well as of isospin symmetry potential is weak on nuclear stopping. The excitation function of $\langle\, Q_{ZZ}/A \,\rangle$ and $\langle\, \mathrm{R} \,\rangle$ however, depends on the form of the medium corrections of two-body cross-sections and on the equation of state of nuclear matter. Moreover, they showed that the behavior of excitation function of $\langle\, Q_{ZZ}/A \,\rangle$ and $\langle\, \mathrm{R} \,\rangle$ can provide clearer information about the isospin dependence of the medium correction of two-body cross-sections. Liu *et al.* [116] studied the nuclear stopping for various colliding systems with different neutron-proton ratios over large domains of incident energy. Nuclear stopping was found to be very sensitive towards the isospin content of in-medium nucleon-nucleon

cross-section above Fermi energy. The results were, however, insensitive towards the symmetry potential. They proposed that nuclear stopping can be used as a new probe to extract the information about the isospin dependence of the in-medium nucleon-nucleon cross-section in intermediate energy heavy ion collisions. However, Li *et al.* [183] showed that, traditional measures of the nuclear stopping power are found to be sensitive to the magnitude of the in-medium nucleon-nucleon cross-sections but they are ambiguous for determining the isospin dependence of the in-medium nucleon-nucleon cross-sections. One of us and co-workers [174, 184, 185, 186, 187] attempted to study the effect of symmetry energy and isospin-dependent nucleon-nucleon cross-section on nuclear stopping. Our findings revealed that the degree of stopping depends weakly on the symmetry energy and strongly on the isospin dependence of nucleon-nucleon cross-section. One more study by our co-worker [188] is carried out by varying the mass asymmetry of colliding pairs with different neutron-proton ratio keeping the total mass of the colliding nuclei fixed. Our findings revealed that, maximum stopping is achieved for nearly symmetric systems. Apart from this, participant-spectator matter plays important role in understanding the nuclear stopping. Sood *et al.* [174, 189] declared that, the participant matter can act as an indicator to nuclear stopping.

Motivated from the above discussion, here we plan to study how stopping (and/or thermalization/equilibrium) is affected when the N/Z ratio of the reacting partners is altered by adding protons to the system keeping the total mass fixed. Our present aim, therefore, is at least three fold:

1. To study the N/Z dependence of participant-spectator matter, anisotropic ratio $\langle R_a \rangle$ and relative momentum $\langle K_R \rangle$, at different incident energies and scaled impact parameters and to examine the influence of isospin-dependence of nucleon-nucleon cross-section on these quantities.

2. To study how the $\langle participant \rangle_{norm}$ (normalized participant matter) & $\langle R_a \rangle$ and $\langle spectator \rangle_{norm}$ (normalized spectator matter) & $\langle K_R \rangle$ are related to each other. Where $\langle R_a \rangle$ and $\langle K_R \rangle$ are the indicator of global and local equilibrium respectively.

3. To pin down the influence of change in N/Z of the system as well as the isospin dependence of nucleon-nucleon cross-section on nuclear stopping.

4.2 Participant-spectator matter and origin of nuclear stopping

The global nuclear stopping is defined as the randomization of one-body momentum space or memory loss of the incoming momentum. At lower incident energies, all projectile and target nucleons form a compound nucleus [190]. This results in fusion and consequently in decay. The formation and the decay of the compound nucleus are completely independent. Thus, the emitted particles do not show any correlation with the entrance channel. However, both the mean-field as well as the nucleon-nucleon collisions are equally important at intermediate energies. The nucleon-nucleon collisions play an important role in destroying the mutual initial correlations and memory of nucleons. More the initial memory of nucleons is erased, better it is stopped and better one has average mixing of projectile and target momentum. The degree of stopping however, may vary drastically with incident energy, mass of colliding nuclei and colliding geometry. The colliding nuclei not only compress each other, they also heat the matter. In addition, the destruction of initial correlations, makes the matter homogeneous and one can have global stopping. A complete knowledge about the degree of stopping is very important since it can be connected to the different properties of the system and in-medium properties of the nucleon-nucleon cross-section. This picture can also be looked at in terms of participant-spectator matter and the fireball concept. Fig.4.1, shows the initial and final phase space of a single event of ${}^{197}_{79}Au_{118} + {}^{197}_{79}Au_{118}$ at an incident energy of 100 MeV/nucleon. Left panels display the results at $\hat{b} = 0$ and right panels at $\hat{b} = 0.9$ respectively. The participants are those nucleons that are located in the geometrical overlap of the projectile and the target. These nucleons interact strongly giving rise to a high density region, known as the fireball. It is clear from the figure that for central collisions (i.e. at $\hat{b} = 0$) the whole of the matter act as the participant matter. But for peripheral collisions (i.e. at $\hat{b} = 0.9$), the number of nucleons participating in the geometrical overlap of the two colliding nuclei decreases (shown by shaded region). Those parts of the nuclei that do not belong to the overlap region between the projectile and target (i.e. the volume that is not cut out of the projectile and target when they are supposed to move through each other on straight lines) are called spectators (shown in upper right panel of Fig.4.1). They are unaffected by the collision except for Coulomb potential and they retain their initial momentum, flying

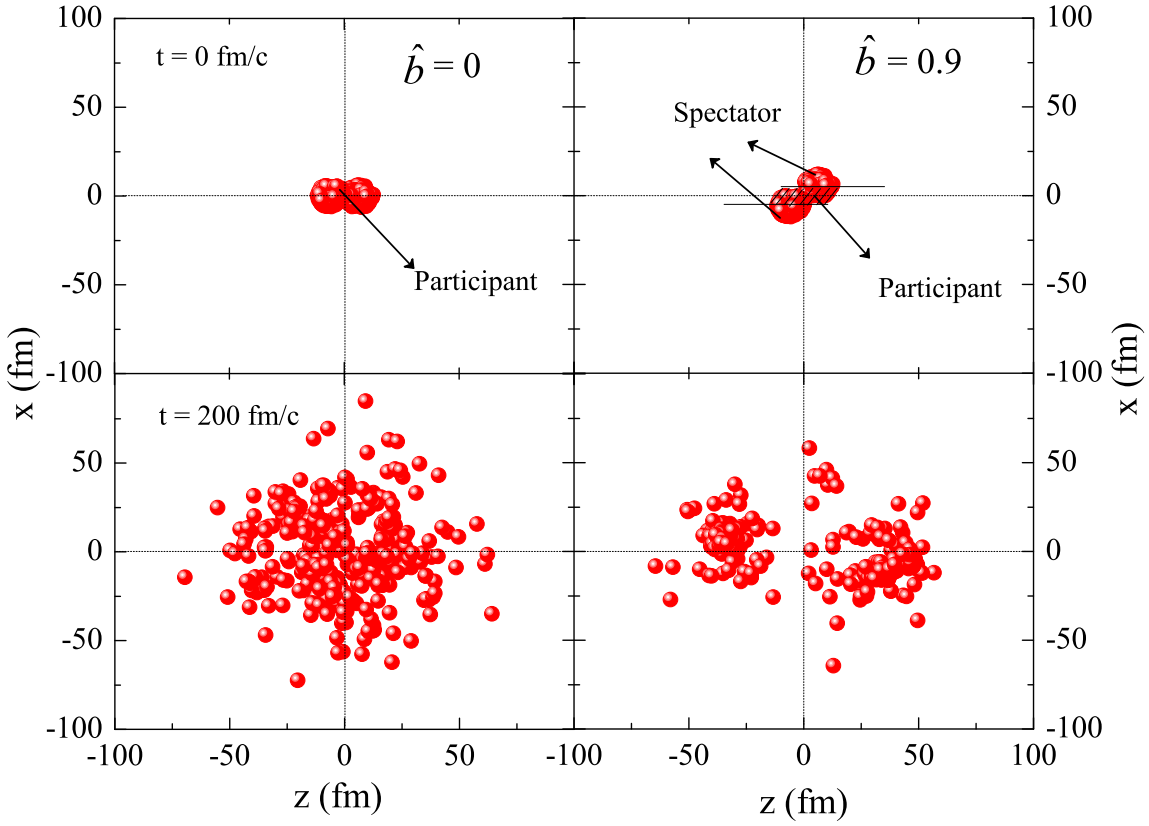

Figure 4.1: *The initial and final phase space of a single event of* $^{197}_{79}Au_{118} + ^{197}_{79}Au_{118}$ *at incident energy of 100 MeV/nucleon. Left panels display the results at* $\hat{b} = 0$ *and right panels at* $\hat{b} = 0.9$*, respectively.*

away from the fireball. The first model which has been developed from this concept is the fireball [191, 192] model. One can see that central collisions lead to complete spherical distribution of particles at the freeze-out time, indicating, spreading of the nucleons in all directions. It means that breaking of initial correlations among nucleons is maximal in this region and, as a result, more randomization and stopping in the hot and compressed nuclear matter occurs. This effect seems to decrease with impact parameter. Puri and co-workers [189] studied the participant-spectator matter and nuclear dynamics for stable systems. Their study revealed that for stable systems, the participant-spectator matter at E_{bal} is quite insensitive to the mass of the colliding nuclei.

Excited nuclear matter is produced in the collision of two nuclei [17, 193] at higher incident energy. Alternatively, one can talk about a shift of rapidity from the beam rapidity towards the mid-rapidity region [194]. This deceleration in the longitudinal direction is

called nuclear stopping power. To quantify the nuclear stopping it is common to look at baryon rapidity distributions, i.e. the number of net-baryons per rapidity bin as a function of rapidity. Since baryon number is a conserved quantity the integral of this distribution is known. It simply equals the number of participants which can be calculated in Monte-Carlo models. The shape of this distribution, and in particular its width, depends strongly on the nature of the successive collisions and is thereby expected to change with the oncoming of new physics [24, 195, 196].

4.3 Parameters for describing Nuclear Stopping

4.3.1 Rapidity distribution

The rapidity distribution $Y(i)$ [61, 112], defined as:

$$Y(i) = \frac{1}{2} ln \frac{E(i) + p_z(i)c}{E(i) - p_z(i)c}, \tag{4.1}$$

Where, $E(i)$ and $p_z(i)$ are the total energy and longitudinal momentum, respectively and c is the velocity of light and its value is taken to be equal to one. For a complete stopping, one expects a single Gaussian shape. Obviously, narrow Gaussian indicate better thermalization compared to broader Gaussian. Very often, the nature of emitting source is defined by analyzing the rapidity distribution.

4.3.2 Anisotropy ratio

The $\langle R_a \rangle$ is defined as [197]:

$$\langle R_a \rangle = \frac{\sqrt{p_x^2} + \sqrt{p_y^2}}{2\sqrt{p_z^2}} = \frac{(\sum_i p_\perp(i))}{2\left(\sum_i p_\parallel(i)\right)} \tag{4.2}$$

This anisotropy ratio is an indicator of the global equilibrium of the system. The word global indicates that this quantity does not depend on the local density and thus represents the equilibrium of the whole system. A global equilibrium is reached when $\langle R_a \rangle$ is close to one. This anisotropy ratio then further improved by the experimental groups in order to achieve the full stopping for fully thermalized systems. The multiplying factor of $\frac{1}{2}$ then replaced by $\frac{2}{\pi}$. The anisotropy ratio then is $\langle$ R $\rangle$ [116], defined as:

$$\langle R \rangle = \frac{2}{\pi} \frac{(\sum_i p_\perp(i))}{\left(\sum_i p_\parallel(i)\right)} \tag{4.3}$$

where $p_{\perp}(i) = \sqrt{(p_x^2(i) + p_y^2(i)}$ and $p_{\parallel}(i) = p_z(i)$ respectively. If $\langle$ R $\rangle$ =1, then it means complete stopping.

4.3.3 Quadrupole Momentum

The quadrupole momentum $\langle\ Q_{ZZ}\ \rangle$ [116], defined as:

$$\langle Q_{ZZ} \rangle = \sum_i \left[2p_z^2(i) - p_x^2(i) - p_y^2(i) \right] \tag{4.4}$$

For complete stopping $\langle\ Q_{ZZ}\ \rangle$ =0.

4.3.4 Relative momentum

The relative momentum $\langle K_R \rangle$ of two colliding Fermi spheres is defined as [198, 199]:

$$\langle K_R \rangle = \langle \frac{|p_P(r,t) - p_T(r,t)|}{\hbar} \rangle \tag{4.5}$$

$$where, \quad p_i(r,t) = \frac{\sum_{j=1}^{A} p_j(t)\rho_j(r,t)}{\rho_j(r,t)} \quad i = 1, 2, \tag{4.6}$$

where, p_j and ρ_j are the momentum and density of the j^{th} particle and i stands for either projectile or target. The $\langle K_R \rangle$ is the indicator of local equilibrium because it depends also on the local position r. In all the above parameters, the averaging in done over the number of events.

4.4 Results and discussion

The ultimate goal to study the role of isospin degree of freedom in both nuclear physics and astrophysics is to extract the information about the isospin dependence of in-medium nuclear effective interactions for the nuclei away from the line of stability. The later quantity especially the symmetry energy term is important for both nuclear physics and astrophysics community. Here we aim to explore the effect of isospin dependence of nucleon-nucleon cross-section on neutron rich colliding systems by taking the concept of participant/spectator and nuclear stopping. For the present analysis, simulations are carried out for the reactions of, ${}^{40}_{Z_1}X_m + {}^{40}_{Z_1}X_m$, where Z_1 = (14, 15, 16, 17, 18, 20, 21 and 23), respectively using soft equation of state and density dependence of symmetry energy with stiffness parameter $\gamma = 0.66$. In addition, the reactions of ${}^{124}_{Z_2}Y_n + {}^{124}_{Z_2}Y_n$, where Z_2 = (47, 48,

49, 50, 53, 55, 56, and 59), respectively are also simulated to see the system mass and N/Z effects on the participant/spectator matter and nuclear stopping at an incident energy between 100 and 300 MeV/nucleon spanning over the entire colliding geometry [200, 201].

4.4.1 The N/Z dependence of participant/spectator matter

4.4.1.1 At fixed colliding geometry

In the present study we define the participant-spectator matter in two different ways:

1. In first case, all nucleons experiencing at least one collision are labeled as participant matter. The remaining nucleons are the part of spectator matter.

2. In second case, we use different rapidity cuts to define participant and spectator matter. These definitions give us the possibility of analyzing the reactions in terms of participant-spectator fireball model.
   The analysis is carried out for the reactions of ${}^{124}_{Z_2}Y_n + {}^{124}_{Z_2}Y_n$, where Z_2 = (47, 50, 53, 56, and 59)

In Fig.4.2, we display the N/Z dependence of participant and spectator matter (defined in terms of number of collisions suffered by the nucleons) at an incident energy between E = 100 and 300 MeV/nucleon for central colliding geometry. Upper (lower) panel displays the participant (spectator) matter. The lines are the linear fit to the theoretical results of the kind:

$$t = t_0 + a \times q, \tag{4.7}$$

where, 'a' is the slope of the curve and t_0 is the t-intercept. We find that:

1. Participant (spectator) matter decreases (increases) with increase in the neutron content of the system. This decrease (increase) in participant (spectator) matter is due to the higher role of repulsive symmetry energy in systems with higher N/Z (which leads to lesser number of collisions due to repulsive nature of symmetry energy).

2. Participant matter increases with increase in the incident energy. This happens because, with increase in incident energy the collision rate increases.

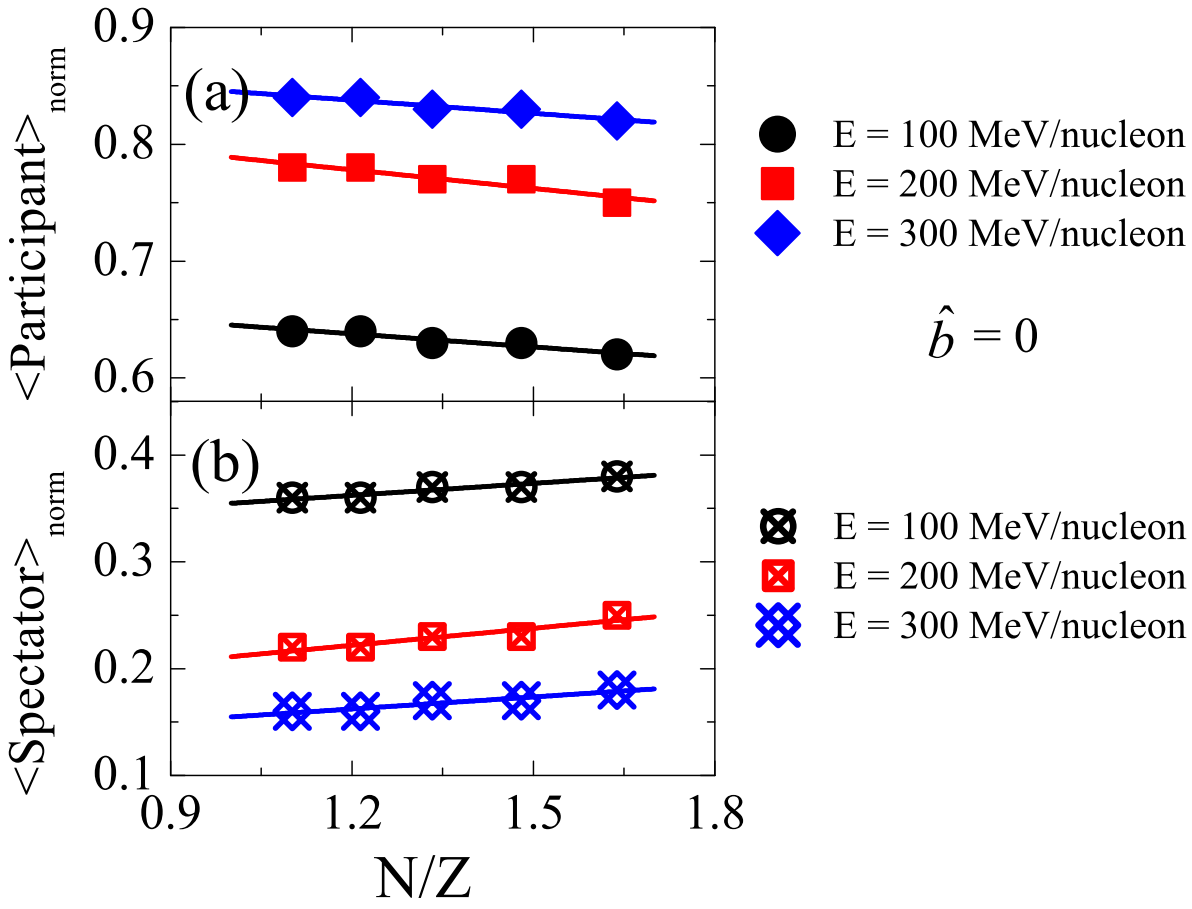

Figure 4.2: *The N/Z dependence of participant and spectator matter for central collision at an incident energy between E = 100 and 300 MeV/nucleon.*

4.4.1.2 At fixed incident energy

As we have discussed in section 4.2, that participant/spectator matter is directly related to the colliding geometry of two nuclei. Therefore, after analyzing the role of incident energy on the N/Z dependence of participant/spectator matter, as a next step, we shall study the role of colliding geometry on the N/Z dependence of participant/spectator matter at fixed incident energy. For this, we display in Fig.4.3, the N/Z dependence of participant and spectator matter at an incident energy of E = 100 MeV/nucleon at different colliding geometry range varying from $\hat{b} = 0.0$ to 0.4. Upper (lower) panel display the participant (spectator) matter. We find that, participant (spectator) matter decreases (increases) slightly with N/Z ratio of the system as explained in Fig.4.2. Moreover, participant matter decreases with increase in the scaled impact parameter. This happens because, as we move from central to semi-peripheral geometry the geometrical overlapping

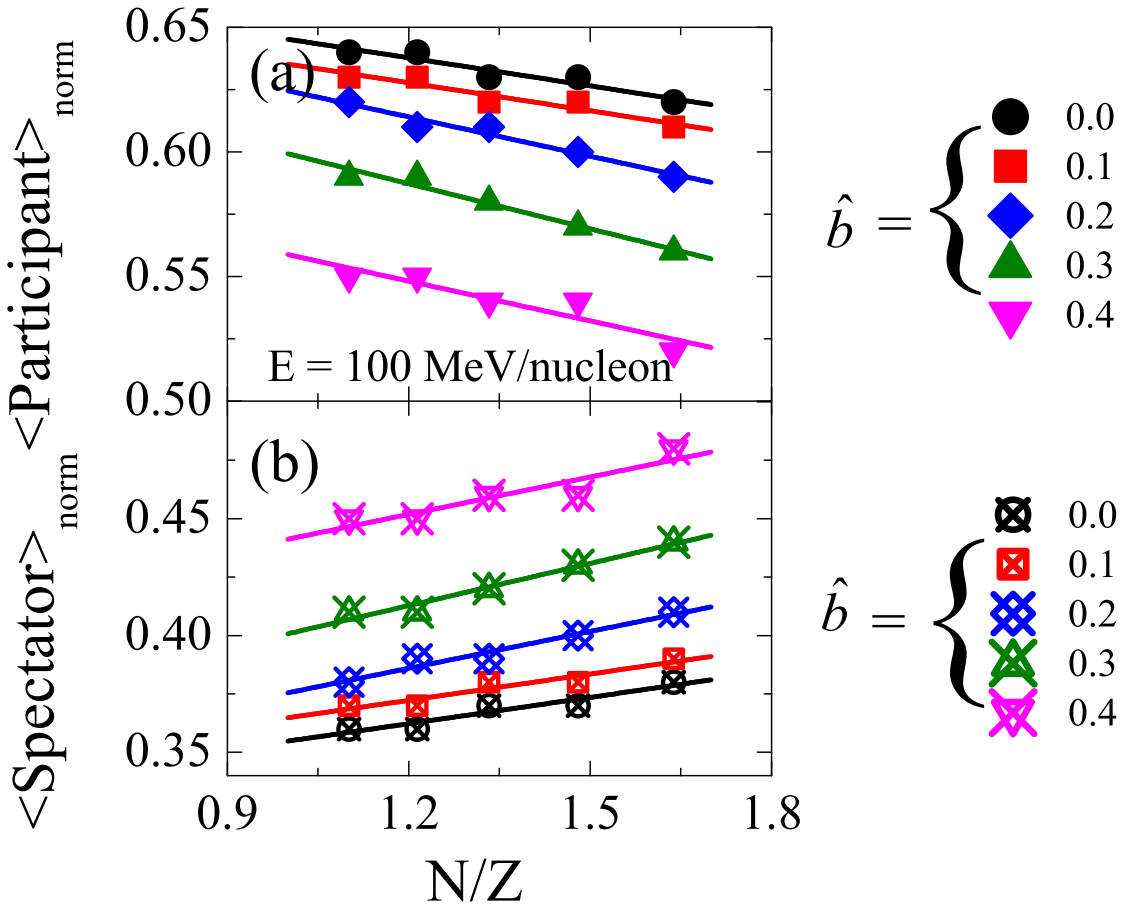

Figure 4.3: *The N/Z dependence of participant and spectator matter at an incident energy of E = 100 MeV/nucleon and for different scaled impact parameters $\hat{b}$ = 0.0, 0.1, 0.2, 0.3 and 0.4.*

region of two colliding nuclei decreases and hence decrease is observed in the participant matter.

4.4.1.3 At fixed colliding geometry for different rapidity bins

In Fig.4.4, we display the N/Z dependence of participant and spectator matter (defined

Table 4.1: *%age of participant matter in different rapidity bins.*

Energy (MeV/nucleon)	BIN 1	BIN 2	BIN 3
100	9.6%	85%	99%
200	10%	90%	99.2%
300	12%	93%	100%

in terms of different rapidity cuts) as: $-0.1 \leq Y^{red} \leq 0.1$ (BIN 1), $-1.0 \leq Y^{red} \leq 1.0$ (BIN 2) and $-1.5 \leq Y^{red} \leq 1.5$ (BIN 3) for central collision at incident energy between

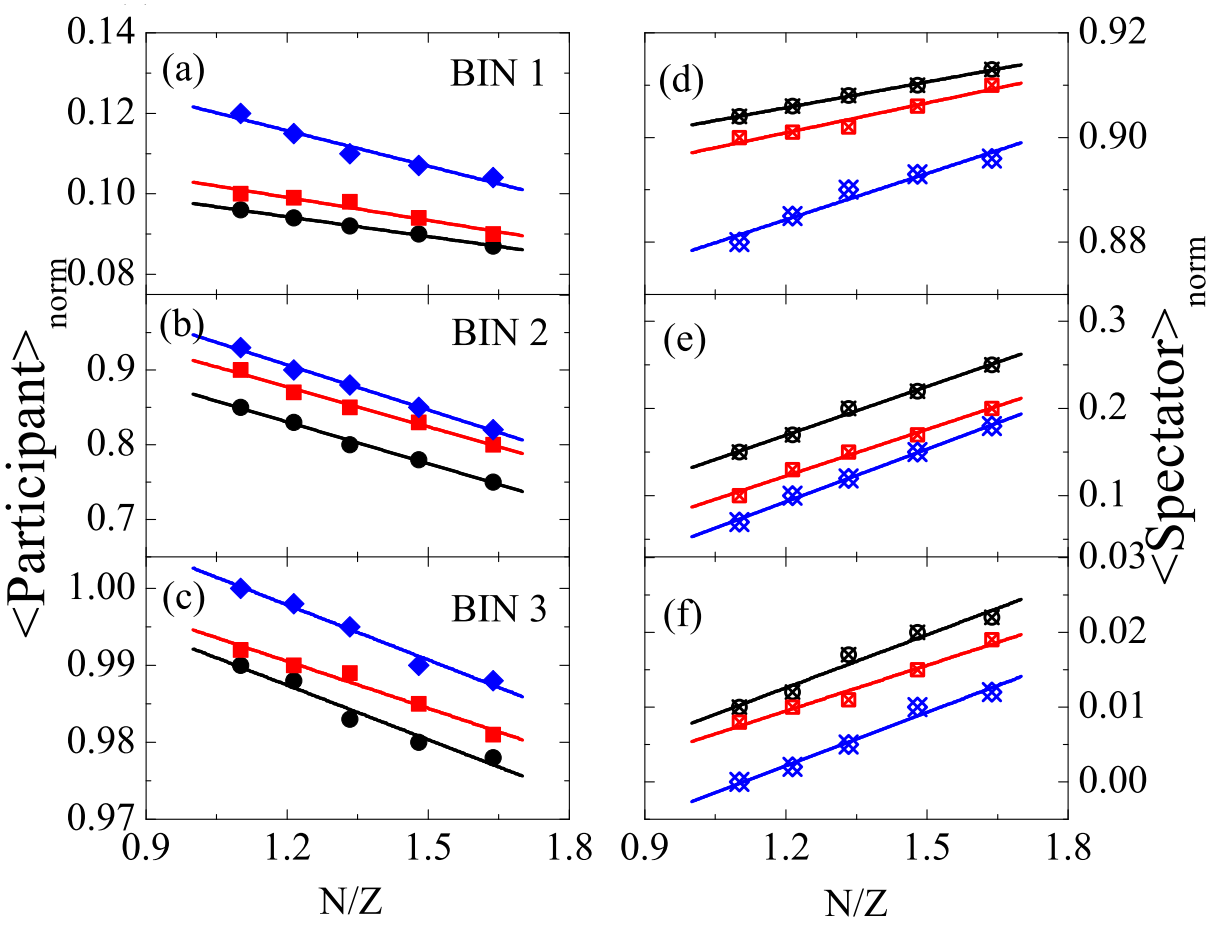

Figure 4.4: *The N/Z dependence of participant and spectator matter for three different rapidity bins at incident energy between E = 100 and 300 MeV/nucleon. Symbols have the same meaning as in Fig.4.2.*

Table 4.2: *%age of spectator matter in different rapidity bins.*

Energy (MeV/nucleon)	BIN 1	BIN 2	BIN 3
100	90.4%	15%	1%
200	90%	10%	0.8%
300	88%	7%	0%

E = 100 and 300 MeV/nucleon. The region $-0.1 \leq Y^{red} \leq 0.1$ is specified as the mid-rapidity region in the literature [85, 202] where $Y^{red} = Y_{c.m.}(i)/Y_{beam}$. The region from -0.1 towards the negative side approaches a target-like (TL) spectator, while the other side is known as projectile-like (PL) spectator. From figure it has been observed that:

1. The participant (spectator) matter decreases (increases) with increase in N/Z of the system as explained in Fig.4.2.

2. The participant (spectator) matter increases (decrease) with incident energy. This is because with increase in incident energy the excitation among the nucleons increases. Therefore, the participant zone expand due to the formation of high density zone, results in the increase in the collision rate.

3. The participant (spectator) matter change drastically by changing these rapidity bins. The percentage change in the value of participant and spectator matter at different incident energies for N/Z = 1.101 is given in the Tables 4.1 & 4.2. It is clear from the tables, that the percentage of participant and spectator change drastically as we move from BIN 1 to BIN 3. This happens because, the number of nucleons participating in the collision increases as we move from BIN 1 to BIN 3.

4.4.1.4 At fixed incident energy for different rapidity bins

As discussed earlier, the geometry of collisions can be well described in terms of participant/spectator matter. The dynamics of participant pieces is described as a superposition of single knock-out & multiple nucleon-nucleon scattering. To study the effect of colliding geometry on the participant-spectator matter for three different rapidity bins, we display in Fig.4.5, the N/Z dependence of participant and spectator matter for three different rapidity bins and the geometry varies from central to semi-peripheral. From figure, one can see that, participant (spectator) matter decreases as we move from central ($\hat{b} = 0$) to semi-peripheral ($\hat{b} = 0.4$) geometry. This is due to the decrease in the participant zone.

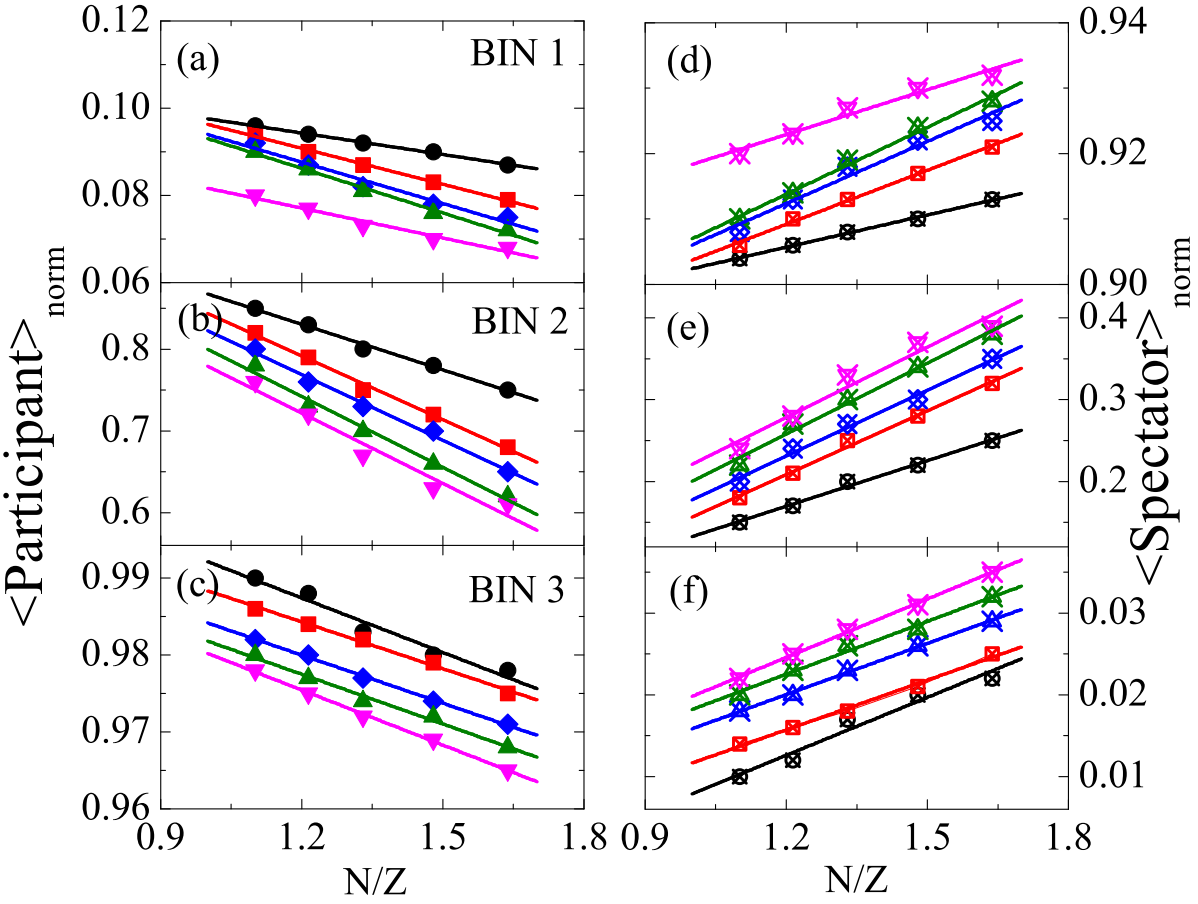

Figure 4.5: *The N/Z dependence of participant and spectator matter for three different rapidity bins and the geometry varies from central to semi-peripheral. Symbols have the same meaning as in Fig.4.3.*

As in Fig.4.4, in this case also, the participant (spectator) matter decrease (increase) with increase in N/Z of the system at all colliding geometries.

On comparing Figs.4.2, 4.3, 4.4 & 4.5 one can conclude that, whatever be the definition of participant matter, it may either in terms of nucleon-nucleon collisions or in terms of different rapidity cuts, the trend remain same. These findings are also in agreement with Ref. [189].

4.4.1.5 At fixed incident energy for isospin dependent and independent cross-sections

Next, to study the influence of isospin dependence of nucleon-nucleon cross-section we calculate the $\langle participant \rangle_{norm}$ and $\langle spectator \rangle_{norm}$ with an isospin independent cross-section. This is done by putting $\sigma_{np} = \sigma_{nn} = \sigma_{pp}$ and labeled as σ_{noiso}. The results are displyed in Fig.4.6, for the N/Z dependence of participant and spectator matter at an incident energy of E = 100 MeV/nucleon and for different scaled impact parameters $\hat{b}$ = 0.0, 0.1, 0.2, 0.3 and 0.4. It has been observed that:

1. Participant matter increases for isospin dependent cross-section. This happens because in the case of isospin dependent cross-section, neutron-proton cross-section is three times larger compared to neutron-neutron and proton-proton cross-section [24, 115] that will enhance binary collisions and hence the participant matter.

2. The difference in the distribution of participant and spectator remain almost same at all colliding geometries.

3. The participant (spectator) matter decreases (increases) with increase in N/Z of the system as explained in Fig.4.2.

4.4.2 N/Z dependence of anisotropy ratio and relative momentum

As we have mentioned in the previous section that in addition to global stopping and randomization of phase space, one may also define the local mixing of target and projectile. Here one studies, the relative momentum of two colliding fermi spheres which indicates the deviation from mixing. The concept of local stopping is used by the hydrodynamical models to simulate the heavy ion reactions. All these definitions will give us glimpse of the degree of stopping or mixing (or equilibrium) reached in a reaction. We display in Fig.

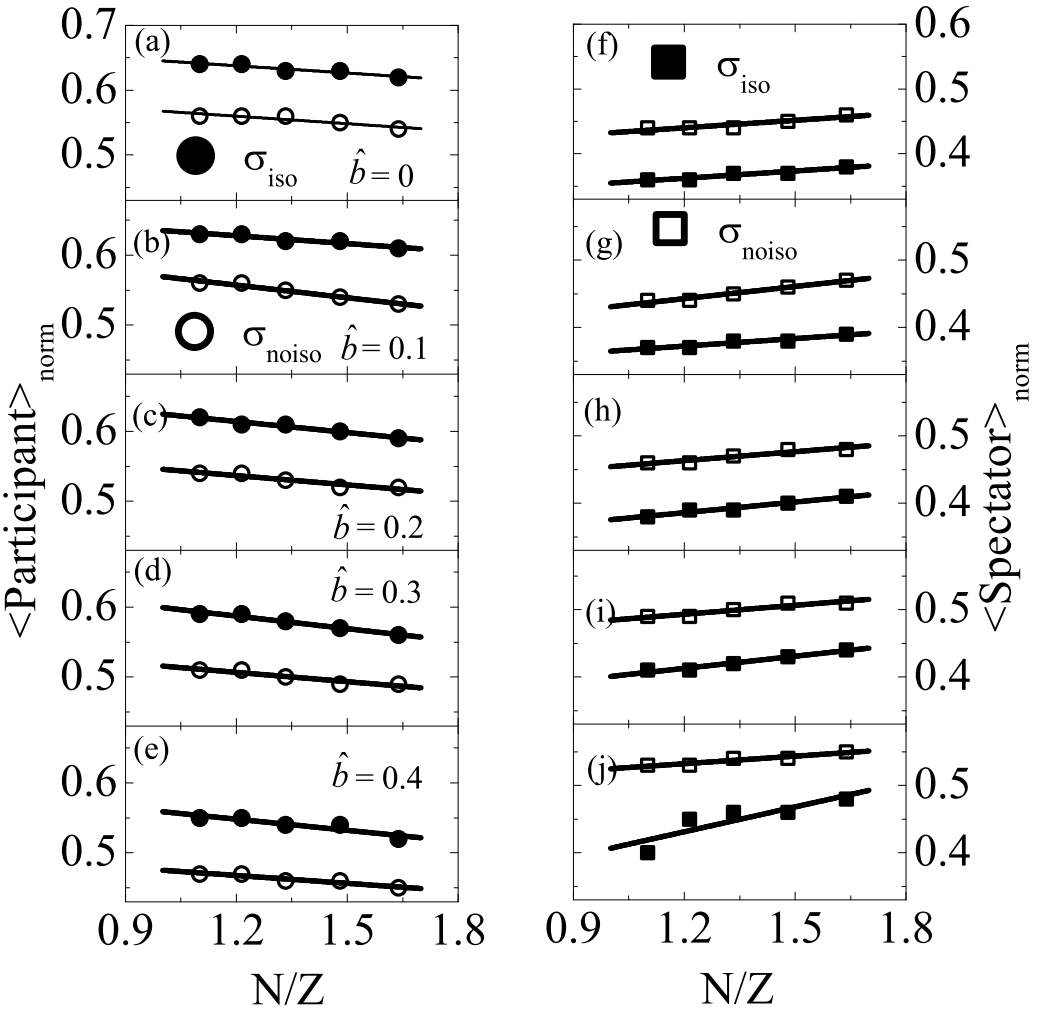

Figure 4.6: *The N/Z dependence of participant and spectator matter for isospin dependent (σ_{iso}) and isospin independent σ_{noiso} cross-section at an incident energy of E = 100 MeV/nucleon and for different scaled impact parameters $\hat{b}$ = 0.0, 0.1, 0.2, 0.3 and 0.4.*

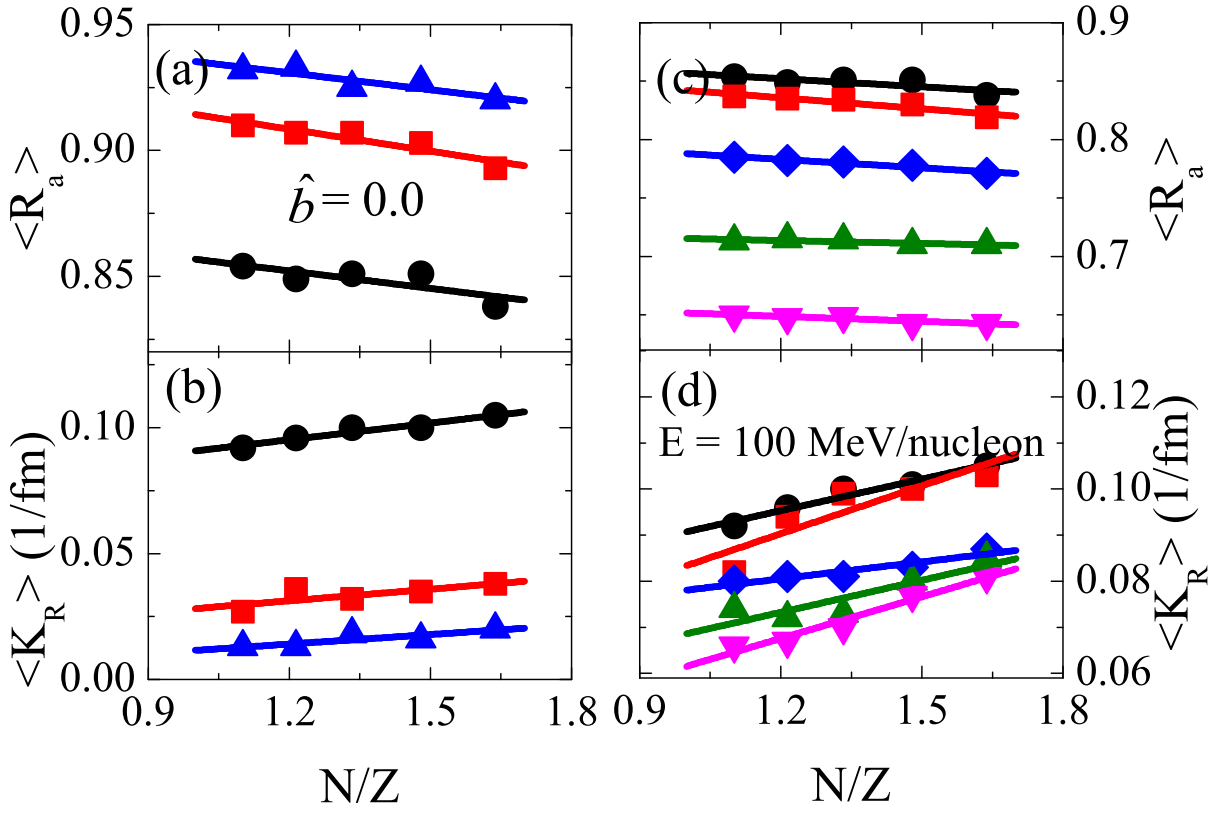

Figure 4.7: *Panels (a) and (b) represents the N/Z dependence of anisotropic ratio* $\langle R_a \rangle$ *and relative momentum* $\langle K_R \rangle$ *for central collision at incident energy between E = 100 and 300 MeV/nucleon and panels (c) and (d) represents the N/Z dependence of anisotropic ratio* $\langle R_a \rangle$ *and relative momentum* $\langle K_R \rangle$ *at incident energy of E = 100 MeV/nucleon for scaled impact parameters* $\hat{b}$ *= 0.0, 0.1, 0.2, 0.3 and 0.4. Symbols have the same meaning as in Fig.4.2 and 4.3.*

4.7(a) and 4.7(b), the N/Z dependence of anisotropic ratio $\langle R_a \rangle$ and relative momentum $\langle K_R \rangle$ (thermalization parameters) for central collision at an incident energy between E = 100 and 300 MeV/nucleon. Figure reveals that, anisotropy ratio decreases with increase in N/Z of the system. This decrease in the charge particle (protons) concentration tends to decrease the nuclear stopping due to the lesser Coulomb repulsion between the target and projectile for higher N/Z values. Moreover, $\langle R_a \rangle$ increases with increase in incident energy. From Fig.4.7(b), we see that, $\langle K_R \rangle$ increases with increase in N/Z of the system. This is because, increase in N/Z of the system leads to change in interaction among the nucleons. That results in increase in their relative momentum. Moreover, $\langle K_R \rangle$ decreases with increase in incident energy. Further, to study the effect of colliding geometry on the anisotropy ratio $\langle R_a \rangle$ and relative momentum $\langle K_R \rangle$, we display in Fig.4.7(c) and 4.7(d), the N/Z dependence of anisotropic ratio $\langle R_a \rangle$ and relative momentum $\langle K_R \rangle$ at an incident energy of E = 100 MeV/nucleon and scaled impact parameters of $\hat{b}$ = 0.0, 0.1, 0.2, 0.3 and 0.4. As stated earlier, the $\langle R_a \rangle$ ratio is a direct indicator of breaking the initial correlation and erasing the memory of nucleons. We can see from Fig.4.7(c) that behavior is similar for both central and semi-peripheral collisions. One can also notices that best stopping ($\langle R_a \rangle$ = 0.854) is observed in case of central collisions for the system with N/Z = 1.101 compared to semi-peripheral collision ($\hat{b}$ = 0.4) where $\langle R_a \rangle$ = 0.65 for same N/Z. This is because, $\hat{b}$ = 0.0 corresponds to an increase in the participant zone due to which the nuclear stopping tends to increase. From Fig.4.7(d), one can see that behavior of $\langle K_R \rangle$ is also similar for both central and semi-peripheral collision. Moreover, $\langle K_R \rangle$ increases with increase in N/Z of the system. Moreover, $\langle K_R \rangle$ decreases with increase in scaled impact parameter. This is because, for central collision the interactions among the nucleons increases due to the increase in the participant zone and thus the relative momentum increases compared to $\hat{b}$ = 0.4.

It is a well known fact that, participant zone contain the nucleons which directly comes from the geometrical overlap of two colliding nuclei. In other words, these nucleons can also act as the barometer for studying the stopping in heavy ion collisions. To study how the $\langle participant \rangle_{norm}$ & $\langle R_a \rangle$ and $\langle spectator \rangle_{norm}$ & $\langle K_R \rangle$ are related to each other we display, in Fig.4.8 the impact parameter dependence of the slope of the curves for $\langle participant \rangle_{norm}$ and $\langle R_a \rangle$, which is extracted from Fig.4.3. It has been observed that,

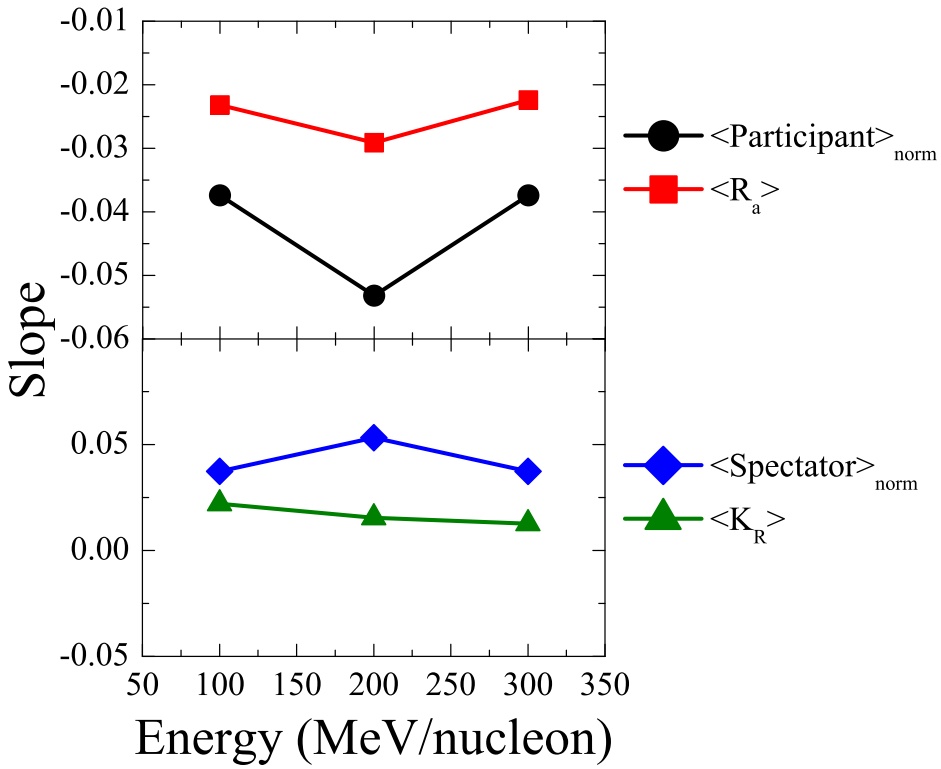

Figure 4.8: *Energy dependence of the slope of the curves for* $\langle participant \rangle_{norm}$ *and* $\langle R_a \rangle$.

slope of both the $\langle participant \rangle_{norm}$ and $\langle R_a \rangle$ (indicator of global equilibrium of the system) follow the similar trend. From this one can see that variation of slope of $\langle participant \rangle_{norm}$ with energy give indication about the global equilibrium of the system. Moreover, slope of both the $\langle spectator \rangle_{norm}$ and $\langle K_R \rangle$ (indicator of local equilibrium of the system) follow the similar trend. Thus, we can say that variation of slope of $\langle spectator \rangle_{norm}$ with energy give indication about the local equilibrium of the system.

From the above study, it has been observed that participant/spectator matter depends crucially on the collision dynamics as well as on the history of nucleons and important changes in the momentum space occur due to the binary nucleon-nucleon collisions experienced during the high density phase. These collisions push the colliding nucleons into mid-rapidity region responsible for the formation of participant matter. This ultimately leads to the thermalization in heavy-ion collisions. To study the effect of isospin dependent cross-section on anisotropy ratio $\langle R_a \rangle$ and relative momentum $\langle K_R \rangle$, we display in Fig.4.9, the N/Z dependence of anisotropic ratio $\langle R_a \rangle$ and relative momentum $\langle K_R \rangle$ for isospin dependent (σ_{iso}) and isospin independent (σ_{noiso}) cross-section for central collision

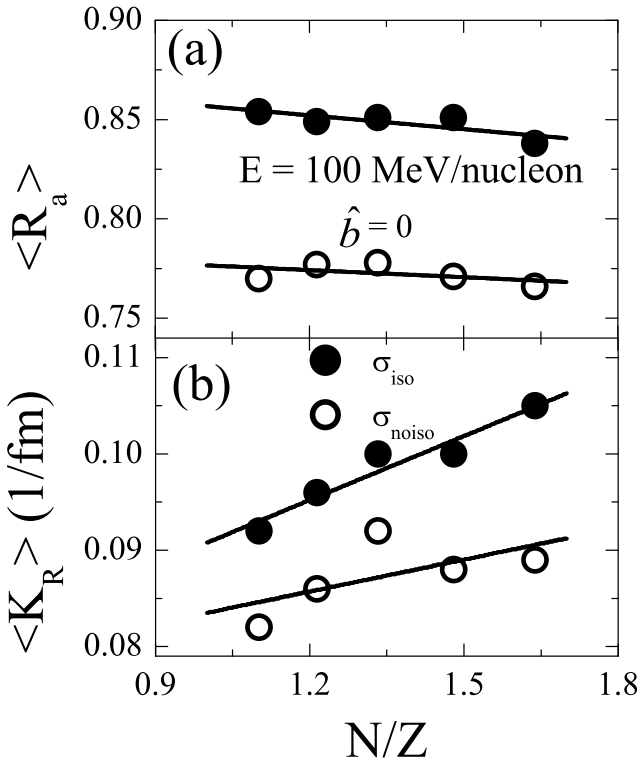

Figure 4.9: *The N/Z dependence of anisotropic ratio $\langle R_a \rangle$ and relative momentum $\langle K_R \rangle$ for isospin dependent (σ_{iso}) and isospin independent σ_{noiso} cross-section for central collision at an incident energy of E = 100 MeV/nucleon.*

at an incident energy of E = 100 MeV/nucleon. It has been observed that $\langle R_a \rangle$ as well as $\langle K_R \rangle$ increases for σ_{iso} compared to σ_{noiso} due to increase in participant zone. Therefore, the nuclear stopping as well as the relative momentum increases.

A study by Dhawan *et al.* [61] suggested that light charged particles (LCP's) can be used as a barometer for studying the stopping in heavy ion collisions. This is because light fragments mostly originate from the mid-rapidity region. Moreover, Vermani *et al.* [173] used rapidity distribution of nucleons to characterize the stopping and thermalization of nuclear matter. They found that nearly full stopping is achieved in heavier systems like Au+Au. Whereas in lighter systems a large fraction of particles is concentrated near the target and projectile rapidities resulting in the broad Gaussian shape, resulting in less stopping. However, all these studies were silent about the change in neutron to proton content of the system as well as the isospin dependence of nucleon-nucleon cross-section on the rapidity distribution of FN's and LMF's. We shall discuss these facts in the following

subsections.

4.4.3 Isospin effects on the rapidity distribution for the emission of FN's and LMF's

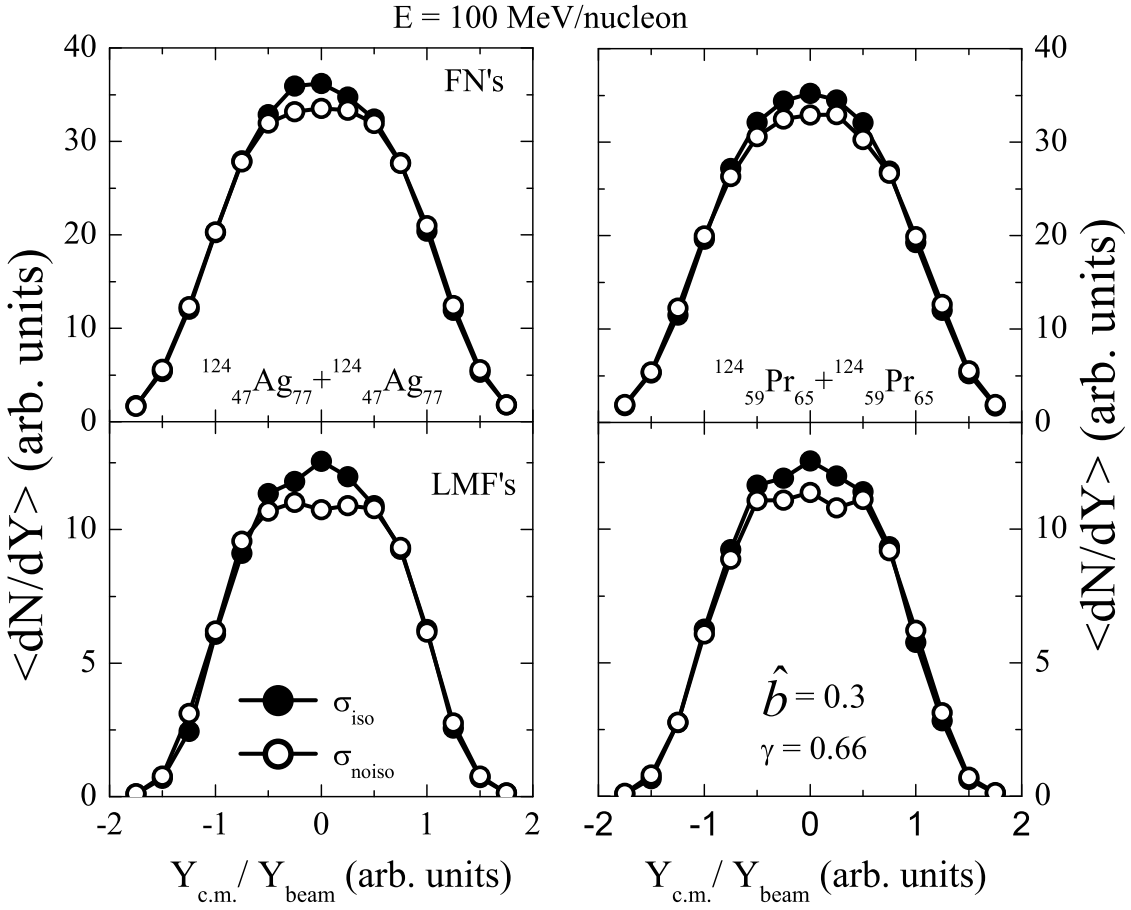

Figure 4.10: *Rapidity distribution of FN's and LMF's.*

Fig.4.10 shows the rapidity distribution $\langle$ dN/dY $\rangle$ for the emission of FN's and LMF's at incident energy of E = 100 MeV/nucleon. This choice of reaction panels will throw light on the change in N/Z ratio of the system on the rapidity distribution for the emission of FN's and LMF's. As noted by many authors, FN's and LMF's are produced from the participant zone whereas IMF's are mostly produced out of the spectator matter.
We also noted clear isospin effects on the rapidity distribution of FN's and LMF's in mid-rapidity region. This is because σ_{iso} (near mid rapidity) will enhance the binary collisions that results in enhanced production. This effect should diminish as we move away from the mid-rapidity region where either target like or projectile like process dominates.

Strikingly, a very little influence (less than 3%) is noted due to the change in N/Z of the colliding systems. Note that while mass remains fixed, charge of the colliding nuclei varies from 47 units to 59 units.

4.4.4 Impact parameter dependence of $\langle$ R $\rangle$ and $\langle$ $1/Q_{ZZ}$ $\rangle$

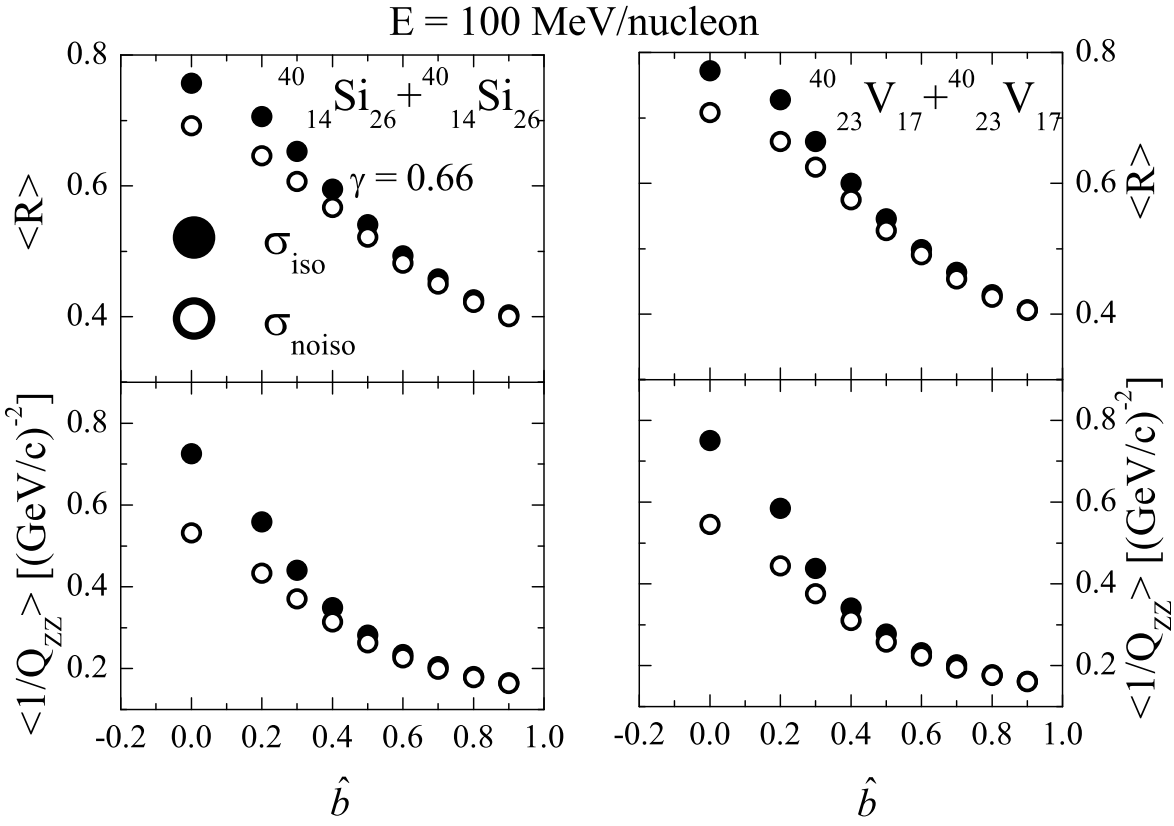

Figure 4.11: *Variation of* $\langle$ R $\rangle$ *and* $\langle$ $1/Q_{ZZ}$ $\rangle$ *as a function of scaled impact parameter for the reactions of* $^{40}_{14}Si_{26}+^{40}_{14}Si_{26}$ *and* $^{40}_{23}V_{17}+^{40}_{23}V_{17}$.

To study the effect of isospin dependence of nucleon-nucleon cross-section on nuclear stopping, we display in Figs.4.11 and 4.12 the impact parameter dependence of the stopping observables ($\langle$ R $\rangle$ and $\langle$ $1/Q_{ZZ}$ $\rangle$) for two different cross-sections i.e isospin dependent (σ_{iso}) and isospin independent (σ_{noiso}). Fine observations are:

1. $\langle$ R $\rangle$ and $\langle$ $1/Q_{ZZ}$ $\rangle$ behave in a similar fashion. The amount of stopping decreases with the impact parameter. Reduced participant matter is the cause for this

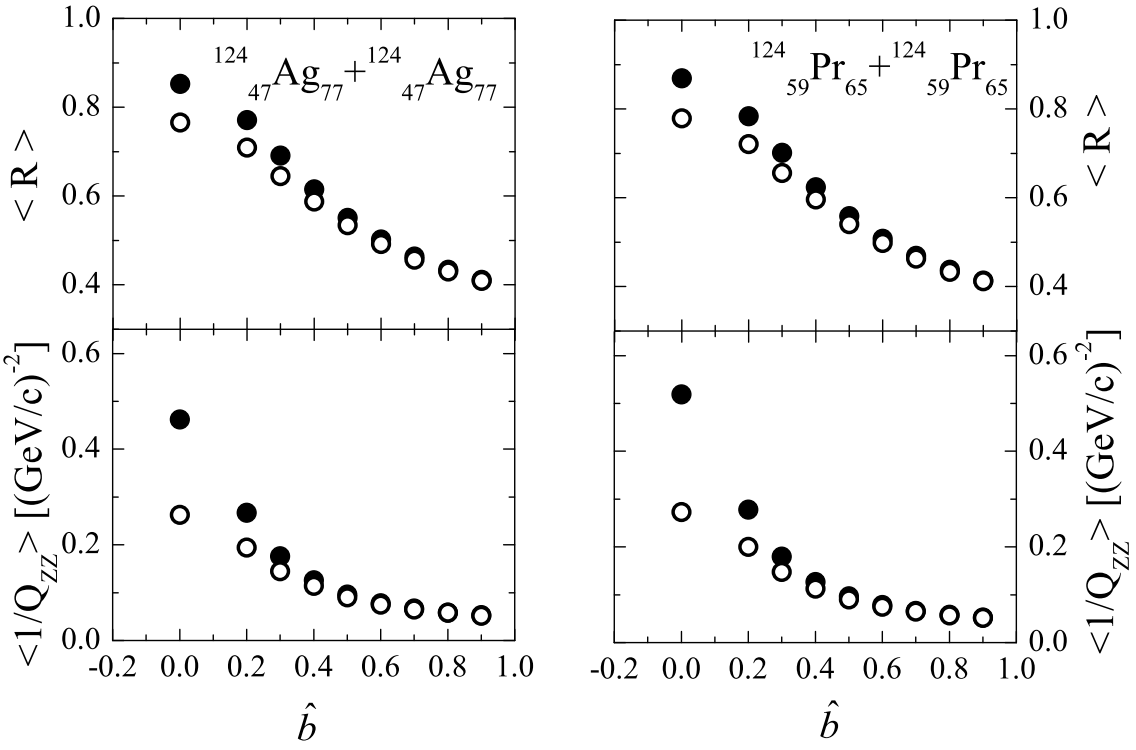

Figure 4.12: *Same as Fig.4.11 but for the reactions of* $^{124}_{47}Ag_{77} + ^{124}_{47}Ag_{77}$ *and* $^{124}_{59}Pr_{65} + ^{124}_{59}Pr_{65}$.

decrease.

2. The value of the stopping is more for σ_{iso} compared to σ_{noiso} (8% in case of $\langle$ R $\rangle$ and 26% in case of $\langle$ $1/Q_{ZZ}$ $\rangle$). This happens because, isospin dependent cross-section will lead to violent nucleon-nucleon collisions that will further causes the transformation of the initial longitudinal motion in other directions and hence thermalization of the system. This dominant role played by the isospin dependent cross-section gradually disappear with the impact parameter. These findings are also in supportive nature with findings of [116].

3. On comparing the value of stopping for both the reacting series, $^{124}_{47}Ag_{77} + ^{124}_{47}Ag_{77}$, $^{124}_{59}Pr_{65} + ^{124}_{59}Pr_{65}$ and $^{40}_{14}Si_{26} + ^{40}_{14}Si_{26}$, $^{40}_{23}V_{17} + ^{40}_{23}V_{17}$, we found that, heavier nuclei lead to better thermalization compared to lighter nuclei.

4.4.5 System charge dependece of $\langle$ R $\rangle$ and $\langle$ $1/Q_{ZZ}$ $\rangle$

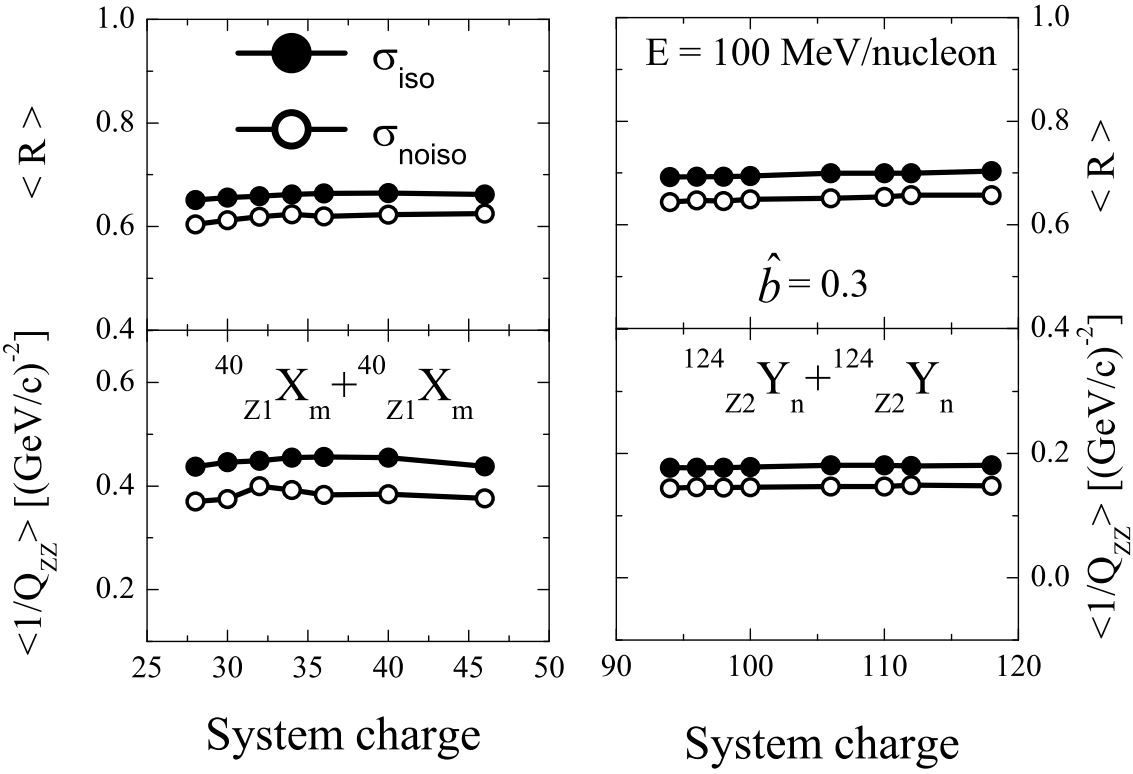

Figure 4.13: *Variation of* $\langle$ R $\rangle$ *and* $\langle$ $1/Q_{ZZ}$ $\rangle$ *with Z, in left panel for the reactions of* ${}^{40}_{Z_1}X_m + {}^{40}_{Z_1}X_m$*, where* Z_1 *= (14, 15, 16, 17, 18, 20, 21 and 23) and in right panels for the reactions of* ${}^{124}_{Z_2}Y_n + {}^{124}_{Z_2}Y_n$*, where* Z_2 *= (47, 48, 49, 50, 53, 55, 56, and 59).*

As noted in the Refs. [116, 186, 203], the production of FN's and LMF's behave in similar fashion as $\langle R \rangle$ and $\langle 1/Q_{ZZ} \rangle$. In order to check the effect of change in neutron to the proton content of the system on the nuclear stopping parameters, we display in Fig.4.13, the variation of stopping parameters as a function of Z for two different cross-sections σ_{iso} and σ_{noiso} for both series of reactions. In the left panels, we use ${}^{40}_{Z_1}X_m + {}^{40}_{Z_1}X_m$ (where Z_1 varies from 14 to 23) whereas in the right panels we use ${}^{124}_{Z_2}Y_n + {}^{124}_{Z_2}Y_n$ (where Z_2 varies from 47 to 59). We note that $\langle$ R $\rangle$ and $\langle$ $1/Q_{ZZ}$ $\rangle$ behave in a similar way. Further, very weak dependence is visible for isobaric nuclei. This result is similar as reported in earlier figures. This observation is in agreement with the observation in Ref. [203].

4.4.6 Incident energy dependence of ⟨ R ⟩

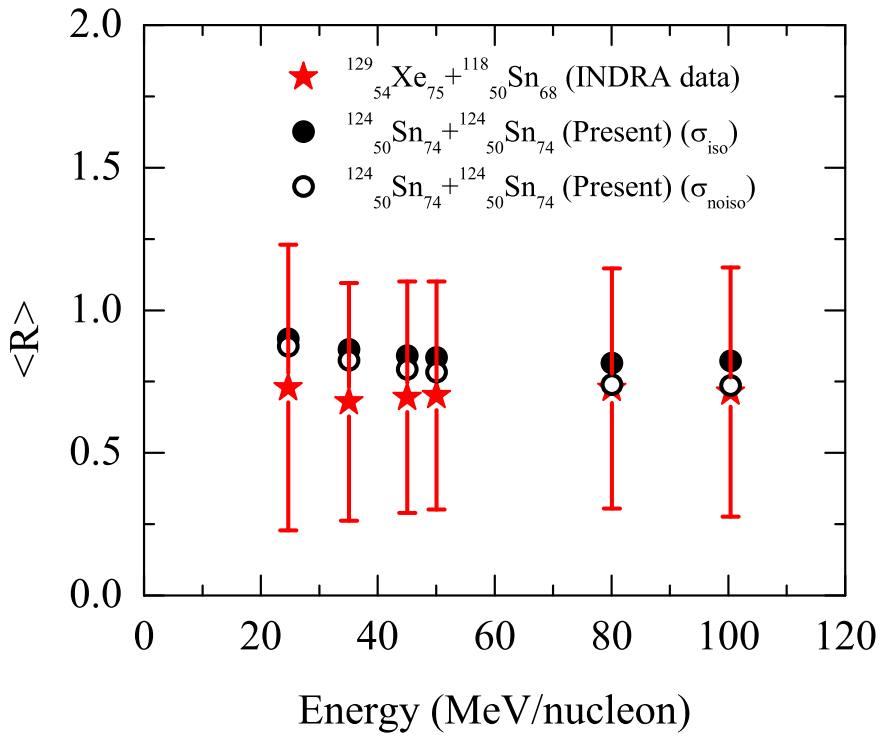

Figure 4.14: *The anisotropy ratio ⟨ R ⟩ as a function of beam energy.*

To further strengthen our interpretation of the results, in Fig.4.14, we display the comparison of theoretical results of anisotropy ratio with the experimental data obtained by the INDRA collaboration [88]. Here simulations are performed for the reaction of $^{124}_{50}Sn_{74}+^{124}_{50}Sn_{74}$ with σ_{iso} reduced by 20%. It is worth mentioning that the results with the above choice of cross-section are in good agreement with the experimental data of Ref. [88]. The choice of reduced cross-section has also been motivated by Ref. [204] as well as many previous studies [205]. The similar results are previously compared by Lehaut *et al.* [88] with the simulation results of IQMD model. A significant difference between them was observed. Theoretical calculations over predict the experimental findings for the incident energy below 60 MeV/nucleon. The gap between the theoretical calculations and the experimental findings becomes small when we factorize the two ingredients i.e. reduce the isospin dependent nucleon-nucleon cross-section by 20% and perform simulations for central collisions. Moreover, the difference between the two different versions of cross-

section is not large. This is because nuclear stopping is a global phenomena. This finding is also in agreement with Ref. [88] in which the theoretical calculations agree with the experimental findings for the collision term without isospin dependence (σ_{noiso}). From Fig.4.14 we also note that anisotropy ratio decreases with increase in the incident energy. This is because transverse component associated with the nucleons decreases with incident energy. These findings are in agreement with the results reported in Ref. [116].

4.5 Summary

We have studied the isospin effects on nuclear stopping for isobaric nuclei. We find that, participant (spectator) matter decreases (increases) with increase in the neutron content of the system whatever be the definition of the participant matter. The variation of slope of $\langle participant \rangle_{norm}$ with energy gives an indication about the global equilibrium of the system and the variation of slope of $\langle spectator \rangle_{norm}$ with energy give an indication about the local equilibrium of the system. Moreover, isospin dependence of nucleon-nucleon cross-section play a significant role in the mid-rapidity region. Change in N/Z ratio of the system has again a small influence on $\langle R \rangle$ and $\langle 1/Q_{zz} \rangle$. Moreover, we have compared our theoretical calculations with the experimental findings of INDRA collaboration. Our calculations have reproduced the experimental findings for the given range of incident energy. Our investigations revealed that strength of nucleon-nucleon cross-section and choice of centrality have a significant role to play in reaction dynamics.

Chapter 5

Isospin effects on collective flow in heavy-ion collisions

5.1 Introduction

The reactions at intermediate energies are violent enough to excite the system to very high temperature leading to the break-up of the initial correlations among nucleons, but not enough to break the internal structure of nucleons and hadrons. The description of the interactions with only hadrons and mesons is sufficient for the intermediate energy reactions. In the following chapter, we shall deal with collective flow. Fourier coefficients of different harmonics reflect the different type of anisotropy in the particle azimuthal distribution. The harmonic $\langle v_1 \rangle$ is called *directed flow*, the harmonic $\langle v_2 \rangle$ *elliptical flow*, the harmonic $\langle v_3 \rangle$ *triangular flow*, and $\langle v_4 \rangle$ as *quadrupole flow* etc. Moreover, when flow harmonics are considered as a function of transverse momentum and rapidity, $v_n(p_t, y)$, one can refer this as differential flow. Mathematically, these harmonics can be written as [206]:

$$\begin{aligned} v_1 &= \langle Cos\phi \rangle = \langle \frac{p_x}{\sqrt{p_x^2 + p_y^2}} \rangle \\ v_2 &= \langle Cos2\phi \rangle = \langle \frac{p_x^2 - p_y^2}{p_x^2 + p_y^2} \rangle \\ v_3 &= \langle Cos3\phi \rangle = \langle \frac{p_x^3 - 3p_x p_y^2}{(p_x^2 + p_y^2)^{3/2}} \rangle \\ v_4 &= \langle Cos4\phi \rangle = \langle \frac{p_x^4 - 6p_x^2 p_y^2 + p_y^4}{(p_x^2 + p_y^2)^2} \rangle \end{aligned} \tag{5.1}$$

where p_x and p_y are the x and y components of the momentum and $\langle ..... \rangle$ denotes average over the azimuthal distribution of particles with transverse momentum p_t.

5.2 Details of different harmonics

5.2.1 Directed flow

The first Fourier coefficient represents an overall shift of the distribution in the transverse plane and is called *directed flow*. Directed flow is a result of the pressure created in the system and is therefore sensitive to the compressibility of the highly thermalized nuclear matter. During the collision of two nuclei (projectile and target), highly excited participant volume is created in the overlapping region. The compression of the participant region depends on the impact parameter of the reaction. It is maximum for semi-central collisions and vanishes for central collisions, due to symmetry, and for very peripheral collisions due to the lack of a sizable pressure gradient [50]. The pressure as well as the density increases in the participant region during collision (becomes 2-3 times the normal nuclear matter density) because the two nuclei tends to occupy the smaller phase space volume. For non central collisions, the resulting anisotropy in the pressure results in the transverse flow of nuclear matter from higher pressure (participant zone) towards the lower pressure (spectator zone). This participant zone de-excite by decaying into the fragments of different mass. The multiplicity of the emitted fragments depends on the reaction conditions like incident energy, impact parameter, system mass etc. Therefore, it could be of interest to study the flow dynamics with respect to the charges of the various fragments created in the reactions of heavy ions throughout the periodic table. Its worth mentioning that, the study of azimuthal anisotropy of the particle distribution as a function of rapidity could reveal important information about the radial and directed flow [206, 207].

In this chapter we plan to address some of the current questions related to $\langle v_1 \rangle$ as well as to the excitation function of reduced flow ($\frac{\partial v_1}{\partial y}|_{midr}$) at intermediate energies. This include:

1. The incident energy as well as the impact parameter dependence of the colliding nuclei on the complex structure of flow in mid-rapidity region (i.e. how the change in neutron content of the colliding nuclei affect the collective momentum transfer in the collision) for the fragments having different mass.

2. The influence of fragment mass on the balance energy throughout the mass range of colliding nuclei for different centrality bins.

3. Consequence of different colliding geometry on directed flow, throughout the mass range.

4. Influence of incident energy on the transverse momentum dependence of directed flow, both in target-like (TL) as well as in projectile-like (PL) regions.

5. Role of isospin dependence of nucleon-nucleon cross section. Discussion will also be made for neutron-proton differential flow [208].

5.2.2 Elliptical flow

The elliptical flow is basically generated due to the anisotropic distribution of the nuclear matter, which is produced due to the non-central collisions resulting in an orthogonal asymmetry in the configuration space and re-scattering. The elliptical flow can only appear if there occur an anisotropic reaction volume as well as the multiple interactions between the particles. Fig.5.1 shows the elliptical shaped (or almond shaped) reaction volume and the way in which particles are emitted from that volume. The value of elliptical flow indicates whether the particle emission is in-plane or out-of-plane. The term *elliptical flow* was introduced in 1997 by H. Sorge [209, 210], a theoretician at SUNY-Stony Brook. The elliptical flow, which is basically the squeeze out of nuclear matter is the counter-balancing of the expansion of compressed excited nuclei to the spectator matter passing time. The balancing of the expanding excited nuclei with that of the spectator matter, moving above the participant region tends to give the transition of the nuclear matter from in-plane to out-of-plane at a particular incident energy (about 100 MeV/nucleon, depending upon the system mass and isospin content) and vice-versa at higher incident energies of the order of few GeV/nucleon. These transitions along the incident energy has further motivated the researchers to carry out the investigation for elliptical flow. The knowledge of the expanding nuclear matter and shadowing of spectator matter can give us crucial information regarding the nuclear matter interactions. This study can also shed light on the various astrophysical phenomenon such as supernova explosion.

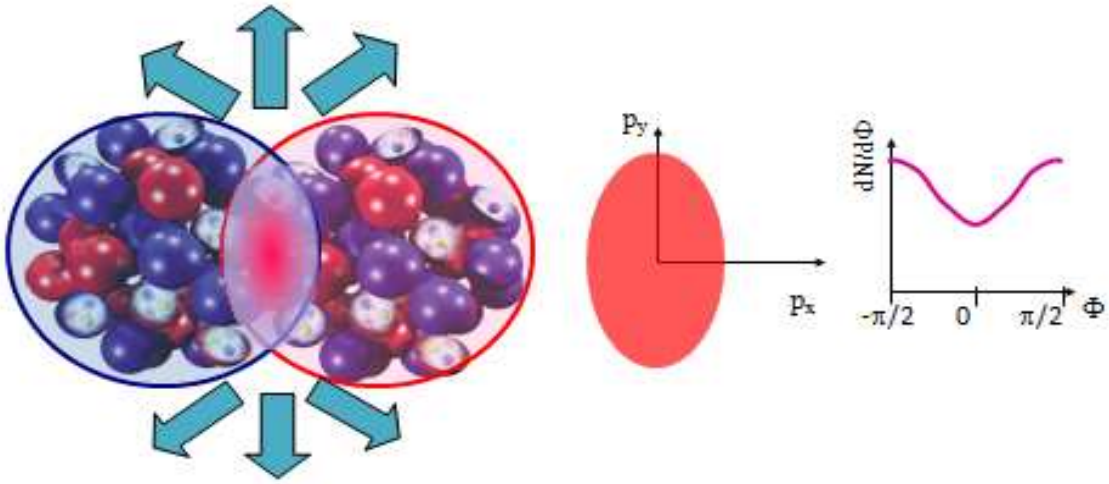

Figure 5.1: Pictorial view of out-of-plane emission of nucleons perpendicular to the reaction plane.

Both mean field and nucleon-nucleon collisions play a significant role at these incident energies. Its worth mentioning that the mean field governs the dynamics at low incident energy. However, at higher incident energy role of mean field diminishes and repulsive nucleon-nucleon interactions dominate.

The elliptical flow generated after the two nuclei collide, diminishes at particular incident energy as the transition from in-plane to out-of-plane and vice-versa takes place. This is a very interesting phenomenon by the virtue of which the transition of the flow between the reaction plane takes place. These transitions actually corresponds to the zero magnitude of elliptical flow and the incident energy at which the elliptical flow becomes zero is said to be the *transition energy* (E_{Trans}). The transition of nuclear matter emitted from in-plane to out of plane emission was first observed by the NAUTILUS Collaboration at GANIL in 1994 using Zn+Ni reaction [84]. For the first time, it has been reported by Bonasera *et*

al. [54, 211] and later on by many others that collective flow is negative at low incident energies, that turns positive with an increase in the incident energies. At a particular incident energy, however, the transition of the particles around the reaction plane takes place. The energy at which this transition observed is dubbed as the transition energy (E_{Trans}).

The transition energy (E_{Trans}), is one of the most interesting aspect in studying elliptical flow. This interesting behavior of the elliptical flow occurs twice with increase in energy from NSCL to AGS via SIS. Although, the in-plane to out of plane flow has been studied by many experimental as well as theoretical groups [186, 212]. Complete systematic study on impact parameter dependence of transition energy is missing. Therefore, a systematic study of impact parameter dependence of transition energy can be performed throughout the mass range. Good agreement of our theoretical calculations with the data motivated us to further investigate the isospin effects on the E_{Trans} throughout the mass range.

5.2.3 Triangular and quadrupole flow

Sorensen [213] reported that fluctuations of the initial collision geometry may lead to higher order Fourier components in the azimuthal correlation function through collective effects. An analysis of higher order components in the Fourier decomposition of azimuthal particle distributions, including the odd terms was proposed by Mishra *et al.,* [214] to probe superhorizon fluctuations in thermalization stage. Recently, Alver *et al.,* [57] reported the importance of triangular flow, which originate from fluctuations in the collision geometry. Unlike the elliptical flow, the triangular flow is less sensitive to the centrality or the impact parameter of the collisions [57, 215]. Since, the odd higher harmonics vanish due to symmetry constraints, therefore, these flow coefficients require the treatment of event-by-event fluctuations. The recent studies in high energy heavy-ion collisions at RHIC and LHC have demonstrated the presence of higher order anisotropic flows ($\langle v_3 \rangle$ & $\langle v_4 \rangle$) of Fourier decomposition [216]. The higher order anisotropic flow ($\langle v_4 \rangle$, in particular) has significant importance even at intermediate energies because it contain important physics of heavy-ion collisions. Theoretically, recent development has been aimed toward a better understanding of the correlation between initial and final state. Most of these models work in a simplified frame work, using e.g. linearized hydro-

dynamics or rotated averaged initial conditions [217]. As discussed above, lots of efforts have already been made in the literature to explore different aspects of directed, elliptical, triangular and quadrupole flow.

Motivated from the above discussion, in addition to the study of various aspects of directed flow mentioned in earlier subsection, we also aim to study the various aspects of higher flow harmonics. These includes:

1. The phase space analysis of participant-spectator matter and the study of the percentage of the nucleons coming from participant matter contributing in flow.

2. To check, whether the distribution of nucleon contributing to elliptical flow are distributed equally along the ellipse or not?

3. The effect of isospin degree of freedom on various aspects of elliptical, triangular and quadrupole flow.

5.3 Results and Discussion

5.3.1 Rapidity dependence of directed flow

As we have mentioned earlier that, directed flow is the ratio of p_x and transverse component of momentum of the particle into the reaction plane see Eqn.5.1. Therefore, in order to study the variation of this projected component along the direction of beam axis, we display in Fig.5.2, the rapidity dependence of directed flow ($\langle v_1 \rangle$) for the reactions of ${}^{40}_{20}Ca_{20}+{}^{40}_{20}Ca_{20}$, ${}^{58}_{28}Ni_{30}+{}^{58}_{28}Ni_{30}$, ${}^{101}_{44}Ru_{57}+{}^{101}_{44}Ru_{57}$, ${}^{139}_{57}La_{82}+{}^{139}_{57}La_{82}$ and ${}^{197}_{79}Au_{118}+{}^{197}_{79}Au_{118}$ at scaled impact parameter of $\hat{b}$ = 0.15 - 0.4 at an incident energy between E = 40 and 400 MeV/nucleon. The vertical columns in figure differentiate the directed flow for different fragments varying from Z = 1 to Z = 4. The rapidity distribution is found to vary drastically with incident energy throughout the range of rapidity, $|\frac{Y_{c.m.}}{Y_{beam}}| \leq 1.75$. Fig.5.2 reveals that, the directed flow of all fragments shows the typical "S-shape" curve. With increase in the incident energy, this curve shows an inverse behavior in both (target-) as well as in (projectile-) like region. This is because, if the incident energy is less than the balance energy (E_{bal}), the nucleon-nucleon collisions get suppressed due to the Pauli exclusion principle, the reaction dynamics are dominated by the attractive mean field.

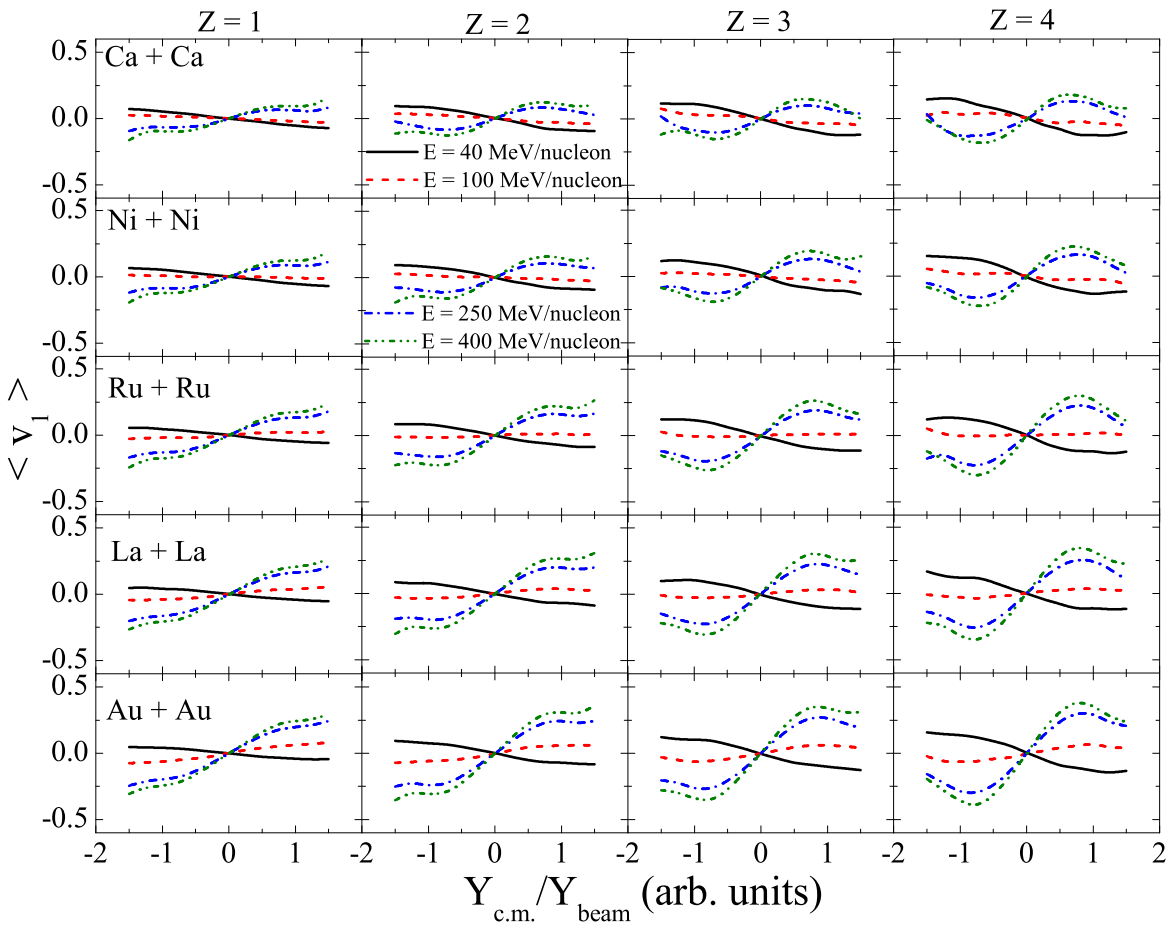

Figure 5.2: *Rapidity dependence of directed flow* ($\langle v_1 \rangle$). *Details are mentioned in the text.*

Due to which the particles gets scattered to the negative angles i.e. away from the projectile side of the reaction plane. If the incident energy becomes greater than the E_{bal}, the mean field is suppressed due to the dominance of nucleon-nucleon collisions. The particles are scattered to the positive angles i.e. towards the projectile side of the reaction plane. The directed flow decreases (increases) monotonically with the increasing rapidity around mid-rapidity for 40 and 100 MeV/nucleon (250 and 400 MeV/nucleon). It reaches the extreme near $Y_{c.m.}/Y_{beam} = \pm 0.7$, and then the absolute value of directed flow goes down with rapidity. The directed flow decompose at the mid-rapidity region. This happens because, the directed flow is basically the sideward deflection of nuclear matter around the participant zone (or mid-rapidity region).

The above scenario is studied by many theoretical groups using different models like *QMD*, *IQMD* [174, 189, 204, 218] and *BUU* [51] etc. But all these studies were concentrated on the directed flow or the balance energy of the whole system. We attempt to study these terms for different fragments throughout the mass range. One can see from the Fig.5.2 that, the directed flow increases with mass of the fragment. This happens because, as the fragment mass increases the thermal energy becomes less important and large fraction of energy associated with a fragment is due to its flow. This result is in agreement with Ref. [219].

Since directed flow is essentially a pressure effect, it is naturally expected to be sensitive to the compressibility of nuclear matter. The strength of the directed flow is usually measured by plotting $\langle v_1 \rangle$ as a function of rapidity and by taking the slope of this at mid-rapidity $|Y^{red}| \leq 0.1$ and is known as *reduced flow*. To study how the compressibility of nuclear matter varies with incident energy and to give more practical interpretation of our results, we display in Fig.5.3, the comparison of our theoretical calculations with the experimental findings of GSI & GANIL collaborations [85] for the incident energy dependence of reduced flow ($\frac{\partial v_1}{\partial y}|_{midr}$). The left panels display the results at scaled impact parameter of $\hat{b} = 0.5$ and right panels display the results at $\hat{b} = 0.1$. From Fig.5.3 one can see that, the at low incident energies the Pauli blocking will block most of the collisions due to the dominance of mean field in the reaction dynamics and we observe a negative slope for all the systems. This observation of a negative flow has already been reported for the lighter systems ${}^{40}_{18}Ar_{22} + {}^{58}_{28}Ni_{30}$, ${}^{58}_{28}Ni_{30} + {}^{58}_{28}Ni_{30}$, and ${}^{129}_{54}Xe_{75} + {}^{nat}Sn$ [220]. But

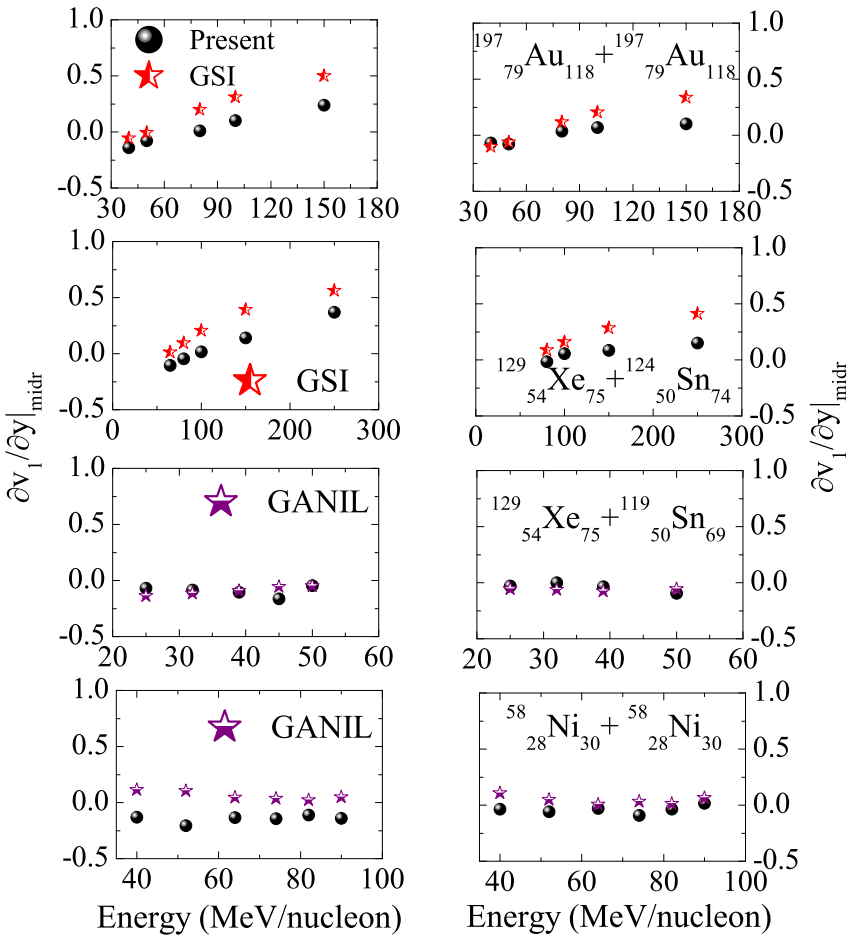

Figure 5.3: *Comparison of our theoretical calculations with the experimental findings of GSI & GANIL collaborations [85] for Z = 2 particles.*

as the incident energy increases both the mean field and the nucleon-nucleon collisions play a significant role therefore, the slope becomes slightly positive. Further increase in the energy leads to dominance of nucleon-nucleon collisions and hence the slope increases drastically. Moreover, the reduced flow is large for the semi-central collisions ($\hat{b} = 0.5$) compared to the central collisions ($\hat{b} = 0.1$). This is due to the pressure gradient. As we have already mentioned that, it is a pressure effect, and for the semi-central collisions the pressure gradient is more which leads to the larger transfer of momentum to nucleons in a direction perpendicular to the beam axis. No such pressure gradient occur for the central collisions and will lead to the isotropic distribution of the particles and fragments. A similar behavior is observed for other fragments like Z = 1 (lesser magnitude than Z = 2) and Z = 3 & 4 (larger magnitude than Z = 2) at both central and semi-central collisions [not shown here].

5.3.2 Influence of colliding geometry on balance energy of fragments and on reduced flow

The role of impact parameter in the determination of the disappearance of flow for the whole system has been reported in literature [40, 51]. Generally, the balance energy increases with the impact parameter and decreases with system mass. This happens because in symmetric collisions the compressed zone (participant or mid-rapidity zone) decreases with increase in impact parameter. Therefore, more energy is required to compensate the effect of mean field in peripheral collisions [40]. Moreover, the increase in balance energy for lighter and medium mass nuclei is due to the interplay between the mean field and nucleon-nucleon scattering but for the heavier colliding nuclei, Coulomb potential is also an important factor.

In order to study the balance energy of different fragments throughout the mass range spanning over the entire colliding geometry, we display in Fig.5.4, the fragment mass dependence of balance energy for the similar set of reactions as in Fig.5.2. The different panels display the results for the different centrality bins (mentioned in caption). It is clear from the figure that, balance energy depends on both the mass as well as on the impact parameter of the colliding nuclei as explained above but is independent of the mass/charge of fragment. Although, the directed flow increases with the mass of the fragment and its magnitude remains same in the projectile as well as target like rapidity

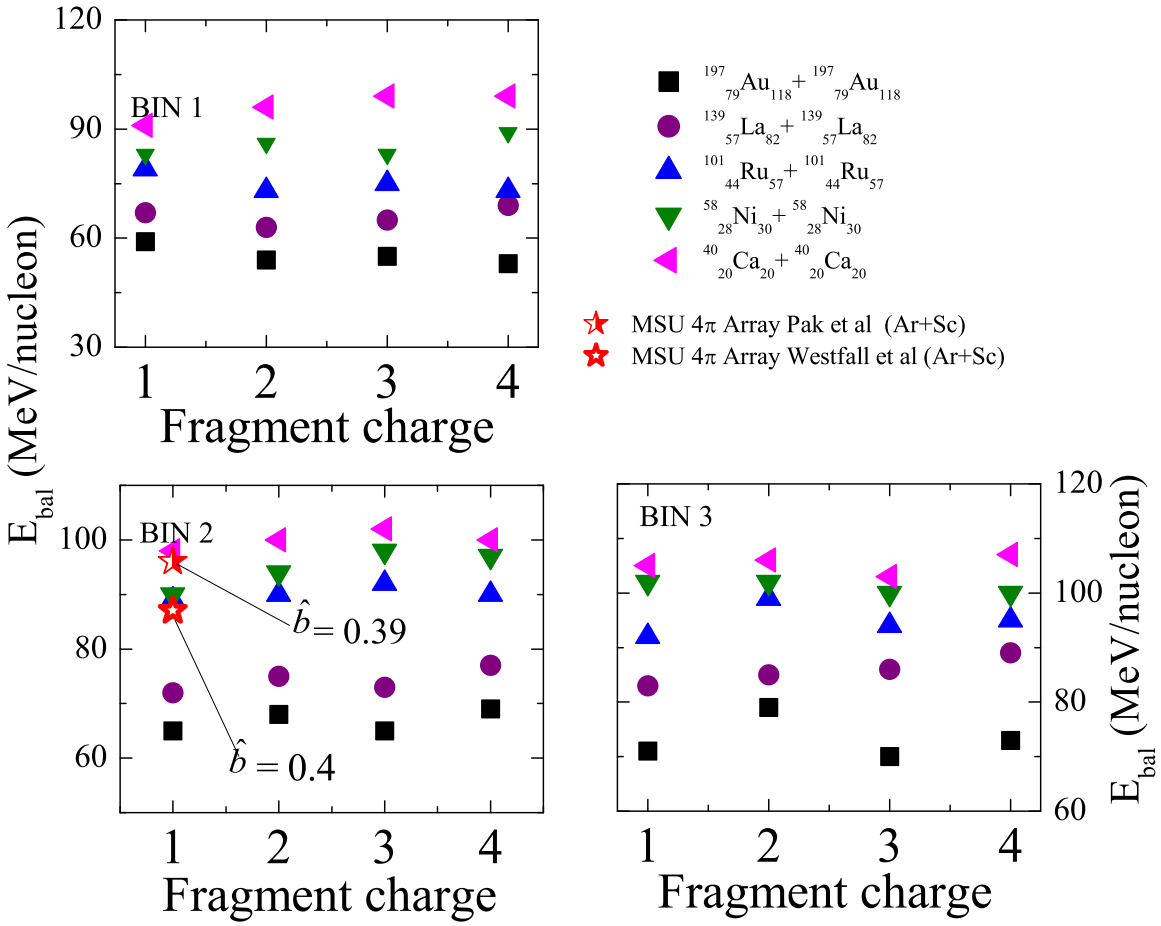

Figure 5.4: *Fragment mass dependence of balance energy for the similar set of reactions as in Fig.1. The different panels represents the results at different centrality bins such as BIN 1 ($\hat{b} = 0.0 - 0.2$), BIN 2 ($\hat{b} = 0.2 - 0.4$) and BIN 3 ($\hat{b} = 0.4 - 0.6$).*

region. Moreover, slope of the directed flow changes with incident energy around mid-rapidity (reduced flow) as discussed in Fig.5.3. But at balance energy interactions among the nucleons are balanced. Therefore, one cannot observe a variation in the balance energy of the fragments having different mass. This result is in agreement with the experimental findings of MSU group reported by Pak *et al.* [118] and Westfall [40]. Moreover, the experimental data of these groups for the reaction of ${}^{40}_{18}Ar_{22} + {}^{45}_{21}Sc_{24}$ has compared with the present results. One can see that, our theoretical calculations are able to reproduce the experimental findings of Ref. [118].

It is now well accepted that directed flow gives wiggle structure (S-shape)(show different behavior for (target-)(TL) as well as (projectile-) (PL) like regions) as a function of rapidity and this structure is influenced by the colliding geometry, system size as well as by the center-of-mass energy [221, 222]. Therefore, it could be of interest to study the different aspects of directed flow separately in these regions. The projectile and target like regions are separated according to different rapidity cuts defined earlier.

5.3.3 Transverse momentum dependence of directed flow

In order to study the neutron-proton differential flow seperately, we plot in Fig.5.5, the transverse momentum dependence of $\langle v_1 \rangle$ for PL [panels (a) & (b)] and TL [panels (c) & (d)] for the protons (left panels) and neutrons (right panels) for the reactions of ${}^{40}_{20}Ca_{20} + {}^{40}_{20}Ca_{20}$, ${}^{58}_{28}Ni_{30} + {}^{58}_{28}Ni_{30}$, ${}^{101}_{44}Ru_{57} + {}^{101}_{44}Ru_{57}$, ${}^{124}_{50}Sn_{74} + {}^{124}_{50}Sn_{74}$, ${}^{124}_{47}Ag_{77} + {}^{124}_{47}Ag_{77}$ and ${}^{197}_{79}Au_{118} + {}^{197}_{79}Au_{118}$. The figure reveals that:

The peak value of $\langle v_1 \rangle$ for the protons is higher compared to the neutrons for all the systems. This clearly indicates that the protons have larger magnitude of the sideward flow around the reaction zone (or participant zone) compared to the neutrons. This happens due to the proton-proton repulsion, that results in the larger scattering of nuclear matter in the sideward directions. In fact, the isospin dependent potentials i.e. Coulomb as well as symmetry potential play a significant role in the directed flow of protons and neutrons. The variation in the directed flow for proton/neutron is due to the interplay of these two potentials. Here, the $[v_1(protons) - v_1(neutrons)]$ reflects the strength of the symmetry energy. This observation is of physical importance as it can give us the glimpse of the behavior of symmetry energy at supra densities ($\rho > \rho_0$). In Refs. [112, 145], pion yield was

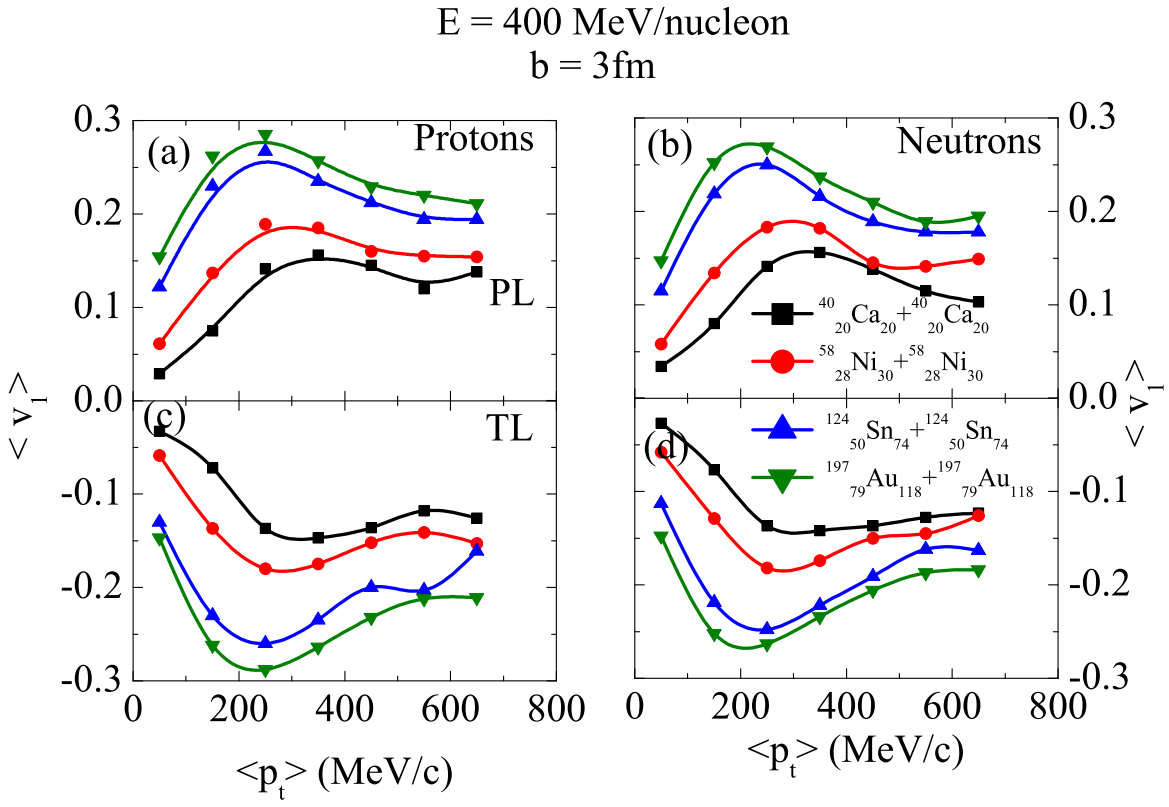

Figure 5.5: *Transverse momentum dependence of sideward flow* $\langle v_1 \rangle$ *for PL [panels (a) & (b)] and TL [panels (c) & (d)] for the neutrons (right panels) and protons (left panels).*

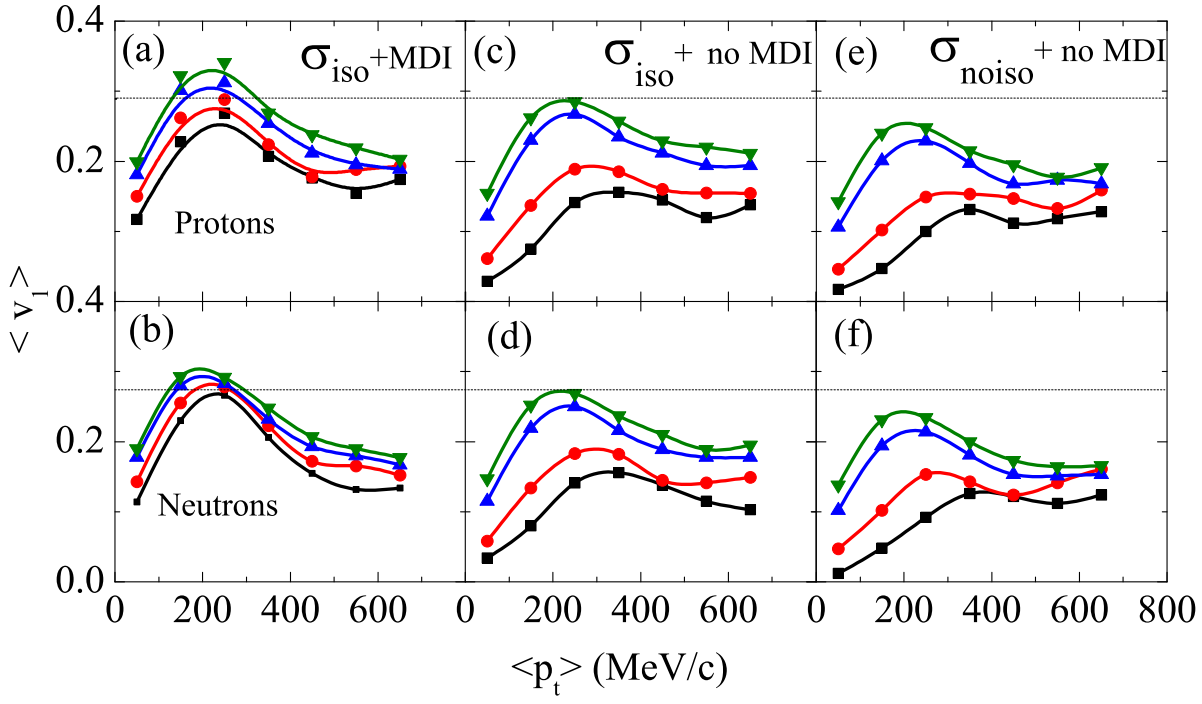

Figure 5.6: *Transverse momentum dependence of v_1 for protons [panels (a), (c) & (e)] and neutrons [panels (b), (d) & (f)] for momentum dependent interactions (first column) the isospin dependent cross-section (σ_{iso}) (second column) (left panels) and isospin-independent cross-section (σ_{noiso}) (third column) for the PL region. The incident energy is 400 MeV/nucleon and b = 3 fm. Symbols have the same meaning as in Fig.5.5.*

found to suppressed by 30 percent once momentum dependent interactions were included in the evolution of the reaction. It could be quite interesting to observe the effect of momentum dependent interactions on the sideward flow of protons and neutrons. In Fig.5.6, we display, the transverse momentum dependence of $\langle v_1 \rangle$ for protons [panels (a), (c) & (e)] and neutrons [panels (b), (d) & (f)]. First column displays the results for momentum dependent interactions, second column displays the results for isospin-dependent (σ_{iso}) and third column for isospin-independent cross-section (σ_{noiso}). The dotted line compare the effect of inclusion of MDI and isospin independent cross-section on the peak value of $\langle v_1 \rangle$ when plotted as a function of p_t.

The MDI and isospin dependence of nucleon-nucleon cross-section are found to affect the sideward flow of both neutrons and protons considerably. The inclusion of MDI results in larger sideward flow of particles. This is due to the repulsive nature of the MDI at the beam energies for which the present analysis is performed. The neutrons and protons with larger relative velocities are expelled more in the sideward direction. Moreover, one can clearly see larger value of sideward flow for the isospin dependent cross-section compared to isospin-independent cross-section. This happens because in the case of isospin dependent cross-section, neutron-proton cross-section is three times larger compared to the neutron-neutron and proton-proton cross-section [24, 115]. This will enhance binary collisions and will further cause more scattering of the neutrons and protons in sideward directions. These findings are in agreement with Ref. [223].

To further strengthen our interpretation of the results, in Fig.5.7, we compare our theoretical findings of transverse momentum dependence of directed flow with the experimental data of FOPI collaboration [224]. The rapidity cut is in accordance with the experimental findings. The theoretical findings are able to explain the FOPI data. The inclusion of MDI results in more negative value of v_1, confirming the momentum dependent interactions play a significant role in p_t-differential sideward flow. This happens because the repulsive forces generated due to the relative velocities of the protons supports the in-plane deflection of matter. We also extend our study to examine the role of constant form of cross-sections in the sideward flow. The literature includes the effects of constant forms of cross-sections on the energy of vanishing flow [174]. It has been concluded that the balance energy depends strongly on the in-medium nucleon-nucleon cross-section [39, 54].

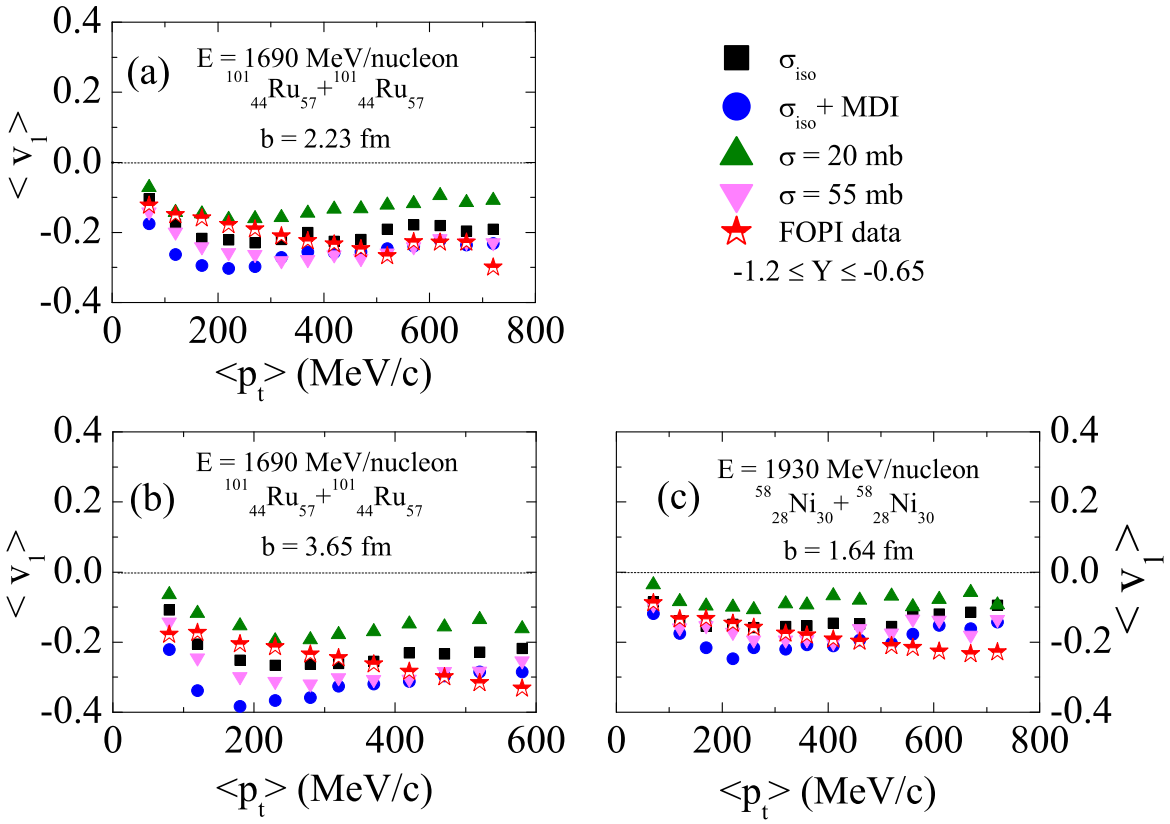

Figure 5.7: *Transverse momentum dependence of* $\langle v_1 \rangle$*, for protons and comparison with the FOPI data [224]. The rapidity bin for this analysis is in accordance with FOPI data i.e.* $-1.2 \leq Y^{red} \leq -0.65$.

We included the nucleon-nucleon constant cross-sections of 20 and 55 mb strength for the present analysis. The effect of constant form of cross-sections (σ = 20 & 55 mb) is also visible in the figure. The sideward flow remains negative along the whole p_t range due to the rapidity cut within the target-like region. Overall, sideward flow is significantly influenced by the MDI and different forms of cross-section.

5.4 Different aspects of elliptical flow

In section 5.2.2, we have discussed the origin and behavior of elliptical flow. In addition to the simple anisotropy in the space and momentum co-ordinates. The physics regarding the elliptical flow is much more complex and interesting. One of the interesting aspect of the elliptical flow is its high sensitivity towards the isospin content of the colliding nuclei. The isospin factor (N/Z > 1) has a considerable effect on the squeeze-out of particles [186, 225]. In addition, elliptical flow is a powerful probe for the symmetry energy. It has been observed that elliptical flow is highly sensitive to the different forms of the density dependence of symmetry energy [212]. The pressure created during a collision can be revealed by studying the elliptical flow with respect to the transverse momenta. In the present section, we aim to shed light on the various aspects of elliptical flow with respect to the isospin content of the system and the isospin dependence of nucleon-nucleon cross-section. For the present analysis, simulations are carried out for the reactions of ${}^{124}_{Z_1}X_n + {}^{124}_{Z_1}X_n$, where Z_1 = (47, 50, 53, 57 and 59) and ${}^{40}_{Z_2}Y_n + {}^{40}_{Z_2}Y_n$, where Z_2 = (14, 16, 18, 21 and 23). The definition of elliptical flow used in the present analysis is the one displayed in Eqn.5.1. The positive value of elliptical flow describes the eccentricity of an ellipse-like distribution and indicates in-plane enhancement of the particle emission. On the other hand, a negative value of $\langle v_2 \rangle$ shows the squeeze-out effects perpendicular to the reaction plane. Obviously, zero value corresponds to an isotropic distribution.

5.4.1 Anisotropic flow in terms of participant and spectator matter

The contribution of the participant and spectator matter [194] in the intermediate energy heavy-ion collisions has motivated us to perform a detailed analysis of anisotropic flow in terms of participant and spectator matter. The important concept of spectator and

participant in collisions was first introduced by Bowman *et al.,* [226]. T. Gaitanos *et al.* [227] studied the spectator and participant decay in heavy ion collisions, they showed that the spectator reaches an equilibrated freeze-out configuration which undergoes simultaneous fragmentation. The fragments from the participant region, on the other hand, do not seem to come from a common fragmenting source in thermodynamical equilibrium. Here we aim to study the phase space analysis of participant-spectator matter and will see what percentage of the nucleons coming from participant matter contributing in flow.

5.4.1.1 Phase space distribution of nucleons

In order to define clearly the most relevant quantities for collective motion in heavy-ion collisions, we display in Fig.5.8, a typical heavy-ion reaction of ${}^{124}_{50}Sn_{74} + {}^{124}_{50}Sn_{74}$ at an incident energy of E = 100 MeV/nucleon and at scaled impact parameter of $\hat{b} = 0.5$ [228]. When two nuclei approach each other, their orientation in space and the initial beam direction define the reaction plane. The panels from top to bottom represents the time evolution of the reaction from 0 fm/c to 200 fm/c. In the initial phase (when t = 0 fm/c), the two matter distributions of projectile and target approach each other and start to overlap. When the matter distributions of projectile and target overlap each other the high density phase (at t = 30 fm/c) is formed. Since the collision is semi peripheral, some of the nucleons (spectators) never undergo a collision with the collision partner. These nucleons experience only the (distorted) mean field of their parent nuclei and propagate with little deflection. The next stage in the reaction scenario is (at t = 70 fm/c), the relaxation of the energy density. At this stage central system undergoes expansion, thereby reducing the temperature and density. Since the collision is semi peripheral, the pressure gradient is largest along the beam direction. Therefore, the system relaxes predominantly longitudinally. Time t = 200 fm/c is commonly referred to as the freeze-out time. The reaction, and the development of collective signatures, stops at this time.

5.4.1.2 The trajectory of nucleons which participate in flow

In Fig.5.9, we display the 3-D snapshot of the trajectory of nucleons which participate in flow for the reaction of ${}^{124}_{50}Sn_{74} + {}^{124}_{50}Sn_{74}$ at different time steps varying from 0 fm/c to 200 fm/c in co-ordinate space at E = 400 MeV/nucleon. For this figure we select those nucleons which suffer maximum number of collisions. Here we increase the size of particles in comparison to previous figure by $\frac{18}{9} = 2$ units. The path of nucleons is shown with the

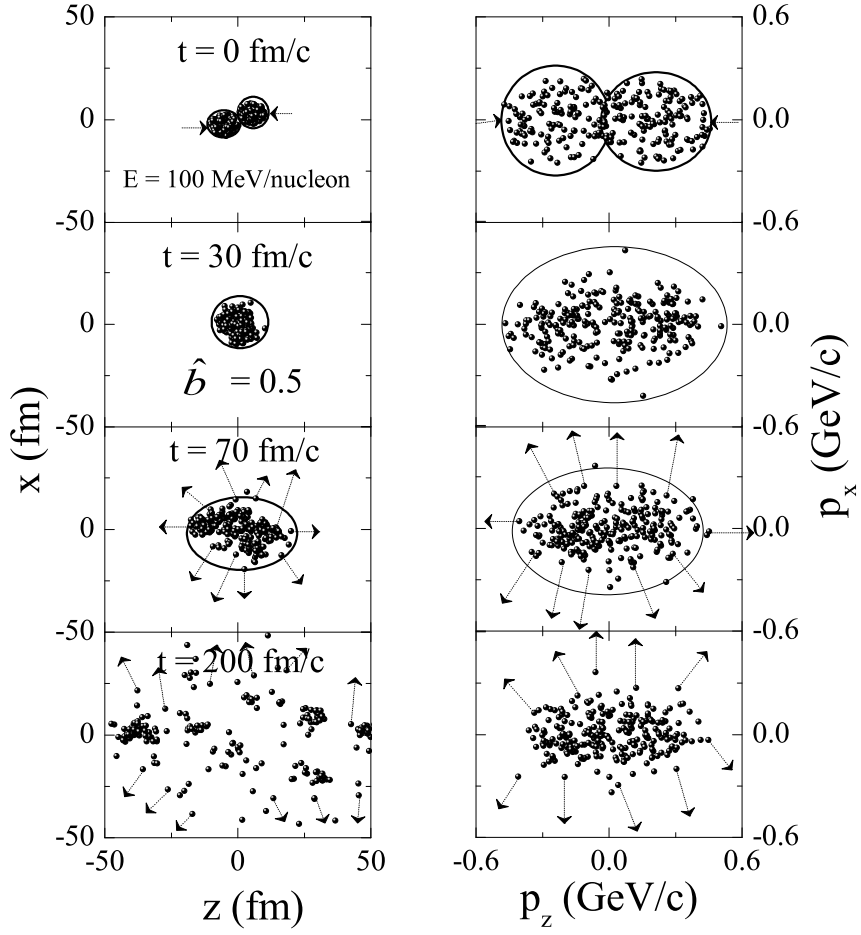

Figure 5.8: *Phase space distribution of* $^{124}_{50}Sn_{74} +^{124}_{50} Sn_{74}$*, x-z plane (left) and* $p_x - p_x$ *plane (right) at incident energy E = 100 MeV/nucleon for semi-peripheral geometry. The panels from top to bottom are representing the positions at different times.*

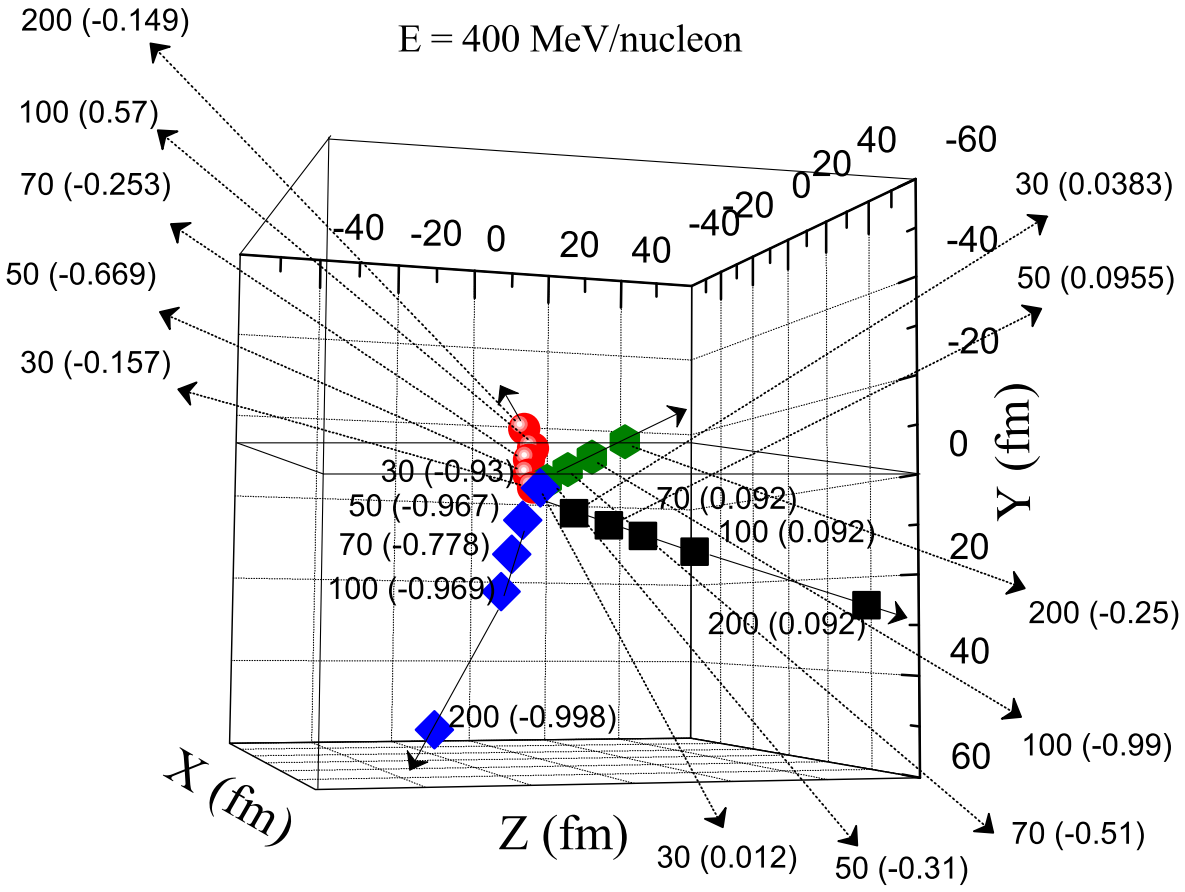

Figure 5.9: *The 3-D snapshots of the trajectory of nucleons which participate in flow for the reaction of* ${}^{124}_{50}Sn_{74} + {}^{124}_{50}Sn_{74}$ *at different time steps varying from 0 fm/c to 200 fm/c in co-ordinate space at E = 400 MeV/nucleon.*

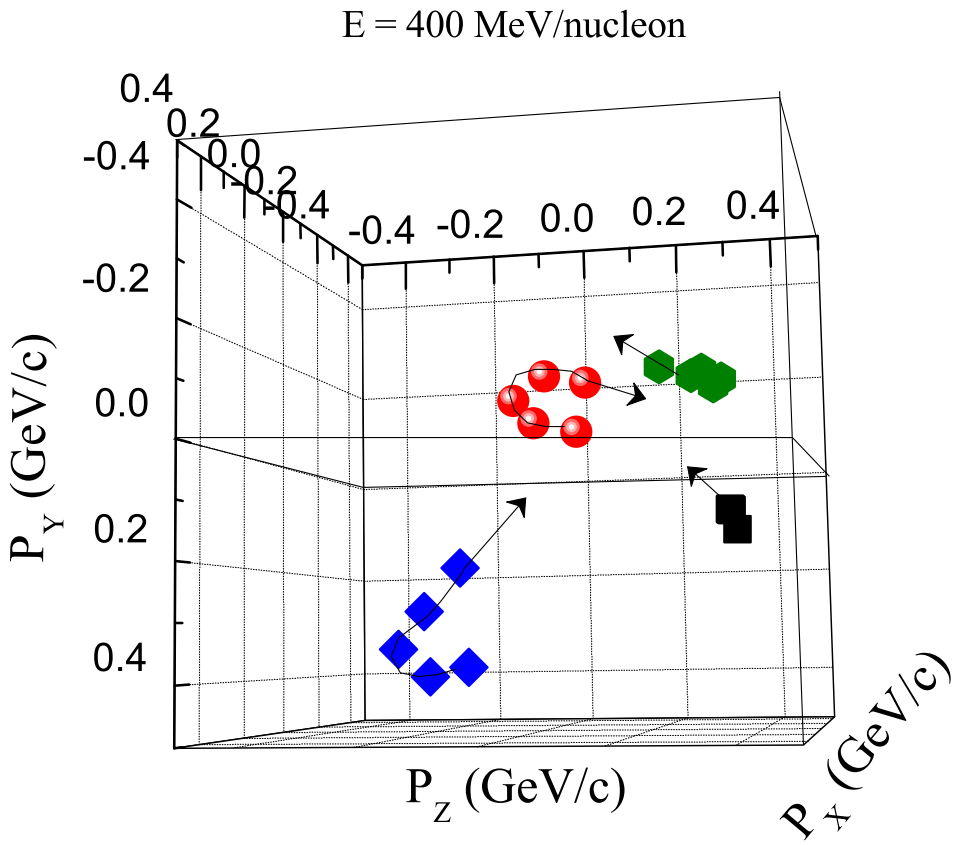

Figure 5.10: *Same as Fig.5.9 but for momentum space.*

help of solid arrows. The numeric values (shown with the help of dotted arrow) in the figure denote time interval (in fm/c) (outside the bracket) during which these collisions happened and the numeric values (inside bracket) denote values of $\langle v_2 \rangle$ for that nucleon. It is clear from the figure that nucleons shows the squeeze-out-flow. The average value of elliptical flow $\langle v_2 \rangle$ for all the nucleons which participate in flow at different time steps is shown in the Table 5.1.

From table we can say that flow is maximum at 50 fm/c and then decreases. This

Table 5.1: The average value of $\langle v_2 \rangle$ for all the nucleons which participate in flow.

Time(fm/c)	$\langle v_2 \rangle$
30	-0.259
50	-0.4596
70	-0.2118
100	-0.2679
200	-0.0061

happens because, the matter distribution of projectile and target overlap each other the high density phase is formed. Since the collision is semi peripheral, participant nucleons shifts in the transverse direction after suffering frequent collisions.

In Fig.5.10, we display the 3-D snapshot of the trajectory of nucleons which participate in flow in momentum space. The arrow show the direction of propagation of each nucleon. From the above discussion we can say that, the nucleons which suffer maximum number of collisions are contributing in anisotropic flow. Moreover, the distribution of nucleons and fragments is not symmetric around the beam axis.

5.4.2 Azimuthal angle dependence of $\frac{dN}{d(\langle Cos2\phi \rangle)}$

5.4.2.1 For two different nucleon-nucleon cross-sections

To further strengthen our interpretation of results, i.e. the distribution of nucleons constituting the LMF's, which are contributing in elliptical flow, is not symmetric around the beam axis, we display in Fig.5.11, the azimuthal angle dependence of $\frac{dN}{d(\langle Cos2\phi \rangle)}$, for FN's (upper panel), LMF's (middle) and IMF's (lower panel) at an incident energy E = 100 MeV/nucleon for the reactions of ${}^{124}_{47}Ag_{77}+{}^{124}_{47}Ag_{77}$ (left panels) and ${}^{124}_{59}Pr_{65}+{}^{124}_{59}Pr_{65}$ (right panels) [229]. One should also keep in mind that, the scattering cross-section depends crucially on the isospin content as discussed in chapter 1. Figure reveals that:

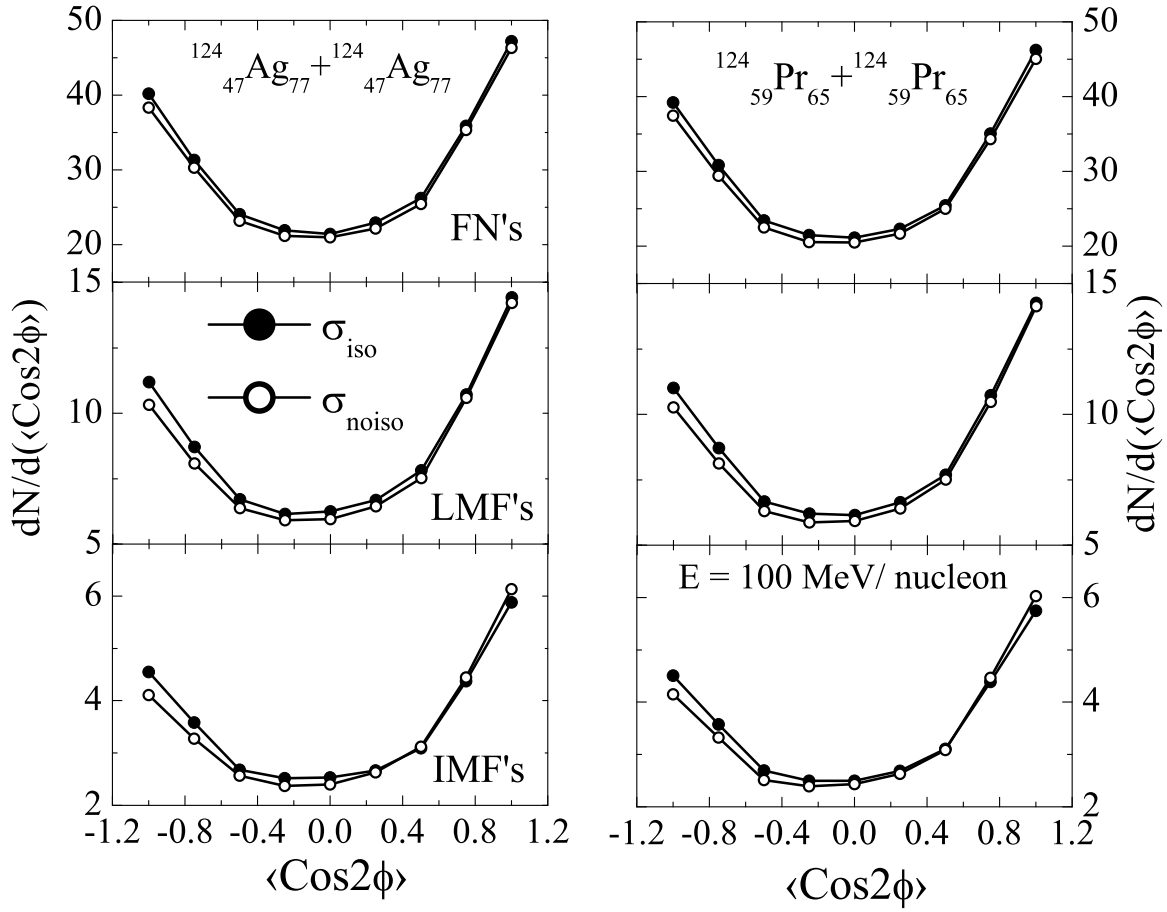

Figure 5.11: *Azimuthal angle dependence of* $\frac{dN}{d(\langle Cos2\phi \rangle)}$*, for FN's (upper panel), LMF's (middle) and IMF's (lower panel).*

1. Minima at 2ϕ=$\pi/2$ indicate predominantly in-plane emission, while the peaks at $2\phi = 0$ and π, corresponds to a preference for azimuthal emission in-plane and perpendicular to the reaction plane, the so-called squeeze-out.

2. Peak is more pronounced at 2ϕ= 0 than at 2ϕ= π, which indicates that number of particles emitted in-plane are larger compared to the number of particles emitted out-of-plane. This indicates that, the ellipse formed is not symmetric around the z-axis i.e in the collision of symmetric nuclei the distribution of nucleon after the collision in momentum space is not uniform.

3. There is a very little influence of isospin asymmetry on the variation of $\frac{dN}{d(\langle Cos2\phi\rangle)}$ with $\langle Cos2\phi\rangle$. $\frac{dN}{d(\langle Cos2\phi\rangle)}$ is higher for neutron rich system ${}^{124}_{47}Ag_{77}+{}^{124}_{47}Ag_{77}$ compared to neutron deficient system ${}^{124}_{59}Pr_{65}+{}^{124}_{59}Pr_{65}$ due to increase in repulsive forces.

4. $\frac{dN}{d(\langle Cos2\phi\rangle)}$ is sensitive to the isospin dependence of nucleon-nucleon cross-section. Its value is more in case of isospin dependent cross-section due to the increase in nucleon-nucleon binary collisions.

5.4.2.2 At different incident energies

As a next step, in order to study the influence of incident energy on the distribution of FN's and LMF's, we display in Fig.5.12, the azimuthal angle dependence of $\frac{dN}{d(\langle Cos2\phi\rangle)}$ for FN's and LMF's at an incident energy between 50 and 250 MeV/nucleon for the reaction of ${}^{124}_{50}Sn_{74}+{}^{124}_{50}Sn_{74}$. Figure reveals that:

As the incident energy increases, slope of the curve increases for both FN's and LMF's. This happens because, as the incident energy increases the thrust will also increase which will enhance the out-of-plane emission of the nucleon. The increase in slope is uniform in case of FN's but non-uniform in case of LMF's. This indicates that emission of FN's is symmetric but emission of LMF's is not symmetric about reaction plane. This is because, since the number of nucleon in both the systems are same but the number of collisions among the nucleon (neutron-neutron, proton-proton and neutron-proton) cannot be same. In addition to this if the colliding nuclear matter is rotating then it could lead to the asymmetric distribution of fragments.

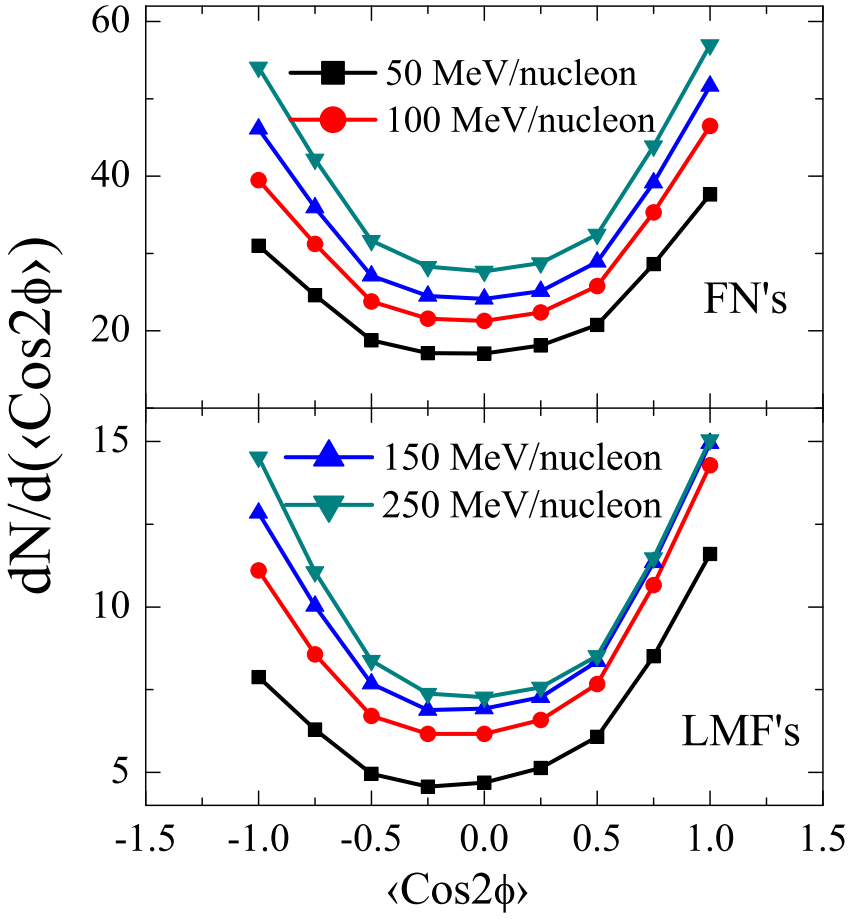

Figure 5.12: *Azimuthal angle dependence of* $\frac{dN}{d(\langle Cos2\phi \rangle)}$ *for FN's (upper panel) and LMF's (lower panel) at incident energies 50, 100, 150 and 250 MeV/nucleon.*

5.4.3 Influence of density dependence of symmetry energy on $\frac{dN}{d(\langle Cos2\phi\rangle)}$ and $\frac{dN}{p_t dp_t}$

To study the effect of density dependence of symmetry energy on $\frac{dN}{d(\langle Cos2\phi\rangle)}$ and $\frac{dN}{p_t dp_t}$, we display in Fig.5.13, the azimuthal angle dependence of $\frac{dN}{d(\langle Cos2\phi\rangle)}$ and the transverse momentum dependence of $\frac{dN}{p_t dp_t}$, for FN's (upper panels) and LMF's (lower panels) at an incident energy E = 400 MeV/nucleon, for the reaction of $^{124}_{50}Sn_{74} + ^{124}_{50}Sn_{74}$. The simulations are carried out for three different parameterizations of density dependent symmetry energy i.e. for $\gamma = 0$, 0.66 and 2. It has been observed that $\frac{dN}{p_t dp_t}$ shifts towards lower values with increase in γ. This is because, the stiffer form of density dependent symmetry energy tends to increase the repulsion at the supra saturation densities, and the value of $\frac{dN}{d(\langle Cos2\phi\rangle)}$ becomes more negative. Moreover, the difference is more in case of LMF's compared to FN's. This is because, the symmetry energy term affect the production of LMF's more compared to FN's.

5.4.4 Incident energy dependence of $\frac{dN}{d(\langle Cos2\phi\rangle)}$

In Fig.5.14, we display, the energy dependence of $\frac{dN}{d(\langle Cos2\phi\rangle)}$ for FN's and LMF's for the reactions of $^{124}_{50}Sn_{74}+^{124}_{50}Sn_{74}$ (N/Z = 1.48) and $^{40}_{16}S_{24}+^{40}_{16}S_{24}$ (N/Z = 1.5) for $\langle Cos2\phi\rangle$ = -1, 0, +1. One can see that, once the FN's and LMF's at $\langle Cos2\phi\rangle = 0$ and -1 are normalized with FN's and LMF's at $\langle Cos2\phi\rangle = +1$ at the starting point of energy, their behavior with respect to the energy is similar for both the FN's and LMF's. Although, the N/Z of both the reactions are nearly equal but the behavior of energy dependence of $\frac{dN}{d(\langle Cos2\phi\rangle)}$ is different for both the reactions. One can see from the Fig.5.14, that out-of-plane emission is more in case of $^{124}_{50}Sn_{74} + ^{124}_{50}Sn_{74}$ than in-plane emission. But the behavior is entirely different for $^{40}_{16}S_{24} + ^{40}_{16}S_{24}$ where the in-plane emission is more than out-of-plane emission. This happens because, $^{124}_{50}Sn_{74} + ^{124}_{50}Sn_{74}$ is proton rich (N/Z = 1.48) and $^{40}_{16}S_{24} + ^{40}_{16}S_{24}$ is neutron rich (N/Z = 1.5). The fragments formed in the collision are not uniformly distributed around the point of collision. The distribution of FN's is equal for in-plane and out-of-plane flow with respect to distribution corresponding to vanishing flow. But for LMF's the distribution is asymmetric.

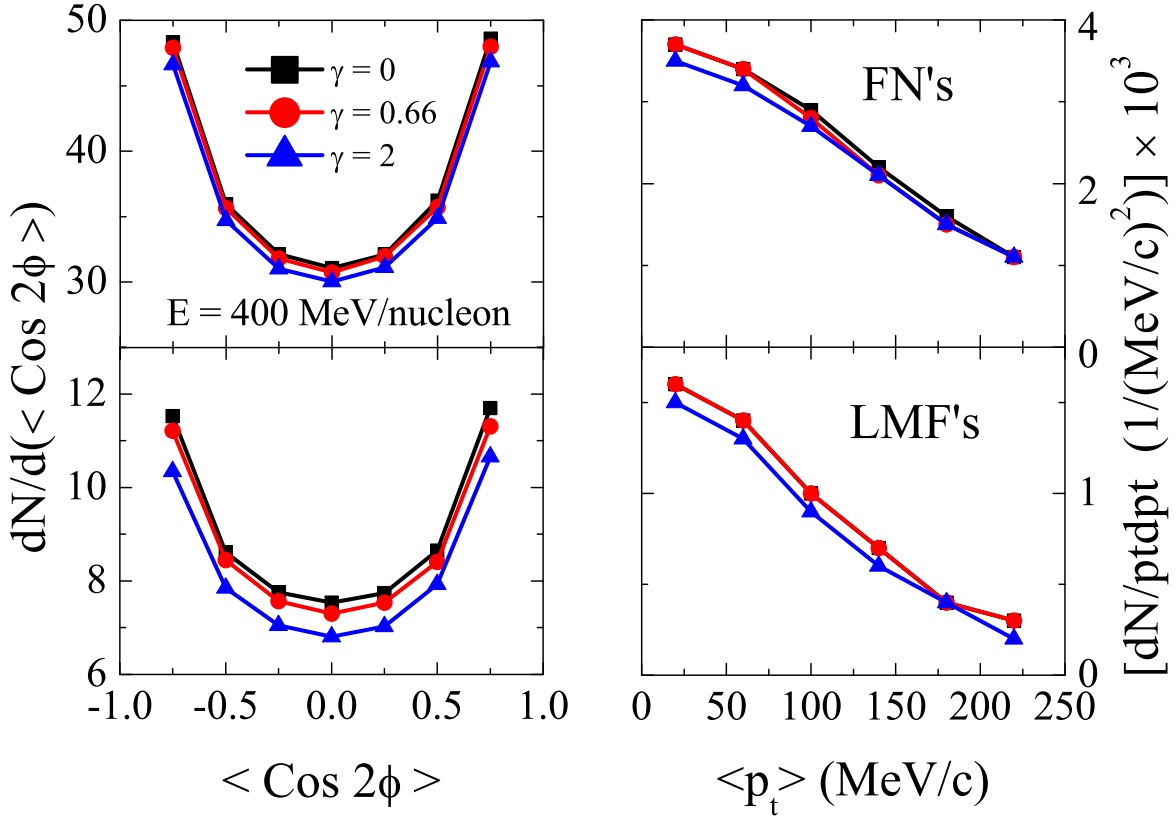

Figure 5.13: *Azimuthal angle dependence of* $\frac{dN}{d(\langle Cos2\phi\rangle)}$ *(Left panels) and transverse momentum dependence of* $\frac{dN}{p_t dp_t}$ *(right panels) for FN's and LMF's at incident energy of E = 400 MeV/nucleon.*

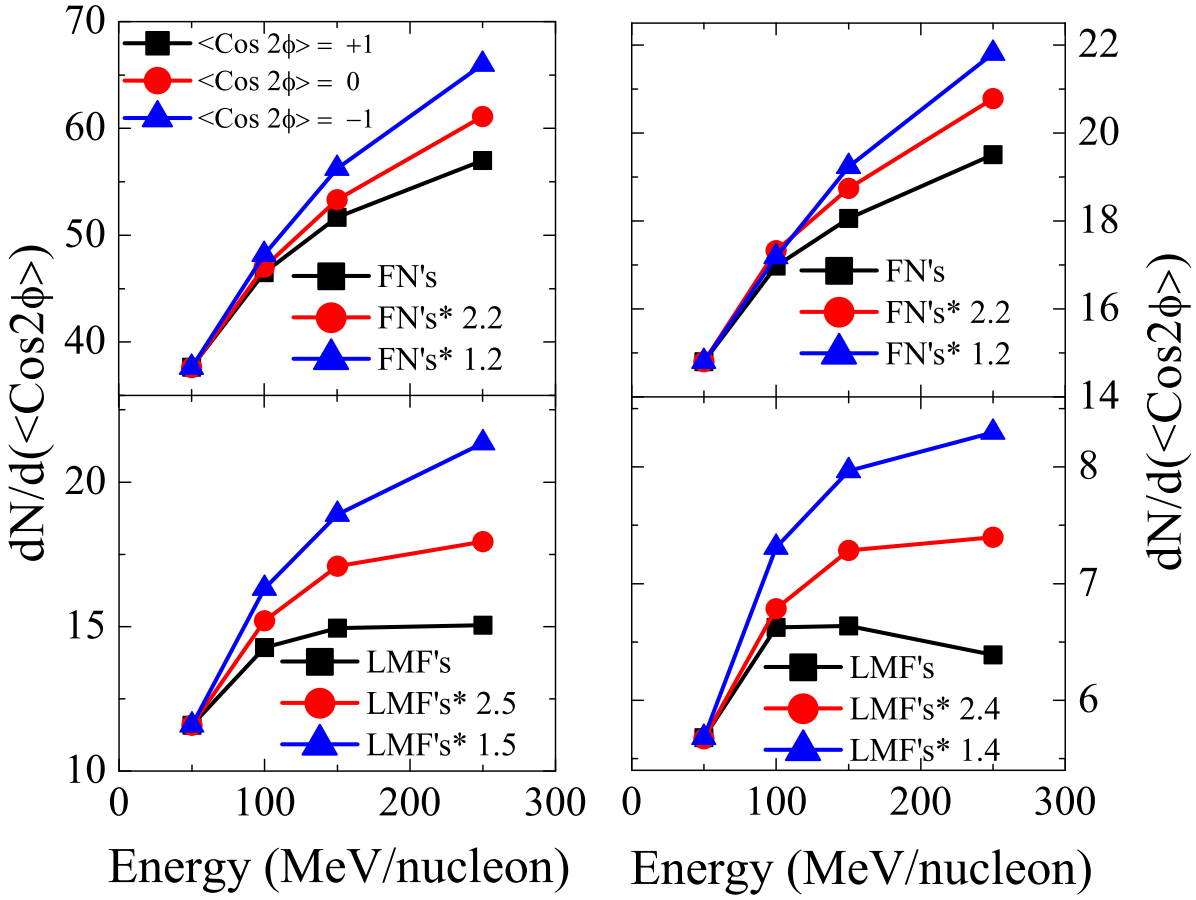

Figure 5.14: *Incident energy dependence of* $\frac{dN}{d(\langle Cos2\phi \rangle)}$ *for the reactions of* ${}^{124}_{50}Sn_{74} + {}^{124}_{50}Sn_{74}$ *and* ${}^{40}_{16}S_{24} + {}^{40}_{16}S_{24}$.

5.4.5 Transverse momentum dependence of elliptical flow

To study the effect of isospin asymmetry on the elliptical flow as a function of $\langle\ p_t\ \rangle$, (where $\langle\ p_t\ \rangle$ is the transverse momentum of the particle and is given by $p_t = \sqrt{(p_x^2 + p_y^2)}$), we display in Fig.5.15, the final state elliptical flow for FN's [(a) & (d)], LMF's [(b) & (e)] and IMF's [(c) & (f)] at an incident energy of E = 50 MeV/nucleon (left panel) and E = 100 MeV/nucleon (right panel) for the reactions of ${}^{124}_{Z_1}\mathrm{X}_n + {}^{124}_{Z_1}\mathrm{X}_n$, where $Z_1 = 47$ and 59 (in Fig.5.15) for isospin dependent cross-section (σ_{iso}). Here elliptical flow is summed over all rapidity bins [230]. Figs.5.15 reveal:

1. A Gaussian shape is obtained for $\langle\ v_2\ \rangle$ in all cases. Note that the elliptical flow is integrated over the entire rapidity range.

2. The peak of the Gaussian shifts towards lower value of $\langle\ p_t\ \rangle$ for heavier fragments. This is because the FN's and LMF's feel the mean field directly, while heavy fragments have weaker sensitivity [186, 231].

3. The neutron rich system ${}^{124}_{47}Ag_{77} + {}^{124}_{47}Ag_{77}$ exhibit weaker squeeze-out flow compared to the neutron deficient systems ${}^{124}_{59}Pr_{65} + {}^{124}_{59}Pr_{65}$. Our findings are in agreement with Ref.[186] where a neutron rich system was found to exhibits weaker squeeze-out flow.

Similar results are obtained for the reactions of ${}^{40}_{Z_2}\mathrm{Y}_n + {}^{40}_{Z_2}\mathrm{Y}_n$, where $Z_2 = 14$ and 20 (not shown here).

To study the effect of isospin dependence of nucleon-nucleon cross-section and change in N/Z of the system (by taking isobaric nuclei) on the elliptical flow, we display in Figs.5.16 and 5.17, the transverse momentum dependence of the elliptical flow for the reactions of ${}^{124}_{47}Ag_{77} + {}^{124}_{47}Ag_{77}$, ${}^{124}_{59}Pr_{65} + {}^{124}_{59}Pr_{65}$ We divide total elliptical flow into contributions from target-like (TL) [(a), (b) & (c)], mid-rapidity [(d), (e) & (f)] and projectile-like (PL) [(g), (h) & (i)] particles at E = 100 MeV/nucleon. The [(a), (d) & (g) panels] represent the FN's, [(b), (e) & (h) panels] represents the LMF's and [(c), (f) & (i) panels] represents the IMF's. Figs. reveal following points:

1. $\langle\ v_2\ \rangle$ is sensitive to isospin dependence of nucleon-nucleon cross-sections. Weaker squeeze-out flow is observed in the case of isospin independent cross-section (σ_{noiso}).

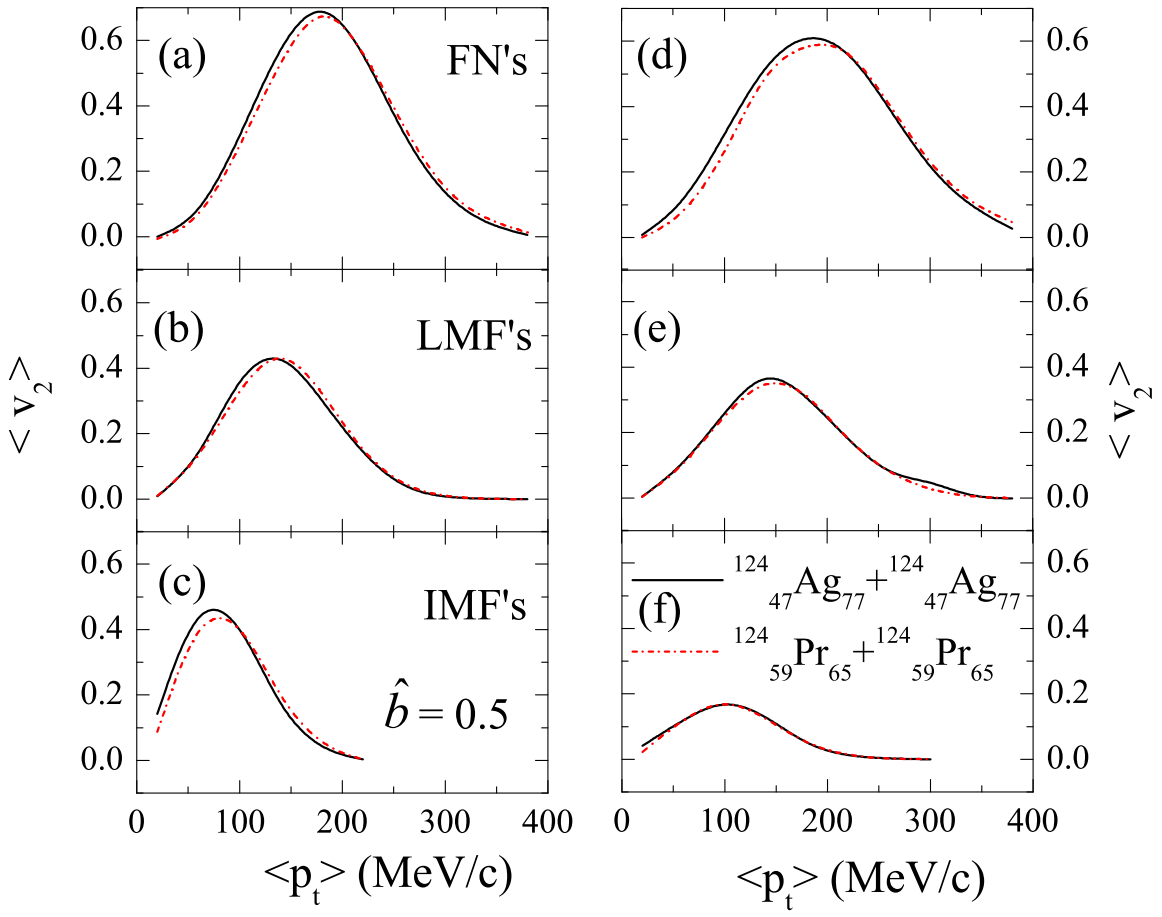

Figure 5.15: *Transverse momentum dependence of the elliptical flow summed over entire rapidity distribution for two different reactions at an incident energy of 50 (left) and 100 (right) MeV/nucleon.*

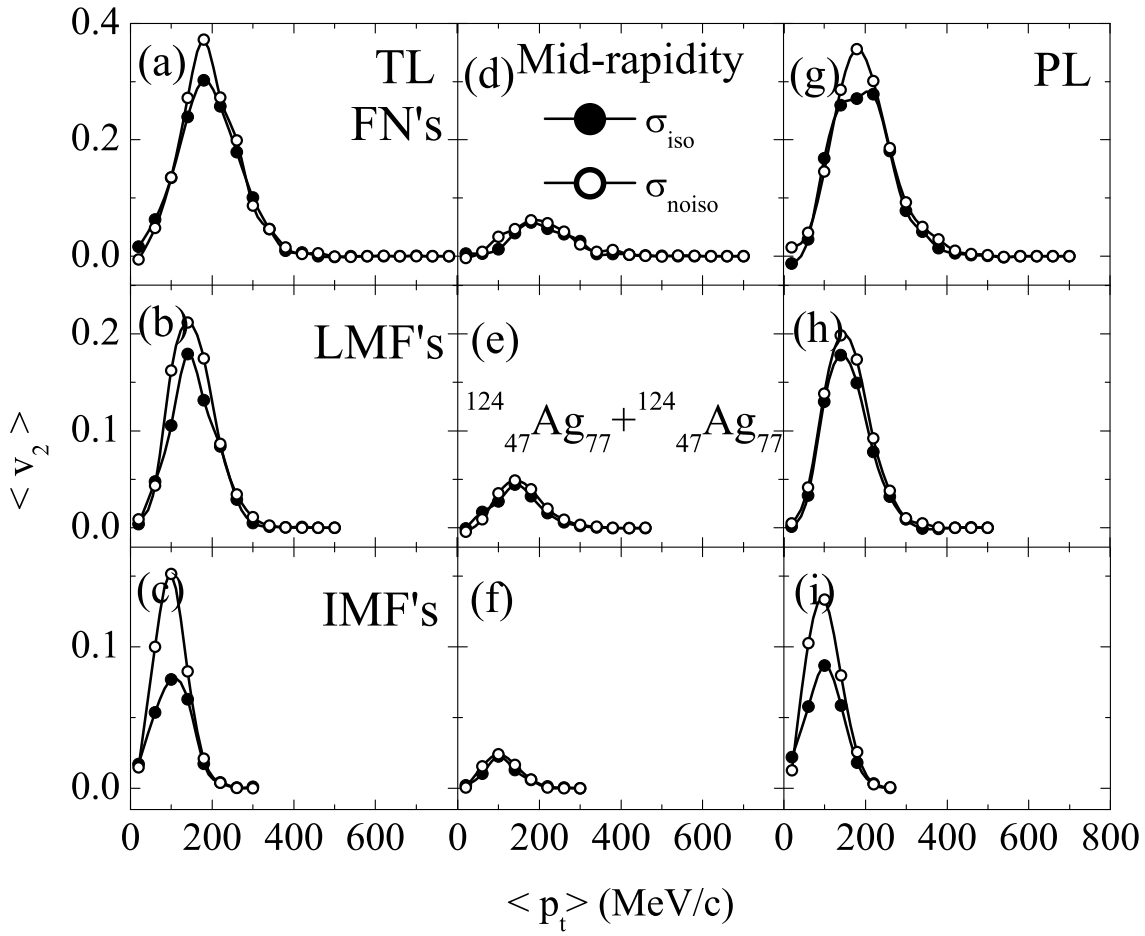

Figure 5.16: *Transverse momentum dependence of the elliptical flow at E = 100 MeV/nucleon for two different cross-sections.*

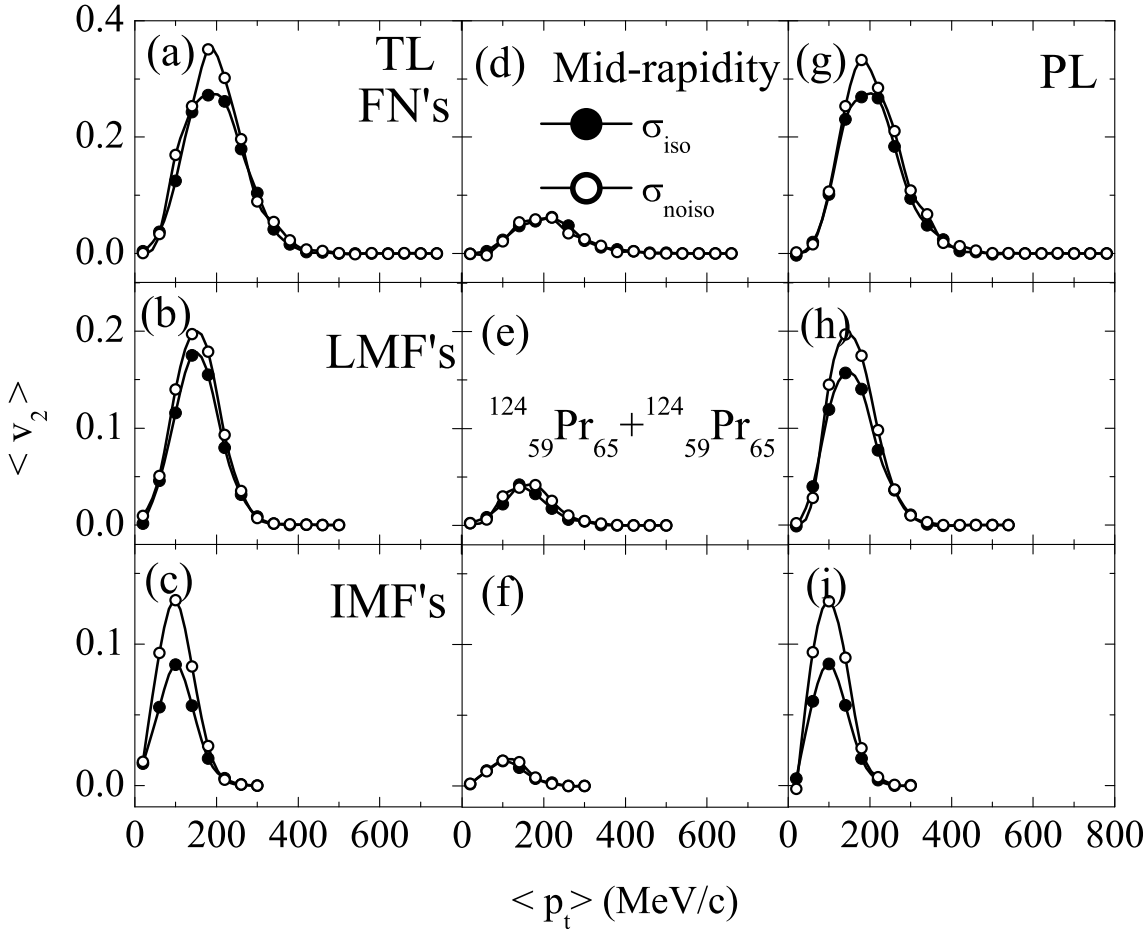

Figure 5.17: *Same as Fig.5.16 but for the reaction* $^{124}_{59}Pr_{65} + ^{124}_{59}Pr_{65}$.

This happens because $\sigma_{iso} = 3\sigma_{noiso}$ [24, 115] that will enhance binary collisions. These findings are in agreement with Ref. [223].

2. For the mid-rapidity region, little influence is observed for the isospin dependent cross-section. This happens because, this zone includes very few nucleons. Moreover, this zone corresponds to the collision (participant) zone, where the violent phase of the collisions occur. Due to which effect of isospin dependent cross-section is not visible.

3. In case of IMF's, the difference between the two cross-sections is large compared to FN's and LMF's. This happens because, the FN's and LMF's are produced from the participant zone and as stated above, due to the occurrence of the violent phase of collisions, various cross-sections don't vary drastically. On the other hand, IMF's are being produced from the spectator matter. Therefore, any change in binary cross-section can have significant effect on the outcome.

Similar results are obtained for the reactions of ${}^{40}_{14}Si_{26} + {}^{40}_{14}Si_{26}$ and ${}^{40}_{20}Ca_{20} + {}^{40}_{20}Ca_{20}$ (not shown here).

5.4.6 Incident energy dependence of elliptical flow

In Figs.5.18 and 5.19, we display the variation of the excitation function of elliptical flow $\langle\ v_2\ \rangle$ for FN's [panel (a)], LMF's [panel (b)] and IMF's [panel (c)] for mid-rapidity region using same set of the reactions considered earlier with isospin dependent cross-section, for $\gamma = 0.66$ in Fig.5.18 and for $\gamma = 2$ in Fig.5.19. We note:

1. The elliptical flow turns negative with beam energy. This is because spectator move faster after $\langle\ v_2\ \rangle$ reaches a minimum value [85, 232]. The energy at which this behavior changes is found to decrease with the size of the fragment. This means that the flow of the heavier fragments is large compared to LMF's and FN's at all beam energies. These findings are in agreement with Ref. [233].

2. There occurs a transition from the in-plane to out-of-plane emission. This happens because, at low incident energy, there is dominance of the mean field. Here, the

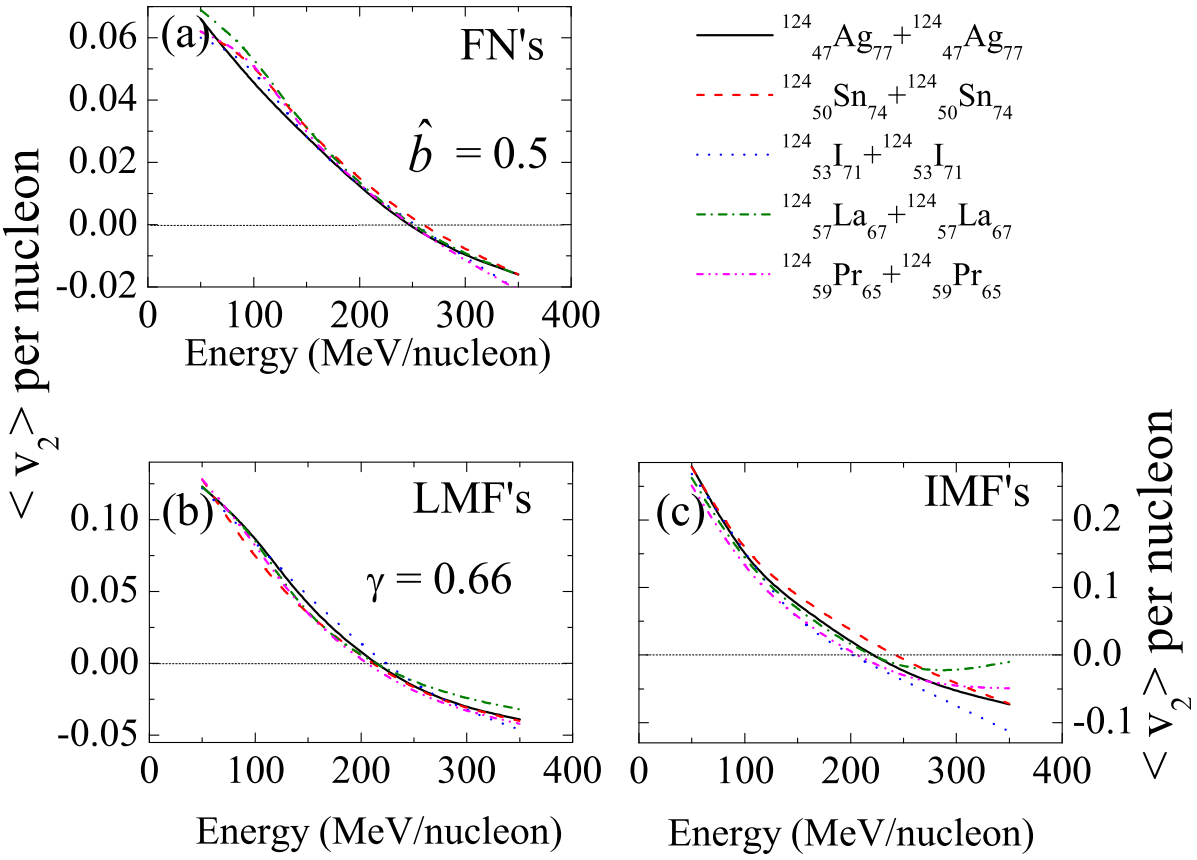

Figure 5.18: *The variation of the elliptical flow with incident energy for the reactions of* $^{124}_{Z_1}X_n + ^{124}_{Z_1}X_n$, *where* $^{124}_{Z_1}X_n$ = ($^{124}_{47}Ag_{77}$, $^{124}_{50}Sn_{74}$, $^{124}_{53}I_{71}$, $^{124}_{57}La_{67}$ *and* $^{124}_{59}Pr_{65}$).

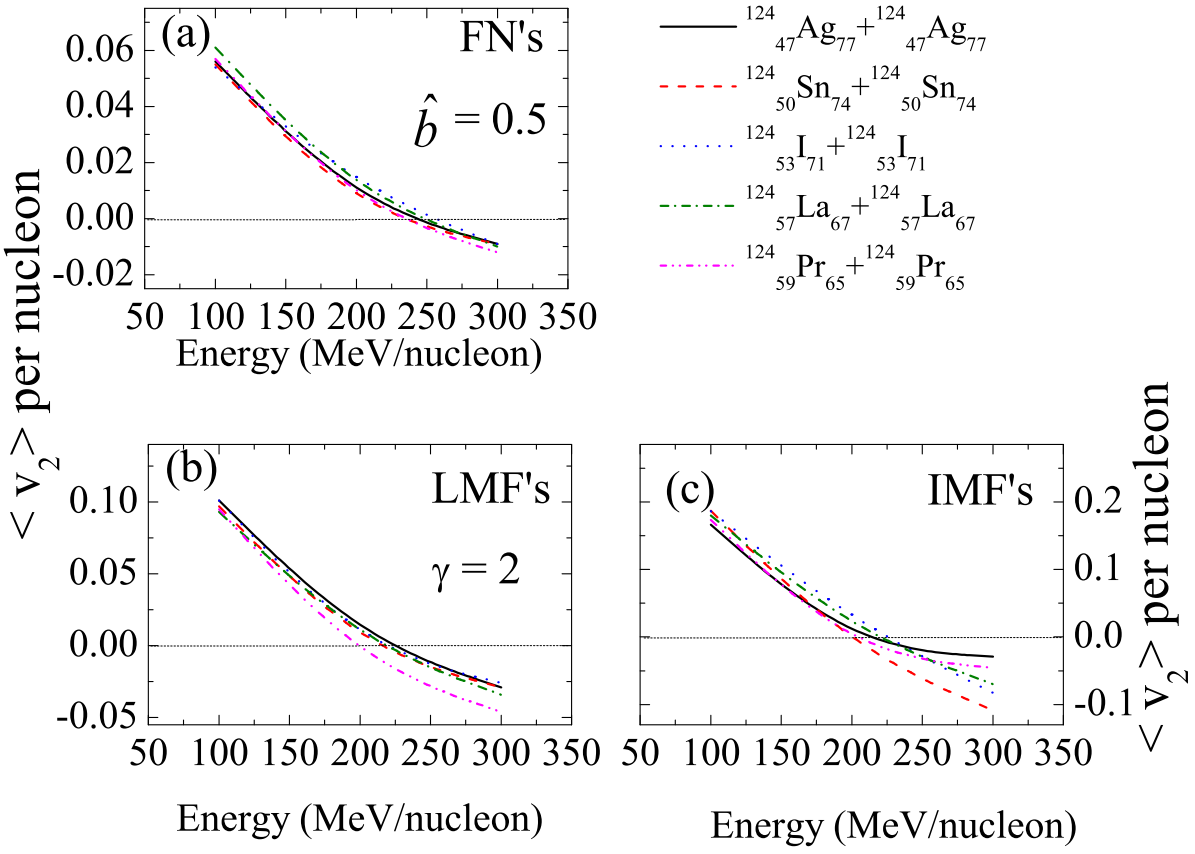

Figure 5.19: *Same as Fig.5.18 but for* $\gamma = 2$.

rotating nucleus corresponding to the dominating spectator matter contributes towards the directed transverse in-plane flow. At higher incident energies, however, the mean field does not play any significant role. The larger compression produced in the participant zone results in the squeeze-out of the nuclear matter. On the other hand, the elliptical flow, which is a representative of hot matter and shadowing of the spectator matter, turns negative at relatively higher incident energies. Similar results are obtained for the reactions in which mass of the colliding nuclei is fixed to be 80 units.

In other words, participant zone is primarily responsible for the transition from the in-plane to out-of-plane.

To further strengthen our interpretation of the results of elliptical flow $\langle\ v_2\ \rangle$, we display in Fig.5.20 a comparison of the theoretical results of elliptical flow with experimental findings reported by the INDRA@(GSI+GANIL) collaboration [85] [panel (a)] for the reaction of ${}^{124}_{50}Sn_{74} + {}^{124}_{50}Sn_{74}$ and with theoretical results [232] [panels (b) and (c)] for the reaction of ${}^{112}_{50}Sn_{62} + {}^{112}_{50}Sn_{62}$. Here simulations are performed with σ_{iso} reduced by 20%. The choice of the reduced cross-section has also been motivated by Ref.[184] as well as many previous studies [205]. Similar data has been compared by one of our collaborator for the reaction of ${}^{129}_{54}Xe_{75} + {}^{124}_{50}Xe_{74}$ [234]. Our theoretical calculations are closer to experimental findings compared to earlier studies with σ_{iso} reduced by 20%. It is worth mentioning that the results with above choice of cross-section are in good agreement with the experimental data of Ref. [85] at higher energies but large difference is observed at lower energies. This can be due to the experimental filters which are not accessible to us. Moreover, in [panels (b) and (c)], the results are not in good agreement with the theoretical results. This is because, in the Ref. [232] percentage of $\langle\ v_2\ \rangle$ is plotted for all the nucleons but in our calculations we have plotted the percentage of $\langle\ v_2\ \rangle$ for FN's only.

5.4.7 N/Z dependence of transition energy

Now to study the effect of change in N/Z of the system on the transition energy of FN's [panels (a) & (d)], LMF's [panels (b) & (e)] and IMF's [panels (c) & (f)], we display in Fig.5.21, the transition energy as a function of the neutron to proton ratio for FN's

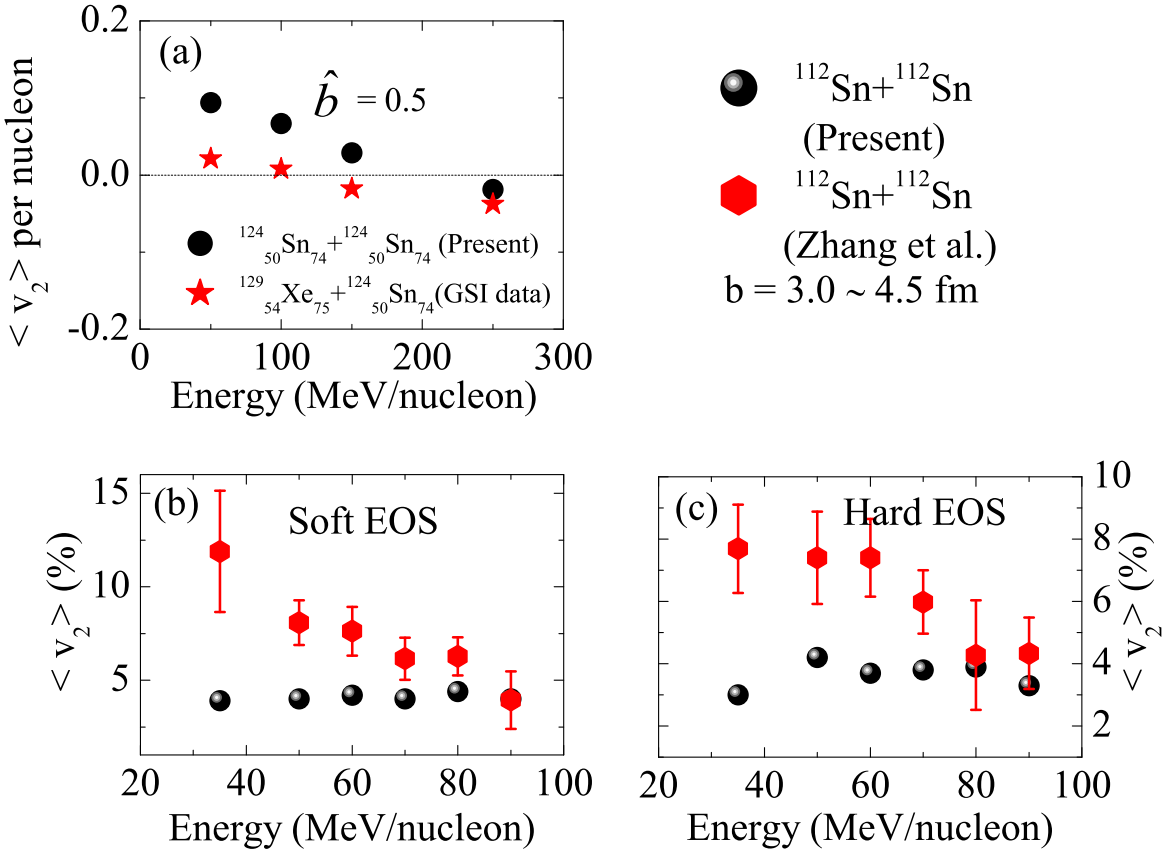

Figure 5.20: *(a) Comparison of* $\langle\, v_2 \,\rangle$ *between theoretical and experimental measurements extracted by the INDRA@(GSI+GANIL) collaboration for the reaction of* $^{124}_{50}Sn_{74} + ^{124}_{50}Sn_{74}$. *(b) & (c) Comparison of our results with theoretical results of Zhang et al. [232] for the reaction of* $^{112}_{50}Sn_{62} + ^{112}_{50}Sn_{62}$.

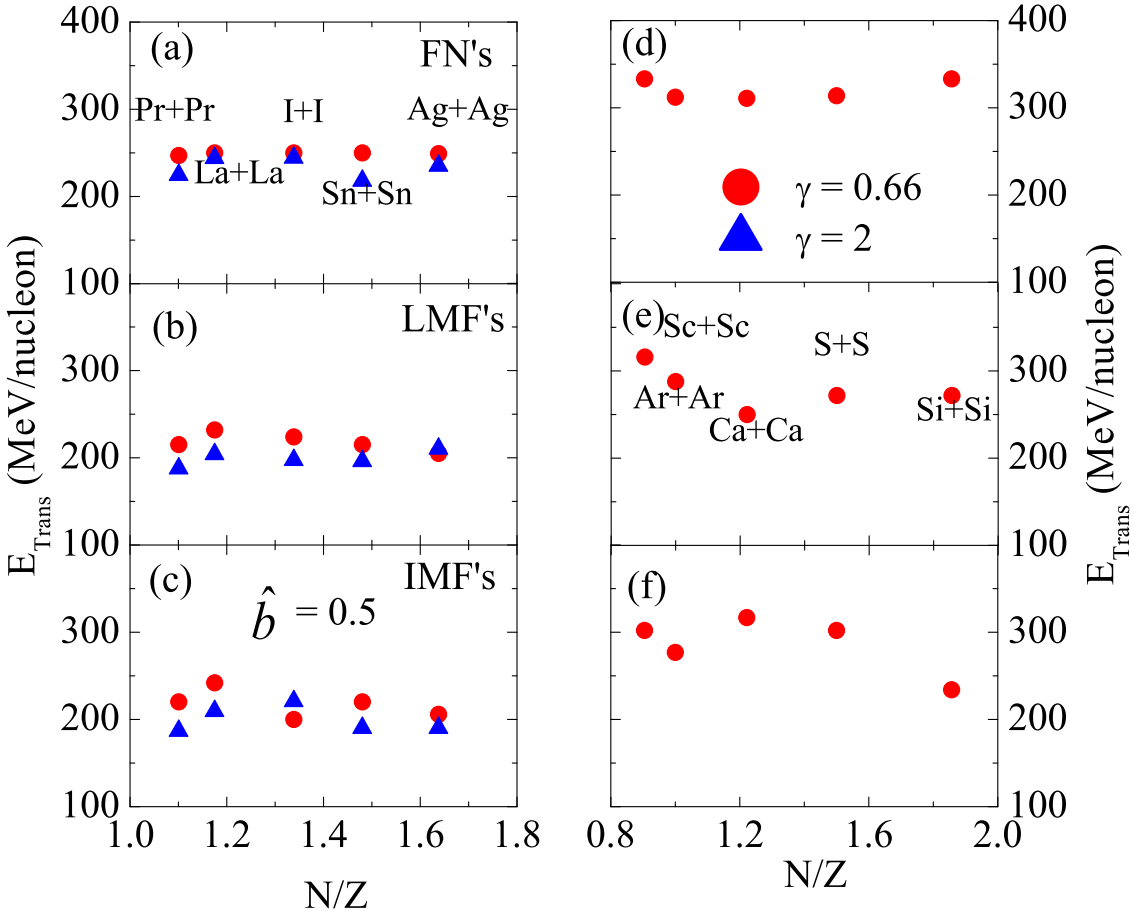

Figure 5.21: *Transition energies (E_{Trans} in MeV/nucleon) as a function of N/Z ratio for FN's [panels (a) & (d)], LMF's [panels (b) & (e)] and IMF's [panels (c) & (f)].*

[panels (a) & (d)], LMF's [panels (b) & (e)] and IMF's [panels (c) & (f)] for $\gamma = 0.66$ and 2 in left panels and for $\gamma = 0.66$ in right panels. From the Figs., it is clear that transition energy remains almost unchanged with the increase in the N/Z of the system. Moreover, (left panels) transition energy decreases with increase in γ. Note that the elliptical flow is strongly influenced by the participant matter, thus, in fact depends on the density reached in a reaction. Larger value of γ corresponds to larger symmetry energy repulsion around the compressed zone (participant zone). Therefore, elliptical flow tends to be affected by the various forms of the density dependent symmetry energy. These findings are in agreement with Ref. [212].

5.5 Different aspects of triangular and quadrupole flow

Higher order anisotropic flows arises due to the medium response to a fluctuating initial state. In recent years, extensive endeavors on harmonic flows has been devoted experimentally and theoretically. The combined investigation of harmonic flow and event plane correlations provide new constraints on the properties of the medium produced in heavy ion collisions. In the previous sections we have discussed the various aspects of elliptical flow, as it usually dominates the other coefficients and being strongly influenced by the elliptical geometry of the overlap region between the colliding nuclei. However, the initial geometry of the produced fireball may have angular moments of several orders: elliptical, triangular and quadrupole etc. due to the fluctuations in the spatial positions of the nucleons in the colliding nuclei. These higher order coefficients typically refer to harmonics higher than the second one, $\langle v_2 \rangle$. These higher order moments in the initial geometry can give rise to measurable higher order flow. Earlier it was thought that the higher order flow are caused by fluctuations in the positions of the participant nucleons and are negligibly small [57, 215]. However, a recent study based on viscous hydrodynamics has shown that $\langle v_3 \rangle$ is more sensitive to the viscosity of the quark-gluon plasma than $\langle v_2 \rangle$ [235]. A study by Kolb [59] shows that, $v_4(p_t)$ might achieve significantly large values at intermediate and large transverse momenta in non-central heavy ion collisions. In the next subsections we shall discuss the isospin effects (by taking isobaric nuclei and isospin dependent nucleon-nucleon cross-section) on triangular ($\langle v_3 \rangle$) and quadrupole ($\langle v_4 \rangle$) flow.

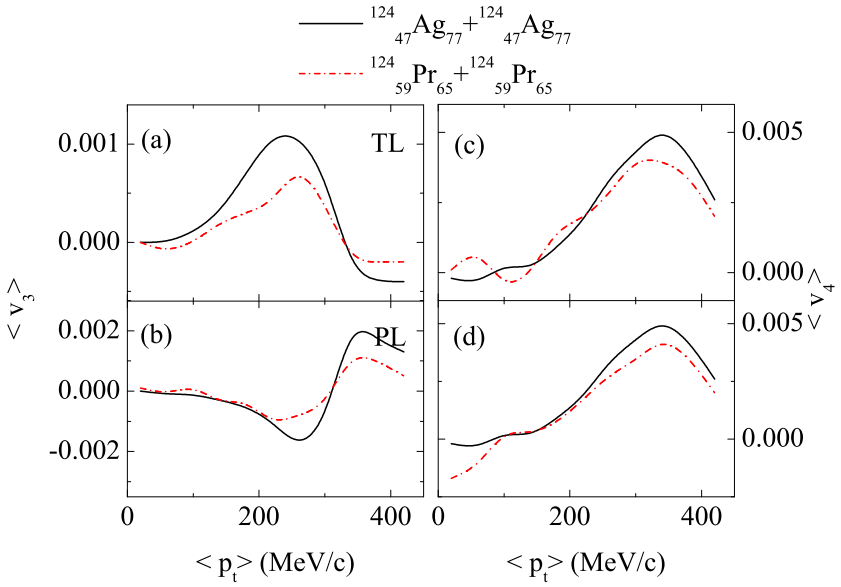

Figure 5.22: *Transverse momentum dependence of triangular and quadrupole flow for two different rections at an incident energy of 100 MeV/nucleon.*

5.5.1 Transverse momentum dependence of triangular and quadrupole flow

As we have discussed earlier, the isospin effects enters the dynamics of heavy ion collisions through symmetry energy and isospin dependence of nucleon-nucleon cross-section. Therefore, to explore isospin effects via these two, we display in Fig.5.22 transverse momentum dependence of $\langle v_3 \rangle$ and $\langle v_4 \rangle$ for the reactions of $^{124}_{47}Ag_{77}+^{124}_{47}Ag_{77}$ and $^{124}_{59}Pr_{65}+^{124}_{59}Pr_{65}$ and in Fig.5.23, transverse momentum dependence of $\langle v_3 \rangle$ and $\langle v_4 \rangle$ for the reactions of $^{124}_{47}Ag_{77}+^{124}_{47}Ag_{77}$ for two different cross-sections, one is isospin dependent and another is isospin independent. We divide the total anisotropic flows into contributions from (target-) and (projectile-) like regions. One can see that, higher order harmonics follow the similar behavior as followed by elliptical flow (see e.g. Fig.5.15) but the percentage change in $\langle v_3 \rangle$ and $\langle v_4 \rangle$ is more for both isobaric colliding nuclei and for isospin dependence of nucleon-nucleon cross-section compared to elliptical flow. This shows that, $\langle v_3 \rangle$ and $\langle v_4 \rangle$ are highly dependent on the initial configuration of the system and its evolution. Therefore, these can act as an important tool to analyze the system history at intermediate energies.

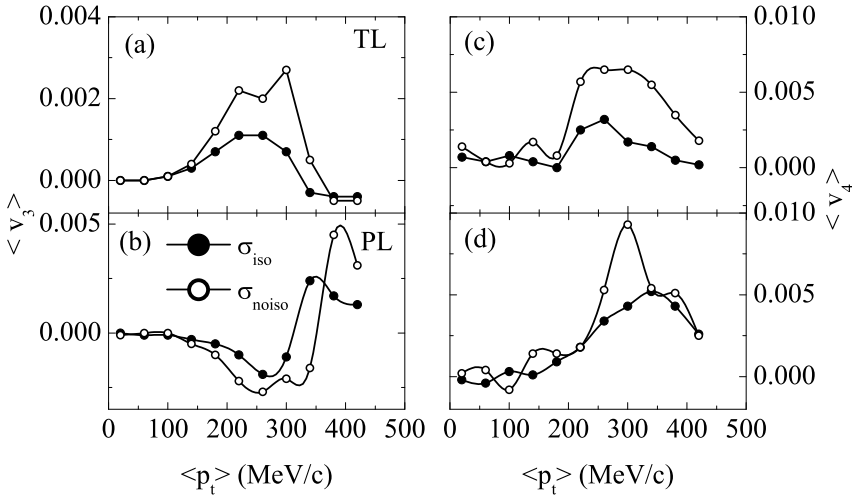

Figure 5.23: *Transverse momentum dependence of triangular and quadrupole flow at an incident energy of E = 100 MeV/nucleon for two different cross-sections.*

5.6 Summary

We studied the role of isospin degree of freedom on directed, elliptical, triangular and quadrupole flow. We found that, the isospin dependence of nucleon-nucleon cross-section has a significant role to play on the neutron/proton differential sideward flow. The results produced with σ_{iso} are found to be more compatible with experimental data. We have proved theoretically for the first time that, fragment charge/mass does not influence the balance energy. In case of elliptical flow, our study revealed that, the distribution of nucleons and fragments is not symmetric around the beam axis. Isospin dependence of nucleon-nucleon cross-section play important role in the transverse momentum dependence of elliptical flow. However, like multifragmentation and nuclear stopping, transition energy also remains unaffected by the change in isotopic content of the system. We have attempted to reproduce the experimental findings of GSI collaboration. Similar data has been compared by one of our collaborator for the reaction of $^{129}_{54}Xe_{75} +^{124}_{50} Xe_{74}$. Our theoretical calculations are closer to experimental findings compared to earlier studies with σ_{iso} reduced by 20%. From this we again conclude that, strength of nucleon-nucleon cross-section play a significant role in the reaction dynamics. Both triangular ($\langle v_3 \rangle$) and

quadrupole flow ($\langle v_4 \rangle$) are more sensitive to the isotopic content as well as to the isospin dependence of nucleon-nucleon cross-section. Which indicates that, these harmonics depends strongly on the initial configuration of the system and its evolution.

Chapter 6

Nuclear stopping around balance energy

6.1 Introduction

As we have already mentioned, heavy-ion collisions at intermediate energies have been found to host a variety of rare phenomena such as multifragmentation, nuclear stopping, collective flow and its disappearance, and subthreshold particle production [36, 175, 176, 186, 236, 237]. Out of these, the first three has been discussed in chapters 3, 4 and 5 respectively. The processes like fusion, fission as well as cluster decay are, however, dominant channels at the lower tail of the energy [177, 238, 239]. Irrespective of the phenomena, lots of investigations have been reported in the literature about the system size effects. Most of the phenomena have been found to have a power law ($\propto A^{\tau}$) dependence. This power law dependence can be in terms of charge/mass of colliding nuclei or in terms of the mass of the fragments [61, 167, 203, 240, 241, 242]. In multifragmentation, the value of the power law parameter τ depends on various physical factors such as incident energy, colliding geometry as well as on the type of the fragment. In collective flow, its disappearance also witnesses such mass (or system size) dependence. The study of the system size dependence may reveal structural effects ranging over entire periodic mass. At the same time, the recent advances in the radioactive ion beam facilities provide the scientific community with a unique opportunity to investigate the isospin effects in heavy-ion collisions [22, 172].

Isospin effects as evident from the literature are found to influence collective flow and its disappearance drastically. It is well known that attractive scatterings (dominating at low incident energies) counter balance repulsive interactions at a particular incident energy,

known as the energy of vanishing flow (EVF) or balance energy [174, 189, 243]. Recently, in a series of papers [204, 244], isospin effects were investigated in collective flow in many isotopes, isobars and isotones covering entire periodic table. One would like to know whether other associated phenomena such as nuclear stopping or thermalization respond to such isospin effects at and around EVF. It is worth mentioning that, the collective flow is generated by the pressure gradient established in the compressed matter while the achieved density is connected to the degree of nuclear stopping. In the present chapter, we plan to address the above points.

6.2 Results and discussion

As stated in the introduction, we shall perform a systematic study of nuclear stopping by taking pairs of isotopes and isobars and shall look for the role of isospin effects and system size dependence spanning over entire colliding geometry at and around (below and above) EVF. This study will give us an indication whether physics phenomena at EVF and below or above is similar or not. First we simulate the reactions with the experimentally available isotopic beams. In particular, we simulate the reactions of $^{40}S+^{40}S$, $^{60}Cr+^{60}Cr$, $^{74}Zn+^{74}Zn$ and $^{124}Sn+^{124}Sn$ having N/Z $\approx$ 1.5 labeled as "$isot_1^{exp}$" and the reactions of $^{44}S+^{44}S$, $^{68}Cr+^{68}Cr$, $^{82}Zn+^{82}Zn$ and $^{142}Sn+^{142}Sn$ having N/Z $\approx$ 1.8 labeled as "$isot_2^{exp}$". Then study has been extended for the reactions of $^{26}_{12}Mg_{14}+^{26}_{12}Mg_{14}$, $^{65}_{30}Zn_{35}+^{65}_{30}Zn_{35}$, $^{91}_{42}Mo_{49}+^{91}_{42}Mo_{49}$, $^{117}_{54}Xe_{63}+^{117}_{54}Xe_{63}$ and $^{164}_{76}Os_{88}+^{164}_{76}Os_{88}$ having N/Z = 1.16 labeled as "$isot_1$" and the reactions of $^{28}_{12}Mg_{16}+^{28}_{12}Mg_{16}$, $^{70}_{30}Zn_{40}+^{70}_{30}Zn_{40}$, $^{98}_{42}Mo_{56}+^{98}_{42}Mo_{56}$, $^{126}_{54}Xe_{72}+^{126}_{54}Xe_{72}$ and $^{177}_{76}Os_{101}+^{177}_{76}Os_{101}$ having N/Z = 1.33 labeled as "$isot_2$" respectively. Similarly, for isobaric study, the reactions of $^{24}_{12}Mg_{12}+^{24}_{12}Mg_{12}$, $^{58}_{29}Cu_{29}+^{58}_{29}Cu_{29}$, $^{72}_{36}Kr_{36}+^{72}_{36}Kr_{36}$, $^{96}_{48}Cd_{48}+^{96}_{48}Cd_{48}$, $^{120}_{60}Nd_{60}+^{120}_{60}Nd_{60}$, $^{135}_{67}Ho_{68}+^{135}_{67}Ho_{68}$ having N/Z = 1.0 labeled as "$isob_1$" and the reactions of $^{24}_{10}Ne_{14}+^{24}_{10}Ne_{14}$, $^{58}_{24}Cr_{34}+^{58}_{24}Cr_{34}$, $^{72}_{30}Zn_{42}+^{72}_{30}Zn_{42}$, $^{96}_{40}Zr_{56}+^{96}_{40}Zr_{56}$, $^{120}_{50}Sn_{70}+^{120}_{50}Sn_{70}$ and $^{135}_{56}Ba_{79}+^{135}_{56}Ba_{79}$ having N/Z = 1.4 labeled as "$isob_2$" respectively were taken. The colliding geometry is divided into four bins that vary from central to peripheral one. We label BIN 1 ($\hat{b}$ = 0.15-0.25), BIN 2 ($\hat{b}$ = 0.35-0.45), BIN 3 ($\hat{b}$ = 0.55-0.65) and BIN 4 ($\hat{b}$ = 0.75-0.85). We simulate the above reactions at the energy of vanishing flow whose values are taken from the work of Gautam *et al.,* [204, 244]. In addition, we have also analyzed the reactions at incident energies above (with maximum

increment of 30 MeV/nucleon from EVF) and below (with maximum decrement of 30 MeV/nucleon from EVF) the energy of vanishing flow.

6.2.1 System mass dependence of nuclear stopping for isotopic pairs

To study the isospin effects on the nuclear stopping, we display in Fig.1, the system mass dependence of $\langle R \rangle$ for two sets of isotopic systems (experimentally available beams). The panels from the top to bottom display the results for $\hat{b} = b/b_{max} = 0.25$, 0.45 and 0.65 where $b_{max} = 1.12(A_P^{1/3} + A_T^{1/3})$ and A_P, A_T are the mass of projectile and target respectively. Different columns display the results below (left column), at (middle column) and above (right column) EVF. Various lines are the power law fits of the kind $\propto A_{tot}^{\tau}$. Fine observations are:

1. A decrease in net stopping is seen in all cases with increase in impact parameter, this is due to the fact that, net reaction volume decreases with impact parameter. This leads to less erase of the initial memory of the colliding pair.

2. The system size effects dominate over the isospin effects throughout the mass range. This is due to the fact that heavier system leads to more compression that populates more nuclear stopping. Inverse happen with increase in the incident energy. This result is in agreement with Refs.[88, 200] where the nuclear stopping was reported to decrease with incident energy. No visible structural changes are seen around the energy of vanishing flow.

To further strengthen our interpretation of results, we display in Fig.6.2, the system mass dependence of $\langle R \rangle$ for two sets of isotopic systems. The panels from the top to bottom display the results for different colliding geometry bins mentioned above. Interestingly, similar results are obtained for the these systems as discussed in Fig.1 for the experimentally available beams. Moreover, theoretical results for this set of reactions can be experimentally verified.

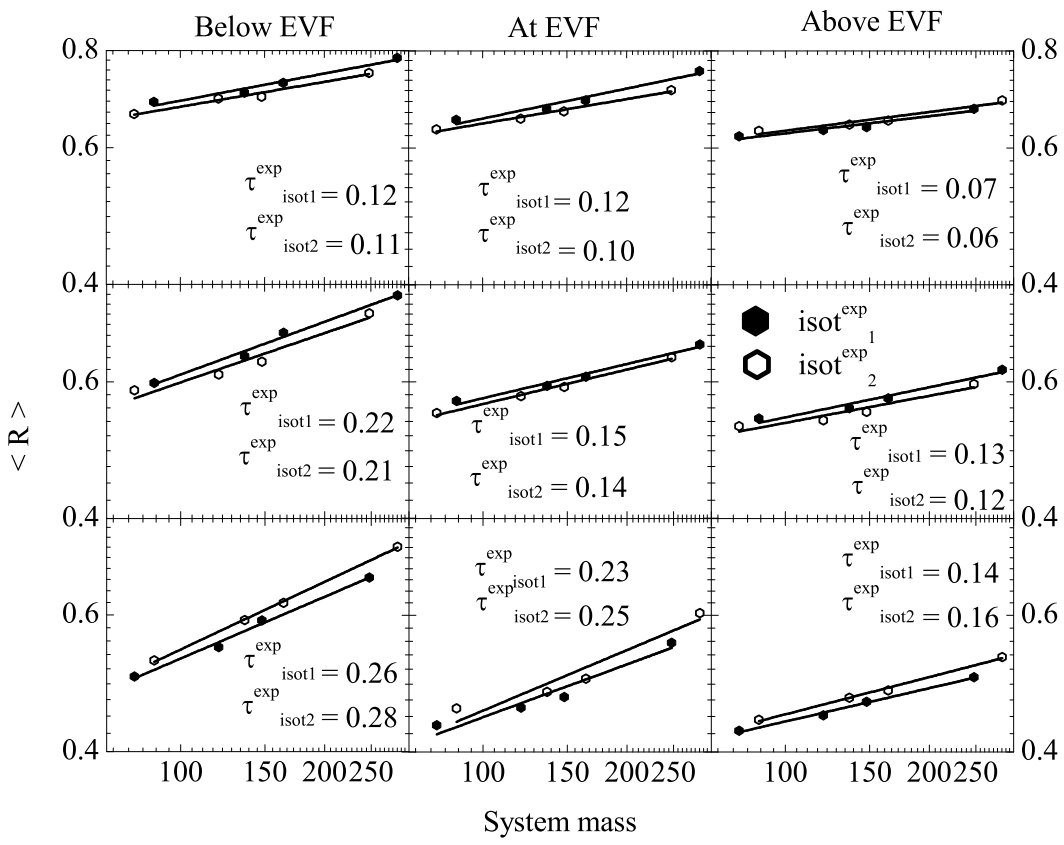

Figure 6.1: *System mass dependence of the nuclear stopping for two isotopic pairs at different colliding geometries.*

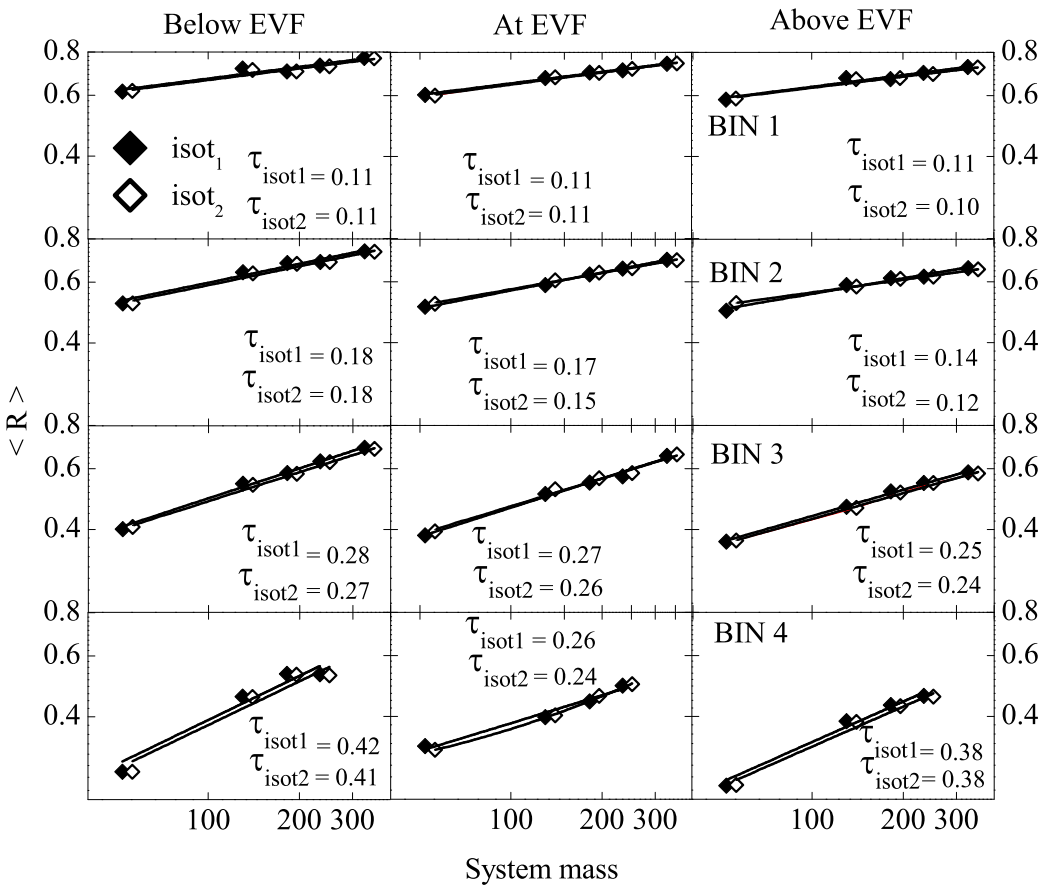

Figure 6.2: *System mass dependence of the nuclear stopping for two isotopic pairs at different colliding geometries. Different columns represents the results at different incident energies. Below EVF (left column), at EVF (middle column) and above EVF (right column).*

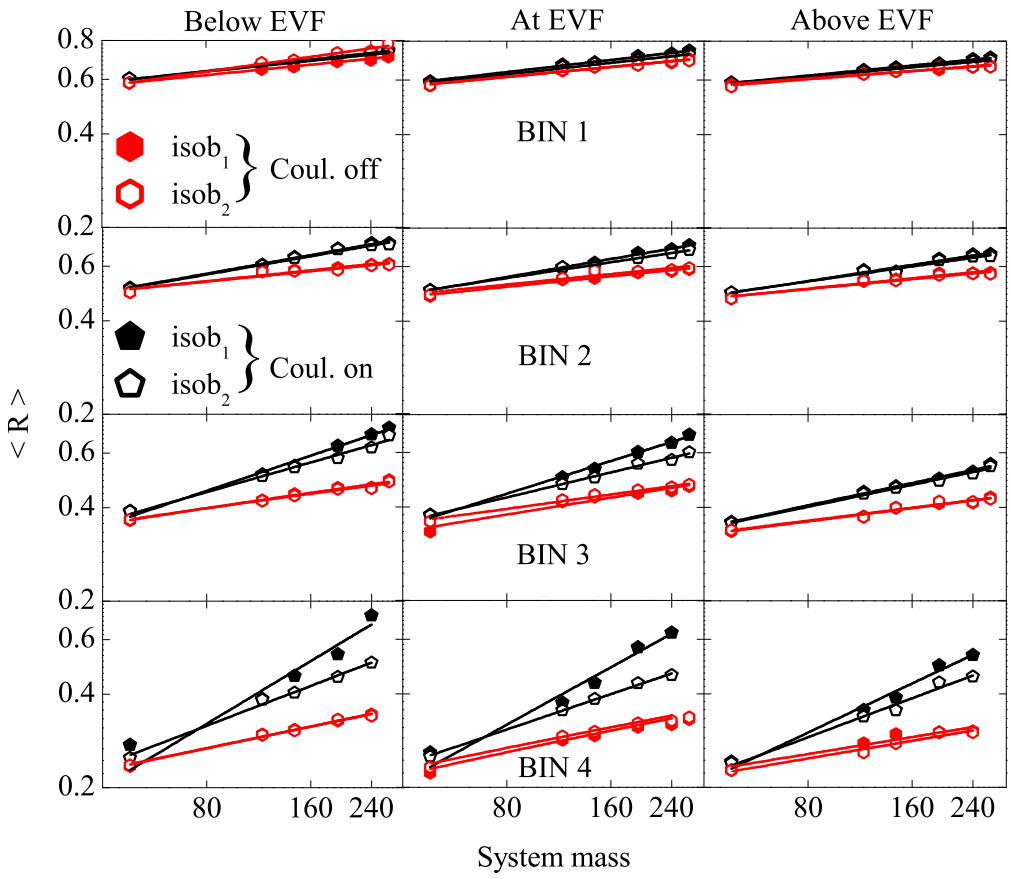

Figure 6.3: *System mass dependence of nuclear stopping for two isobaric pairs at different colliding geometries. The pentagon (hexagon) are for the calculations with (without) Coulomb potential.*

6.2.2 System mass dependence of nuclear stopping for isobaric pairs

As a next step, we carried out the study for the isobaric pairs throughout the mass range. Fig.6.3 displays the system mass dependence of $\langle R \rangle$ for two sets of isobaric systems. The N/Z ratio is varied by changing the number of protons at a fixed local reacting mass. The values of τ for both with and without Coulomb potential are listed in Table 6.1 & 6.2.

Table 6.1: *The values of slope parameter τ for different N/Z ratios with Coulomb potential.*

	Below EVF		At EVF		Above EVF	
$\hat{b}$	τ_{isob_1}	τ_{isob_2}	τ_{isob_1}	τ_{isob_2}	τ_{isob_1}	τ_{isob_2}
BIN 1	0.12	0.11	0.12	0.12	0.10	0.10
BIN 2	0.19	0.19	0.19	0.17	0.17	0.15
BIN 3	0.37	0.31	0.34	0.26	0.23	0.23
BIN 4	0.67	0.42	0.61	0.37	0.52	0.41

Table 6.2: *The values of slope parameter τ for different N/Z ratios without Coulomb potential.*

	Below EVF		At EVF		Above EVF	
$\hat{b}$	τ_{isob_1}	τ_{isob_2}	τ_{isob_1}	τ_{isob_2}	τ_{isob_1}	τ_{isob_2}
BIN 1	0.11	0.15	0.10	0.10	0.07	0.08
BIN 2	0.12	0.16	0.11	0.11	0.11	0.10
BIN 3	0.16	0.19	0.18	0.15	0.14	0.13
BIN 4	0.23	0.23	0.21	0.20	0.18	0.18

Our findings are as:

1. Nuclear stopping is less for the neutron rich systems throughout the mass range as described above. Clearly, the different values of τ for isobaric pairs is due to the role of Coulomb interactions for the systems having higher proton content in heavier systems.

2. As mentioned above, the role of symmetry energy dominates the reaction dynamics (which will reduce the nuclear stopping) for the system having more neutron content, whereas repulsive Coulomb interactions dominate the reaction dynamics for the systems having more proton content. Therefore, in order to study the dominance of Coulomb interactions, we have also calculated the nuclear stopping for the above

mentioned isobaric pairs throughout the mass range without Coulomb potential. The dominance of the Coulomb repulsion is visible in the system mass dependence as well as in the isospin effects. We also notice reduced role of τ in reactions without Coulomb potential.

3. Isospin effects become more pronounced with impact parameter. Moreover, the stopping decreases for the neutron rich system as explained above. The magnitude of the isospin effects increases with the increase in the mass of the system at all colliding geometries. The effect is much more pronounced at higher impact parameters. This difference is clearly visible from the values of τ for $isob_1$ and $isob_2$. Situation becomes more interesting if we check the role of Coulomb potential at different colliding geometry. The nuclear stopping decreases if we switch off Coulomb potential. Moreover, the difference between the two isobaric pairs is negligible at all colliding geometries. This behavior is in contrast with the situation for full Coulomb. The above mentioned behavior is independent of the incident energy irrespective of whether it is energy of vanishing flow or below/above the energy of vanishing flow.

6.2.3 Impact parameter dependence of slope parameter τ

From the above discussion, it is clear that, Coulomb interactions play a significant role in the collision of heavier mass systems and effect becomes more pronounced at higher impact parameters. Therefore, in order to study the variation of the slope parameter (τ) with colliding geometry, we display in Fig.6.4, the impact parameter dependence of the slope parameter both with $A_{tot} = 48$ and without $A_{tot} = 48$ as explained in Ref.[204, 244]. The solid symbols are for the case with $A_{tot} = 48$, square (circle) represents the results for $isob_1$ ($isob_2$) with Coulomb potential and diamond (upper triangle) for $isob_1$ ($isob_1$) without Coulomb potential respectively. The corresponding open symbols are shown for the case without $A_{tot} = 48$. One can see that, for full Coulomb the value of τ increases for both $isob_1$ and $isob_2$ with increase in impact parameter. But this increase remain independent of the inclusion of $A_{tot} = 48$ for $isob_2$, but shows a sharp increase with impact parameter for $isob_1$ when we take into account only heavier masses compared to the case where lighter masses are also included. The values of parameter τ with and without $A_{tot} = 48$ are listed in Tables 6.3 & 6.4.

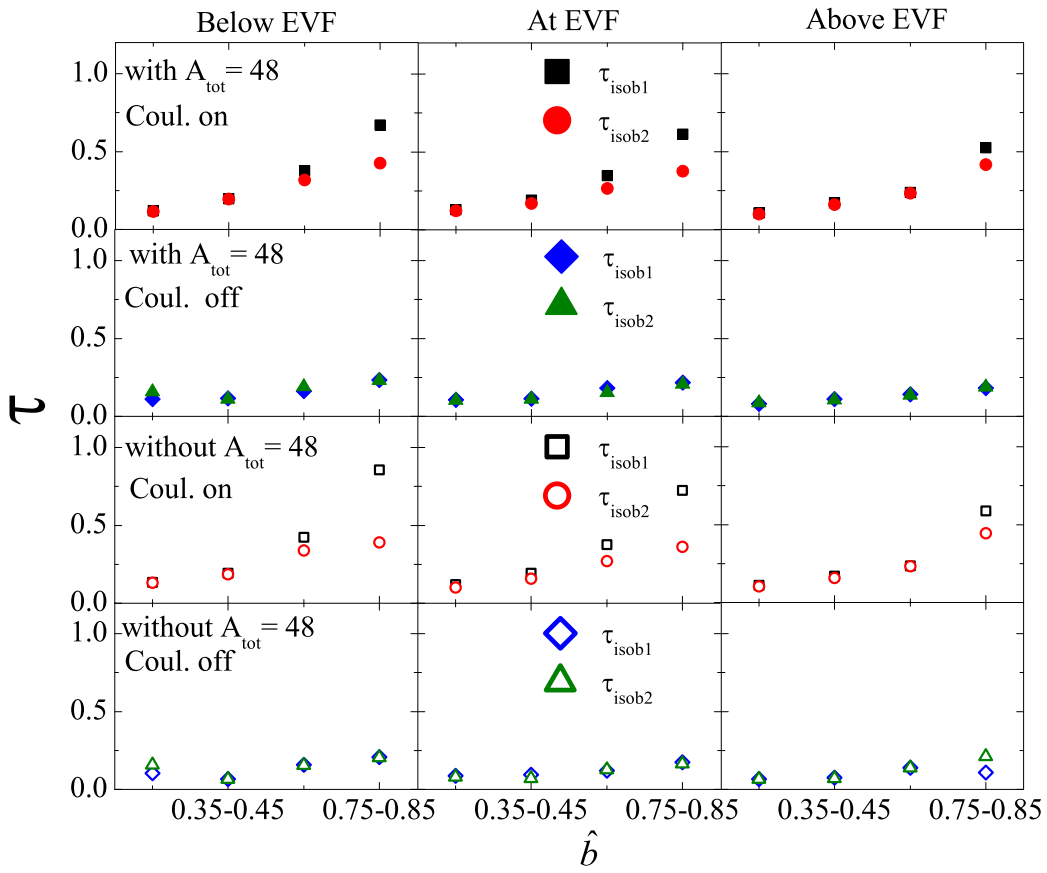

Figure 6.4: *Impact parameter dependence of slope parameter τ for both with and without Coulomb potential with and without $A_{tot} = 48$.*

Table 6.3: *The values of slope parameter τ for different N/Z ratios with Coulomb potential and without A_{tot} = 48.*

	Below EVF		At EVF		Above EVF	
$\hat{b}$	$isob_1$	$isob_2$	$isob_1$	$isob_2$	$isob_1$	$isob_2$
BIN 1	0.13	0.13	0.12	0.10	0.11	0.10
BIN 2	0.19	0.18	0.19	0.15	0.17	0.15
BIN 3	0.42	0.34	0.37	0.27	0.23	0.23
BIN 4	0.85	0.39	0.72	0.36	0.58	0.44

Table 6.4: *The values of slope parameter τ for different N/Z ratios without Coulomb potential and without A_{tot} = 48.*

	Below EVF		At EVF		Above EVF	
$\hat{b}$	$isob_1$	$isob_2$	$isob_1$	$isob_2$	$isob_1$	$isob_2$
BIN 1	0.10	0.15	0.08	0.08	0.06	0.06
BIN 2	0.06	0.06	0.09	0.07	0.07	0.07
BIN 3	0.15	0.15	0.12	0.12	0.14	0.13
BIN 4	0.20	0.20	0.17	0.16	0.10	0.21

Moreover, this difference decreases as we move from lower to higher incident energies. This again indicates the dominance of the Coulomb interactions at lower incident energies and decreases at higher incident energies due to the dominance of the nucleon-nucleon collisions. As noted earlier, the variation of τ with scaled impact parameter remains same for both isobaric pairs if we switch off the Coulomb interactions.

6.2.4 Impact parameter dependence of nuclear stopping, with and without Coulomb potential

To further strengthen interpretation of our results, we display in Fig.6.5, the scaled impact parameter dependence of the nuclear stopping for the total masses 116 and 240 for both with and without Coulomb potential at an incident energy below, at and above EVF. The solid symbols square (pentagon) represents the results with (without) Coulomb potential for $isob_1$ and the corresponding open symbols display the results for $isob_2$. The study of reactions without Coulomb repulsion helps to find the relative contribution of nucleon-nucleon collisions and mean field. The figure reveals that:

1. For both with and without Coulomb potential, at all colliding geometries the nuclear stopping decreases for $isob_2$ spanning over the entire colliding geometry. This is due to the fact that, the increase (decrease) in the neutron (proton) content will lead to

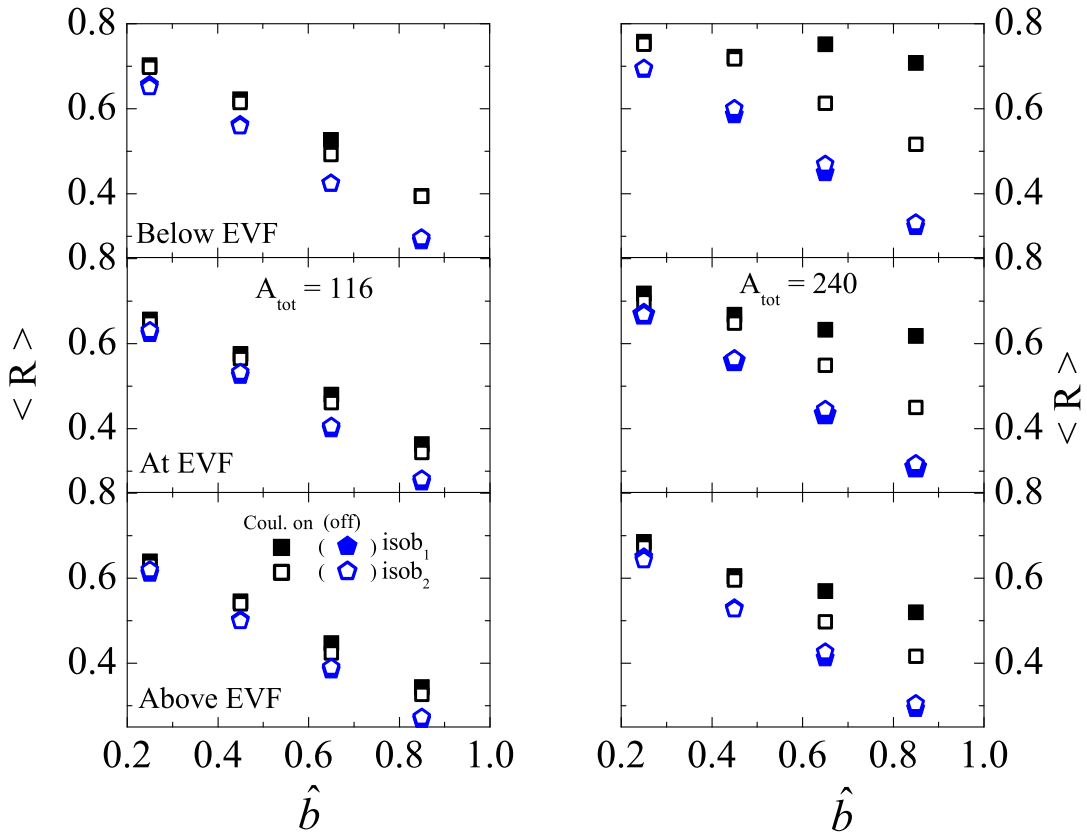

Figure 6.5: *Impact parameter dependence of nuclear stopping for the different system masses having A_{tot} = 116 (left columns) and A_{tot} = 240 (right columns). The results are displayed for both with and without Coulomb potential.*

the reduction in the repulsive interactions and increase the probability of nucleon-nucleon collisions that leads to overall decrease in stopping.

2. In contrast without Coulomb potential, the difference in the nuclear stopping for a given mass pair increases with increase in the impact parameter. This happens due to the presence of Coulomb interactions, the repulsion in the heavier systems increases with impact parameter. This ultimately leads to the decrease in the collision probability. Moreover, for both with and without Coulomb potentials, the nuclear stopping decreases with increase in the impact parameter. This is because participant zone decreases with increase in the impact parameter.

3. The dominance of the Coulomb repulsion is also visible at higher colliding geometry, from the higher value of nuclear stopping for $isob_1$ compared to $isob_2$.

6.2.5 Impact parameter dependence of nuclear stopping, with and without collisions

In order to study the relative contribution of the Coulomb repulsion and nucleon-nucleon cross-section, we switched off the collision term and then calculated the nuclear stopping for the similar systems as in previous figure at all the four impact parameter bins. The results are displayed in Fig.6.6 for below, at and above EVF. In both the systems, the nuclear stopping decreases by large magnitude at lower impact parameters and in small magnitude at higher impact parameters. This behavior clearly indicates the importance of nucleon-nucleon cross-section. In such cases, the mean field which contribute to the formation of a rotating compound system dominates. In other words, the collective expansion process based on the nucleon-nucleon scattering becomes less important. As a result, lesser nuclear matter gets thermalized, which leads to overall decrease in the nuclear stopping. Moreover, the above behavior remain same for the case below, at and above the EVF.

From the above discussion, it is clear that, incident energy plays a dominant role over Coulomb interactions. This is because the slope of the incident energy dependence of nuclear stopping is steeper at low incident energies compared to the case at higher incident energies. In fact, at higher incident energies, the cross-section remains almost independent of the incident energy [245].

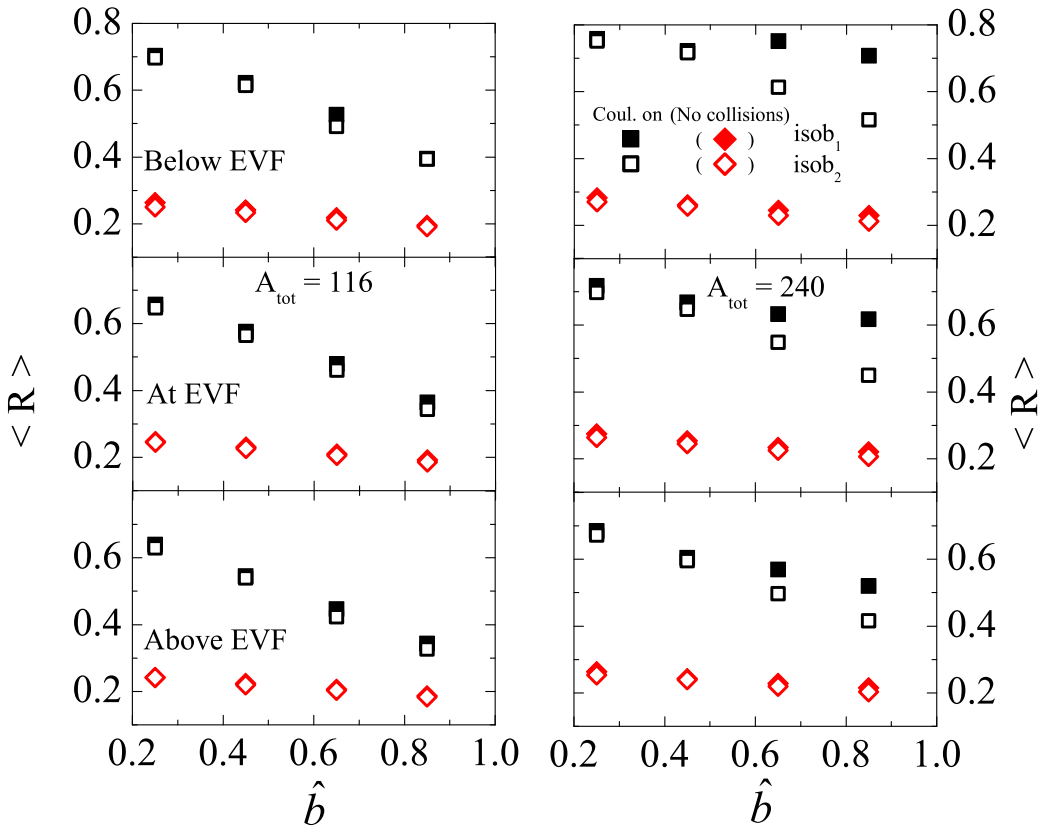

Figure 6.6: *Same as Fig.6.5 but the results are displayed for the full Coulomb and without nucleon-nucleon collisions.*

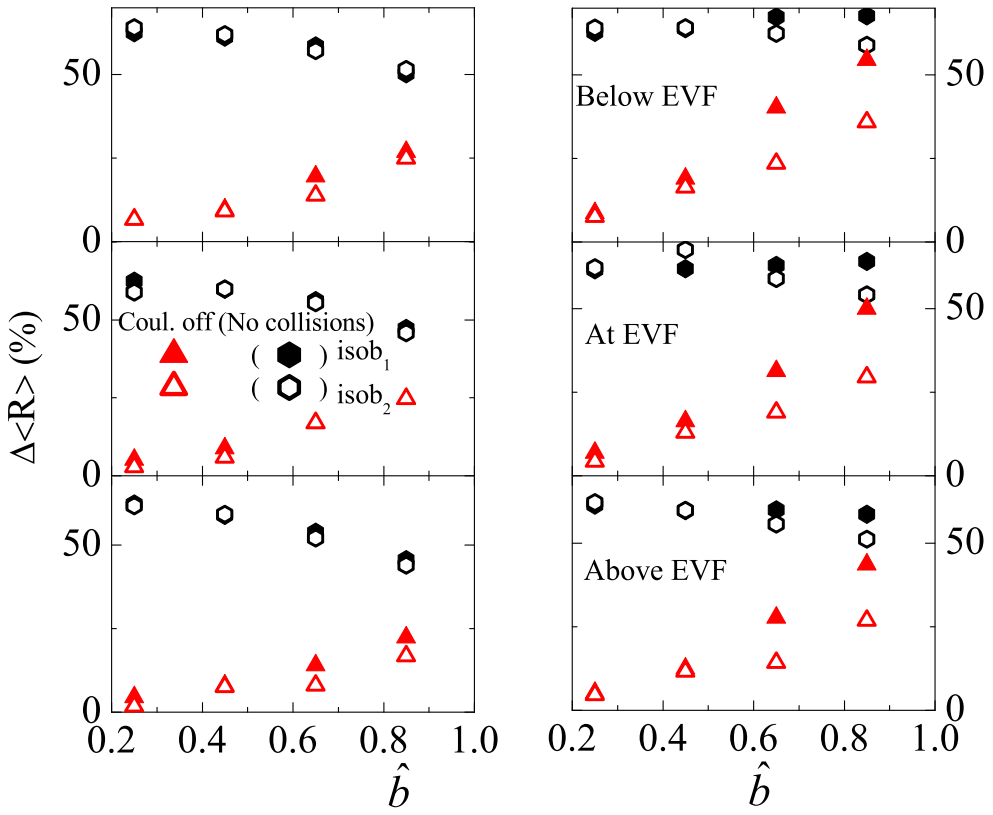

Figure 6.7: *The percentage change in nuclear stopping without Coulomb potential and without nucleon-nucleon binary collisions for the reactions as in Fig.6.5 & 6.6.*

6.2.6 Relative effect of Coulomb potential and nucleon-nucleon binary collisions on nuclear stopping

Further, in order to study the percentage change in the nuclear stopping without Coulomb potential and nucleon-nucleon collisions, we display in Fig.6.7, the impact parameter dependence of $\Delta\langle R\rangle(\%)$. First we calculate the percentage change in the nuclear stopping without Coulomb potential by $\Delta\langle R\rangle\ (\%) = \frac{\langle R\rangle - \langle R\rangle^{Coul.off}}{\langle R\rangle} \times 100$ (upper triangles) and without nucleon-nucleon collisions $\Delta\langle R\rangle\ (\%) = \frac{\langle R\rangle - \langle R\rangle^{Nocoll.}}{\langle R\rangle} \times 100$ (hexagons). Solid symbols display the results for $isob_1$ and open symbols display the results for $isob_2$. One can see that, the percentage change in nuclear stopping is more if we exclude the nucleon-nucleon collisions from the system compared to the case when we switch off the Coulomb potentials. This clearly indicates the dominance of nucleon-nucleon cross-section over Coulomb interactions for semi-central geometries and the difference decreases if one moves to the peripheral collisions. Moreover, the system mass dependence plays a less important role as the percentage change is nearly the same for both $A_{tot} = 116$ & $A_{tot} = 240$ systems. Nearly the same difference is observed both without Coulomb potential and nucleon-nucleon collisions at peripheral geometry. This indicate that, effect of cross-section become less important at higher impact parameters. Moreover, this statement holds good for the heavier mass systems compared to the lighter mass systems.

6.3 Summary

We studied the effect of isospin degree of freedom on nuclear stopping throughout the mass range between 50 and 350 for two sets of isotopic systems first with N/Z $\approx$ 1.5 and 1.8, second with N/Z = 1.16 and 1.33 as well as isobaric systems with N/Z = 1.0 and 1.4. Analysis is carried out at an incident energy below, at, and above the energy of vanishing flow (EVF). Our findings revealed that nuclear stopping does not show any particular behavior at EVF. Moreover, system size effects dominate the isospin effects throughout the range of colliding geometry. The Coulomb effects becomes important at higher colliding geometry. The comparative study of counterbalancing of Coulomb and mean field by removing the nucleon-nucleon collisions clearly indicates the dominance of nucleon-nucleon cross-section over the repulsive Coulomb potential. But on can see the dominance of Coulomb potential at higher impact parameter.

Chapter 7

Summary and outlook

7.1 Summary

In the present thesis, we presented the effect of introducing the isospin dependence of nucleon-nucleon cross-section on various observables like multifragmentation, collective flow (directed, elliptical, triangular and quadrupole) and nuclear stopping. The study was carried out using the Isospin dependent Quantum Molecular Dynamics (IQMD) model. We first presented an introduction to the field of heavy-ion collisions. Then we presented the discussion of various phenomena that occur at intermediate energies like multifragmentation, collective flow (directed, elliptical, triangular and quadrupole) and nuclear stopping. Discussion has been carried out on the review of experimental attempts for the isospin effects on multifragmentation, collective flow and nuclear stopping. Brief review of various realizations of QMD model is also discussed. In particular we discussed the IQMD model which we have used for the present study. The charge asymmetry means the collision of nuclei in which neutron number is not equal to the proton number. We have fixed the mass of colliding nuclei but varied their proton number (isobaric nuclei). To see the influence of isospin asymmetry on fragment production, we have chosen two sets of reactions, one where the mass of the each colliding nuclei is fixed to be 40 units, but charge varies from 14 to 23. For the second set we have chosen the reactions for which the mass of the each colliding nuclei is fixed to be 124 units, but charge varies from 47 to 59. Our study revealed that N/Z of the system play less significant role compared to the mass of the colliding nuclei. The study also revealed that influence of isospin dependence of nucleon-nucleon cross-section is uniform on the N/Z dependence of FN's and LMF's. Moreover, in multifragmentation we cannot pin down which of the two forms of nucleon-

nucleon cross-section (i.e. σ_{iso} or σ_{noiso}) is more realistic.

As a next step, efforts have been made to study the isospin effects in nuclear stopping at intermediate energies. Isospin dependence of nucleon-nucleon cross-section shows its influence in the rapidity distribution of FN's and LMF's only in the mid-rapidity region. Interestingly, we for the first time, could successfully reproduce the experimental findings. We have also investigated the reasons of disagreement of earlier theoretical attempt performed by using IQMD model. Our study revealed that the strength of nucleon-nucleon cross-section and the centrality was responsible for the disagreement with data in the study carried by other groups.

To explore the isospin effects on collective flow, we studied the role of isospin degree of freedom on directed, elliptical, triangular and quadrupole flow. We found that, isospin dependence of nucleon-nucleon cross-section has a significant role to play on the neutron/proton differential sideward flow. We have proved theoretically for the first time that, fragment charge/mass does not influence the balance energy. In case of elliptical flow, our study revealed that, the distribution of nucleons and fragments is not symmetric around the beam axis. Isospin dependence of nucleon-nucleon cross-section play important role in the transverse momentum dependence of elliptical flow. We have tried to reproduce the experimental findings of GSI collaboration. Our theoretical calculations are closer to experimental findings compared to earlier studies with σ_{iso} reduced by 20%. From this we again conclude that, strength of nucleon-nucleon cross-section play a significant role in the reaction dynamics. Both triangular ($\langle v_3 \rangle$) and quadrupole flow ($\langle v_4 \rangle$) are more sensitive to the isotopic content as well as to the isospin dependence of nucleon-nucleon cross-section. Which indicates that, these harmonics depends strongly on the initial configuration of the system and its evolution.

As a last step, to explore the effect of Coulomb potential on nuclear stopping, we studied the nuclear stopping throughout the mass range between 50 and 350 for two sets of isotopic systems with N/Z = 1.16 and 1.33 as well as isobaric systems with N/Z = 1.0 and 1.4. Our study revealed that, nuclear stopping does not show any particular behavior at EVF. Moreover, system size effects dominate the isospin effects throughout the range of colliding geometry.

In last we conclude that, isospin dependence of nucleon-nucleon cross-section affect the

reaction dynamics significantly in case of collective flow. But very little influence can be seen in case of fragmentation and nuclear stopping.

7.2 Outlook

Though, we studied the role of isospin content of colliding nuclei, isospin dependence of nucleon-nucleon cross-section, density dependence of symmetry energy in reaction dynamics via multifragmentation, nuclear stopping, directed, elliptical, triangular and quadrupole flow. In addition, the influence of isospin effects on the system mass dependence of nuclear stopping around balance energy is studied in detail there are many challenges yet to be solved. One can elaborate the influence of density dependent symmetry energy, isospin dependence of nucleon-nucleon cross-section on the above mentioned observables for highly asymmetric collisions (collision of light projectile on heavy target). Experimentalist can think of designing the experiment to carry out such studies. Moreover, directed flow in the mid-rapidity region for highly asymmetric nuclei can be of further interest in the future. This study could of great use for the new facility called ANURIB (Advanced National facility for Unstable & Rare-Isotope Beams) at VECC Kolkata. The study is useful not only to understand the nuclear forces and supernova explosion but also to help in the discovery of many isotopes, which could have great applications in the field of medicine and material science.

Bibliography

[1] S. V. S. Sastry, S. Kailas, A. K. Mohanty, and A. Saxena, Pramana J. of Physics **64**, 47 (2005).

[2] A. Yadav *et al.,* Phys. Rev. C **86**, 014603 (2012).

[3] L. G. Moretto and G. J. Wozniak, Annu. Rev. Nucl. Part. Sci. **43**, 379 (1993).

[4] L. C. Vaz, J. M. Alexander and G. R. Satchler, Phys. Rep. **69**, 373 (1981); M. Beckerman, Rep. Prog. Phys. **51**, 1047 (1988); R. K. Puri, Ph.D Thesis, P.U. Chandigarh (1990); M. K. Sharma, Ph.D Thesis, P.U. Chandigarh (1998).

[5] P. J. Brussaard and P. W. M. Glaudemans, *Shell-model applications in nuclear spectroscopy, North-Holand, Amsterdmm (1977).*

[6] E. P. Prendergast, Ph.D thesis, London (1971).

[7] C. Y. Wong, *Introduction to high-energy heavy-ion collisions, World Scientific, Singapore (1994).*

[8] C. De Troyes, Artherian Legends, Troyes, France (1160-1172).

[9] K. H. Kampert, J. Phys. G: Nucl. Phys. **15**, 691 (1989).

[10] H. H. Gutbrod, A. M. Poskanzer and H. G. Ritter, Rep. Prog. Phys. **52**, 1267 (1989).

[11] H. R. Schmidt, Int. J. Mod. Phys. **6**, 3865 (1991).

[12] H. R. Schmidt and J. Schukraft, J. Phys. G: Nucl. Part. Phys. **19**, 1705 (1993).

[13] D. K. Srivastava and J. I. Kapusta, Phys. Rev. C **48**, 1335 (1993); E. Muller, J. Phys. G: Nucl. Phys. **16**, 1571 (1990).

[14] T. K. Jha, P. K. Raina, P. K. Panda and S. K. Patra, Phys. Rev. C **74**, 055803 (2006).

[15] G. Peilert, H. Stöcker and W. Greiner, Rep. Prog. Phys. **57**, 533 (1994).

[16] J. M. Eisenberg and W. Greiner Nuclear Theory **1**, 3rd edn (Amslerdam: Notih Holland) (1987).

[17] W. Scheid, R. Ligensa and W. Greiner W, Phys Rev. Lett. **21**, 1479 (1968); W. Scheid, H. Miiller and W. Greiner, Phys Rev. Len **32**, 741 (1974).

[18] R. Stock, Nucl. Phys. A **237**, 365 (1975).

[19] J. P. Blaizot, Phys. Rep. **64**, 171 (1980).

[20] A. Bohr and B. R. Mottelson, Nuclear Structure **1**, (Benjamin, New York) (1996).

[21] C. F. V. Weizsäcker, Z. Physik **96**, 431 (1935); H. A. Bethe and R. F. Bacher, Rev. Mod. Phys. **8**, 82 (1936).

[22] B. A. Li, C. M. Ko and W. Bauer, Int. J. Mod. Phys. E **7**, 147 (1998).

[23] B. A. Li and S. J. Yennello, Phys. Rev. C **52**, R1746 (1995); B. A. Li, Z. Ren, C. M. Ko, S. J. Yennello, Phys. Rev. Lett. **76**, 4492 (1996).

[24] C. Hartnack *et al.,* Eur. Phys. J. A **1**, 151 (1998); C. Hartnack *et al.,* Phys. Rep. **510**, 119 (2012).

[25] R. K. Tripathi, J. W. Wilson and F. A. Cucinotta, Nucl. Instr. and Meth. in Phys. Res. B **194**, 229 (2002).

[26] J. Cugnon, T. Mizutani, and J. Vandermeulen, Nucl. Phys. A **352**, 505 (1981); J. P. Bondrof, P. I. Siemens, S. Garpman, and E. C. Halbert, Z Phys. A **279**, 385(1976).

[27] M. Schmidt, G. Röpke, and H. Schulz, Ann. Phys. (N.Y.) **202**, 57 (1990).

[28] J. Cugnon, A. Lejeune, and P. Grange, Phys. Rev. C **35**, 861 (1987).

[29] A. Faessler, Nucl. Phys. A **495**, 103c (1989).

[30] G. Q. Li and R. Machleidt, Phys. Rev. C **48**, 1702 (1993); *ibid* Phys. Rev. C **49**, 566 (1994).

[31] T. Alm, G. Röpke and M. Schmidt, Phys. Rev. C **50**, 31 (1994).

[32] W. Cassing and U. Mosel, Prog. Part. Nucl. Phys. **25**, 235 (1990).

[33] A. Faessler, W. H. Dickhoff and M. Trefz, Nucl. Phys. A **428**, 271c (1981); M. Trefz, A. Faessler and W. H. Dickhoff, Nucl. Phys. A **443**, 499 (1985).

[34] T. Izumoto, S. Krewald and A. Faessler, Nucl. Phys. A **341**, 319 (1980); *ibid.* **357**, 471 (1981).

[35] N. Ohtsuka, R. Linden, A. Faessler and F. B. Malik, Nucl. Phys. **A 465**, 550 (1987).

[36] A. Bohnet, N. Ohtsuka, J. Aichelin, R. Linder, and A. Faessler, Nucl. Phys. A **494**, 349 (1989); R. K. Puri, N. Ohtsuka, E. Lehmann, A. Faessler, M. A. Matin, D.T. Khoa, G. Batko, and S.W. Huang, Nucl. Phys. **A 575** , 733 (1994).

[37] B. A. Li, L. W. Chen and C. M. Ko, Phys. Rep. **464**, 113 (2008).

[38] R. Pak *et al.,* Phys. Rev. C **53**, R1469 (1996).

[39] C. A. Ogilivie *et al.,* Phys. Rev. C **42**, R10 (1990).

[40] G. D. Westfall *et al.,* Phys. Rev. Lett. **71**, 1986 (1993); D. Klakow, G. Welke, W. Bauer, Phys. Rev. C **48**, 1982 (1993); M. J. Huang *et al.,* Phys. Rev. Lett. **77**, 3739 (1996).

[41] R. Wada *et al.,* Phys. Rev. Lett. **58**, 1829 (1987); R. Pak *et al.,* Phys. Rev. Lett. **78**, 1022 (1997); L. G. Sobotka *et al.,* Phys. Rev. C **55**, R1272 (1994); F. Rami *et al.,* Phys. Rev. lett. **84**, 1120 (2000).

[42] M. Farine *et al.,* Z. Phys. **339**, 363 (1991); H. Müller and B. D. Serot, Phys. Rev. C **52**, 2072 (1995); G. Kortmeyer, W. Bauer and G. J. Kunde, Phys. Rev. C **55**, 2730 (1997); J. Pan and S. Das Gupta, Phys. Rev. C **57**, 1839 (1998); V. Baran *et al.,* Nucl. Phys. A **632**, 287 (1998).

[43] N. Marie *et al.,* Phys. Rev. C **58**, 256 (1998); W. Loveland *et al.,* Phys. Rev. C **59**, 1472 (1999).

[44] L. Phair *et al.,* Phys. Lett. B **285**, 10 (1992); M. B. Tsang *et al.,* Phys. Rev. Lett. **71**, 1502 (1993).

[45] J. Lukasik *et al.,* Phys. Rev. C **66**, 064606 (2002).

[46] C. A. Ogilvie *et al.,* Phys. Rev. Lett. **67**, 1214 (1991); J. Hubele *et al.,* Phys. Rev. C **46**, R1577 (1992).

[47] J. Colin *et al.,* Phys. Rev. C **67**, 064603 (2003); J. D. Frankland *et al.,* Phys. Rev. C **71**, 034607 (2005).

[48] S. Goyal, Phys. Rev. C **84**, 044614 (2011).

[49] W. Reisdorf and M. G. Ritter, Ann. Rev. Nucl. Sci. **47**, 663 (1997).

[50] L. Bhattacharya and P. Roy, Phys. Rev. C **81**, 054902 (2010).

[51] B. A. Li, Phys. Rev. C **48**, 2415 (1993); W. M. Zhang *et al.,* Phys. Rev. C **42**, R491 (1990); G. F. Bertsch, W. G. Lynch and M. B. Tsang, Phys. Lett. B **189**, 384 (1987).

[52] M. B. Tsang *et al.,* Phys. Rev. Lett. **57**, 559 (1986).

[53] P. Danielewicz and G. Odyniec, Phys. Lett. B **157**, 146 (1985); J. W. Harris, Nucl. Phys. A **471**, 241 (1987).

[54] J. J. Molitoris and H. Stöcker, Phys. Lett. B **162**, 47 (1985); D. Krofcheck *et al.,* Phys. Rev. Lett. **63**, 2028 (1989); J. Peter, Nucl. Phys. A **545**, 173 (1992).

[55] B. Zhang, M. Gyulassy and C. Ko, Phys. Lett. B **455**, 45 (1999).

[56] J. Ollitrault, Phys. Rev. D **48**, 1132 (1993).

[57] B. Alver and G. Roland, Phys. Rev. C **81**, 054905 (2010); D. Teaney and L. Yan, Phys. Rev. C **83**, 064904 (2011).

[58] L. W. Chen and C. M. Ko, Phys. Rev. C **73**, 014906 (2006); L. W. Chen and C. M. Ko, Phys. Rev. C **73**, 044903 (2006); J. Xu and C. M. Ko, Phys. Rev. C **84**, 044907 (2011).

[59] P. F. Kolb, Phys. Rev. C **68**, 031902(R) (2003).

[60] Y. G. Ma *et al.,* Nucl. Phys. A **787**, 611c (2007).

[61] J. K. Dhawan, N. Dhiman, A. D. Sood, and R. K. Puri, Phys. Rev. C **74**, 057901 (2006) and the refrences therein; P. B. Gossiaux and J. Aichelin, Phys. Rev. C **56**, 2109 (1997).

[62] A. W. Strong, I. V. Moskalenko and V. S. Ptuskin, Ann. Rev. Nucl. & Part. Sci. **57**, 285 (2007).

[63] E. Schopper, Naturwissenschaftler **5**, 557 (1937); I. I. Gurevich *et al.,* Dokl. Akad. Nauk SSSR **18**, 169 (1938).

[64] O. V. Lozhkin and N. A. Perfilov, J. Exp. Theo. Phys. **31**, 913 (1956).

[65] B. Jakobsson *et al.,* Z. Phys. A **307**, 293 (1982).

[66] A. I. Warwick *et al.,* Phys. Rev. C **27**, 1083 (1983).

[67] P. J. Siemens, Nature **305**, 410 (1983).

[68] J. E. Finn *et al.,* Phys. Rev. Lett. **49**, 1321 (1982); A. S. Hirsh *et al.,* Phys. Rev. C. **29**, 508 (1984).

[69] V. Avdeichikov *et al.,* Yad. Fiz. **48**, 1736 (1988).

[70] R. Ogul *et al.,* Phys. Rev. C **83**, 024608 (2011).

[71] S. P. Avdeyev *et al.,* Nucl. Inst. Meth. Phys. Res. A **332**, 149 (1993).

[72] V. V. Kirakosyan *et al.,* Inst. and Exp. Tech. **51**, 159 (2008).

[73] see http://www-aladin.gsi.de.

[74] C. Sfienti *et al.,* in Proceedings of the XLI International Winter Meeting on Nuclear Physics, Bormio, Italy, 2003, Ed. I. Iori, A. Moroni, Ricerca Scientifica ed Educazione Permanente Suppl. # 120, Milano 2003, p. 323.

[75] C. Sfienti *et al.,* Acta. Phys. Polo. B **37**, 193 (2006); *ibid.* Phys. Rev. Lett. **102**, 152701 (2006).

[76] S. Z. Belenkij, L. D. Landau, Usp. Fiz. Nauk **56**, 309 (1955); Nuovo Cimento Suppl. **3**, 15 (1956).

[77] A. E. Glassgold, W. Heckrotte, K. M. Watson, Ann. Phys. (NY) **6**, 1 (1959).

[78] H. A. Gustafsson *et al.,* Phys. Rev. Lett. **52**, 1590 (1984); R. E. Renfordt *et al.,* Phys. Rev. Lett. **53**, 763 (1984).

[79] H. Ströbele *et al.,* Phys. Rev. C **27**, 1349 (1983).

[80] A. Baden *et al.,* Nucl. Instr. Meth. **203**, 189 (1982).

[81] M. Demoulins *et al.,* Phys. Lett. B **241**, 476 (1990).

[82] H. H. Gutbroad *et al.,* Phys. Lett. B **216**, 267 (1989).

[83] H. Stöcker *et al.,* Phys. Rev. C **25**, 1873 (1982).

[84] R. Popescu *et al.,* Phys. Lett. B **331**, 285 (1994).

[85] J. Lukasik, G. Auger, and M. L. Begemann-Blaich *et al.,* Phys. Lett. B **608**, 223 (2005); A. Andronic *et al.,* Nucl. Phys. A **679**, 765 (2001); *ibid.* Phys. Lett. B **612**, 173 (2005); J. Lukasik, *et al.,* INDRA Collaborations, Int. Workshop on Multifragmentation and related topics (IWM 2003) Caen, France (2003).

[86] P. Crochet *et al.,* Nucl. Phys. A **624**, 755 (1997).

[87] J. Lukasik *et al.,* Proc. of INPC **2**, 513 (2007).

[88] G. Lehaut *et al.,* Phys. Rev. Lett. **104**, 232701 (2010).

[89] W. Reisdorf *et al.,* Phys. Rev. Lett. **92**, 232301 (2004); W. Reisdorf *et al.,* Nucl. Phys. A **848**, 366 (2010).

[90] Y. Yano, "The RIKEN RI Beam Factory Project: A status report": Nucl. Instr. Meth, **B261**, 1009 (2007).

[91] J. W. Xia, Y. J. Yuan and Y. Liu, Proceedings of PAC09, Vancouver, BC, Canada, 3048-3052; X. Cai *et al.,* J. of Phys. Con. Ser. **163**, 012113 (2009).

[92] INFN-LNL Report **238**, 1828-8545 (2012).

[93] G. D. Alton and J. R. Beene, J. Phys. G: Nucl. Part. Phys. **24**, 1347 (1998); See, e.g., http://www.phy.ornal.gov.

[94] See, e.g., http://www.gsi.de/fair/index-e.html.

[95] See e.g. Physics News, *Bulletin of the Indian Physics Association*, Vol. 42, October (2012).

[96] See http://www.indianexpress.com.kolkata-to-house-asia-s-second-lab-to-study-supernova-conditions/1055235.

[97] J. P. Bondorf *et al.,* Phys. Rep. **257**, 133 (1995).

[98] D. H. E. Gross, Rep. Prog. Phys. **53**, 605 (1990).

[99] D. V. Fedorov, A. S. Jensen and E. Garrido, Acta. Phys. Hungarica **18**, 203 (2003).

[100] J. Pan, S. D. Gupta, Phys. Lett. B **344**, 29 (1995); J. Pan, S. D. Gupta, Phys. Rev. C **51**, 1384 (1995); S. D. Gupta and J. Pan, Phys. Rev. C **53**, 1319 (1996).

[101] W. A. Friedman, Phys. Rev. C **42**, 667 (1990).

[102] J. P. Bondorf, R. Donangelo, I. N. Mishustin, C. J. Pethick, H. Schulz, and K. Sneppen, Nucl. Phys. A **443**, 321 (1985); *ibid* **444**, 460 (1985); *ibid* **448**, 753 (1986); G. A. Souliotis *et al.,* Phys. Rev. C **75**, 011601 (2007); S. Pal, S. K. Samaddar, J. N. de, and B. Djerroud, Phys. Rev. C **57**, 3246 (1998); A. Das, M. Mishra, M. Satpathy, and L. Satpathy, J. Phys. G: Nucl. and Part. **19**, 319 (1993).

[103] J. Aichelin J and H. Stöcker, Phys. Lett. B **163**, 59 (1985); S. E. Koonin, Ph.D Thesis (MIT) (1975); P. Bonche, S. E. Koonin, and J. W. Negele, Phys. Rev. C **3**, 1226 (1976).

[104] C. Y. Wong, J. A. Maruhn, and T. A. Welton, Nucl. Phys. A **253**, 469 (1975); C. Y. Wong, T. A. Welton, and J. A. Maruhn, Phys. Rev. C **15**, 1558 (1977); C. Y. Wong, Phys. Rev. C **17**, 1832 (1978); C. Y. Wong and H. H. K. tang, Phys. Rev. Lett. **40**, 1070 (1978).

[105] H. Flocard, S. E. Koonin, and M. S. Weiss, Phys. Rev. C **17**, 1682 (1978); P. Bonche, B. Grammaticos and S. Koonin, Phys. Rev. C **17**, 1700 (1978); J. W. Negele, S. E. Koonin, P. Moller, J. R. Nix, and A. J. Sierk, Phys. Rev. C **3**, 1098 (1978).

[106] E. Suraud, C. Gregoire, and B. Tamain, Prog. Part. Nucl. Phys. **23**, 357 (1989).

[107] Proceeding of 5^{th} International Conference "On fission and properties of neutron rich nuclei" held at Sanibel Island, Florida, USA Nov. 4-10 (2012).

[108] A. Uehling and G. E. Uhlenbeck, Phys. Rev **43**, 552 (1933); G. F. Bertsch, H. Kruse and S. D. Gupta, Phys. Rev. C **29**, 673 (1984).

[109] Thorsten Fliessbach, Statistische Physik. Spektrum, Heidelberg Berlin, (1999).

[110] A. Bonasera, G. F. Burgio, and M. D. Toro, Phys. Lett. B **221**, 233 (1989); A. Bonasera, G. Russo, and H. H. Wolter, Phys. Lett. B **246**, 337 (1990).

[111] L. Wilets, Y. Yariv, and R. Chestnut, Nucl. Phys. A **301**, 359 (1978); A. R. Bodmer, C. N. Panos, and A. D. MacKellar, Phys. Rev. C **22**, 1025 (1980).

[112] J. Aichelin, Phys. Rep. **202**, 233 (1991); J. Aichelin and H. Stöcker, Phys. Lett. B **176**, 14 (1986).

[113] M. Colona *et al.,* Phys. Rev. C **57**, 1410 (1998).

[114] B. A. Li, Phys. Rev. Lett. **88**, 192701 (2002) and refs. therein.

[115] S. A. Bass, C. Hartnack, H. Stöcker, and W. Greiner, Phys. Rev. C **51**, 3343 (1995); B. J. VerWest and R. A. Arndt, Phys. Rev. C **25**, 1979 (1982); H. Kruse, B. V. Jacak, and H. Stöcker. Phys. Rev. Lett. **54**, 289 (1985); J. J Molitoris and H. Stöcker, Phys. Rev C **32**, R346 (1985).

[116] J. Liu, W. Guo, S. Wang, W. Zuo, Q. Zhao and Y. Yang, Phys. Rev. Lett. **86**, 975 (2001).

[117] J. Y. Liu *et al.,* Phys. Rev. C **70**, 034610 (2004); J. Y. Liu *et al.,* Chin. Phys. Lett. **21**, 1914 (2004).

[118] R. Pak *et al.,* Phys. Rev. C **54**, 2457 (1996)

[119] S. Jones and E. Remler, Ann. of Phys. (NY) **180**, 152 (1987); P. Carruthers and M. Zachariasen, Rev. Mod. Phys. **55**, 245 (1983).

[120] E. Lehmann *et al.,* Prog. Part. Nucl. Phys. **30**, 219 (1993).

[121] G. Peilert, J. Konopka, M. Blann, M. G. Mustafa, H. Stöcker and W. Greiner, Phys. Rev. C **46**, 1457 (1992); G. Peilert *et al.,* Phys. Lett. B **260**, 271 (1991).

[122] C. Dorso, S. Duarte and J. Randrup, Phys. Lett. B **188**, 287 (1987); C. Dorso and J. Randrup, Phys. Lett. B **215**, 611 (1988).

[123] N. Metropolis, A. W. Metropolis, M. N. Rosenbluth, A. H. Teller and E. Teller, J. Chem. Phys. **21**, 1087 (1953).

[124] J. Konopka, H. Stöcker and W. Greiner, Nucl. Phys. A **583**, 357c (1995).

[125] L. Jianye and Z. S. Guang, Z. Phys. A **348**, 31 (1994).

[126] C. Ngo, H. Ngo, S. Leray, M. E. Spina, Nucl. Phys. A **499**, 148 (1989).

[127] K. A. Waged, Phys. Rev. C **63**, 024618 (2001).

[128] S. Y. Shmakov, V. V. Uzhinskii, and A. M. Zadorozhny, Comput. Phys. Commun. **54**, 125 (1989), and references therein.

[129] A. Bohnet *et al.,* Phys. Rev. C **44**, 2111 (1991).

[130] M. Begemann-Blaich *et al.,* Phys. Rev. C **48**, 610 (1993); W. F. J. Müller *et al.,* Phys. Lett. B **298**, 27 (1993); S. C. Jeong *et al.,* Phys. Rev. Lett. **72**, 3468 (1994); P. B. Gossiaux *et al.,* Phys. Rev. C **51**, 3357 (1995).

[131] S. Huber and J. Aichelin, Nucl. Phys. A **573**, 587 (1994).

[132] M. Papa, T. Maruyama and A. Bonasera, Phys. Rev. C **64**, 024612 (2001); M. Papa, G. Giuliani and A. Bonasera, J. Comp. Phys. **208**, 403 (2005).

[133] H. Sörge, H. Stöcker, and W. Greiner, Ann. Phys. **192**, 266 (1989).

[134] D. G. Currie, T. F. Jordan, and E. C. G. Sudarshan, Rev. Mod. Phys. **35**, 350 (1963).

[135] M. Belkacem *et al.,* Phys. Rev. C **58**, 1727 (1998); A. Dumitru *et al.,* Phys. Rev. C **57**, 3271 (1998); S. A. Bass *et al.,* Prog. Part. Nucl. Phys. **41**, 255 (1998).

[136] C. Nonaka and S. A. Bass, Phys. Rev. C **75**, 014902 (2007); J. Steinheimer, M. Bleicher, H. Petersen, S. Schramm, H. Stöcker, and D. Zschiesche, Phys. Rev. C **77**, 034901 (2008).

[137] S. A. Bass and A. Dumitru, Phys. Rev. C **61**, 064909 (2000).

[138] D. Teaney, J. Lauret, and E. V. Shuryak, Phys. Rev. Lett. **86**, 4783 (2003); T. Hirano, U. W. Heinz, D. Kharzeev, R. Lacey, and Y. Nara, Phys. Lett. B **636**, 299 (2006).

[139] H. Feldmeier, Nucl. Phys. A **515**, 147 (1990); H. Feldmeier and J. Schnack, Prog. Part. Nucl. Phys. **39**, 393 (1997).

[140] H. Horiuchi, Nucl. Phys. A **522**, 257c (1991); H. Horiuchi, T. Maruyama, A. Ohnishi and S. Yamaguchi, Preprint, KUNS **1028**, Kyoto University; C. Coriano, R. Parwani and H. Yamagishi, Nucl. Phys. A **522**, 591 (1991).

[141] L. Wilet, E. M. Henley, M. Kraft and A. D. MacKellar, Nucl. Phys. A **282**, 341 (1977).

[142] A. Ono, H. Horiuchi, T. Maruyama, and A. Ohnishi, Phys. Rev. Lett. **68**, 2898 (1992); A. Ono, H. Horiuchi, T. Maruyama, and A. Ohnishi, Prog. Theo. Phys. **87**, 1185 (1992).

[143] A. Bohnet, Ph.D Thesis, University of Heidelberg (1988).

[144] A. K. Kerman and S. E. Koonin, Ann. Phys. (NY) **100**, 332 (1976).

[145] J. Aichelin, A. Rosenhauer, G. Peilert, H. Stöcker and W. Greiner, Phys. Rev. Lett. **58**, 1926 (1987).

[146] L. G. Arnold *et al.,* Phys. Rev. C **25**, 936 (1982); G. Passatore, Nucl. Phys. A **95**, 694 (1967).

[147] Y. Yariv and Z. Frankel, Phys. Rev. C **20**, 2227 (1979); J. Cugnon. Phys. Rev. C **22**, 1885 (1980).

[148] P. Danielewicz and G. F. Bertsch, Nucl. Phys. A **533**, 712 (1991).

[149] B. A. Li, Phys. Rev. C **67**, 017601 (2003).

[150] V. Greco *et al.,* Phys. Lett. B **562**, 215 (2003).

[151] W. P. Tan *et al.,* Phys. Rev. C **64**, 051901(R) (2001).

[152] M. B. Tsang *et al.,* Phys. Rev. Lett. **86**, 5023 (2001).

[153] H. Xu *et al.,* Phys. Rev. Lett. **85**, 716 (2000).

[154] L. W. Chen, C. M. Ko, B. A. Li, Phys. Rev. C **76**, 054316 (2007). Z. H. Li, U. Lombardo, H. J. Schulze, W. Zuo, L. W. Chen, and H. R. Ma, Phys. Rev. C **74**, 047304 (2006).

[155] B. A. Brown, Phys. Rev. Lett. **85**, 5296 (2000); A. Szmaglinski, W. Wojcik, M. Kutschera, Acta Phys. Polon. B **37**, 227 (2006); L. W. Chen, C. M. Ko and B. A. Li, Phys. Rev. C **72**, 064309 (2005).

[156] M. Lopez-Quelle *et al.,* Nucl. Phys. A **483**, 479 (1988); V. Baran *et al.,* Nucl. Phys. A **703**, 603 (2002); L. W. Chen and B. A. Li, Phys. Rev. Lett. **94**, 032701 (2005).

[157] Z. Q. Feng, Phy. Rev. C **84**, 024610 (2011); D. V. Shetty, S. J. Yennello and G. A. Souliotis, Phys. Rev. C **75**, 034602 (2005).

[158] D. V. Shetty, S. J. Yennello, and G. A. Souliotis Phys. Rev. C **76**, 024606 (2007) and references therein.

[159] C. Zeitlin *et. al.,* Phys. Rev. C **56**, 388 (1997).

[160] R. Wada *et al.,* Phys. Rev. C **69**, 044610 (2004).

[161] O.V. Lozhkin and W. Trautmann, Phys. Rev. C **46**, 1996 (1992).

[162] J. F. Dempsey *et al.,* Phys. Rev. C **54**, 1710(1996).

[163] N. Buyukcizmeci *et al.,* Eur. Phys. J. A **25**, 57 (2005).

[164] K. Schmidt *et al.,* Acta Phys. Polo. B, **41** (2010).

[165] J. B. Garcia and C. Cerruti, Nucl. Phys. A **578**, 597 (1994).

[166] Y. K. Vermani and R. K. Puri, J. Phys. G: Nucl. Part. Phys. **36**, 105103 (2009).

[167] A. Jain and S. Kumar, Pramana Journal of Physics **78**, 749 (2012).

[168] L. W. Chen, C. M. Ko and B. A. Li, Phys. Rev. C **68**, 017601 (2003).

[169] C. Xu, B. A. Li and L. W. chen, Phys. Rev. C **82**, 054607 (2010); Y. Zhang, P. Danielewicz, M. Famiano, Zhuxia Li, M. B. Tsang *et. al.,* Phys. Rev. Lett. **102**, 122701 (2009); Z. Y. Sun *et. al.,* Phys. Rev. C **82**, 051603(R) (2010).

[170] J. Randrup, Nucl. Phys. A **314**, 429 (1979).

[171] J. Cugnon, T. Mizutani and J. Vandermeulen, Nucl. Phys. A **359**, 345 (1981); Z. X. Li *et al.,* Nucl. Phys. A 559, 603 (1993).

[172] H. Johnston, T. White, J. Winger, D. Rowland, B. Hurst, F. G. Nogues, D. Okelly, and S. J. Yennello, Phys. Lett. B **371**, 186 (1996); S. J. Yennello *et al.,* Phys. Lett. B **321**, 15 (1994); M. D. Toro *et al.,* Prog. Nucl. Part. Phys. **42**, 125 (1999).

[173] J. Singh, S. Kumar, and R. K. Puri, Phys. Rev. C **62**, 044617 (2000); *ibid* **65**, 024602 (2002); S. Kumar and R. K. Puri, Phys. Rev. C **58**, 1618 (1998); Y. K. Vermani, S. Goyal, and R. K. Puri, Phys. Rev. C **79**, 064613 (2009).

[174] A. D. Sood and R. K. Puri, Phys. Rev. C **70**, 034611 (2004); S. Kumar, M. K. Sharma, and R. K. Puri, Phys. Rev. C **58**, 3494 (1998), A. D. Sood, R. K. Puri, and J. Aichelin, Phys. Lett. B **594**, 260 (2004).

[175] R. K. Puri, C. Hartnack, and J. Aichelin, Phys. Rev. C **54**, R28 (1996); Y. K. Vermani and R. K. Puri, Eur. Phys. Lett. **85**, 62001 (2009); P. B. Gossiaux, R. K. Puri, C. Hartnack, and J. Aichelin, Nucl. Phys. A **619**, 379 (1997).

[176] C. Fuchs *et al.,* J. Phys. G: Nucl and Part. **22**, 131 (1996).

[177] R. K. Puri *et al.,* Phys. Rev. C **43**, 315 (1991); R. K. Puri *et al.,* Eur. Phys. J. A **3**, 277 (1998); R. K. Puri and R. K. Gupta, Phys. Rev. C **45**, 1837 (1992); R. K. Puri and R. K. Gupta, J. Phys. G: Nucl. and Part. **18**, 903 (1992); R. K. Puri, S. S. Malik and R. K. Gupta, Eur. Phys. Lett. **9**, 767 (1989); R. K. Puri *et al.,* Eur. Phys. J. A **23**, 429 (2005); S. S. Malik *et al.,* Parmana J. Phys. **32**, 419 (1989).

[178] S. A. Bass, *et al.,* GSI Scientific Report **94** GSI (Germany) 66 (1995).

[179] W. Bauer, Phys. Rev. Lett. **61**, 2534 (1988); B. A. Li and C. M. Ko, Nucl, Phys. A **601**, 457 (1996).

[180] G. Peilert, A. Rosenhauer, J. Aichelin, H. Stcker, and W. Greiner, Phys. Rev. C **39**, 1402 (1989).

[181] F. Fu *et al.,* Phys. Lett. B **666**, 359 (2008).

[182] Q. Li and Z. Li, Chin. Phys. Lett. **19**, 321 (2002).

[183] B. A. Li, P. Danielewicz and W. G. Lynch, Phys. Rev. C **71**, 054603 (2005).

[184] S. Gautam *et al.*, J. Phys. G **37**, 085102 (2010); S. Kumar, S. Kumar and R. K. Puri, Phys. Rev. C **81**, 014601 (2010).

[185] S. Kumar and R. K. Puri, Phys. Rev. C **60**, 054607 (1999).

[186] S. Kumar, S. Kumar and R. K. Puri, Phys. Rev. C **81**, 014611 (2010); V. Kaur, S. Kumar and R. K. Puri, Phys. Lett. B **697**, 512 (2011).

[187] S. Kumar and R. K. Puri, Phys. Rev. C **58**, 320 (1998); J. Singh and R. K. Puri, *ibid.* **62**, 054602 (2000).

[188] V. Kaur, S. Kumar, and R. K. Puri, Nucl. Phys. A **861**, 37 (2011).

[189] A. D. Sood and R. K. Puri, Phys. Rev. C **73**, 067602 (2006); A. D. Sood and R. K. Puri, Int. J. of Mod. Phys. E **15**, 899 (2006); A. D. Sood and R. K. Puri, Phys. Rev. C 79, 064618 (2009).

[190] V. Weisskopf, Phys. Rev. **52**, 295 (1937).

[191] G. D. Westfall, J. Cosset, P. J. Johannsen, A. M. Poskanzer, W. G. Meyer, H. H Gulbrod, A. S. Sandoval and R. Stock, Phys. Rev. Lett. **27**, 1202 (1976).

[192] J. Gosset, H. H. Gutbrod, W. G. Mayer, A. M. Poskanrer, A. Sandoval, R. Stock and G. Westfall, Phys. Rev. C **16**, 629 (1977).

[193] G. F. Chapline *et al.,* Phys. Rev. D **8**, 4302 (1973).

[194] S. Kumar, V. Kaur and S. Kumar, Cent. Eur. J Phys. **9(4)**, 986 (2011).

[195] M. Berenguer *et al.,* J. Phys. G: Nucl. Part. Phys. **18**, 655 (1992).

[196] W. Schmidt *et al.,* Phys. Rev. C **47**, 2782 (1993).

[197] R. K. Puri, E. Lehmann, A. Faessler and S. W. Huang, J. Phys. G: Nucl. Part. Phys. **20**, 1817 (1994).

[198] H. Stöcker, *et al.,* Phys. Rep. **137**, 277 (1986).

[199] R. K. Puri, E. Lehmann, A. Faessler and S. W. Huang, Z. Phys. A **351**, 59 (1995).

[200] A. Jain, S. Kumar and R. K. Puri, Phys. Rev. C **84**, 057602 (2011).

[201] A. Jain and S. Kumar, Phys. Scr. **85**, 065306 (2012).

[202] Y. Zhang, Z. Li, Phys. Rev. C **74**, 014602 (2006).

[203] T. Gaitanos *et al.,* Phys. Lett. B **595**, 209 (2004); M. Di Toro *et al.,* Nucl. Phys. A **787**, 585 (2007).

[204] S. Gautam and A. D. Sood, Phys. Rev. C **82**, 014604 (2010).

[205] F. Daffin and W. Bauer, arXiv:nucl-th/9809024v1.

[206] S. Voloshin, Phys. Rev. C **55**, R1630 (1997).

[207] W. Reisdorf *et al.,* Nucl. Phys. A **876**, 1 (2012).

[208] A. Jain, K. S. Vinayak and S. Kumar, **334**, 334 (2013).

[209] H. Sörge, Phys. Rev. Lett. **78**, 2309 (1997).

[210] J. Ollitrault, Phys. Rev. D **46**, 229 (1992).

[211] J. J. Molitoris and H. Stöcker, Phys. Lett. B **162**, 47 (1985); D. Krofcheck *et al.,* Phys. Rev. Lett. **63**, 2028 (1989); J. Peter, Nucl. Phys. A **545**, 173 (1992).

[212] K. S. Vinayak and S. Kumar, Eur. Phys. J. A **47**, 144 (2011).

[213] P. Sorensen, J. Phys. G **37**, 094011 (2010).

[214] A. P. Mishra *et al.,* Phys. Rev. C **77**, 064902 (2008).

[215] B. H. Alver *et al.,* Phys. Rev. C **82**, 034913 (2010); H. Petersen, G. Y. Qin, S. A. Bass and B. Miiller, Phys. Rev. C **82**, 041901 (2010).

[216] K. Aamodt *et al.,* Phys. Rev. Lett. **107**, 032301 (2011); K. Aamodt *et al.,* Phys. Lett. B **708**, 249 (2012).

[217] G. Y. Qin, H. Petersen, S. A. Bass and B. Muller, Phys. Rev. C **82**, 064903 (2010).

[218] P. Danielewicz and M. Gyulassy, Phys. Lett. B **129**, 283 (1983).

[219] R. Pak, Ph.D Thesis, MSU (1996).

[220] D. Cussol *et al.,* Phys. Rev. C **65**, 044604 (2002).

[221] L. V. Bravina, A. Faessler, C. Fuchs and E. E. Zabrodin, Phys. Rev. C **61**, 064902 (2000).

[222] R. J. M. Snellings, H. Sörge, S. A. Voloshin, F. Q. Wang and N. Xu, Phys. Rev. Lett. **84**, 2803 (2000).

[223] J. Liu, W. J. Guo, Y. Z. Xing and H. Liu, Nucl. Phys. A **726**, 123 (2003).

[224] P. Crochet *et al.,* Phys. Lett. B **486**, 6 (2000).

[225] J. Liu *et al.,* Phys. Rev. Lett. **86**, 975 (2001).

[226] J. D. Bowman, W. J. Swiatecki and C. F. Tsang, *Lawrence Berkeley Laboratory Report No. LBL-2908* (unpublished) (1973).

[227] T. Gaitanos, H. H. Wolter and C. Fuchs, Phys. Lett. B **478**, 79 (2000).

[228] A. Jain and S. Kumar, Int. J of Mod. Phys. E **21**, 1250071 (2012).

[229] A. Jain and S. Kumar, Nucl. Phys. A **876**, 109 (2012).

[230] A. Jain, S. Kumar and R. K. Puri, Phys. Rev. C **85**, 064608 (2012).

[231] Y. T. Zhi, M. Y. Gang, C. X. Zhou, F. D. Qing, G. Wei, M. C. Wang, S. W. Qing, T. W. Dong, and W. Kun, Chin. Phys. **16**, 2676 (2007).

[232] H. Y. Zhang *et al.,* Eur. Phys. J. A **15**, 399 (2002).

[233] H. Y. Zhang *et al.,* J. Phys. G **28**, 2397 (2002).

[234] V. Kaur, S. Kumar and R. K. Puri, Phys. Lett. B **861**, 37 (2011).

[235] B. Schenke, S. Jeon and C. Gale, Phys. Rev. Lett. **106**, 042301 (2011).

[236] R. K. Puri *et al.,* J. Comp. Phys. **162**, 245 (2000).

[237] S. W. Huang *et al.,* Phys. Lett. B **298**, 41 (1993).

[238] I. Dutt and R. K. Puri, Phys. Rev. C **81**, 047601(2010); *ibid* **81**, 044615 (2010); *ibid* **81**, 064608 (2010).

[239] I. Dutt and R. K. Puri, Phys. Rev. C **81**, 064609 (2010).

[240] S. Kumar, S. Kumar and R. K. Puri, Phys. Rev. C **78**, 064602 (2008).

[241] J. Singh, R. K. Puri and J. Aichelin, Phys. Lett. B **519**, 46 (2001); J. Dhawan and R. K. Puri, Phys. Rev. C **74**, 054610 (2006).

[242] W. Reisdorf *et al.,* Proceedings of International Workshop on Gross Properties of Nuclei and Nuclear Excitation **17**, 82 (1999), Hirschegg, Austria; D. Sisan *et al.,* Phys. Rev. C **63**, 027602 (2001).

[243] A. D. Sood and R. K. Puri, Phys. Rev. C **69**, 054612 (2004).

[244] S. Gautam, A. D. Sood, R. K. Puri, and J. Aichelin, Phys. Rev. C **83**, 014603 (2011).

[245] S. W. Huang, Ph.D thesis, Tubingen (Germany) (1994).